TECHNISCHE UNIVERSITÄT MÜNCHEN

Wissenschaftszentrum Weihenstephan für Ernährung, Landnutzung und Umwelt

Lehrstuhl für Analytische Lebensmittelchemie

Linking the sulfur and carbon cycle by ultrahigh resolution characterization of dissolved organic matter

Sabine Eva-Maria Dvorski

Vollständiger Abdruck der von der Fakultät für Wissenschaftszentrum Weihenstephan für Ernährung, Landnutzung und Umwelt der Technischen Universität München zur Erlangung des akademischen Grades eines

Doktors der Naturwissenschaften

genehmigten Dissertation.

Vorsitzende: Univ.-Prof. Dr. Dr. h.c. I. Kögel-Knabner

Prüfer der Dissertation:

1. apl. Prof. Dr. P. Schmitt-Kopplin
2. Univ.-Prof. Dr. M. Rychlik
3. Assistant Professor M. Gonsior, Ph.D., University of Maryland/USA

Die Dissertation wurde am 07.11.2016 bei der Technischen Universität München eingereicht und durch die Fakultät Wissenschaftszentrum Weihenstephan für Ernährung, Landnutzung und Umwelt am 19.01.2017 angenommen.

Summary

The chemical properties of dissolved organic matter (DOM) are highly dependent on the ecosystem of its origin and the diverse interaction points with microorganisms and other chemical elements. Hence, DOM reflects key ecosystem characteristics. As a major contributor to the global carbon cycle, the interplay of DOM with the unique sulfur redox chemistry, occupying oxidation states from –II to +VI, links two important geochemical processes, the carbon and sulfur cycle.

However, the current knowledge on the global elemental cycles is primarily based on inorganic analyses. Therefore, the aim of this thesis was the characterization of DOM from aquatic ecosystems with intensive sulfur cycling by advanced organic and inorganic analytical techniques. Besides structural spectroscopy, in particular ultrahigh resolution mass spectrometry was applied. The DOM characteristics were set into relation with prevailing geochemical parameters and particularly the inorganic sulfur chemistry, so that especially the dependency between the ecosystem conditions and the sulfur organic compound formation was evaluated.

Two freshwater aquatic ecosystems with characteristic sulfur chemistry were studied: First, DOM from hypolimnic (sulfide-rich) water of a meromictic lake and second, DOM from a well-defined petroleum hydrocarbon contaminated aquifer with intensive bacterial sulfate reduction was investigated. At both field sites a distinct enrichment of sulfur organic compounds was found in water samples with reactive inorganic sulfur species. For the comparison of the findings from field sites, laboratory experiments on the abiotic formation of sulfur organic compounds by reaction of DOM with inorganic sulfur species under similar conditions were performed. These experiments, revealed especially sulfide and sulfite to be involved in the formation of sulfur organic compounds. The great accordance of the field and laboratory investigations corroborated that the formation of sulfur organic compounds in DOM is predominantly an abiotic process. The obtained details of the laboratory experiments can be considered as a library of sulfur organic compounds in aquatic ecosystems. Moreover, new insights into the interplay of the aquatic carbon and sulfur cycle were found. Since DOM acts as a sulfide sink, it is presumably a beneficial key player in the mediation of sulfide.

iv

Zusammenfassung

Die chemischen Eigenschaften von gelösten organischen Substanzen (DOM) sind abhängig von diversen Faktoren, wie beispielsweise deren Ursprungsökosystem, den vielfältigen Interaktionen mit Mikroorganismen und anderen chemischen Elementen. Demnach spiegelt DOM wichtige Ökosystemeigenschaften wider und spielt eine wesentliche Rolle im globalen Kohlenstoffkreislauf. Die zwei zentralen geochemischen Prozesse, der Kohlenstoff- und Schwefelkreislauf, werden durch die Interaktion von DOM mit der einzigartigen Schwefelredoxchemie, die die Oxidationsstufen -II bis +VI besetzt, verbunden.

Derzeit basiert das Wissen über die globalen Stoffkreisläufe in erster Linie auf anorganischen Analysen. Ziel dieser Arbeit war es daher mittels moderner organischer und anorganischer analytischer Techniken DOM aquatischer Ökosysteme, die eine intensive Schwefelredoxchemie aufweisen, zu charakterisieren. Neben spektroskopischen Verfahren wurde hierfür insbesondere ultrahoch auflösende Massenspektrometrie angewandt. Die ermittelten geochemischen Parameter und die Eigenschaften der DOM ermöglichten die Beschreibung der Bildung von schwefelorganischen Verbindungen unter spezifischen Ökosystembedingungen.

Es wurden zwei Süßwasserökosysteme mit charakteristischer Schwefelredoxchemie untersucht. Zum einen wurde hypolimnisches (sulfid-reiches) Wasser eines meromiktischen Sees und zum anderen ein gut erforschtes kontaminiertes Grundwasser, in dem insbesondere mittels bakterieller Sulfatreduktion Erdölkontaminationen abgebaut werden, analysiert. Beide Feldstudien zeigten eine deutliche Anreicherung von schwefelorganischen Verbindungen in Wasserproben, in denen reaktive anorganische Schwefelspezies anwesend waren. Zusätzlich wurden Laborexperimente unter Ökosystem ähnlichen Bedingungen durchgeführt, um die abiotische Bildung von schwefelorganischen Verbindungen durch die Umsetzung von DOM mit anorganischen Schwefelspezies zu untersuchen und mit den Feldstudien zu vergleichen. Diese Experimente zeigten, dass insbesondere Sulfid und Sulfit an der Bildung von schwefelorganischen Verbindungen beteiligt sind.

Das hohe Maß an Parallelen zwischen den Feld- und Laborstudien bestätigte, dass die Bildung von schwefelorganischen Verbindungen in DOM primär ein abiotischer Prozess ist. Die detaillierten Ergebnisse der Laborexperimente können als Bibliothek

schwefelorganischer Verbindungen in wässrigen Ökosystemen dienen. Zudem wurden neue Erkenntnisse über das Zusammenspiel des aquatischen Kohlenstoff- und Schwefelkreislaufs erlangt. Da DOM einen wesentlichen Anteil am Umsatz von Sulfid hat, spielt es wahrscheinlich eine Schlüsselrolle bei der Mediation von Schwefelwasserstoff.

Acknowledgements

Only the support of wonderful people made this thesis possible.

First of all, I would like to thank my supervisor Prof. Dr. Philippe Schmitt-Kopplin who gave me the opportunity to be part of his exceptional group. Thank you for the encouraging way of training and trusting into my abilities. I will always be impressed by your provision of an environment of scientific freedom and creative thinking.

I thank Dr. Norbert Hertkorn for his extraordinary scientific support and promotion of sampling trips, which are memorable experiences.

I am grateful to Prof. Michael Gonsior for his scientific advice and the possible to visit his laboratory at the Chesapeake Biological Laboratory of the University of Maryland.

I thank Prof. Gregory K. Druschel and Fotios Christos Kafantaris for their collaboration in the laboratory experiments with DOM and inorganic sulfur species. Thank you very much Greg for giving me the opportunity to join your laboratory at the Indiana University-Purdue University Indianapolis and to learn from the sulfur expert.

I want to thank Dr. Christian Griebler for his support starting from the sampling trip to proof-reading in the Düsseldorf Flingern collaboration. Further, I want to thank Dr. Tillmann Lueders and Anna Róza Szalay for their efforts with the bacterial community data in the Düsseldorf Flingern collaboration. I also want to thank all group members of the IGOE who assisted during measurements and sampling trips, as well as the joint scientific discussions.

I thank all my colleagues form the BGC for the great time we spent together and the delicious coffees we enjoyed. In particular, I want to thank Dr. Marianna Lucio for her support in statistics. Further, I thank Brigitte Look and Silvia Thaller for their support in the laboratory. I am also thankful to Dr. Basem Kanawati and Alexander Ruf for their assistance at the FT-ICR-MS. I thank Prof. Dr. Bernhard Michalke and Peter Grill for their support in inorganic sulfur speciation. I want to thank Astrid Bösl for her efforts and good words, which were always present at the right time and place. Thank you very much Kirill Smirnov, Dr. Franco Moritz and Daniel Hemmler for the data analysis discussions and programming support. Special thanks go to my office 020: Theresa Bader, Tanja Verena Maier, Yan Li, Kirill Smirnov and Dr. Chloé Roullier-Gall; it was a musical and

Table of content

List of abbreviations

(−)	Negative ionization mode
(+)	Positive ionization mode
^{13}C-DEPT NMR	Carbon distortion less enhancement by polarization transfer
AC	Acenaphthene-5-carboxylic acid
ANOVA	Analysis of variance
APCI	Atmospheric pressure chemical ionization
APPI	Atmospheric pressure photo ionization
B	Magnetic field strength
BIX	Freshness index
bls	Below the surface
BTEX	Benzene, toluene, ethylbenzene, and xylenes
CDOM	Chromophoric dissolved organic matter
C_f	Concentration factor
CHNO	Carbon, hydrogen, nitrogen and oxygen containing compounds
CHNOS	Carbon, hydrogen, nitrogen, oxygen and sulfur containing compounds
CHO	Carbon, hydrogen and oxygen containing compounds
CHOS	Carbon, hydrogen, oxygen and sulfur containing compounds
CID	Collision induced dissociation
CRAM	Carboxyl-rich alicyclic molecules
CSIA	Contaminant-specific stable isotope analysis
CV	Cyclic voltammetry
DEPT HSQC	Distortion less enhanced by polarization transfer heteronuclear single quantum coherence
DME	Dropping mercury electrode
DOC	Dissolved organic carbon
DOM	Dissolved organic matter
DOS	Dissolved organic sulfur
ED	Elector dialysis
EEM	Excitation emission matrix
ESI	Electrospray ionization
FA	Fulvic acid
FDOM	Fluorescent dissolved organic matter
FI	Fluorescence index
F_L	Lorentz force
FT-ICR-MS	Fourier transform ion cyclotron resonance mass spectrometry
FTIR	Fourier transform infrared spectroscopy
GC-MS	Gas chromatography coupled to mass spectrometry
H/C	Hydrogen to carbon ratio
HA	Humic acid
HIX	Humification index

HPLC	High performance liquid chromatography
HPLC-UV/VIS	High performance liquid chromatography coupled to a ultraviolet visible detector
HR-MLW	High resolution multilevel well
HS	Humic substances
ICP-MS	Inductively coupled plasma mass spectrometry
ICP-OES	Inductively coupled plasma optical emission spectrometry
JRES	J-resolved NMR spectroscopy
LOD	Limit of detection
m	Mass
M	Molar
m/z	Mass to charge ratio
MALDI	Matrix assisted laser desorption ionization
mg/L	Milligram per liter
MNA	Methylnaphthoic acid
MNMS	Methylnaphthyl-2-methylsuccinic acid
MS/MS	Tandem mass spectrometry
n.d.	Not determined
NMR	Nuclear magnetic resonance
NMS	Naphthyl-2-methyl-succinic acid
NOM	Natural organic matter
O/C	Oxygen to carbon ratio
OPLS	Orthogonal partial least squares analysis
OPLS-DA	Orthogonal partial least squares discriminant analysis
OTU	Operational taxonomic unit
PAH	Polycyclic aromatic hydrocarbon
PARAFAC	Parallel factor analysis
PCA	Principal component analysis
PN	Pine needle extract
POM	Particulate organic matter
Py-GC-MS	Pyrolysis gas chromatography coupled to mass spectrometry
q	Charge
R	Resolution
r	Radius of trajectory movement
RO	Reversed osmosis
RO-ED	Reversed osmosis coupled to elector dialysis
SEC	Size exclusion chromatography
SPE	Solid phase extraction
SPE-DOM	Solid phase extracted dissolved organic matter
SRFA	Suwannee River Fulvic Acid
TOCSY	Total correlation NMR spectroscopy
UK	United Kingdom
USA	United States of America
XANES	X-ray absorption near edge structure

YNP	Yellowstone National Park
δ	Chemical shift
ν	Velocity
ω	Angular velocity

Glossary

$CHOS_1$	sulfur organic compound with one sulfur atom
$CHOS_2$	sulfur organic compound with two sulfur atom
$CHOS_3$	sulfur organic compound with three sulfur atom
$CHOS_4$	sulfur organic compound with four sulfur atom
$CHOS_x$	polysulfurized sulfur organic compound
desulfurization	release of sulfur from organic molecules
polysulfane monosulfuric acids	$HS_xO_3^-$
polysulfanes	H_2S_x
polysulfide	S_x^{2-}, salt of polysulfanes
polysulfur sulfonic acids	$R\text{-}S_xO_3H$
polysulfurized	organic molecules with multiple sulfur atoms
polythiol	$R\text{-}S_x\text{-}SH$
polythionate	$S_xO_6^{2-}$
sulfide	S^{2-}
sulfite	SO_3^{2-}
sulfonate	$R\text{-}OSO_3^-$
sulfonation	incorporation of sulfonic acid functionalities
sulfonic acids	$R\text{-}SO_3^-$
sulfurization	incorporation of reduced sulfur functionalities
thiol	$R\text{-}SH$
thiosulfate	$S_2O_3^{2-}$

List of tables

List of figures

1. General introduction

1.1. Thesis structure and motivation

Freshwater dissolved organic matter (DOM) ranges among the most complex organic mixtures on earth and is a major contributor to the global carbon cycle. Through its diverse interaction possibilities with other elements, such as metals and particularly sulfur species, it is directly interacting with the sulfur cycle. Therefore, DOM reflects key ecosystem characteristics, e.g., it is influencing the availability of organic and inorganic nutrients and contaminants. The sulfur cycle is major geochemical cycle, because of the unique redox chemistry of sulfur occupying oxidation states from –II to +VI.

The current knowledge on the geochemical elemental cycles is primarily based on inorganic and isotopic ratio analyses. Hence, less is known about the linkage of the carbon cycle and sulfur cycle. Therefore, the motivation of this thesis was the characterization of DOM from aquatic ecosystems with intensive sulfur cycling by advanced analytical techniques. Particularly, ultrahigh resolution mass spectrometry, due to its unique capability of unambiguous assignment of sulfur organic molecules (CHOS), was applied. The DOM characteristics were set into relation with prevailing geochemical parameters and particularly the inorganic sulfur chemistry, so that especially the dependency between ecosystem conditions and CHOS compounds formation was evaluated. The obtained results provide new insights into the interplay of the aquatic carbon and sulfur cycle.

An overview of the thesis structure is provided in Figure 1-1. This thesis includes field investigations from two field sites with characteristic sulfur cycling. First, DOM from hypolimnic (sulfide-rich) water of a meromictic lake was investigated (chapter 2). Second, DOM from a well-defined petroleum hydrocarbon contaminated aquifer with intensive bacterial sulfate reduction was studied (chapter 3). For the comparison of the findings from field sites, laboratory experiments on the abiotic formation of sulfur organic compounds by reaction of DOM with inorganic sulfur species under similar conditions as found in ecosystems, were performed (chapter 4). The obtained results from the field sites and laboratory experiments were set into relation in the overall summary and conclusion (chapter 5).

The Supplementary Information includes additional figures and tables of the results and discussion sections from chapters 3–5. The specific materials and methods sections are

integrated in the respective chapters. Additionally, extended information on method details are included in the Appendix (chapter 7).
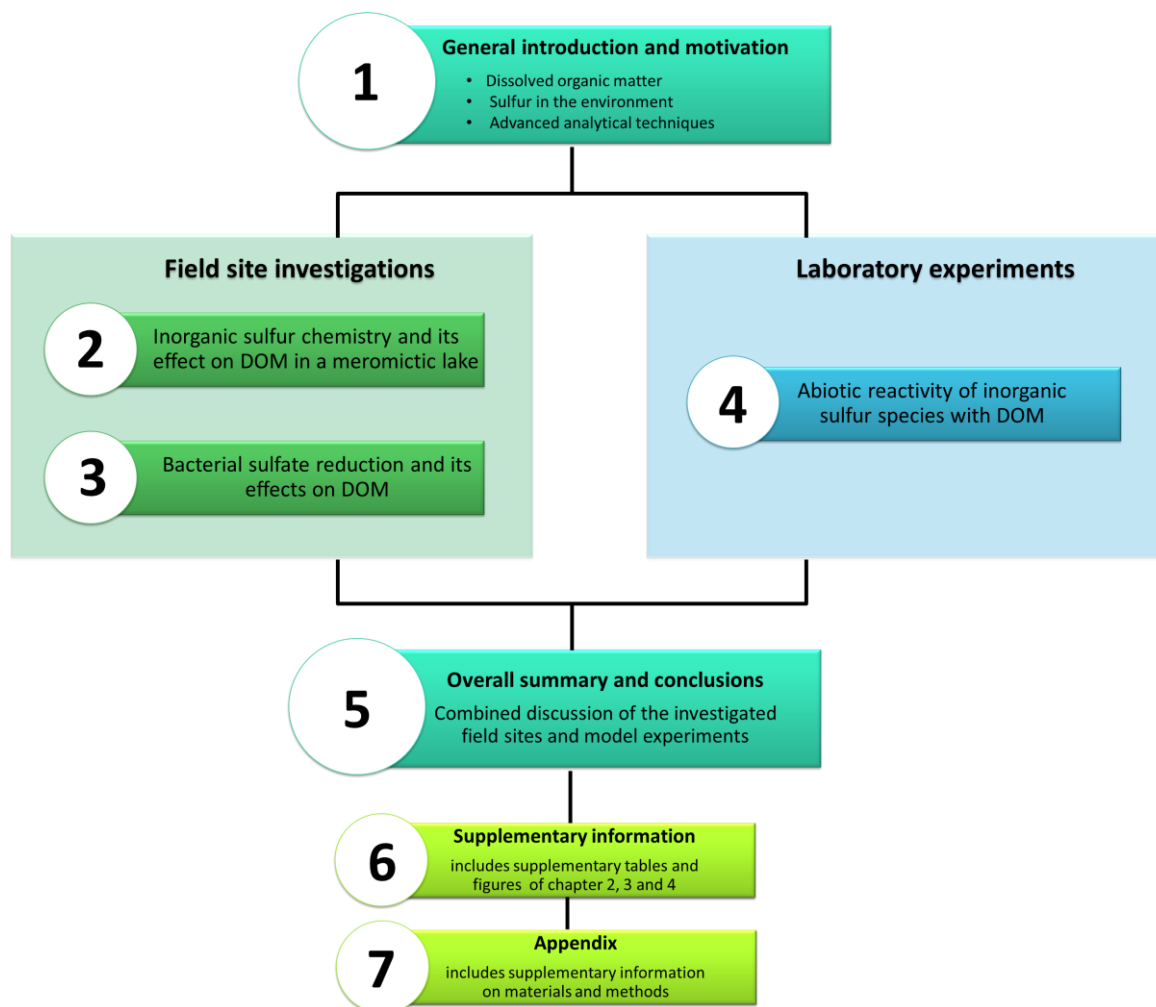
Figure 1-1: Overview of the thesis structure.

1.2. Dissolved organic matter

Natural organic matter (NOM) is an ubiquitous and highly complex mixture of organic compounds in aquatic and terrestrial environments (Nebbioso and Piccolo 2013). In aquatic environments NOM is subdivided into two groups: Particulate organic matter (POM) and dissolved organic matter (DOM) (vanLoon and Duffy 2011). The definition of DOM is operationally as the fraction that passes through a filter of a nominal pore size varying from 0.1 μm to 1.0 μm (Mopper et al. 2007). DOM is involved in numerous aquatic ecosystem processes (Nebbioso and Piccolo 2013); hence it reflects key characteristics of the ecosystem from where it is derived.

1.2.1. Origin and composition of DOM

DOM originates from the decay of living organisms and anthropogenic processes (Mostofa et al. 2009, vanLoon and Duffy 2011). The chemical properties of DOM are highly dependent on the ecosystem of its origin. The sources of DOM are subdivided into terrestrial and aquatic sources (Lin 2015, vanLoon and Duffy 2011). Terrestrial derived DOM is also called allochthonous when it is derived from, e.g. degradation of plants in the surrounding watersheds, soil organic matter, as well as animals, and anthropogenic when derived from, e.g. agriculture, industry, and sewage effluents (Mostofa et al. 2009, vanLoon and Duffy 2011). Autochthonous DOM is directly derived from the aquatic environment, which includes sources such as the degradation and excretion of algal biomass, submerged aquatic vegetation, seagrass, bacteria, and phytoplankton (Figure 1-2) (vanLoon and Duffy 2011). The composition of DOM is altered by chemical reactions and photochemical reactions, the so called abiotic transformation, and microbial processes, the so called biotic transformation (Lin 2015, Mostofa et al. 2013). Thus, physicochemical analysis of DOM, particularly its composition, is essential to understand aquatic ecosystem processes (Figure 1-2).
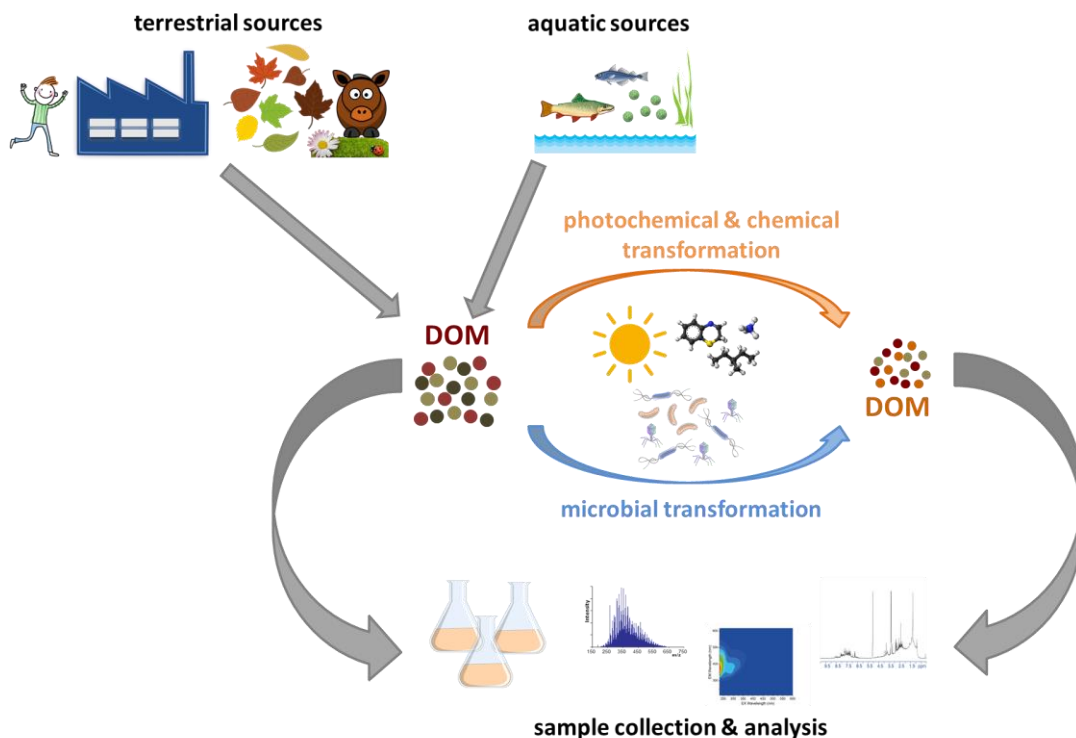
Figure 1-2: Overview of DOM.
Schematic overview of the sources of DOM and its transformation processes in combination with the characterization of DOM.

The concentration of DOM versus inorganic solutes varies for the different types of aquatic environments and is obtained by analyzing the dissolved organic carbon (DOC) and inorganic carbon (DIC) concentration. Seawater represents the extreme case where inorganic matter is 30,000 times more concentrated than organic matter. Other extremes are swamps, marshes and bogs where the organic matter concentration is greater than the inorganic matter concentrations. Lakes and rivers as well as groundwaters represent intermediate conditions with about 10 to 100 times more inorganic matter, respectively (Thurman 1985).

Furthermore, the DOC concentration differs substantially for the mentioned water body types. Sea and groundwaters have the lowest average DOC concentrations with 0.5 mg/L and 0.7 mg/L, respectively. Pristine streams have with 1 to 3 mg/L slightly lower average DOC concentrations than rivers and lakes with values in the range of 2 to 10 mg/L. Swamps, mashes, and bogs have concentrations of DOC from 10 to 60 mg/L and are representatives for ecosystems where organic compounds dominate the water chemistry (Thurman 1985).

The chemical composition of DOM ranges on the one side from largely aliphatic to highly unsaturated aromatic compounds and on the other side from hydrophobic to hydrophilic compounds (Matilainen et al. 2011, Thurman 1985). The heterogeneous mixture of molecules carries all sorts of functional groups whereby carboxyl, hydroxyl, amide and keto groups are the most prominent (Leenheer and Croué 2003). The hydrophobic DOM fraction is rich in aromatic carbon, phenolic structures, and conjugated double bonds (Matilainen et al. 2011). The mainly hydrophobic acids, also refer to as humic substance (HS) (Matilainen et al. 2011), account for more than 50% of the DOC in aquatic ecosystems (Aiken et al. 1986, Thurman 1985). Dissolvable HS are subdivided into two groups according to their behavior at different pH values. Humic acids (HA) which are soluble in base and fulvic acid (FA) which are soluble in both acid and base (Kördel et al. 1997, Thurman 1985). The structure of HS is strongly related to the biological component, e.g. phenols, lignins, and tannins, from which they derive (Kördel et al. 1997, Thurman 1985). The non-humic DOM fraction consist of more hydrophilic molecules such as carbohydrates and peptides and their free building blocks sugars and amino acids (Matilainen et al. 2011, Perdue and Ritchie 2003, Thurman 1985). These substrates are biologically directly available and show a greater turnover and lower concentration than the recalcitrant HS (Perdue and Ritchie 2003, Thurman 1985). Although DOM has been subject to broad variety of studies and analysis techniques DOM remains largely unknown at the molecular level.

1.2.2. DOM functions in the environment and its role in the global carbon cycle

1.2.2.1. DOM functions in the environment

Based on the chemical diversity of the DOM composition, DOM holds important environmental functions (Kördel et al. 1997, vanLoon and Duffy 2011, Minor et al. 2014) and plays key roles in biogeochemical cycling (Kruger, Dalzell and Minor 2011).

Chromophoric dissolved organic matter (CDOM) is the light absorbing fraction of DOM and of ecological importance as it is attenuating harmful ultraviolet (UV) as well as photosynthetically active radiation (Blough and Del Vecchio 2002, Hiriart-Baer and Smith 2005, Morris et al. 1995, Bracchini et al. 2004).

Owing to the high number of carboxyl groups, DOM acts as a pH buffer in water bodies which lack inorganic proton acceptors such as hydrogen carbonate (vanLoon and Duffy 2011, Oliver, Thurman and Malcolm 1983). Additionally, humic substances were shown to be redox active and can serve as electron acceptor and shuttle in microbial redox processes (Kappler et al. 2004, Klupfel et al. 2014, Lovley et al. 1996, Heitmann et al. 2007, Aeschbacher et al. 2011).

Besides the association of DOM to solids (vanLoon and Duffy 2011), DOM is a known complexing agent for metal ions (vanLoon and Duffy 2011, Kördel et al. 1997, Sholkovitz and Copland 1981, Ravichandran 2004, Perdue and Ritchie 2003). Additionally, DOM is a reactant, chelator and sorbent for anthropogenic pollutants (vanLoon and Duffy 2011, Kördel et al. 1997, Minor et al. 2014). Hence, DOM influences the chemical degradation, volatilization and toxicity of pollutants (Kördel et al. 1997). In addition, the photolysis of anthropogenic pollutants is affected by DOM because DOM can act both as photosensitizer (Miller and Chin 2005, Zeng and Arnold 2013, Remucal 2014) and inhibitor (Wenk, von Gunten and Canonica 2011) in photolysis of contaminants. Furthermore, DOM alters the mobility (Moeckel et al. 2014, Kördel et al. 1997), bioavailability (Traina, McAvoy and Versteeg 1996, Kördel et al. 1997) and ultimate fate of organic contaminants and trace metals (Minor et al. 2014, Kördel et al. 1997).

Moreover, DOM is an important energy source for heterotrophic aquatic organisms (Azam et al. 1983, Boyer et al. 2006, Pace et al. 2007, Amon and Benner 1996b, Hertkorn et al. 2002). It was shown that the chemical structure and size of DOM components are essential factors for the DOM bioavailability and nutrient value (Amon and Benner 1996a).

The above presented DOM ecosystem functions are linked to biogeochemical cycling (Kruger et al. 2011). Together with biota, DOM is an essential member of the global carbon cycle.

1.2.2.2. Role of DOM in the global carbon cycle

Some of the above presented ecosystem functions of DOM have a direct linkage to biogeochemical cycles (Kruger et al. 2011), particularly the global carbon cycle. Oceanic DOM is one of the Earth's largest reactive carbon pools and therefore a major contributor to the global carbon cycling (Hedges 1992, Hansell and Carlson 2001). Only recently, it

was found that, despite only a comparably small area of the Earth is covert with freshwater systems, its contribution to the carbon cycle by carbon dioxide evasion is remarkable (Cole et al. 2007, Battin et al. 2009, Raymond et al. 2013, Wehrli 2013).
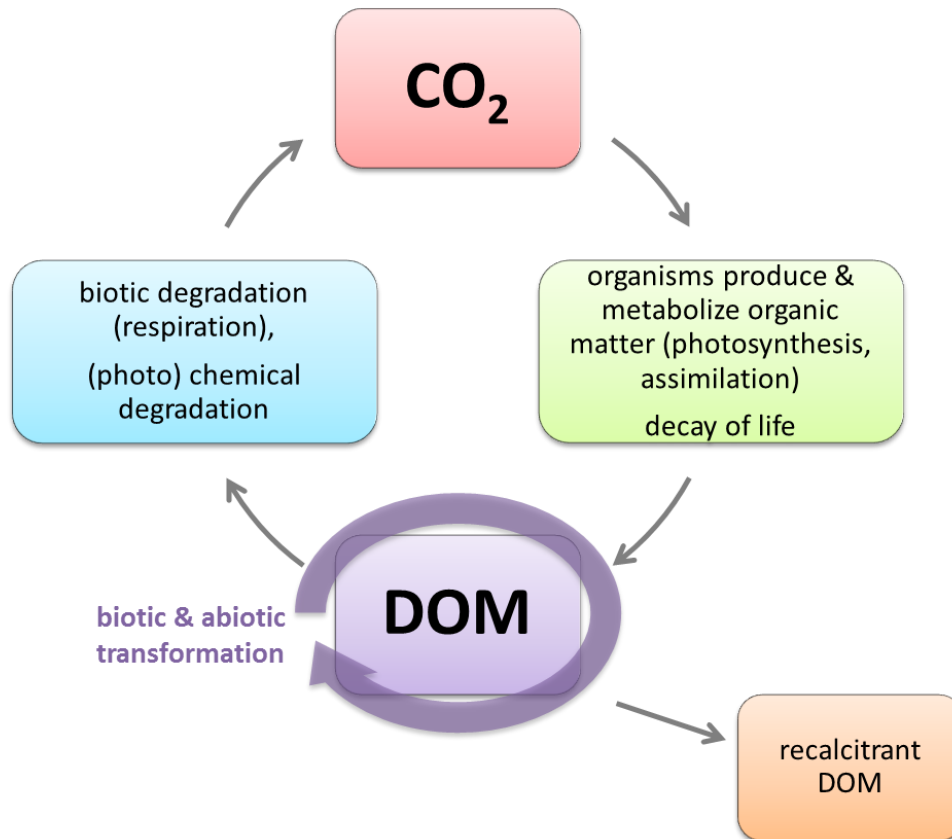
Figure 1-3: The role of DOM in the global carbon cycle.

Generally, DOM plays an essential role in the transport of carbon and nutrients from soils into streams, rivers, and the oceans (Kruger et al. 2011). The carbon turnover via DOM and therefore the role of DOM in the global carbon cycle is highlighted in Figure 1-3. The first step is the fixation of carbon dioxide by photosynthetic active organisms into metabolites and serves as a nutrient and is therefore further metabolized by all sorts of organisms (Thurman 1985). Besides the release of metabolites to the DOM pool, the decay of live is the major source for DOM (cf. paragraph 1.2.1) (Mostofa et al. 2009, vanLoon and Duffy 2011). DOM, if it is not recalcitrant or buried, finally underlies photo-induced and microbial or biological degradation (Mostofa et al. 2013, Fasching et al. 2014, Thurman 1985). A major end product of both DOM degradation pathways is carbon dioxide, the major starting form of carbon in the global carbon cycle (Mostofa et al. 2013).

1.3. Sulfur in the aquatic environment

Sulfur is an essential element for all forms of live (Brown 1982, Bailey et al. 2002, vanLoon and Duffy 2011) and plays a pivotal role in biogeochemical cycles (Bailey et al. 2002, vanLoon and Duffy 2011). Sulfur organic compounds have been identified as key players for the biotic and abiotic DOM chemistry (Herzsprung et al. 2010, Sleighter et al. 2014, Yu et al. 2015a, Yu et al. 2015b, Durham et al. 2015). Both organic and inorganic sulfur occupies all possible sulfur oxidation states, from the most reduced oxidation state –II, i.e. hydrogen sulfide (H_2S) and thiols, to the most oxidized redox state +VI, i.e. sulfate (SO_4^{2-}) and organosulfates (Bailey et al. 2002, vanLoon and Duffy 2011).

Sulfate is a principle ionic species in aquatic environments, with average concentrations of 28 mmol L^{-1} in the oceans and 0.12 mmol L^{-1} in rivers and lakes (vanLoon and Duffy 2011). The majority of H_2S in aquatic ecosystems is produced by bacteria in widely spread anaerobic, sulfate rich environments such as marine sediments (Brown 1982). Besides H_2S and sulfate, also other small sulfur molecules such as thiosulfate ($S_2O_3^{2-}$), thiocyanates (R/H-SCN), methane thiol (CH_3SH), dimethyl sulfide ((CH_3)$_2$S), dimethyl disulfide ((CH_3)$_2$S$_2$), carbonyl sulfide (COS) and carbon sulfide (CS_2) are produced and released during the degradation of sulfur containing organic matter such as proteins in aquatic ecosystems (Brown 1982, Bailey et al. 2002). Some sulfur compounds are directly toxic such as H_2S (Brown 1982, vanLoon and Duffy 2011), others are indirectly toxic, e.g. production of acidity by sulfuric acid (Brown 1982). Inorganic and organic sulfur species interact with metals by mineralization and complexation, whereby especially iron is of importance (Hellige et al. 2012, Rickard and Luther III 2007, Luther III and Church 1992).

1.3.1. Aquatic sulfur cycle

As already hinted, a variety of biochemical and geochemical processes occurring in soils, sediments, and water play an essential role in the natural circulation of sulfur in ecosystems (Brown 1982, vanLoon and Duffy 2011). Figure 1-4 summarizes the aquatic sulfur cycle based on the major inorganic sulfur species as well as abiotic and biotic formation and decomposition processes. These processes control the rate at which sulfur is captured in insoluble forms such as pyrite or mobilized as soluble forms such as sulfate and volatile forms such as hydrogen sulfide (Brown 1982). The sulfur cycle is controlled by microbes and fungi which convert sulfur species, especially by inorganic sulfur species

metabolizing bacteria which carry out oxidation and reduction reactions (Brown 1982, Lyons, Fike and Zerkle 2015). Besides the two redox endmembers sulfide and sulfate also elemental sulfur and thiosulfate have been shown to be key intermediates in both oxidative and reductive conversions in the microbial energy metabolism (Bak and Cypionka 1987, Bak and Pfennig 1987, Jørgensen 1990, Lyons et al. 2015). Sulfur organic molecules are formed from organic molecules and inorganic sulfur species by abiotic and biotic pathways (Amrani 2014, Brown 1982, Aizenshtat et al. 1995, Amrani et al. 2007, Bailey et al. 2002, Durham et al. 2015). They are also part of the organic matter pool. Therefore, organic matter contributes to the formation of inorganic sulfur species, both by the decomposition of sulfur organic molecules and by providing substrates for bacterial sulfur redox processes, such as bacterial sulfate reduction (Brown 1982, Bailey et al. 2002).
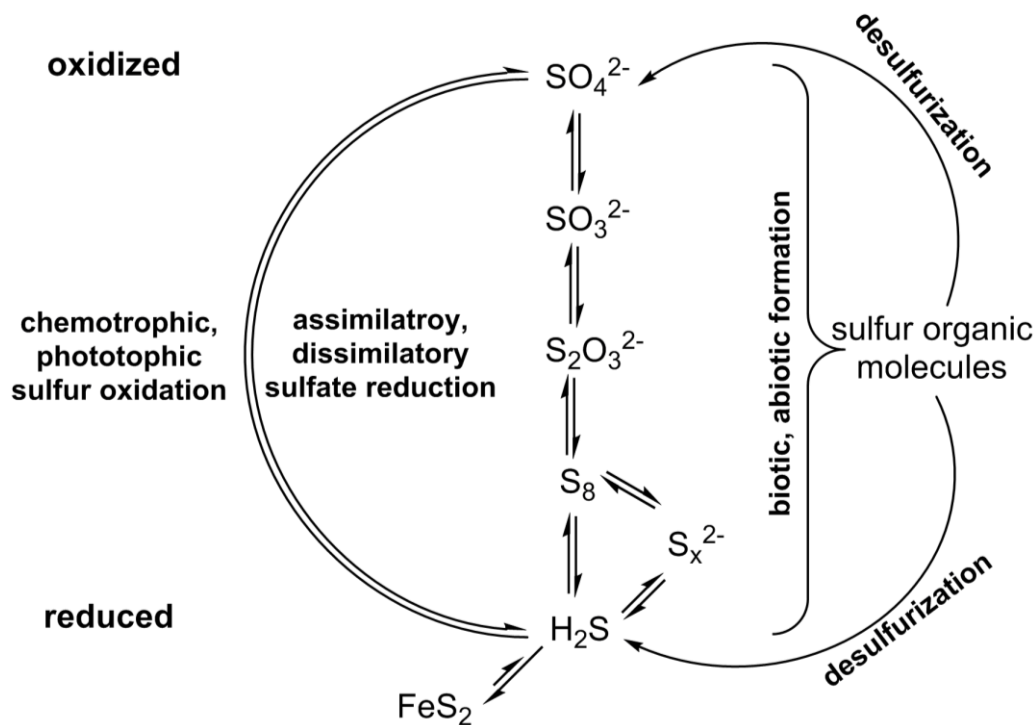
Figure 1-4: The aquatic sulfur cycle.

1.3.2. Role of sulfur species in abiotic and biotic processes

In the following section the role of different sulfur species involved in abiotic and biotic processes of the sulfur cycle is addressed in detail.

The most prominent biotic process involved in the sulfur cycle is sulfate reduction. Dissimilatory sulfate reduction is a respiratory process used by some bacteria and archaea

to generate energy under anaerobic conditions, whereby sulfate serves as the terminal electron acceptor leading to the production of sulfide (vanLoon and Duffy 2011, Jørgensen 1977, Brown 1982). This process is called bacterial sulfate reduction (BSR) (Jørgensen 1977) or more precise microbial sulfate reduction (MSR) (Amrani 2014), which includes also sulfate reduction by archaea. Accompanied by continuous sulfur cycling, bacterial sulfate reduction has been identified as crucial respiratory pathway in both marine (Jørgensen 1982) and freshwater ecosystems (Heitmann et al. 2007). Another important biotic process that involves the reduction of sulfate is assimilatory sulfate reduction (Schiff and Fankhauser 1981). This process enables the production of the thiol amino acid cysteine, an essential protein building block and a precursor for other sulfur organic metabolites, and is carried out by many organisms such as plants and chemosynthetic sulfur bacteria (Schiff and Fankhauser 1981).

The complementary process in the biotic sulfur cycling is the oxidation of sulfide. The first step of this process is the oxidation of sulfide to elemental sulfur, followed by oxidation of elemental sulfur to sulfite or directly to sulfate for the production of energy by bacteria and archaea (Maier 2009). In aerobic ecosystems chemoautotrophs and in anaerobic ecosystems photoautotrophs (Purple and Green Sulfur Bacteria) are carrying out microbial sulfide oxidation (Maier 2009, vanLoon and Duffy 2011).

Besides sulfur oxidation and reduction some microbes are specialists in the disproportionation of sulfur species with intermediate redox states such as elemental sulfur and thiosulfate (Vairavamurthy et al. 1993, Poser et al. 2013, Thamdrup et al. 1993, Finster, Liesack and Thamdrup 1998, Jørgensen 1990, Lyons et al. 2015, Hardisty et al. 2013). Furthermore, desulfurization, the release of sulfur during the microbial decomposition of sulfur organic molecules from the organic matter pool, takes place in aquatic environments (vanLoon and Duffy 2011). Desulfurization leads to the release of H_2S and sulfate (vanLoon and Duffy 2011).

Recently, the studies of diverse environments, from the deep sea to the human gut, showed that many essential ecosystem processes are mediated not by a single species, but by the metabolic interaction of microbial communities (Milucka et al. 2012, Devkota et al. 2012, Pfeffer et al. 2012).

Aside from the variety of biotic processes involving and releasing sulfur species also abiotic reactions with sulfur species, such as the mineralization of sulfur in the form of

pyrite, are crucial to biogeochemical cycling (Rickard and Luther III 2007, Amrani 2014). The abiotic reactivity of inorganic sulfur species with organic matter is of particular interest for this thesis. It was shown that sulfur is incorporated into organic molecules by reaction of sulfide and polysulfide with organic molecules in diverse ecosystem settings to form thiols (Vairavamurthy and Mopper 1987, LaLonde, Ferrara and Hayes 1987, Schouten et al. 1994, Aizenshtat et al. 1995, Adam, Philippe and Albrecht 1998, Perlinger et al. 2002, Amrani and Aizenshtat 2004b, Amrani et al. 2007, Amrani 2014, Yu et al. 2015b). Additionally, organosulfonates and –sulfonic acids are major contributors to the sulfur organic compounds in organic matter, formed by the reaction of thiosulfate, sulfite and sulfuric acid with organic matter (Vairavamurthy et al. 1994, Aizenshtat et al. 1995, Schmitt-Kopplin et al. 2010, Yu et al. 2015b).

1.4. Advanced analytical techniques for the characterization of DOM

Although DOM is a highly complex mixture of organic molecules, which vary in size, structure, and functionality, many studies are based on bulk chemical parameters such as DOC, C/N elemental ratios, and bulk isotopic and elemental compositions (Mopper et al. 2007, Leenheer and Croué 2003, Minor et al. 2014, Thurman 1985). Other approaches are focused on studying general chemical properties such as determination of the acid-base chemistry by titration, UV/VIS absorption (e.g. $SUVA_{254}$) and fluorescence characteristics (Thurman 1985, Ritchie and Perdue 2003, Leenheer and Croué 2003, Minor et al. 2014). Traditionally, knowledge of molecular structural characteristics of organic matter is obtained by Fourier transform infrared (FTIR), X-ray absorption near edge structure (XANES), ^{13}C nuclear magnetic resonance (NMR) spectroscopy and chemical degradation followed gas chromatography coupled to mass spectrometry (GC-MS) and direct pyrolysis Py-GC-MS (Derenne and Nguyen Tu 2014, Leenheer and Croué 2003, Thurman 1985). Recently, advanced analytical techniques such as Fourier transform ion cyclotron resonance mass spectrometry (FT-ICR-MS), solution state NMR and excitation-emission matrix (EEM) fluorescence spectroscopy enabled detailed structural characterization and adequate assessment of DOM and its interaction in abiotic and biotic processes (Minor et al. 2014, Stubbins et al. 2014, Simpson and Simpson 2014, Simpson, Simpson and Soong 2012, Hertkorn et al. 2013, Hertkorn et al. 2007, Nebbioso and Piccolo 2013, Mopper et al. 2007). Further details about these methods are addressed

later in this chapter, since these techniques were primarily used for the characterization of DOM in this thesis.

Additionally, isolation and fractionation of DOM is of great importance for the DOM characterization. On the one hand it is able to give rise to size and chemical properties of DOM and on the other hand it is required as a sample preparation step prior methods, such as FT-ICR-MS and NMR spectroscopy (Minor et al. 2014, Nebbioso and Piccolo 2013, Mopper et al. 2007). Membrane based isolation and fractionation include ultra-(UF) and nanofiltration (NF), reversed osmosis (RO), electro dialysis (ED) and the combination RO-ED (Perdue and Ritchie 2003, Mopper et al. 2007, Nebbioso and Piccolo 2013, Minor et al. 2014). Chromatography based isolation and fractionation include size exclusion chromatography (SEC), high performance liquid chromatography (HPLC) and solid phase extraction (SPE) (Perdue and Ritchie 2003, Mopper et al. 2007, Leenheer and Croué 2003, Thurman 1985, Nebbioso and Piccolo 2013, Minor et al. 2014). Further, capillary electrophoresis has been applied for the characterization of DOM and when used in combination with mass spectrometry enables an in-depth characterization of DOM (Egeberg and Bergli 2002, Schmitt-Kopplin and Kettrup 2003, Gaspar et al. 2010).

SPE is superior when isolation of DOM is needed as sample preparation step (desalination and concentration) for a large number of samples since it is applicable without sophisticated instrumentation and electrical power compared to RO and ED (Dittmar et al. 2008). Thus, SPE can be performed under rough field conditions with a large number of samples in parallel (Dittmar et al. 2008). Historically XAD resins were used for the isolation and fractionation of DOM since the 1970s but were unfortunately taken from the market (Aiken et al. 1979, Thurman and Malcolm 1981). Today mainly silica based C-18 and styrene divinyl benzene polymer based PPL (only available from Agilent Technologies Inc.) SPE cartridges are used for the isolation of DOM (Kim et al. 2003b, Dittmar et al. 2008). Hydrophobic Silica-based sorbents have the drawback that they undergo phase collapse in aqueous matrices which leads to the loss of the retention (Dittmar et al. 2008). Furthermore, the isolation of DOM with polymer based PPL cartridges showed a higher DOC recovery rate compared to silica-based as well as other polymer based SPE resins (Dittmar et al. 2008, Chen et al. 2016).

1.4.1. Fourier transform ion cyclotron resonance mass spectrometry

Among all types of mass spectrometers FT-ICR-MS offers highest mass accuracy (< 100 ppb) and resolving power (Nikolaev, Kostyukevich and Vladimirov 2014). FT-ICR-MS is able to distinguish several thousands of ions with substantial concentration differences in parallel. Modern computational power and approaches enable to unravel the molecular formulas from the detected ions (Koch et al. 2005, Sleighter and Hatcher 2007, Tziotis, Hertkorn and Schmitt-Kopplin 2011). These unique analytical characteristics made FT-ICR-MS an important tool for the characterization of complex mixtures in -omics approaches such as proteomics, metabolomics, petroleomics as well as in the understanding of DOM (Nikolaev et al. 2014, Mopper et al. 2007, Sleighter and Hatcher 2011, Nebbioso and Piccolo 2013, Minor et al. 2014). Molecular level information obtained by FT-ICR-MS has been proven to be a powerful approach for the identification of biogeochemical transformations and transport processes of DOM (Kim, Kramer and Hatcher 2003a, Kujawinski et al. 2009, Kim, Kaplan and Hatcher 2006, Koch et al. 2005, Schmidt et al. 2011).
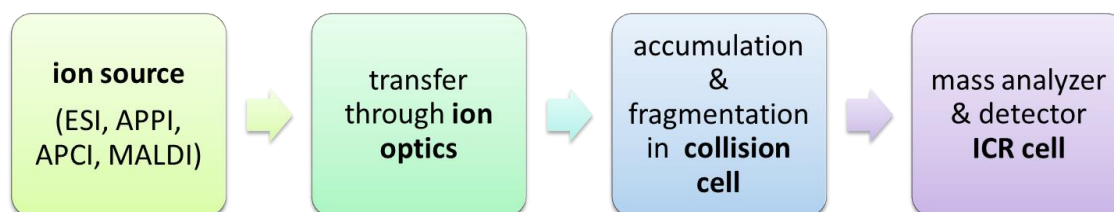
Figure 1-5: Schematic overview of the FT-ICR-MS instrumental setup.

The fundamentals behind FT-ICR-MS were reviewed in detail by Marshall et al. and Nikolaev et al. (Marshall, Hendrickson and Jackson 1998, Nikolaev et al. 2014). Figure 1-5 illustrates schematically the FT-ICR-MS instrumental setup. After ionization of the molecules, the ions are focused by the funnel system of the ion optics and a quadrupole. The ions enter the collision cell, where they are accumulated before they reach the ICR cell. The collision cell is an additional quadrupole mass analyzer, which enables a selective ion filtration and by infusion of collision gas MS/MS fragmentation can be performed. The ions enter the ICR cell which is embedded in a spatial uniform magnetic field and an electrical field excites the ions on higher trajectories. The ions with the mass m and an electrical charge q are subject to Lorentz Force F_L (Equation 1-1) in a magnetic field B which is orthogonal to the ion's velocity v (Marshall et al. 1998).

$$F_L = q \cdot v \cdot B$$

Equation 1-1: Lorentz Force
Lorentz force F_L that acts on electrical charge q which passes a magnetic field B with the velocity v.

The magnetic field bends the ion path into a circle of the radius r in a homogenous magnetic field. The Lorentz and centrifugal force are in equilibrium (Equation 1-2).

$$\frac{m \cdot v^2}{r} = q \cdot v \cdot B \quad or \quad \frac{m}{q} = \frac{B \cdot r}{v}$$

Equation 1-2: Equilibrium between the centrifugal and Lorentz force
Equilibrium between the centrifugal and Lorentz force (m = mass, v = velocity, r = radius of trajectory movement, q = charge, B = magnetic field).

The angular velocity ω of an ion is called cyclotron frequency and is only dependent of the mass m, charge q and the magnetic field strength B (Equation 1-3).

$$\omega = \frac{q \cdot B}{m}$$

Equation 1-3: Angular velocity
The angular velocity ω (cyclotron frequency) (ω = angular velocity, q = charge, B = magnetic field strength, m = mass).
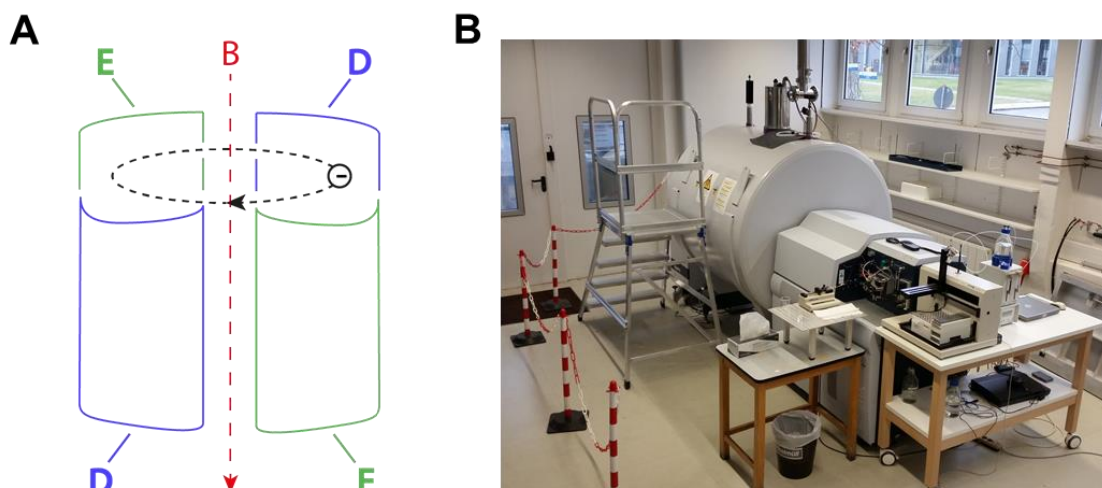
Figure 1-6: Principles of FT-ICR-MS.
A) Scheme of the trajectory of a negatively charged ion in the ICR cell as explained in the text (B = magnetic field, D = detection plates, E = excitation plates). B) Bruker Daltonik SolariX Qe FT-ICR-MS equipped with a 12 T superconducting magnet in the laboratory of the research unit Analytical BioGeoChemistry at the Helmholtz Zentrum München.

In order to enable detection of ions their radius has to be increased. Therefore, so called excitation plates apply an alternating electrical field orthogonal to the magnetic field. A second pair of plates, which is rotated 90° to the excitation plates, detects the ions due to the occurrence of alternating currents between the two detection plates (Figure 1-6). Fourier transformation is required to convolute the mass spectrum from the so called image current, which is a superimposition of several frequencies caused by ions with different masses.

It is possible to couple various ionization sources, such as electrospray ionization (ESI), atmospheric pressure photoionization (APPI), atmospheric pressure chemical ionization (APCI), and matrix assisted laser desorption ionization (MALDI) with FT-ICR mass spectrometers. Negative mode (–)ESI is mainly applied for the analysis of organic matter, due to the high number of acidic functional groups in NOM (Sleighter and Hatcher 2007, Sleighter and Hatcher 2011). In contrast to ESI, which ionizes polar functional groups of the molecules, APPI ionizes non-polar molecules such as condensed aromatics (Sleighter and Hatcher 2011). Both ESI and APPI are soft ionization techniques, thus charged intact molecules are detected in the ICR cell (Sleighter and Hatcher 2011). The use of multiple ionization methods is able to deliver comprehensive information on the sample (Sleighter and Hatcher 2007, Hertkorn et al. 2008, Sleighter and Hatcher 2011).

There are several strategies to assign molecular formulas from FT-ICR mass spectra, reaching from matching of possible molecular formulas with databases to network approaches (Koch et al. 2005, Kujawinski and Behn 2006, Koch et al. 2007, Tziotis et al. 2011, Green and Perdue 2015). Besides chemical constraints, such as the double bond equivalent and elemental constraints, matching of the isotopic pattern of assigned formulas is crucial for molecular formula assignment (Koch and Dittmar 2006, Kind and Fiehn 2007, Sleighter and Hatcher 2011). The unique capability of unambiguous assignment of molecular formulas from FT-ICR mass spectra is based on the high mass accuracy and particularly the ultrahigh resolution (R), which allows e.g. the unambiguous differentiation of molecules only consisting of carbon, hydrogen and oxygen (CHO) from sulfur containing organic molecules (CHOS) (Figure 1-7). FT-ICR-MS was applied by several studies focused on CHOS molecules in complex NOM mixtures, e.g. Herzsprung et al. studied the photodegradtion of CHOS in pore water (Herzsprung et al. 2010), Schmitt-Kopplin et al. showed the formation of CHOS from sulfuric acids in secondary organic aerosols (Schmitt-Kopplin et al. 2010) and Sleighter et al. suggested suflur

16

incorporation in wetland DOM (Sleighter et al. 2014). Therefore, FT-ICR-MS is a powerful technique for the anaylsis of CHOS molecules in complex DOM mixtures to link the carbon and sulfur cycle.
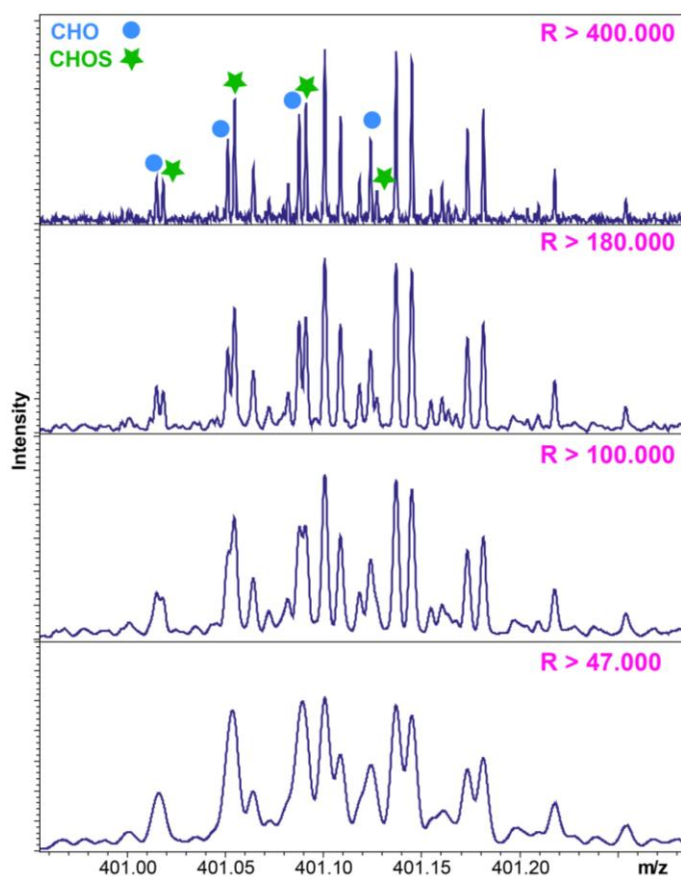
Figure 1-7: Assignment of molecular formulas enabled by ultrahigh resolution.
(–)ESI FT-ICR mass spectrum of a sulfur rich thermal spring SPE-DOM from Yellowstone National park at four different resolutions (R) highlights the influence of the resolution on the peak capacity of a mass spectrum and the mass accuracy that enables unambiguous differentiation and assignment of CHO and CHOS compounds.

Typically assigned molecular formulas from FT-ICR mass spectra of DOM are visualized by means of van Krevelen diagrams in which the hydrogen to carbon ratio (H/C) is plotted against the oxygen to carbon ratio (O/C), from which mass peaks are assigned to distinct compound groups (e.g. lignins, carbohydrates, lipids, tannins, condensed hydrocarbons) (van Krevelen 1950, Sleighter and Hatcher 2007, Schmitt-Kopplin et al. 2010). However, it is important to note that a molecular formula derived from FT-ICR-MS can represent an enormous variety of isomers (Hertkorn et al. 2007). Therefore, categorization of molecular formulas is ambiguous and FT-ICR-MS does not supply any direct structural information.

1.4.2. Nuclear magnetic resonance spectroscopy

The most extensively used technique for structural characterization of organic molecules is undoubtedly NMR spectroscopy (Mopper et al. 2007). Although NMR spectra of complex mixtures such as DOM show less structural details than NMR spectra of single molecules, due to broader peaks as a result of overlapping resonances if multiple DOM components are present, solid and solution state NMR spectroscopy is wildly used for the characterization of DOM (Mopper et al. 2007, Simpson, McNally and Simpson 2011, Simpson et al. 2012). Solution state NMR is the method of choice for the analysis of DOM, since DOM is by definition the soluble fraction of organic matter. In addition, solution state NMR provides highest resolution data (Simpson et al. 2012). NMR spectra of DOM provides substantial knowledge of DOM compound classes as well as individual compounds (Hertkorn et al. 2006, Lam et al. 2007, Perdue, Hertkorn and Kettrup 2007, Mitchell, Simpson and Simpson 2014).

NMR spectroscopy utilizes the differences in the nuclei's magnetic properties, which depend on the chemical environment in vicinity of the nuclei. In the strong magnetic field of NMR instruments nuclies orient themselves in the lowest possible energy configuration. A short radio frequency (RF) pulse excites the nuclei to a higher energy state. During the relaxation back to the lower energy state, electromagnetic radiation is emitted, detected and transformed into a chemical shift (δ) spectrum.

NMR is quantitative, non-destructive, and applicable to all major elements of organic matter (H, C, N, O, S, P) (Hertkorn 2014). Mainly ^{1}H and ^{13}C NMR spectroscopy are applied, due to the high sensitivity compared to other elements and high abundance of hydrogen and carbon in organic matter. Figure 1-8 depicts the general structural information obtained by ^{1}H NMR spectroscopy of DOM. Besides one-dimensional NMR experiments a variety of homo- and hetero-correlated multidimensional NMR experiments enable even in depth structural characterization of DOM (Hertkorn et al. 2006, Lam et al. 2007).

NMR spectroscopy utilizes in combination with FT-ICR-MS provides complementary information of complex DOM and in depth assessment of structural details according to ecosystem characteristics (Kim et al. 2003b, Hertkorn et al. 2006, Hertkorn et al. 2007, Hertkorn et al. 2013).
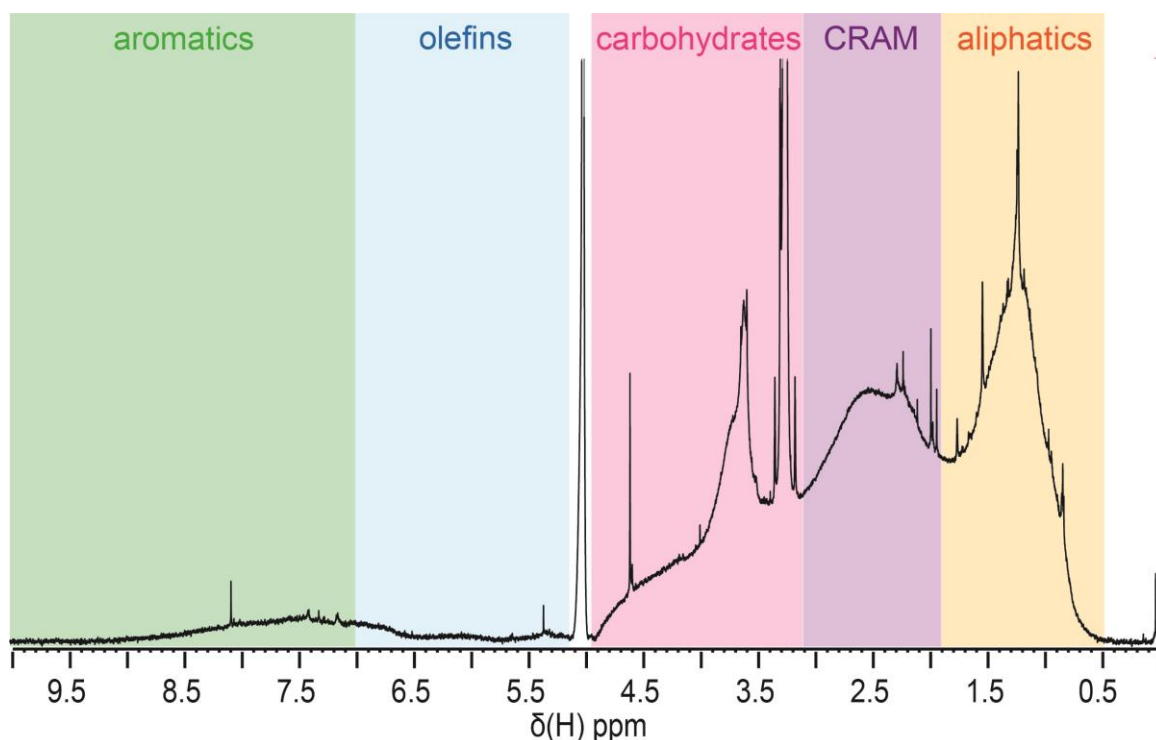
Figure 1-8: ¹H NMR spectrum of SPE-DOM.
¹H NMR spectrum of Suwannee River SPE-DOM with the main structural regions (aromatic, olefins, carbohydrates, carboxyl-rich alicyclic molecules (CRAM) and aliphatics) highlighted.

1.4.3. Excitation emission matrix (EEM) fluorescence spectroscopy

Fluorescence spectroscopy of aquatic organic matter has gained wide popularity and has recently been described in detail and reviewed by Coble et al. (Coble et al. 2014). EEM fluorescence spectroscopy especially in conjunction with parallel factor (PARAFAC) analysis is a powerful tool to study fluorescent dissolved organic matter (FDOM) (Stedmon, Markager and Bro 2003, Murphy et al. 2013). Although only the fluorescent fraction of DOM is accessible by this method (Coble et al. 2014), EEM fluorescence spectroscopy is widely applied for the characterization of DOM and improved significantly the understanding of DOM dynamics and transport (Yamashita et al. 2008, Mostofa et al. 2009, Jaffé, Cawley and Yamashita 2014), photo-reactivity and degradation of DOM (Mostofa et al. 2007, Timko et al. 2014, Timko, Gonsior and Cooper 2015a), phytoplankton (Zhang et al. 2009) and microbial degradation of DOM (Lønborg et al. 2010, Fasching et al. 2014). Since PARAFAC analysis for the extraction of characteristic FDOM components from an EEM fluorescence spectra sample set was introduced by Stedmon et al., it became the most frequently utilized method for the characterization of organic matter EEM fluorescence spectra (Stedmon et al. 2003, Murphy et al. 2013, Coble et al. 2014). PARAFAC components can be compared and assigned to identified

regions of observed fluorescence peaks in EEM fluorescence spectra of DOM (cf. Table 1-1) (Coble 1996, Parlanti et al. 2000).

Table 1-1: DOM fluorescence peaks.
Identified regions of observed fluorescence peaks in EEM fluorescence spectra of DOM (Coble 1996, Parlanti et al. 2000).

Component	Ex [nm]	Em[nm]	Coble 1996	Parlanti et al. 2000
Humic-like	330–350	420–480	C	α
Humic-like	250–260	380–480	A	α'
Marine humic-like	310–320	380–420	M	β
Tyrosine-like, protein-like	270–280	300–320	B	γ
Tryptophane-like, protein-like or phenol-like	270–280	320–350	T	δ

Besides PARAFAC modeling, also indices such as the fluorescence index (FI) as a proxy for the DOM source (i.e. microbial versus terrigenous derived DOM) (McKnight et al. 2001, Cory 2010), the humification index (HIX) indicating the degree of humification (Zsolnay 1999), and the freshness index (BIX) indicating the proportion of recently produced DOM (Parlanti et al. 2000, Huguet et al. 2009) are used for the characterization of DOM (Coble et al. 2014).

Only recently the combined characterization of DOM by EEM fluorescence spectroscopy and FT-ICR-MS has benefited the understanding of processes such as photo-degradation of DOM (Gonsior et al. 2009, Gonsior, Schmitt-Kopplin and Bastviken 2013, Timko et al. 2015b), change of DOM during drinking water production (Lavonen et al. 2015) and Stubbins et al. showed that FDOM gives insights into a more extensive proportion of the DOM pool (Stubbins et al. 2014).

2. Effects of the inorganic sulfur chemistry on the DOM of a meromictic lake
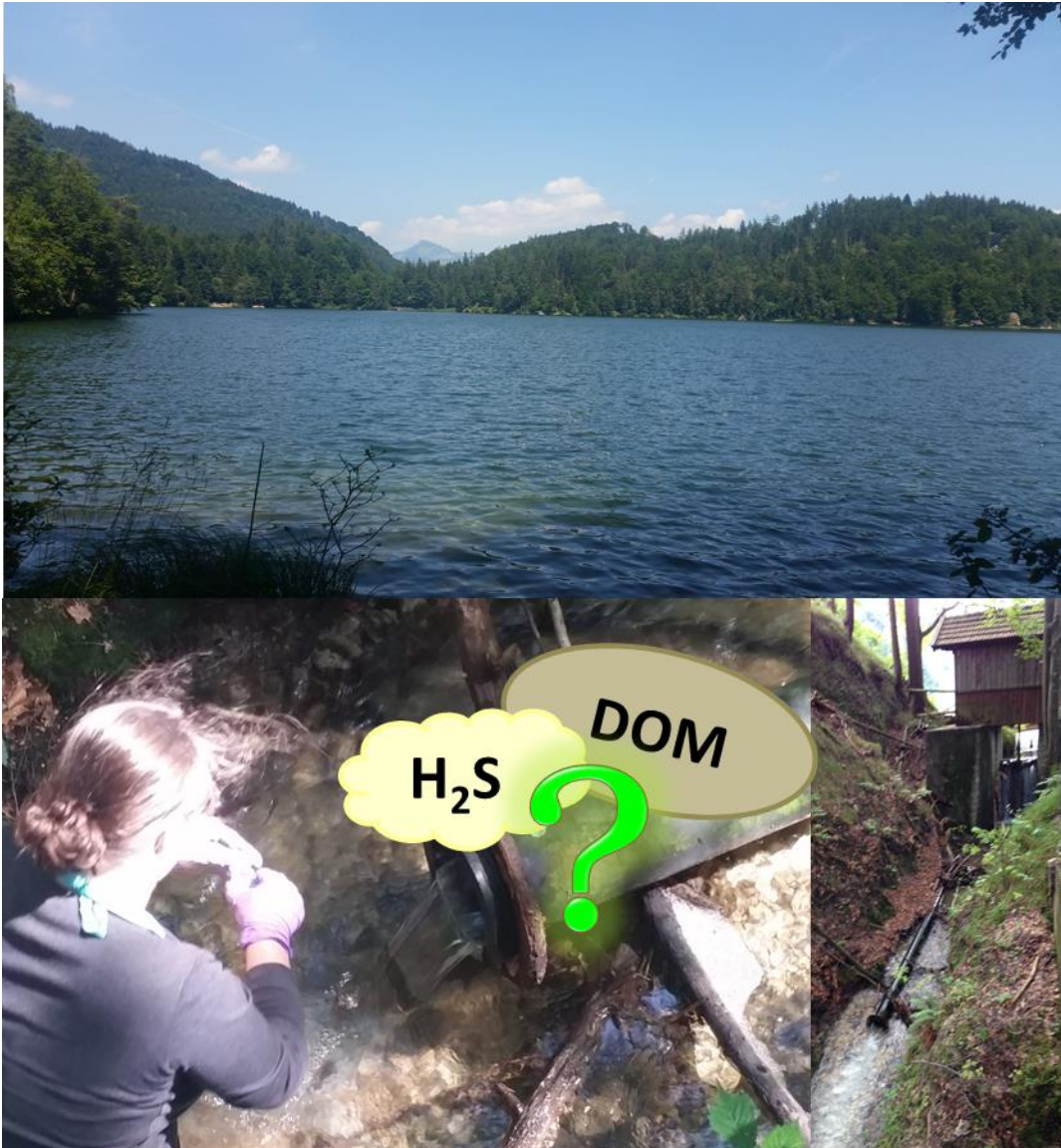
2.1. Introduction to meromictic lakes

In contrast to holomictic lakes, meromictic lakes do not show intermixing of their water layers (Wetzel 2001). Meromictic lakes are subdivided into three layers (Figure 2-1) (Walker 1974). The so called mixolimnion is the top layer, consisting of the epi-, meta- and hypolimnion. The mixolimnion has mixing conditions similar to holomictic lakes (Walker 1974). Generally, the oxygen concentration decreases from the very top layer, the epilimnion, towards the deeper water layers. The mixolimnion and the bottom water layer, the so called monimolimnion, are separated by the chemocline (Walker 1974). The water body of the hypo- and monimolimnion is anoxic and rich in nutrients (Nürnberg 1987). As a result of the anaerobic conditions, the hypo- and monimolimnion is often enriched with hydrogen sulfide, the product of bacterial sulfate reduction (cf. 1.3.1) (Nürnberg 1987, Cook 1992).
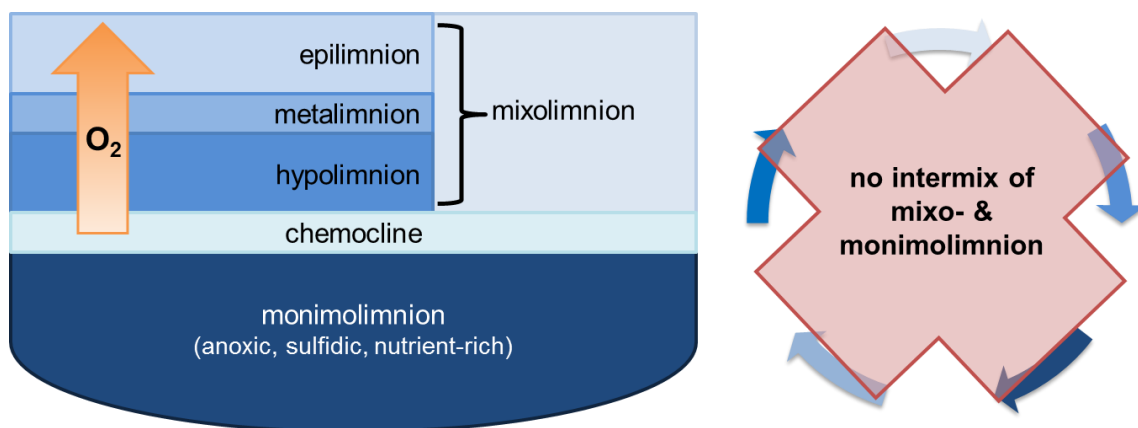
Figure 2-1: Scheme of a meromictic lake and its water layers.

Hypolimnetic (oxygen depleted) water withdrawal is an often applied lake restoration technique. Benefits are the decrease of anoxia to improve fish habitats, as well as the decrease of epilimnetic nutrient concentration, which leads to the limitation of phytoplankton and algae growth, thus combating the negative effect of eutrophication (Nürnberg 1987). Commonly hypolimnetic water withdrawal is performed by the installation of an Olszewski pipe, first proposed by the Polish limnologist Olszewski in 1961, and has been reviewed in detail by Nürnberg (Olszewski 1961, Klapper 1980, Nürnberg 1987, Nürnberg 2007).

In 1973 an Olszewski pipe was installed at the meromictic lake Hechtsee in Austria to withdraw anoxic, hydrogen sulfide and nutrient rich deep water (Pechlaner 1978, Aigner

2015). In order to protect the recreational environment from the odors of the hydrogen sulfide rich water, the pipe was installed in 25 m depth instead of the lakes maximum depth of 56.5 m (Pechlaner 1978). The restoration resulted in a decrease of the nutrient concentration in Hechtsee. But in contrast to most other studied lakes, the anaerobic conditions of Hechtsee remained unchanged (Nürnberg 1987, Nürnberg 2007, Aigner 2015).

2.2. Objectives

Sleighter et al. proposed the abiotic sulfur and nitrogen incorporation in pore water DOM from Prairie wetland and suggested abiotic incorporation of heteroatoms into DOM (Sleighter et al. 2014), whereby sulfide incorporation into specific organic molecules and organic matter had been shown experimentally before (De Graaf, Damsté and de Leeuw 1992, Schouten et al. 1993, Schouten et al. 1994, Perlinger et al. 2002, Heitmann and Blodau 2006, Amrani et al. 2007). Furthermore, a mediating role of DOM in wetland photochemical and redox reactions was suggested, which indicates a crucial role of DOM in the biogeochemical cycling of major elements not only in wetlands (Sleighter et al. 2014). This chapter addresses the research question whether sulfur incorporation into DOM occurs also in hypolimnic water of meromictic lakes. So far, the focus of meromictic lake investigations was on the interplay of biotic and abiotic sulfur cycling (Overmann et al. 1996, Zerkle et al. 2010). Oduro et al. suggested a combination of biotic and abiotic process as well as lignins to be involved in the formation of volatile organic sulfur compounds (Oduro et al. 2013).

Hechtsee was chosen as model site for a meromictic lake because its anoxic deep water is known to be enriched with hydrogen sulfide (Kiefersfelden 2009). As a result of presumably high sulfide concentrations in the anoxic water layers, an increased number of organosulfur compounds is expected to be present in the DOM sampled from the respective depth. This is investigated by means of FT-ICR-MS. Additionally; the degree of sulfurization of DOM is investigated by analyzing the sulfur concentration of the SPE-DOM extracts. In conjunction with the peak intensities and number as well as the molecular formula of CHOS, the dissolved organic sulfur (DOS) concentration gives rise to the sulfur functional groups found in the SPE-DOM. Comprehensive inorganic sulfur speciation was performed to allow conclusions whether only sulfide, expected as the most relevant based on the literature and chemical properties, is involved in the formation of

organosulfur compounds. Because dissolved organic matter chemistry is highly influenced by ecosystem settings, typical water characteristics, such as the pH value and DOC concentration were measured. In order to get further in depth knowledge about the DOM origin and chemical composition, spectroscopic parameters, such as humification index (HIX) and freshness index (BIX), were investigated from EEM fluorescence spectroscopic analyses and set into relation with FT-ICR-MS derived molecular formulas.

2.3. Materials and Methods

2.3.1. Sampling site

Hechtsee is located at the Austrian German border (47°36'33.25"N 12°09'47.38" E) in the Alps (Figure 2-2A) and belongs to the city of Kufstein, Austria (Figure 2-2B). The lake is a major recreational attraction in the region, especially for bathing during the summer time.
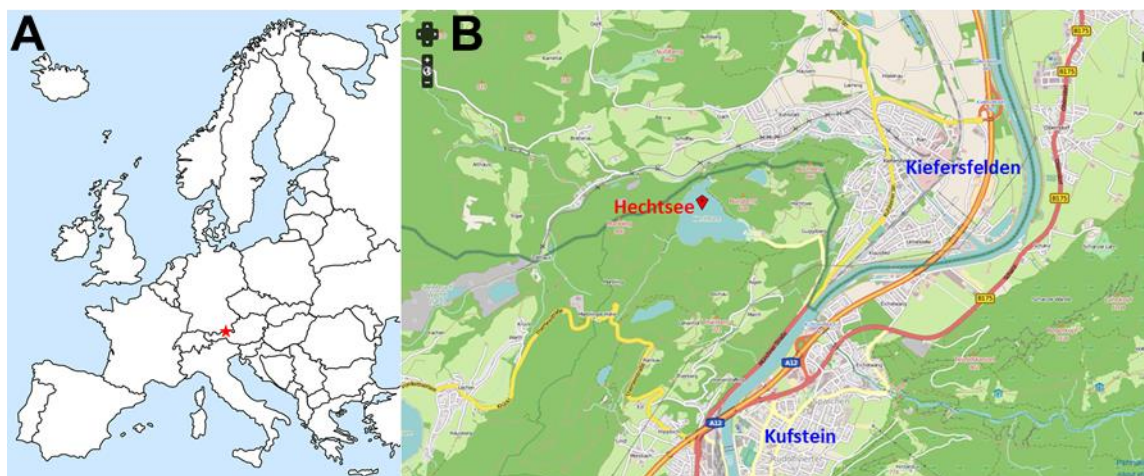
Figure 2-2: Location of the Hechtsee sampling site.
A) Map of Europe, the red star indicates the Hechtsee right at the Austrian German border. B) The red pin marks Hechtsee close to Kufstein (Austria) and Kiefersfelden (Germany). Source: http://www.openstreetmap.de (5.1.2016)

In order to protect the recreational environment from the odors, a plastic tube (diameter 18 cm) was installed in 1973 not at the lakes maximum depth of 56.5 m but in 25 m depth (Pechlaner 1978, Nürnberg 1987, Kiefersfelden 2009). The tube discharge from the 26.3 ha lake ranges between 1.2 and 1.8 m^3min^{-1} and caused already in the first years after construction a drastic decline of the total phosphorous and thus nutrient concentration in the lake (Nürnberg 1987, Cooke et al. 2005, Nürnberg 2007). Anoxia of the lakes deep

water remained (Nürnberg 1987, Nürnberg 2007). In the last years Hechtsee showed very low total phosphate concentrations (≤ 10 µg L^{-1}), phytoplankton biomass (≤ 0.8 g m^{-3}) and no multiplication of cyanobacteria (Aigner 2015). Hechtsee is classified as a mesotrophic lake (Aigner 2015).

The sampling was performed on July 10th 2015.

2.3.2. Sulfur speciation[1] and major water parameters

At each sampling site, pH and voltammetry measurements were undertaken on site immediately, and samples were preserved for transport and later analysis. pH measurements were accomplished on a Fisher Scientific™ (Thermo Fisher Scientific Inc., Waltham, MA, USA) accumet™ AB15 field pH meter using a double junction combination pH electrode from Sensorex (Garden Grove, CA, USA). A three electrode system consisting of a silver/silver chloride reference electrode, a platinum counter electrode, and an Au-amalgam working electrode was used in voltammetric analyses after Brendel and Luther (Brendel and Luther 1995).Voltammetric signals are produced when redox-active dissolved or nanoparticulate species interact with the surface of an Au-amalgam (Au-Hg alloy) working electrode. Electron flow, resulting from redox half-reactions occurring at specific potentials on the surface of a 100 µm diameter Au-amalgam working electrode, is registered as a current that is proportional to concentration (Taillefert and Rozan 2002). Cyclic voltammetry was performed between -0.1 and -1.8 V (vs. Ag/AgCl) at a scan rate of 1000 mVs^{-1} with a 2 s conditioning step. Aqueous and nanoparticulate sulfur species that are electroactive at the Au-amalgam electrode surface include H_2S, S_8, polysulfides (S_x^{2-}), $S_2O_3^{2-}$, HSO_3^{-}, and $S_4O_6^{2-}$ (Luther III et al. 2001, Druschel et al. 2003b). Detection limits with this technique vary for each species, matrix, and scan condition. In the conditions of this study the detection limit is for sulfide and polysulfide about 100 nmol L^{-1}, for thiosulfate and bisulfite about 10 µmol L^{-1}. Voltammetric analyses were carried out with an Analytical Instrument Systems, Inc. (Ringoes, NJ, USA) DLK-70 potentiostat and computer controller. Briefly, 25 mL aliquots of water were collected, unfiltered, from each sampling location and immediately analyzed by voltammetry. Analyses were carried out in sets of at least 10 sequential scans

---

[1] Sulfur speciation was predominantly performed by the collaboration partner Prof. Gregory K. Druschel from the Indiana University – Purdue University Indianapolis.

at each sampling point, with the first three scans discarded (allowing the electrode response to stabilize).

Sample aliquots from each sampling site were also preserved for high performance liquid chromatography (HPLC) analysis of polysulfides by Methyl trifluoromethanesulfonate (98%, Sigma Aldrich, Taufkirchen, Germany) derivatization (Kamyshny et al. 2004, Kamyshny et al. 2007, Kamyshny, Borkenstein and Ferdelman 2009), thiosulfate and sulfite by Bromobimane ($\geq$ 95% (HPCE), Sigma Aldrich, Taufkirchen, Germany) derivatization (Rethmeier et al. 1997, Zopfi, Ferdelman and Fossing 2004). Analyses were carried out on a UltiMate 3000 HPLC system (Thermo Fisher Scientific Inc., Waltham, MA, USA) utilizing a Thermo Scientific™ Acclaim™ 120 C_{18} column, UV-Vis and Fluorescence detectors after established protocols (Rethmeier et al. 1997, Zopfi et al. 2004, Kamyshny et al. 2004). Elemental sulfur was extracted with methanol from water samples (v/v 50:50) and concentrations were measured by HPLC-UV/VIS (Zopfi et al. 2004, Kamyshny et al. 2009).

The nitric acid (ROTIPURAN®, $\geq$65 %, p.a., Carl Roth GmbH & Co. KG, Karlsruhe, Germany) used for the stabilization of samples for ICP-OES analysis was purified by an IR-Subboiling-Apparatur BSB-939-IR (Berghof GmbH, Eningen, Germany). Sulfate, phosphate and nitrate concentrations were determined by a Dionex ICS-1500 ion chromatograph (Thermo Fisher Scientific Inc., Waltham, MA, USA) from 0.45 µm (Millex-HV, Merck KGaA, Darmstadt, Germany) filtered water samples. Total sulfur and iron concentrations were measured by a CIROS VISION ICP-OES Spectrometer (Spectro Analytical Instruments Inc., Mahwah, Germany) from onsite 0.45 µm Millex-HV (Merck KGaA, Darmstadt, Germany) filtered and nitric acid stabilized water samples. For the determination of sulfur concentrations in SPE-DOM, the methanol was evaporated from the extract and DOM was re-dissolved in purified water (MilliQ-Integral, Merck KGaA, Darmstadt, Germany) and stabilized by the addition of nitric acid. The measurements were performed by a CIROS VISION ICP-OES Spectrometer (Spectro Analytical Instruments Inc., Kleve, Germany).

Dissolved organic carbon (DOC) concentrations were measured from in the field 0.45 µm filtered (Millex-HV, Merck KGaA, Darmstadt, Germany) and acidified with hydrochloric acid (32%, p.a., Merck KGaA, Darmstadt, Germany) water samples on an Shimadzu (Duisburg, Germany) TOC-5000A TOC analyzer.

2.3.3. Isolation of SPE-DOM

Water samples were filtered through GF/F Glass microfiber filters (GE Healthcare Life Science Whatmann™, Chalfont St Giles, UK), which were baked out for 5 h at 450°C prior usage. Isolation of DOM was performed by an established SPE method described by Dittmar et al. (Dittmar et al. 2008). Briefly, 500 mg Bond Elut PPL SPE cartridges (Agilent Technologies Inc., Santa Clara, CA, USA) were rinsed with methanol (Chromasolv® LC-MS grade methanol, Sigma Aldrich, Taufkirchen, Germany) and purified acidified (pH 2) water (MilliQ-Integral, Merck KGaA, Darmstadt, Germany; hydrochloric acid 32%, p.a., Merck KGaA, Darmstadt, Germany). Then 1 L of each water sample was acidified to pH 2 and gravity fed through a Bond Elut PPL SPE cartridge. After that, the cartridges were rinsed with acidified purified water and dried under vacuum. The DOM was eluted with 5 mL methanol. The SPE-DOM samples were stored at -20°C. The recovery of the SPE isolation was determined by measuring the TOC concentrations of SPE-DOM after vaporization of the methanol.

2.3.4. Ultrahigh resolution mass spectrometry of SPE-DOM

FT-ICR mass spectra were acquired with a SolariX Qe FT-ICR-MS (Bruker Daltonik GmbH, Bremen, Germany) equipped with a 12 Tesla superconducting magnet. (–)ESI FT-ICR-MS analyses were performed with an Apollo II ESI source (Bruker Daltonik GmbH, Bremen, Germany). Prior to (–)ESI FT-ICR-MS analysis, the SPE-DOM samples were diluted 1:40 with methanol and continuously infused with a flowrate of 120 μL h^{-1}. Detailed information on the FT-ICR-MS parameters is displayed in the Appendix 7.1.1 Table 7-1.

The mass spectra were internally calibrated to known and high abundant masses of DOM with a mass accuracy of 0.1 ppm. Only singly charged molecular ions were found. Mass spectra were exported from m/z 150 to 750 and at a S/N > 4. Spectra were aligned with the in-house written software Matrix Generator. Noise was eliminated by a mass defect filter. The formula assignment of the mass spectra, based on a network approach, was performed with the in-house written software tool NetCalc (Tziotis et al. 2011). The mass accuracy window for the formula assignment was set to ±0.2 ppm. The assigned formulas were validated by setting sensible chemical constraints (N rule; O/C ratio ≤ 1; H/C ratio ≤ 2n+2 (C_nH_{2n+2}), double bond equivalents) in conjunction with isotope pattern comparison.

Final formulas were classified into molecular groups containing CHO (blue), CHNO (orange), CHOS (green), or CHNOS (red).

Principal component analysis (PCA) on the base peak normalized intensities of molecular formula assigned mass peaks was performed with SIMCA-P 9.0 (Umetrics, Umeå, Sweden). The most representative and characteristic molecular formulas for samples or groups of samples, respectively, were extracted by taken the individual vector position of the molecular formulas in the PCA score plot into account (Sleighter et al. 2010). The results were visualized by the use of van Krevelen diagrams in which the hydrogen to carbon ratio (H/C) was plotted against the oxygen to carbon ratio (O/C) (van Krevelen 1950).

2.3.5. EEM fluorescence spectroscopy of SPE-DOM

Excitation emission matrix fluorescence spectroscopy of SPE-DOM was measured using a Jobin Horiba Instruments (Kyoto, Japan) Aqualog spectrofluorometer. Prior analysis the methanol from 300 µL SPE-DOM was evaporated under a gentle stream of nitrogen. The sample was re-dissolved in Barnstead™ Nanopure™ water (Thermo Fisher Scientific, Waltham, USA) whereby the concentration was adjusted to a maximum UV absorbance at 300 nm of 0.2. Excitation scans were conducted from 600 nm to 231 nm in 3 nm steps, and the emission wavelength ranged from 211.0 nm to 617.1 nm in ~3 nm increments. The integration time was set to 1 s. Inner filter effects and Rayleigh scattering were corrected by the Aqualog software. The spectra were normalized to a Starna$^{®}$ Scientific Ltd. (Hainault, UK) Quinine Sulfate Standard of 1 ppm. Fluorescence units were then given in quinine sulfate units (QSU).

Spectroscopic indices such as the fluorescence index (FI) (McKnight et al. 2001), which was calculated including the instrument correction (Cory and McKnight 2005, Cory 2010) from the EEM fluorescence spectra. Furthermore, the humification index (HIX) (Zsolnay 1999) and the index of recent autochthonous contribution/freshness index (BIX) (Huguet et al. 2009) were calculated. Additionally, the $SUVA_{254}$ as a proxy for aromaticity (Weishaar et al. 2003), spectral slope (S_R) (Helms et al. 2008) and a_{254}/a_{365} (Berggren, Laudon and Jansson 2009), which are both associated with the DOM molecular weight, were calculated from the UV-absorption spectra. The UV-absorption spectra were simultaneously recorded with the EEM fluorescence spectra. Spearman rank correlation between molecular formulas derived from FT-ICR-MS and the fluorescence

indices HIX and BIX was performed according to Herzsprung et al. (Herzsprung et al. 2012).

2.4. Results and Discussion

2.4.1. Water characteristics and inorganic sulfur species

To obtain comprehensive knowledge on the inorganic sulfur chemistry and its effect on dissolved organic matter of a meromictic lake, sampling was carried out at 8 sampling spots (Figure 2-3A). The inlet (IN) sample is taken closely before the Hechtbach, the main water source of Hechtsee, enters the lake. Representatives for the oxic epilimnion water are the lake top (LT), lake 2 m below the surface (bls) (L2m) as well as the overflow (OF) sample. The sample taken at the pipe (PIPE) is hypolimnic and sulfide enriched water from the hypolimnion or even monimolimnion, which is getting mixed with water from the overflow right below the pipe outlet (mixing water (MIX)). The outlet stream flows into the Kieferbach by passing a waterfall (waterfall top (WFT), waterfall bottom (WFB)). The water characteristics including the inorganic sulfur speciation are summarized in Table 2–1.
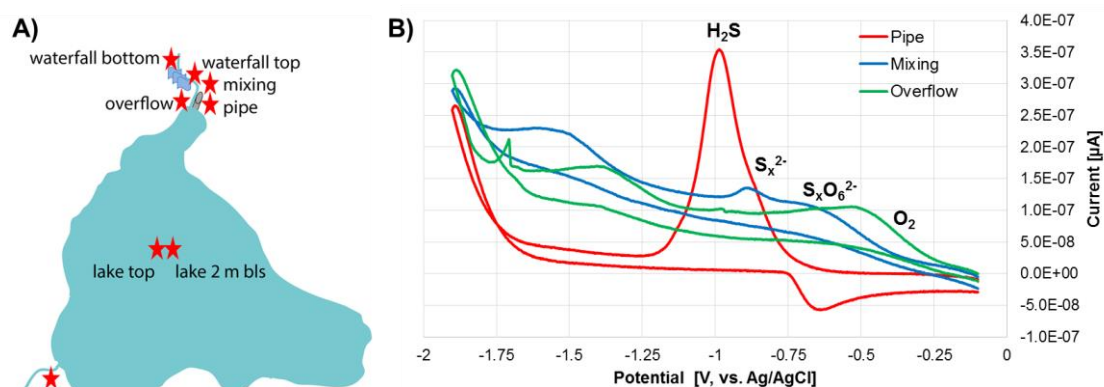
Figure 2-3: Hechtsee sampling spots and cyclic voltammograms.
A) Sampling positions B) Cyclic voltammograms proof high abundance of sulfide in the anoxic pipe water (red), compared to the oxic overflow water (green). The mixing water is oxic with little amounts of sulfide.

2.4.1.1. Inorganic sulfur speciation

Sulfur speciation by cyclic voltammetry (Figure 2-3B) revealed the abundance of sulfide (~ −1.0 V) in the anoxic pipe water (red graph). Additionally, little amounts of polysulfide (~ −0.9 V) and elemental sulfur (~ −0.8 V) were present in the hypolimnic pipe water. The overflow water (green graph) represents a typical cyclic voltammogram of the oxic

lake water samples and showed no traits of reduced sulfur species. The mixing water (blue graph) was almost fully oxic. In comparison with the pipe water (920 µmol L^{-1}), the water from the mixing zone (56 µmol L^{-1}) had only little concentrations of sulfide (Table 2–1). The large decrease in sulfide concentration from the pipe to the mixing water results from multiple factors. First, the water is a combination of the highly sulfidic pipe water and the sulfide free overflow water. Second, hydrogen sulfide is getting oxidized under aerobic conditions. Third, volatile hydrogen sulfide (H$_2$S) gas is getting released by the water phase. As a consequence of hydrogen sulfide outgassing heavy odors were present in the surrounding area.

Although the cyclic voltammogram of the pipe water showed little amounts of polysulfide, the concentration was below the limit of quantification ($<$ 10 µmol L^{-1}). Likewise, additional analysis following the protocol of Kamyshny (Kamyshny et al. 2004) did not show a quantifiable polysulfide concentration for any chain length of polysulfide (where limits of detection (LOD) are between 3 and 10 µmol L^{-1}). Unexpectedly the HPLC analyses did not show any extractable elemental sulfur, with a limit of detection of approximately 0.1 µmol L^{-1}. Thus, it was not possible to specify the small amount of elemental sulfur in the cyclic voltammogram (Figure 2-3B) of the pipe water. Also the bimane derivatized samples did not display quantifiable levels of sulfite or thiosulfate (with LODs for our method at about 1 µmol L^{-1}). However, the cyclic voltammogram of the mixing water indicated the presence of polythionates. Sulfate as the most stable oxidized sulfur species was present in rather similar concentrations (mean concentration of 46 µmol L^{-1}) throughout all sampling spots. The total sulfur concentrations indicate (considering the analytical accuracy) that almost all sulfur is present in the form of the two redox species endmembers sulfate and sulfide. The discrepancy between the total sulfur concentrations and the sulfide concentrations in the pipe and mixing water sample can be explained by tremendous outgassing of highly volatile H$_2$S during acidification of the samples for the analysis by ICP-OES.

Table 2-1: Sulfur speciation and major water parameters.
Inorganic sulfur species (sulfate, total sulfur and sulfide), dissolved organic carbon (DOC), nitrate, iron and manganese concentrations as well as pH values of the water samples. (n.d. = not determined, LOD = limit of detection)

Sample	DOC [mg L^{-1}]	pH [-]	NO$_3^-$ [μmol L^{-1}]	Fe [μmol L^{-1}]	Mn [μmol L^{-1}]	SO$_4^{2-}$ [μmol L^{-1}]	HS$^-$ [μmol L^{-1}]	S$_{total}$ [μmol L^{-1}]
Inlet (IN)	2.73	7.20	57.74	0.03	< LOD	49.97	< LOD	45.85
Lake top (LT)	3.69	n.d.	20.65	0.04	< LOD	42.68	< LOD	42.11
Lake 2 m bls (L2m)	4.29	7.60	27.26	0.04	0.04	43.51	< LOD	43.36
Overflow (OF)	3.88	7.29	19.36	0.03	< LOD	42.37	< LOD	43.36
Pipe (PIPE)	2.79	7.95	1.53	2.81	2.04	50.49	920	304.43
Mixing (MIX)	4.45	7.24	11.65	0.89	0.69	47.78	56	58.95
Waterfall top (WFT)	3.66	7.48	17.90	0.20	0.14	44.56	< LOD	43.36
Waterfall bottom (WFB)	4.63	n.d.	22.26	0.13	0.09	45.91	< LOD	43.98

2.4.1.2. Water characteristics

The dissolved organic carbon (DOC) concentration reached levels from ~ 2.8 mg L^{-1} for the pipe and inlet sample to 4.63 mg L^{-1} for the sample taken at the bottom of the waterfall from the outlet of the lake. These DOC concentrations are in agreement with the lakes mesotrophic classification (Aigner 2015, Thurman 1985) and usual riverine DOC levels (Thurman 1985). The pH values (Table 2−1) with a mean value of 7.5 were in the typical range for streams and lakes (Kemker 2013). The hypolimnic pipe water had with 7.95 compared to the other samples an elevated pH value. This increased pH value most likely results from the high concentration of dissolved hydrogen sulfide in the pipe water. Additionally, the pipe water showed an increased abundance of redox cycle relevant metals, such as iron and manganese (Table 2−1), hinting towards active redox cycling in

the anaerobic water layers. Nitrate was depleted in the anaerobic pipe water (Table 2−1), suggesting that besides bacterial sulfate reduction also denitrification was active. Generally, the nitrate concentration was much higher in the inlet water compared to all samples taken from the lake and outlet. In agreement with previous studies (Aigner 2015), the total phosphorous (< 0.31 µmol L^{-1}) and phosphate (< 0.51 µmol L^{-1}) concentration was below the LOD, confirming that no eutrophication of the lake takes place.

2.4.2. Spectroscopic analysis of the DOM

Spectroscopic parameters give rise to the chemical characteristics and origin of DOM in natural waters. Thus, they are important indicators for the active processes in aquatic ecosystems. In this study, the spectroscopic parameters support inorganic chemical findings, which have been discussed in the previous paragraph (2.4.1). Additionally, spectroscopic indices, such as the $SUVA_{254}$, are associated with molecular attributes. They provide complementary information to FT-ICR mass spectrometric analysis of DOM, which is addressed in detail in the following paragraph (2.4.3). Furthermore, correlation analysis of fluorescence indices with FT-ICR-MS derived molecular formulas assists in obtaining a deeper knowledge on the DOM chemical composition and its formation processes.

Table 2-2: Fluorescence and UV-Absorption Indices for the Hechtsee sampling spots.

Sample	Fluorescence Indices			UV-Absorption Indices		
	HIX	BIX	FI_{cor}	$SUVA_{254}$	S_R	a_{254}/a_{365}
Inlet (IN)	7.95	0.60	1.44	0.22	0.81	5.89
Lake top (LT)	2.64	0.77	1.27	0.16	0.79	6.25
Lake 2 m bls (L2m)	2.79	0.87	1.50	0.12	0.93	8.29
Overflow (OF)	2.75	0.86	1.54	0.15	0.94	8.37
Pipe (PIPE)	6.69	0.64	1.44	0.20	0.86	6.33
Mixing (MIX)*	2.65	0.69	1.20	0.16	0.63	4.68
Waterfall top (WFT)	2.99	0.76	1.37	0.16	0.86	6.52
Waterfall bottom (WFB)	3.11	0.80	1.49	0.12	0.89	7.85

* EEM fluorescence spectra and spectroscopic indices of the mixing water sample were quite different from those of the other samples.

Table 2–2 summarizes the spectroscopic indices for the 8 sampling spots at Hechtsee. Due to the interference of complex hydrological and geological effects, which are not subject of this study, the EEM fluorescence spectra and spectroscopic indices of the mixing water sample were quite different from those of the other samples. Therefore, the spectroscopic indices of the mixing water sample will not be discussed in detail and are not part of the following discussion of the results.

2.4.2.1. UV-Absorption spectroscopic characteristics

The specific UV-absorption SUVA$_{254}$ value suggests an increased degree of aromaticity for the inlet and pipe water DOM compared to the DOM from the other lake and outlet samples. The inlet is surrounded by forest, thus plant derived aromatic compounds such as lignins are a major source of the DOM. The pipe water is representative for the lakes deeper water layers, hence represents further degraded organic matter, which is commonly enriched with recalcitrant aromatic compounds. The slope ratio (S_R) and the absorption coefficient a$_{254}$/a$_{365}$ are both inversely related to the molecular weight of DOM. The two indices are focused on the absorption at different wavelengths (Helms et al. 2008, Berggren et al. 2009). Both indices revealed that lower molecular weight DOM was present in the lake water samples 2 m bls, overflow and waterfall samples. This implies that at these sampling spots DOM degradation takes place. The degradation process is more likely to be microbial due to the limited exposure to light of the water body below the surface and the waterfall being located in the forest. This is further corroborated by the fact that the inlet and lake top sample, which have the highest input of fresh organic matter derived from the lakes surrounding, had the lowest S_R and a$_{254}$/a$_{365}$ values.

2.4.2.2. EEM fluorescence spectroscopic characteristics

The fluorescence index (FI) is an indicator to distinguish the source of DOM (McKnight et al. 2001, Jaffé et al. 2004). Typically FI values range from 1.3 − 1.9, whereby a FI index of ~ 1.4 is associated with terrestrial derived DOM and a FI value of ~ 1.9 with microbially derived DOM (McKnight et al. 2001). The FI of all samples ranged from (FI$_{cor}$ = 1.20 − 1.54), hence indicated a mainly terrestrial source of the DOM. This is in agreement with the lakes mesotrophic status, which is suggested by the found low phosphate values in the current and regular samplings (cf. 2.4.1) as well as by the non-eutrophication status of the lake (Aigner 2015). These findings are further corroborated

by the found BIX values (Table 2–2). The BIX value is an indicator for the biological activity (Huguet et al. 2009). Table 2–3 summarizes the range of the BIX index and the related level of biological activity. The BIX values of the inlet and pipe were indicative for low biological activity, whereas the BIX values of the lake and outflow samples were indicative for average to high biological activity corresponding to the mesotrophic state of Hechtsee. This is in agreement with the above discussed lower molecular weight of DOM of those samples, suggested by the S_R and a_{254}/a_{365}.

The state of humification of DOM is associated with the HIX value (Table 2–3) (Parlanti et al. 2000, Huguet et al. 2009). This index is complementary to the BIX index (Wagner et al. 2015a). The DOM from the inlet and pipe water showed an important humic and recent autochthonous component. The inlet water stream is forested, thus the DOM is expected to be partially derived from humified organic molecules from the soils. The pipe is installed in 25 m depth, hence, parts of the DOM found in the pipe water is originated from further degraded and in consequence more humified material. The HIX values of all other lake and outlet samples were indicative for (aquatic) biological derived DOM, in agreement with the pervious discussed BIX values.

Table 2-3: DOM characteristics associated with HIX and BIX values.
DOM characteristics associated with the range of values for HIX and BIX from estuarine and seawater samples (Huguet et al. 2009).

Index	Value ranges	Characteristics of the DOM
BIX	0.6 – 0.7	Low biological activity
	0.7 – 0.8	Average biological activity
	0.8 – 1	High biological activity
	> 1	Biological or aquatic bacterial origin
HIX	16 – 10	Strongly humic character or an important terrestrial contribution
	10 – 6	Important humic component and recent autochthonous component
	6 – 4	Low humic character and important recent autochthonous component
	< 4	Biological or aquatic bacterial origin

2.4.2.3. Association of the spectroscopic indices with FT-ICR-MS derived molecular formulas

The above discussed optical indices are often applied proxies for the general DOM composition (Fasching et al. 2014, Wagner et al. 2015a, Lavonen et al. 2015, Hertkorn et al. 2016). However, they do not give rise of the molecular signatures that are associated with the optical indices. Only recently, correlation analysis of spectroscopic measures and

FT-ICR mass spectra derived molecular formulas has been employed to overcome this knowledge gap (Herzsprung et al. 2012, Stubbins et al. 2014, Wagner et al. 2015a). Hence, Spearman's correlation of the spectroscopic indices ($SUVA_{254}$, a_{254}/a_{365}, BIX and HIX), that showed the major discrimination between the samples, with the FT-ICR-MS derived molecular formulas was performed. Figure 2-4 displays the molecular formulas which positively correlate ($r > 0.48$; $p < 0.1$) with the four optical indices.

The correlation of the $SUVA_{254}$ with molecular formulas was chosen as a proof-of-principle, since the aromaticity proxy $SUVA_{254}$ is expected to correlate with aromatic compounds with an $H/C < 1.5$. The actual analysis confirmed this assumption, since the $SUVA_{254}$ index mainly correlates with aromatic CHO and CHNO compounds in the lignin and tannin region of the van Krevelen diagram (Figure 2-4). Similar results were found by Wagner et al. 2015. In this study also ~ 50% of the molecules associated with the $SUVA_{254}$ were CHO compounds with a similar molecular weight distribution and van Krevelen space coverage (Wagner et al. 2015a). Thus, correlation of optical indices and FT-ICR mass spectra derived molecular formulas is a powerful tool for the in-depth characterization of DOM. This is further corroborated by correlation analysis with the absorption coefficient ratio a_{254}/a_{365}. As discussed above, this index is inversely related to the molecular weight and correlation analysis revealed that a_{254}/a_{365} is mainly associated with molecular formulas having a m/z-ratio < 400 (Figure 2-4). Additionally, primarily sulfur and nitrogen containing compounds correlate with the a_{254}/a_{365}, implying that lower molecular weight DOM is formed during biotic metabolic processes. This hypothesis is confirmed by the fact that similar molecules are correlating with the BIX index, the optical measure for biological activity (Figure 2-4). Indeed, 48.5% of the molecular formulas which correlate with the BIX also correlate with the a_{254}/a_{365}. Such strong association of the BIX (also referred to as freshness index) with low molecular weight CHNO and CHOS compounds was also found by Wagner et al. 2015. These types of molecules are likely to be highly bioavailable and assumingly metabolites from bacterial activity. The HIX index on the contrary correlated with mostly CHO molecules in the core of the lignin region of the van Krevelen diagram (Figure 2-4). The HIX index associated molecules do not show a trend in their molecular weight. Their molecular characteristics are converse to those associated with the BIX index. This suggests that these molecules are recalcitrant endmembers of the humification of organic matter.
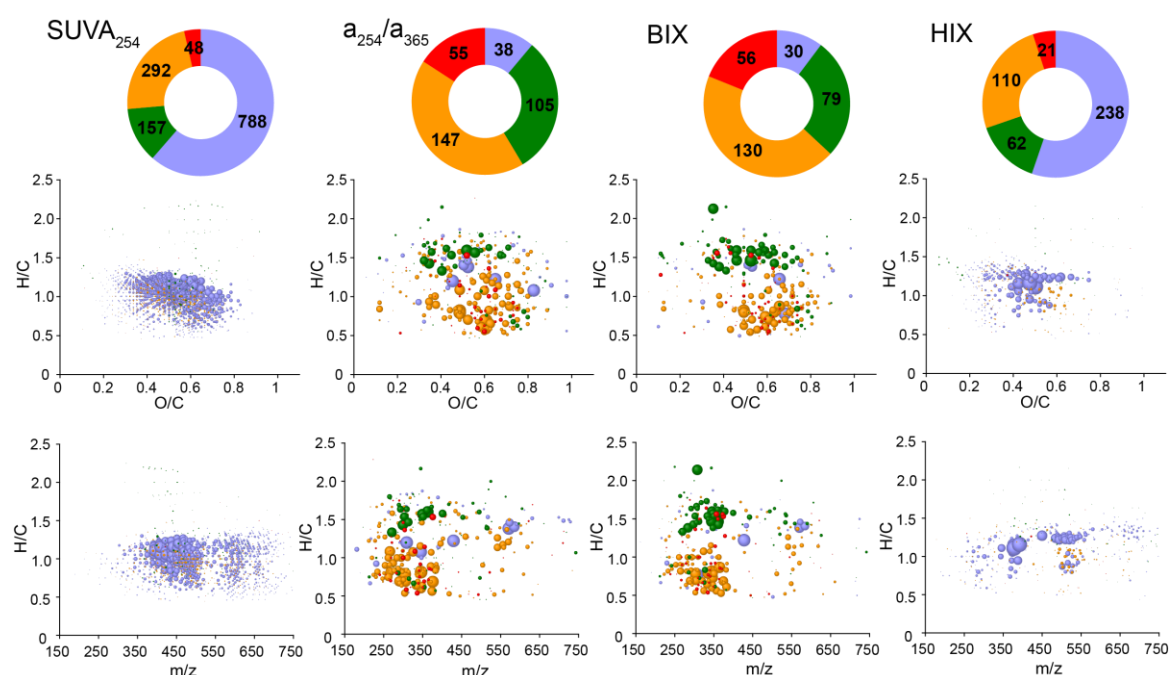
Figure 2-4: Molecular formulas positively correlating with optical indices.
FT-ICR mass spectrometry derived molecular formulas positively correlating (Spearman's correlation ($r > 0.48$; $p < 0.1$)) with the optical indices $SUVA_{254}$, a_{254}/a_{365}, BIX and HIX. The ring charts in the top row depict the count of molecular formulas, whereby the elemental composition is represented as CHO (blue), CHNO (orange), CHOS (green), and CHNOS (red). The middle row displays the van Krevelen diagrams and the bottom row the m/z-resolved H/C atomic ratio. The bubble area depicts the mean mass peak intensity within all samples.

2.4.3. Ultrahigh resolution mass spectrometric characterization of DOM

2.4.3.1. Mass spectrometric characterization of the CHNOS chemical space

Ultrahigh resolution mass spectrometry with its ability to resolve molecular formulas is a powerful tool for the characterization of the elemental composition of DOM. Hence, FT-ICR-MS enables the in depth characterization of especially heteroatom containing compounds, which makes it a suitable technique to study the formation of sulfur organic compounds in meromictic lakes. (–)ESI FT-ICR-MS of the SPE-DOM was performed because all naturally expected sulfur organic functional groups, from the most oxidized sulfonates and sulfones to the most reduced form i.e. thiols, are ionizable by deprotonation. Table 6-1 in the Supplementary Information includes the detailed information on the mass spectrometry derived annotated molecular formulas for the 8 sampling spots. The proportions of the elemental composition classes, i.e. CHO, CHNO, CHOS and CHNOS, at the respective sampling spot are displayed by the ring charts in Figure 2-5. In general, the analysis of the SPE-DOM revealed similar distributions and assigned molecular formulas for all of the Hechtsee sampling spots. Furthermore, the van

Krevelen diagrams of all sampling spots do not show any distinct patterns for any of the sampling spots (Figure 6-1). Only the total number of assigned molecular formulas is lower and especially CHOS and CHNOS annotations are less for the inlet (IN) then for the other sampling spots (Figure 2-5). Interestingly, the average molecular mass is with 444.30 Da higher than for the other samples, which has a mean average molecular mass of 417.79 Da.

However, the number of CHOS compounds was with 1100 for the sulfidic pipe (PIPE) and with 1010 for the mixing (MIX) samples significantly higher than for the other lake and outlet samples, in which on average 757 CHOS molecular compositions were assigned. Thus, the general hypothesis that DOM from hypolimnic and hydrogen sulfide containing water is enriched in sulfur organic compounds was confirmed. However, only the number of CHOS compounds was elevated for the SPE-DOM from sulfidic waters. The CHNOS annotations did not differ substantially for the lake and outlet samples (Figure 2-5, Figure 6-1 and Table 6-1). Hence, sulfide presumably reacts with CHO compounds in anoxic aquatic systems. Incorporation of sulfur into organic molecules in ecosystems with elevated sulfide concentrations is a common biogeochemical process (Casagrande et al. 1979, Casagrande, Gronli and Sutton 1980, Henneke et al. 1997, Heitmann et al. 2007). Additionally, several laboratory experiments with DOM and model organic compounds confirmed the incorporation of sulfur by the reaction of sulfide with organic functionalities, such as single and activated double bonds (Michael systems, Quinones) (Vairavamurthy and Mopper 1987, Perlinger et al. 2002, Heitmann and Blodau 2006, Yu et al. 2015b).
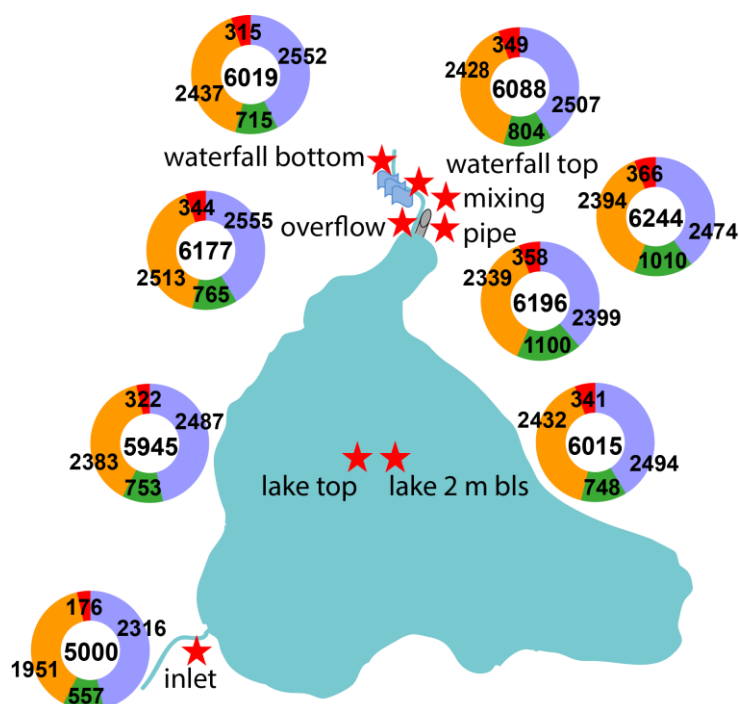
Figure 2-5: FT-ICR-MS assigned elemental composition groups of DOM.
Sketch of the sampling positions, indicted by red stars, at Hechtsee. The ring charts display the count of assigned elemental compositions classified into molecular groups containing CHO (blue), CHNO (orange), CHOS (green), or CHNOS (red).

Since visual comparison of the van Krevelen diagrams of the 8 sampling spots did not show any clear differences, PCA based on all assigned molecular formulas was performed (Figure 2-6A). Likewise to the above discussed specifics, the inlet (IN) sample was separated in the PCA analysis from all other sampling locations (Figure 2-6A). The two waterfall samples from the top (WFT) and bottom (WFB) showed highest similarity with the top surface water sample (LT). Although the pipe (PIPE) and mixing (MIX) sample were enriched with CHOS compounds, PCA based on all assigned molecular formulas was not able to clearly separate the two samples from the overflow (OF) and lake water sampled from 2 meters depth (L2m). Most probably this was caused by the low abundance, based on the intensity weighted compositions of assigned molecular formulas (Table 6-1), of CHOS (mean = 3.2%, includes the pipe water SPE-DOM sample) compared to CHNO (mean = 13.6%) and especially CHO (mean = 82.6%) compounds.
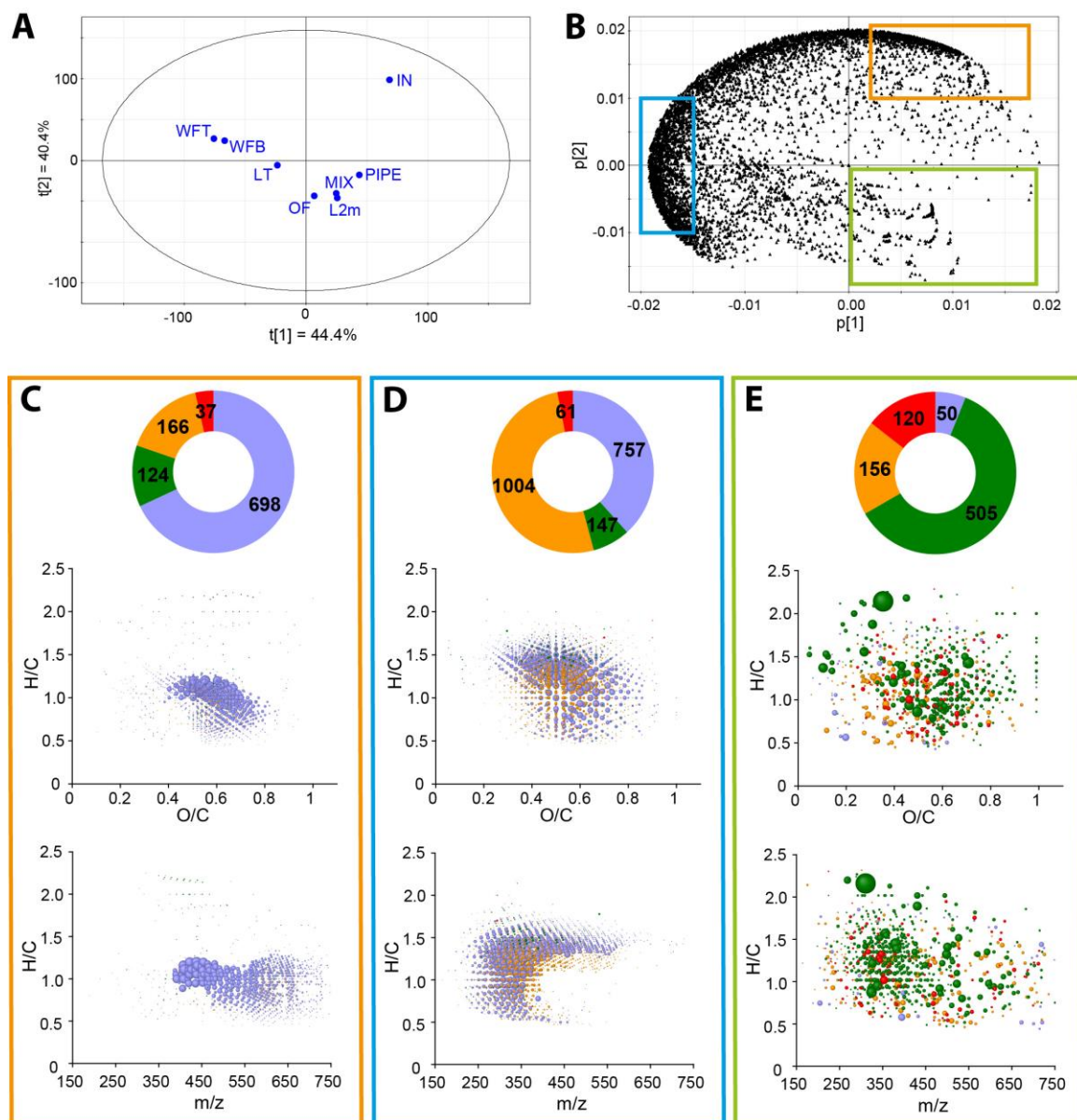
Figure 2-6: PCA based on all assigned molecular formulas.
A) Scores and B) loadings plot of the PCA based on all assigned molecular formulas. C-E) Depiction by ring diagrams, van Krevelen diagrams and m/z-resolved H/C ratios of the molecular compositions characteristic for the C) inlet (IN) sample, D) lake top (LT) and waterfall samples (WFT, WTB) and E) other lake samples: overflow (OF) and lake 2 m bls (L2m) as well as the pipe (PIPE) and mixing (MIX) sample.

However, the PCA further corroborates the findings from the above discussed optical proxies (2.4.2). The characteristic molecular formulas for the inlet SPE-DOM were primarily aromatic CHO compounds in the tannin and lignin region of the van Krevelen diagram (Figure 2-6C). The inlet stream is surrounded by forest, which explains the enriched lignin-type-molecule abundance in the inlet SPE-DOM. Additionally; the characteristic compounds are in agreement with the increased $SUVA_{254}$ value, an aromaticity proxy (Table 2–2). Furthermore, the m/z-resolved H/C ratio plot shows, a

great number of high molecular weight (m/z > 550) CHO, which account for the higher average molecular weight found for the inlet SPE-DOM (Table 6-1). The two optical molecular weight indices (S_R, a_{254}/a_{365}) also suggested an increased molecular weight for the inlet SPE-DOM (Table 2–2). The waterfall top (WFT) and bottom (WFB) SPE-DOM were very similar in their composition and mainly characterized by CHO and CHNO molecules in the tannin region of the van Krevelen diagram, with an m/z value < 400 (Figure 2-6D). In comparison of the inlet SPE-DOM the molecules are less aromatic (see above, (Table 2–2). All lake and outlet samples, especially the waterfall, SPE-DOM showed an increased abundance of CHNO compounds (Table 6-1) and also the PCA revealed CHNO compounds to be characteristic for those samples (Figure 2-6D, E). Most likely, nitrate is metabolized and incorporated into DOM molecules, which is also suggested by the depletion of nitrate in the lake and outlet samples compared to the inlet water sample (Table 2–1). Although the SPE-DOM from the sulfidic pipe (and mixing) water was not separated clearly from other lake water DOM, mainly low molecular weight CHOS compounds are characteristic for the PCA quadrant where the pipe sample is located (Figure 2-6E). This again testifies the enrichment of CHOS compounds in the hypolimnic water layer.

2.4.3.2. Mass spectrometric characterization of the sulfur organic chemistry

In order to distinguish CHOS molecules formed under hypolimnic conditions from those also present in the lakes inlet and oxic top layer waters, PCA analysis of the CHOS molecular formulas and their respective abundance was performed (Figure 2-7A). Based on its CHOS composition, the sulfide enriched pipe water SPE-DOM was clearly separated from all other samples.
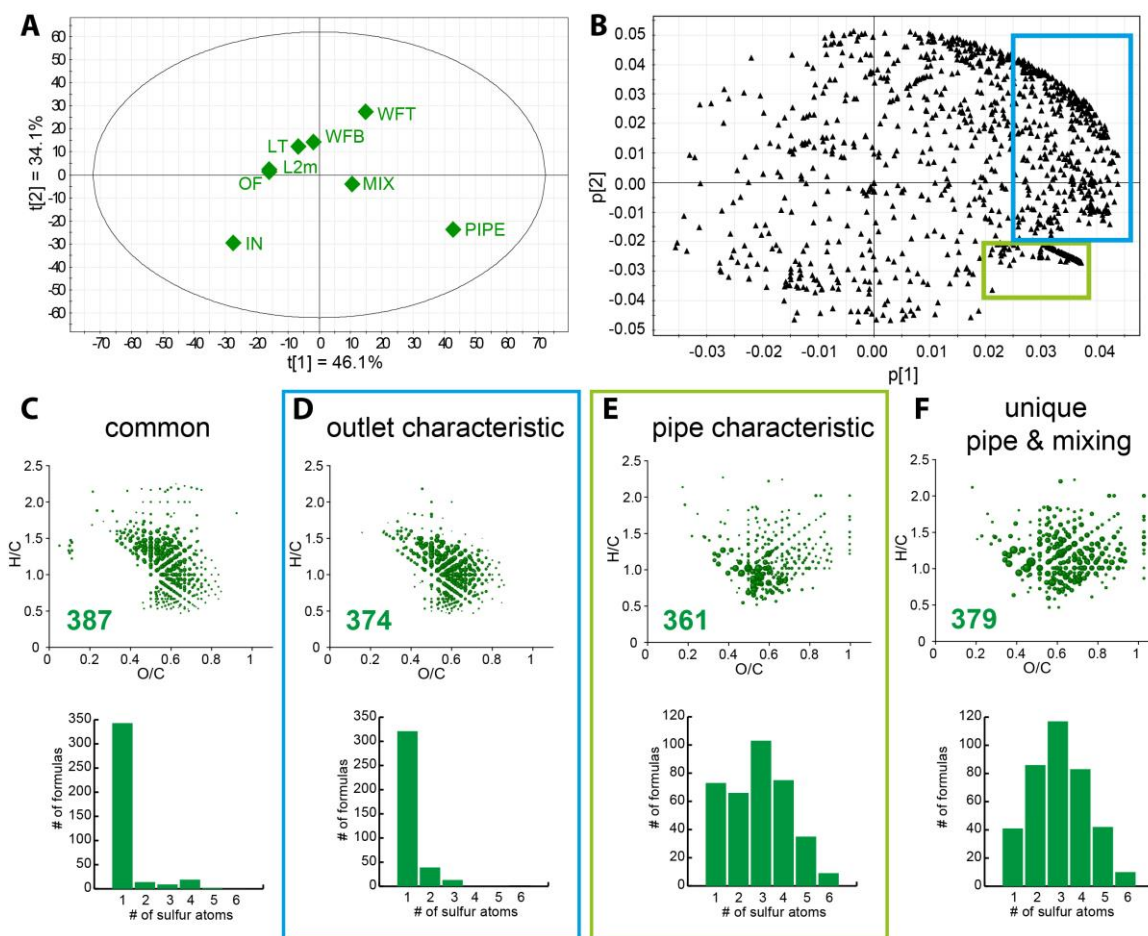
Figure 2-7: PCA based on assigned CHOS molecular formulas.
A) Scores and B) loadings plot of the PCA based on assigned CHOS molecular formulas. C-F) Van Krevelen diagrams and bar charts, which depict the number of sulfur atoms in the assigned CHOS molecular formulas, of the C) common CHOS molecular formulas to all samples, D) the characteristic CHOS for outlet samples which were in touch with hypolimnic pipe water, E) characteristic CHOS of the pipe (PIPE) sample and F) unique CHOS molecular formulas to the pipe and mixing SPE-DOM.

There were 387 CHOS molecular formulas identified in all SPE-DOM samples from Hechtsee (Figure 2-7C), which cover an often reported van Krevelen space for CHOS class molecules (Sleighter et al. 2014, Dubinenkov et al. 2014, Wagner et al. 2015b). The great majority of common CHOS compounds were $CHOS_1$ molecules (Figure 2-7C), which were also present in DOM in a variety of ecosystems (Schmidt et al. 2009, Schmidt et al. 2014, Dubinenkov et al. 2014). The first component of the PCA (Figure 2-7A) accounts for the separation of the sulfidic pipe water itself and the outlet samples which were mixed with pipe water. The representative molecular formulas for these samples were extracted from the score plot (Figure 2-7B) and are displayed in Figure 2-7D. The sulfur organic molecules resemble in their chemical space coverage as well as being mainly $CHOS_1$ type molecules those common to all Hechtsee SPE-DOM samples.

Indeed, > 50% of these molecular formulas coincided, hence, were enriched in those samples highly affected by the sulfidic pipe water. The PCA score plot (Figure 2-7B) also revealed molecular formulas very characteristic to the pipe (PIPE) water SPE-DOM (Figure 2-7E). The majority of these CHOS molecular formulas have multiple sulfur atoms incorporated and have higher H/C and O/C ratios. The coverage of the van Krevelen space resembles organic matter enriched in sulfonic acids (Yassine et al. 2012, Schmitt-Kopplin et al. 2012). But the detailed inspection of the molecular formulas ensured that both, the number of carbon and oxygen atoms in those molecular formulas decrease with an increasing number of sulfur atoms (Figure 2-8A and B). With the given ratio of oxygen to sulfur atoms in the molecules, the presence of sulfur only in its oxidized form, i.e. sulfonates and sulfones, is impossible (Table 6-2). Thus, formation of reduced sulfur CHOS compounds occurred in the sulfide enriched water layer of the meromictic lake. Furthermore, the low abundance of the $CHOS_x$ compounds might be a result of the lower ionization efficiency of thiols compared to acid functional groups (i.e. carboxylic and sulfonic acids). Additionally, the sulfur based Kendrick mass defect plot of all assigned CHOS in the pipe water SPE-DOM (Figure 2-8D and E) shows molecular series differing only in the number of sulfur atoms in the molecules. This additionally hints towards sulfur being present as sulfides, the most reduced sulfur oxidation state, and most likely also polysulfides.
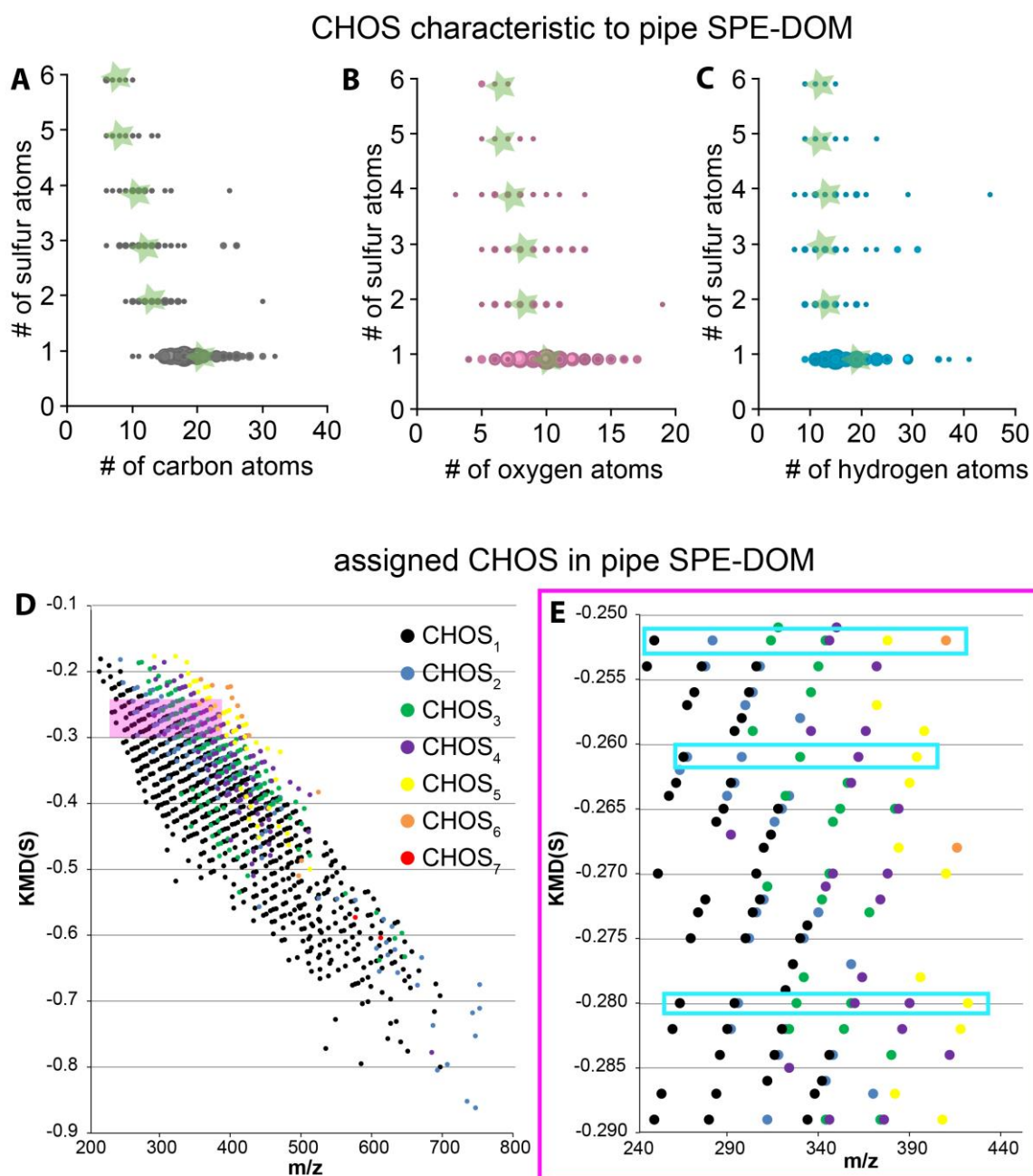
Figure 2-8: Characteristics of pipe water CHOS molecular formulas.
Plot of the number of A) carbon, B) oxygen and C) hydrogen atoms vs. number of sulfur atoms for the pipe characteristic CHOS molecular formulas. The bubble area depicts the abundance and the green stars highlight the average number of the respective atom in the molecular formula. D) Sulfur based Kendrick mass defect (KMD) plot for all assigned CHOS molecular formulas in the pipe water SPE-DOM. E) Enlarged part of the KMD(S) plot with molecular sulfur series highlighted in cyan.

The reaction of inorganic sulfides with CHO molecules was further investigated by evaluating the presence of putative precursor CHO compounds and formed CHOS compounds after incorporation of H_2S and H_2S_3, most likely occurring at double bonds and activated double bonds (Vairavamurthy and Mopper 1987, Perlinger et al. 2002, Heitmann and Blodau 2006, Yu et al. 2015b). Precursor CHO and resulting CHOS

compounds cover a wide range of molecular weight (Figure 2-9). Hence, sulfur incorporation is not limited by the size of the organic molecules. For the formation of $CHOS_1$ molecular formulas 77% and of $CHOS_3$ molecular formulas 72% of the precursor CHO molecules were present in the pipe water sample (Figure 2-9). Thus, most probably sulfur is present in the form of R-CH_2-CH_2-S_xH and not in the form of oxidation resistant sulfur heterocycles. This is further endorsed by a great overlap (83%) of the CHOS molecules characteristic for the pipe SPE-DOM and those unique to the pipe and mixing water SPE-DOM. Hence, pipe specific CHOS molecules formed under anoxic conditions in the presence of hydrogen sulfide are labile under oxic conditions and thus not present in the outlet samples further downstream (WFT and WFB).
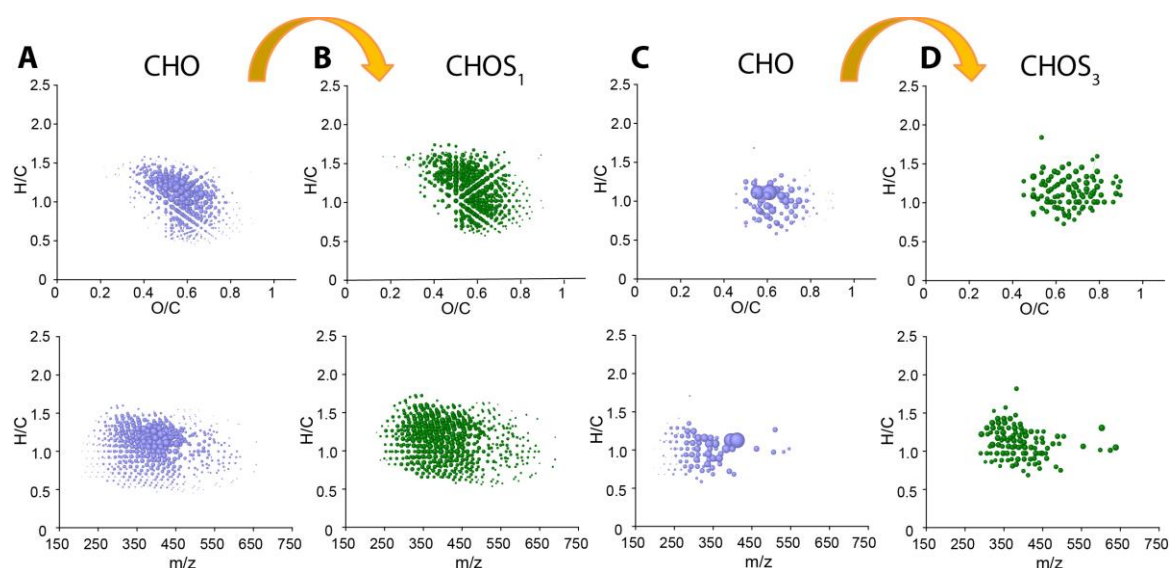
Figure 2-9: Putative CHO precursor molecules present in pipe water SPE-DOM.
Van Krevelen diagrams and m/z-resolved H/C ratio plots of the CHO putative precursor molecules present in the pipe water SPE-DOM of the formation of A) $CHOS_1$ and C) $CHOS_3$. Van Krevelen diagrams and m/z-resolved H/C ratio plots of the B) $CHOS_1$ and D) $CHOS_3$ formed by incorporation of H_2S and H_2S_3 present in the pipe water SPE-DOM, respectively.

2.4.3.3. Presence of polythionates and polysulfane monosulfuric acids in SPE-DOM

Ultrahigh resolution mass spectra of SPE-DOM predominantly contain signals from organic compounds, because ideally inorganic salts are not retained by the SPE sorbent. However, polythionates and polysulfane monosulfuric acids were found in the SPE-DOM from the sulfide enriched pipe water as well as from the mixing zone and the outlet stream before the waterfall (Figure 2-10). Also the cyclic voltammogram of the mixing water indicated polythionates (Figure 2-3). The presence of inorganic polysulfur species in the SPE-DOM extracts was verified by the comparison with the corresponding isotopic

patterns (c.f. Appendix Figure 6-2 and Figure 6-3). Possibly due to their lability (Steudel 2003), the completely reduced polysulfides were not present in any of the samples. The retention of polythionates by PPL resins is most likely possible due to the nonpolar sulfur chain in the center of the molecule. Furthermore, polythionates are e.g. fully retained by the Bio-Rad anion-exchange resins AG1-X8 (Druschel et al. 2003c). Both PPL and AG1-X8 are based on a styrene divinylbenzene copolymer.
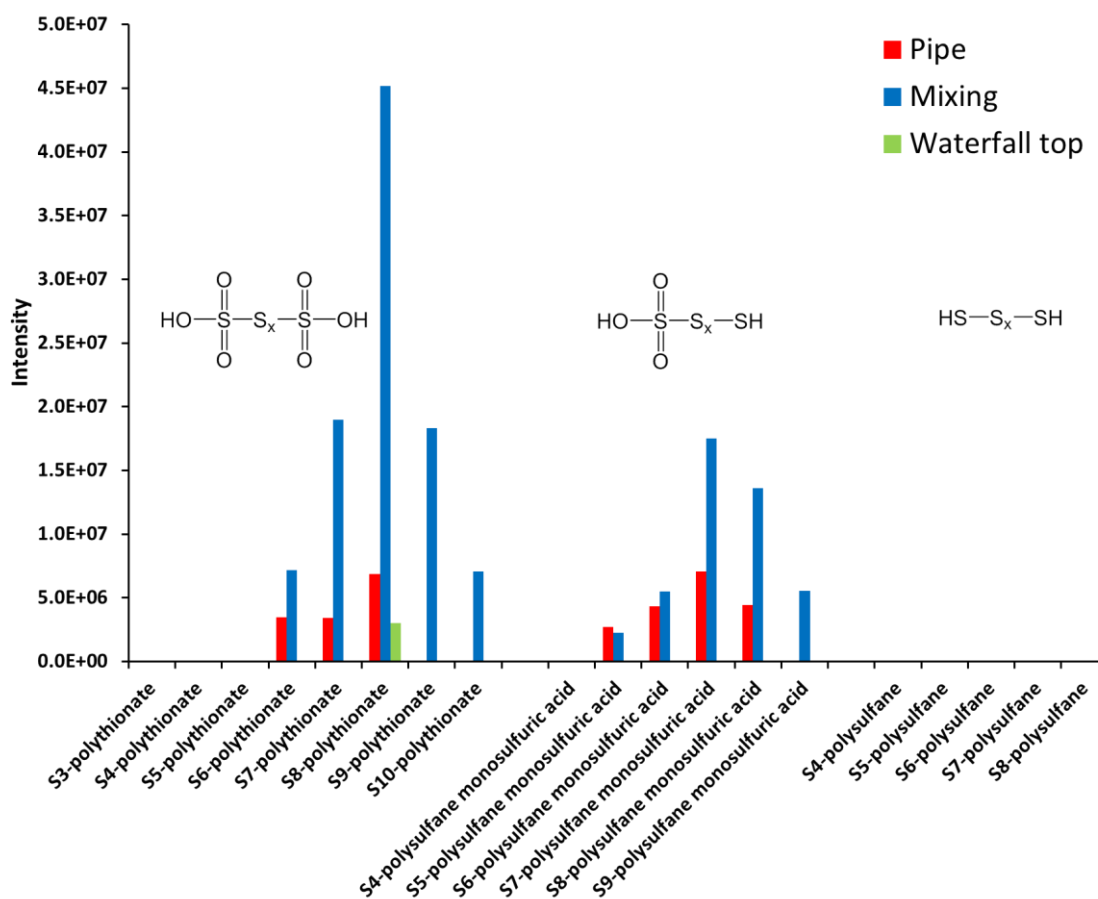
Figure 2-10: FT-ICR-MS based inorganic polysulfur speciation.
Polythionates and polysulfane monosulfuric acids present in the FT-ICR mass spectra of the pipe, mixing and waterfall top SPE-DOM extract.

Polythionates are important intermediates of abiotic sulfur redox transformations in the environment as well as in the metabolism of sulfur oxidizing and reducing microorganisms (Steudel et al. 1987, Takano and Watanuki 1988, Kelly 1999, Schippers, Rohwerder and Sand 1999, Suzuki 1999, Xu et al. 2000, Druschel et al. 2003c). Many sulfur bacteria producing polythionates as metabolites are dependent on the presence of iron (Steudel et al. 1987, Schippers et al. 1999). Abiotic formation of polythionates occurs via the reaction of sulfur dioxide with hydrogen sulfide (Schmidt and Heinrich 1958, Druschel, Hamers and Banfield 2003a) or the oxidation of thiosulfate in the presence of

metal sulfides such as pyrite (Xu and Schoonen 1995). Although inorganic sulfur speciation did not confirm the presence of thiosulfate, which has been shown to be a major product of the hydrogen sulfide oxidization in oxic water (Chen and Morris 1972, O'Brien and Birkner 1977, Zhang and Millero 1993), increased iron concentrations in the pipe water (Table 2–1) and low bacterial activity (low BIX values, c.f. Table 2–2) hint towards polythionate formation via the second abiotic pathway (Rickard and Luther III 2007). This is further corroborated by the fact that polythionates and polysulfane monosulfuric acids were more abundant in the SPE-DOM from the mixing water spot, where hydrogen sulfide oxidation takes place as a result of the intermix of anaerobic pipe and aerobic overflow water. Polysulfane monosulfuric acids are formed during the hydrolysis of polythionates (Meyer and Ospina 1982, Steudel et al. 1987). Besides the hydrolysis of polythionates, dilution and mixing of inorganic and organic molecules in the water further downstream the inorganic polysulfur intermediates were almost completely absent in the sample from the top of the waterfall (Figure 2-10).

2.4.4. The dissolved organic sulfur concentration in relation to mass spectrometric analysis of sulfur organic compounds

DOC and dissolved organic sulfur (DOS) concentrations of the SPE-DOM extracts were determined for all sampling spots to obtain an ionization efficiency independent assessment on the enrichment of sulfur organic compounds in the hypolimnic water layers. The results are summarized in Table 6-3 in the Appendix.

The DOS concentration was 271 µmol L^{-1} for the SPE-DOM from the pipe water and 228 µmol L^{-1} for the SPE- DOM from the mixing water. Thus, DOS was increased by the factor of two compared to SPE-DOM from the other lake waters (mean 128 µmol L^{-1}). The molar DOS/DOC ratios of the lake water SPE-DOM was with 0.0047 similar to those found in sea water (Pohlabeln and Dittmar 2015), whereas the molar DOS/DOC ratios for the pipe and mixing water were with 0.0121 and 0.0088 also increased by a factor of 2.6 and 1.9, respectively.
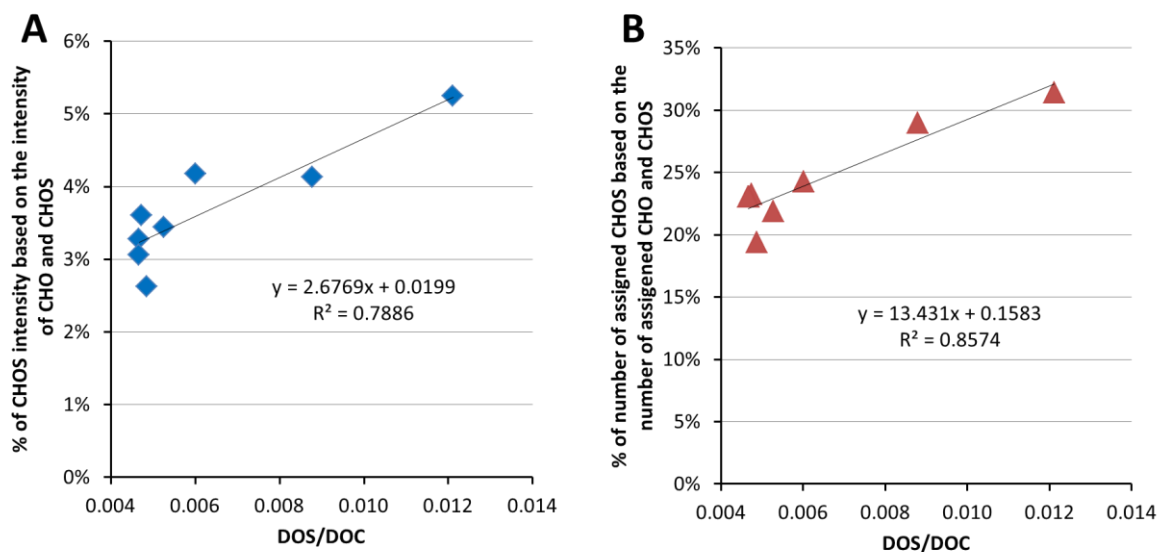
Figure 2-11: Dissolved organic sulfur concentration in relation to mass spectrometric analysis of sulfur organic compounds.
Linear regression analysis on the molar DOS/DOC ratio and the percentage of the A) summed CHOS mass peak intensity compared to the total intensity of CHO and CHOS compounds and B) number of assigned CHOS compared to the total number of assigned CHO and CHOS compounds. Both the number of assigned CHOS as well as their total mass peak intensity includes the counts and intensity, respectively, of the identified polythionates and polysulfane monosulfuric acids (Table 6-1). CHNO and CHNOS mass peaks were excluded due to their low variability between the samples.

In order to evaluate the relationship between molar DOS/DOC ratios and the percentage of the CHOS mass peak intensity and the percentage of number of assigned CHOS compounds, a linear regression analysis was performed (Figure 2-11). The linear correlation between the molar DOS/DOC ratio and the CHOS mass peak intensity had a correlation coefficient R^2 of 0.7886 and a slope of 2.7. Both, the correlation coefficient ($R^2 = 0.8574$) and the slope (13.431) were higher for the correlation of the molar DOS/DOC ratio with the number of assigned CHOS compounds. The reason is the competitive ionization process of ESI (Sleighter and Hatcher 2011). CHOS molecules including an acid functional group such as sulfonic acid have a higher ionization efficiency in (–)ESI compared to those including a thiol (Sleighter and Hatcher 2011). Thus, the correlation between molar DOS/DOC ratio and the number of assigned CHOS molecules, mostly ionization efficiency independent, corresponds more to the actual enrichment of hypolimnic SPE-DOM with sulfur organic compounds. The factor of five between the two slopes of the linear regressions, clearly indicates that sulfur organic compounds present in the hypolimnic water to be thiols with polysulfur chains. Hence, this result is in agreement with the findings from ultrahigh resolution mass spectrometry

(2.4.3.2). Additionally, the molar DOS/DOC ratio increases substantially, when individual molecule formulas include multiple sulfur atoms, like the majority of characteristic CHOS molecules of the pipe water SPE-DOM (cf. Figure 2-7E). The number of assigned molecular formulas does not increase in such way, because an induvial molecule in mass spectrometric analysis with soft ionization methods, such as ESI, only produces one mass peak from which the molecular formula is assigned. This is reflected by the pipe water being below the linear trend line (Figure 2-11B) and the correlation coefficient being clearly below 1.

2.5. Summary and conclusions

Hechtsee was chosen as a model site to investigate the incorporation of sulfur into DOM in anoxic and sulfide rich aquatic ecosystems. Inorganic sulfur speciation confirmed the presence of ~ 1 mmol L^{-1} sulfide in the anoxic water layer sampled directly from the installed Olszewski pipe of the meromictic lake. Furthermore, active sulfur cycling in the anaerobic zone was confirmed by the presence of elevated iron concentrations and traits of polysulfide, elemental sulfur, polythionates and polysulfane monosulfuric acids. The latter two were predominantly found in the mixing water (zone where the lake overflow is mixed with pipe water), thus, are primarily formed during the oxidation of hydrogen sulfide. The mesotrophic classification of the lake was confirmed by the florescence spectroscopy index BIX, which was clearly below 1, as well as the found DOC concentrations. Additionally, the total phosphorous and phosphate concentrations were below the limit of detection. Hence, no eutrophication took place at Hechtsee.
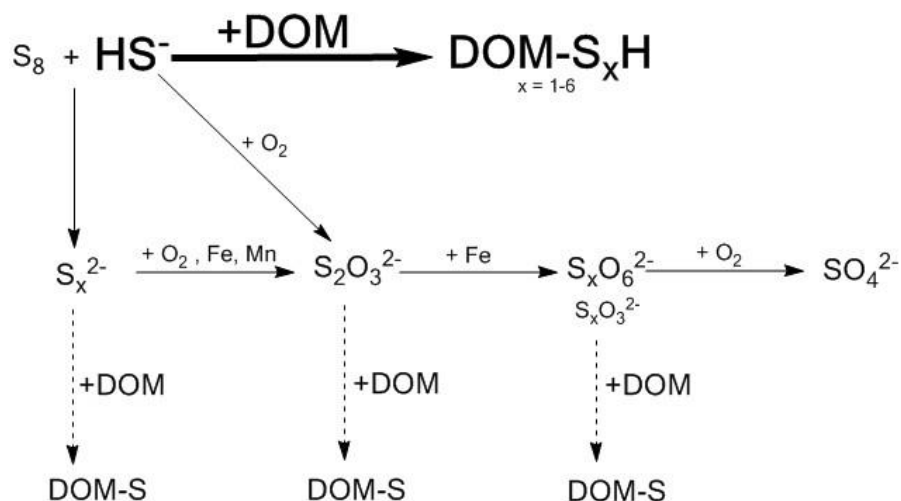
Figure 2-12: Reaction scheme of DOM with reduced sulfur species.
Hydrogen sulfide reacts with DOM to form CHOS molecules with thiols and most likely polythiol functional groups in the anaerobic water layer of meromictic lakes. Possibly DOM also reacts with polysulfide, thiosulfate, polythionates and polythiol monosulfuric acid to form CHOS molecules (indicated by dashed arrows).

Figure 2-12 illustrates the reaction scheme of DOM with inorganic sulfur species in meromictic lakes resulting from the findings at Hechtsee. Both ultrahigh resolution mass spectrometry of SPE-DOM and molar DOS/DOC ratios confirmed the enrichment of DOM with CHOS compounds in the anaerobic and sulfide rich pipe water (cf. Figure 2-5, Figure 2-7, Table 7-1, Table 6-3). Hence, sulfurization of DOM takes place in the hypolimnic water layer of the meromictic lake. Although the molar DOS/DOC ratio increased by the factor of 2.6, the total number of mass peaks as well as the intensity (< 5% of the total mass peak intensity of the assigned molecular formulas) of CHOS molecules only increased by the a factor of ~ 1.5. Furthermore, the low mass peak intensities and chemical composition of the characteristic CHOS molecular formulas, including multiple sulfur atoms and not enough oxygen atoms to carry only oxidized sulfur functional groups (Figure 2-8), proofs that sulfur must be present in the form of thiols and most probably also polythiols. These species have lower ionization efficiencies compared to sulfonic acids in (–)ESI (Sleighter and Hatcher 2011). The majority of DOM molecules in the pipe water SPE-DOM, like for all other sampling spot, were CHO compounds (Table 6-1). Hence, despite high concentrations of free hydrogen sulfide (Table 2–1), the formation of stable CHOS is limited in the anaerobic water layer of the lake. Thus, the formation of CHOS by reaction of CHO with the strong nucleophile sulfide is rather depending on the chemical composition of available reaction sites in CHO molecules than on the sulfide concentration. This is in agreement with laboratory

experiments, that showed that sulfurization of organic molecules occurs at double bonds and activated double bonds (Vairavamurthy and Mopper 1987, Perlinger et al. 2002, Hebting, Adam and Albrecht 2003), which are not the predominate functional groups in DOM molecules (Thurman 1985). It is also possible that polysulfurized CHOS resulted from the reaction of polysulfide with DOM. This has to be studied further in depth by laboratory experiments, because only traits of polysulfide were detectable with CV at Hechtsee. Low polysulfide concentrations potentially indicate fast reactivity of polysulfide with DOM. Similarly, the reaction of thiosulfate (not detected in the Hechtsee water samples), the major oxidation product of hydrogen sulfide (Chen and Morris 1972, O'Brien and Birkner 1977, Zhang and Millero 1993), cannot be precluded from the findings. Additionally, reactions between DOM and polythionates as well as polysulfane monosulfuric acid (both present in the anaerobic pipe water and almost fully oxic mixing water) with DOM cannot be entirely excluded by our finding. Therefore, future studies should also focus on the reactivity of DOM with intermediate redox state sulfur species.

Besides the proposed laboratory studies with diverse inorganic sulfur species, field studies at different meromictic lakes (e.g. Mahoney Lake, BC, Canada; Fayetteville Green Lake, NY, USA) should be performed. These studies should focus on the combination of organic and inorganic sulfur speciation as well as microbial activity and community determination. This would allow an even further extended comprehensive understanding on the interplay of the abiotic and biotic sulfur cycle with the carbon cycle.

3. Bacterial sulfate reduction and its effect on dissolved organic matter

Petroleum hydrocarbon degradation by bacterial sulfate reduction and its effect on groundwater dissolved organic matter
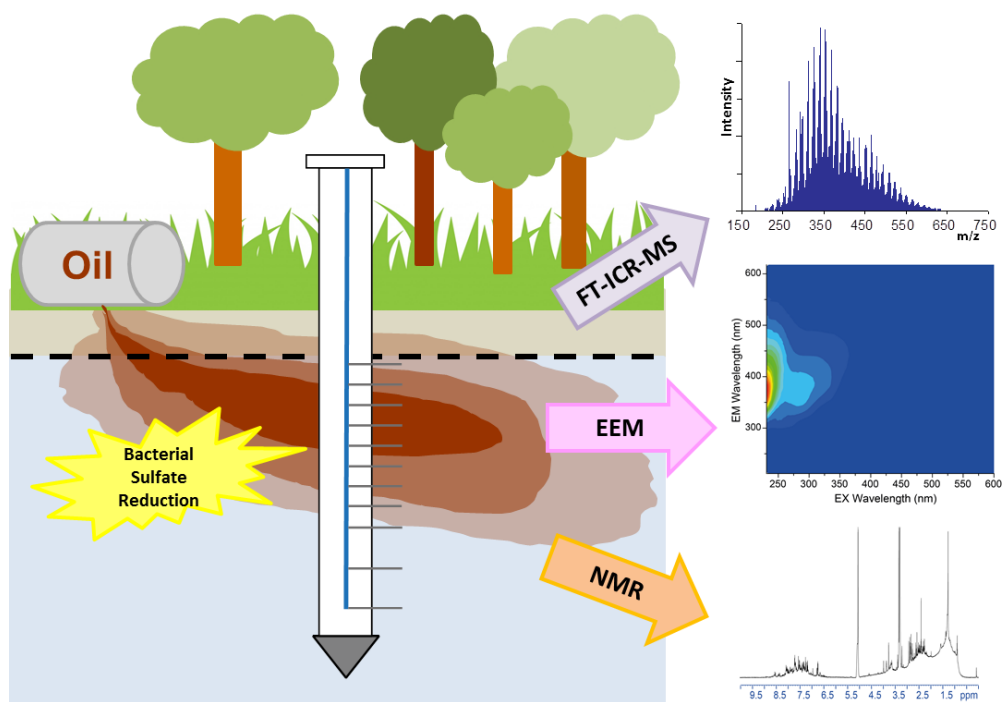
Reprinted (adapted) with permission from (Dvorski et al. 2016). Copyright (2016) American Chemical Society.

Parts of this chapter are published in:
Dvorski, S. E.-M., M. Gonsior, N. Hertkorn, J. Uhl, H. Müller, C. Griebler & P. Schmitt-Kopplin (2016) Geochemistry of Dissolved Organic Matter in a Spatially Highly Resolved Groundwater Petroleum Hydrocarbon Plume Cross-Section. Environmental Science & Technology, 50, 5536–5546.

3.1. Introduction

Concentration and composition of DOM are pivotal parameters related to water quality (Shen et al. 2014). Groundwater ecosystems are typically poor in organic carbon and energy and, consequently, systems of low productivity (Thurman 1985, Griebler and Lueders 2009). DOM concentrations in pristine oxic groundwater are as little as 0.1 mg L^{-1} to a few mg L^{-1} (Thurman 1985, Fitts 2012). However, numerous groundwater sites worldwide are contaminated with organic chemicals thus exhibiting significantly higher DOM concentrations (Vogt and Richnow 2014, Meckenstock et al. 2015). Prominent organic groundwater contaminants are petroleum hydrocarbons with benzene, toluene, ethylbenzene and xylenes (BTEX) and polycyclic aromatic hydrocarbons (PAHs) being the most common (Eberhardt and Grathwohl 2002, Jobelius et al. 2011). In contaminated systems, natural DOM may act as a reactant, chelator, and sorbent for hydrophobic organic contaminants influencing their bioavailabilty, mobility, and fate (Minor et al. 2014, Moeckel et al. 2014).

From the point source, pollutants partly dissolved in groundwater are transported along with the water flow, thereby forming a contaminant plume (Meckenstock et al. 2015). The fate and transformation of organic contaminants in a mature plume are related to several abiotic processes such as dilution, diffusion, and microbial degradation (Wiedemeier et al. 1999). Current research underlined that contaminant plumes in porous aquifers are characterized by steep and small-scale gradients in the range of centimeters to decimeters with high biodegradation activities occurring at the fringes of the plume (Anneser et al. 2008a, Anneser et al. 2010). This 'plume fringe concept' is founded on the typically occuring depletion of dissolved electron acceptors in the plume core (Meckenstock et al. 2015, Bauer et al. 2008). Biodegradation with oxygen, nitrate, or sulfate reduction can then only take place at the fringes of the plume where electron acceptors are replenished from surrounding groundwater by dispersion and diffusion. In the plume core, biodegradation may alternatively be driven by reduction of solid electron acceptors such as Fe(III)- or Mn(IV), and also by methanogenesis (Foght 2008).

Natural DOM interacts with not only organic pollutants but also inorganic reactive species that may directly be related to the dominant terminal redox processes coupled to contaminant biodegradation. Reactive sulfur species such as sulfide are a prominent example (Vairavamurthy and Mopper 1987, Heitmann and Blodau 2006, Yu et al.

2015b). In fact, sulfate reduction is the quantitatively most important redox process in petroleum hydrocarbon contaminated aquifers (Wiedemeier et al. 1999). Bacterical sulfate reduction was also identfied as the key redox process involved in the contaminant biogradtion at the petroleum hydrocarbon plume in Düsseldorf Flingern (Winderl et al. 2008, Anneser et al. 2008a, Anneser, Richters and Griebler 2008b, Anneser et al. 2010).

3.2. Objectives

So far, detailed insight into the role of natural DOM for petroleum hydrocarbon contaminated groundwater ecosystems is missing on a molecular level. An improved fundamental understanding of contaminant biodegradation bottlenecks and development of successful remediation strategies need detailed investigations of the mutual influence, the dominating redox reactions and products, and characteristics and distribution of contamination as well as its interaction with natural DOM.

The aim of this study was to combine on-site high resolution spatial sampling across a well-defined petroleum hydrocarbon plume with high resolution molecular characterization of DOM in an effort to study the interaction of the contaminants in addition to redox processes and their reaction products with natural DOM. Particularly the effect of bacterial sulfate reduction on the DOM characteristic was studied in detail by evaluating the formation of sulfur organic compounds at elevated sulfide concentration resulting from bacterial sulfate reduction.

Comprehensive analyses of solid phase extracted DOM (SPE-DOM) from groundwater of the petroleum hydrocarbon contaminated sandy aquifer in Düsseldorf Flingern by means of (−)ESI and (+)APPI FT-ICR-MS, NMR, and EEM fluorescence spectroscopy was performed. The purpose and advantages of the analytical techniques is summarized in the following paragraphs.

 (+)APPI FT-ICR-MS favors the detection of aromatic and less polar compounds (Hertkorn et al. 2008, D'Andrilli et al. 2010, Sleighter and Hatcher 2011), hence, favors the detection of petroleum derived compounds. (−)ESI FT-ICR-MS is selective towards DOM molecules containing carboxylic acids and other polar functional groups (Hertkorn et al. 2008, Sleighter and Hatcher 2011), thus, preferably applied for the characterization of natural DOM.

Owing to the high abundance of aromatic molecules in mineral oils and their degradation products, EEM fluorescence spectroscopy is useful to assess distribution, influence, and transformation of petroleum products in the environment (Zhou and Guo 2012, Zhou et al. 2013, Mendoza, Riemer and Zika 2013, Bianchi et al. 2014).

NMR does not suffer from potential distortions, such as ionization efficiency and selective detection of fluorophores, and provides quantitative depiction of relevant structural features in complex organic mixtures (Hertkorn et al. 2007). Furthermore, NMR spectroscopy has been employed for the analysis of oils from various sources and to study the interaction of natural organic matter and organic pollutants (Mazzei and Piccolo 2015, Sudasinghe et al. 2014, Meckenstock et al. 2014, Kim et al. 2015).

In order to enable an enhanced and meaningful discussion of the linkage between the abiotic and biotic processes contributing to the DOM characteristics of the specific zones, multi-data correlation based on the (–)ESI FT-ICR-MS derived molecular formulas from DOM, bacterial community data as well as geochemical and contamination properties was performed.

3.3. Materials and methods

3.3.1. Sampling site

The sampling site is located at a former gasworks site in Düsseldorf Flingern, Germany 51°13'19.83" N 6°49'05.44" E (Figure 3-1, Figure 3-2). The sediment shows a relatively homogenous composition predominantly of quaternary sand with gravel inclusions > 12 m below land surface (bls) (Anneser et al. 2008a). In the samples section of the aquifer groundwater follows a hydraulic gradient of about 6‰ from east to west with velocity of $0.1 - 2$ m day^{-1} (Anneser et al. 2008a).

Figure 3-1: Location of Düsseldorf in Europe.
Map of Europe, the red star indicates the sampling location Düsseldorf Flingern.
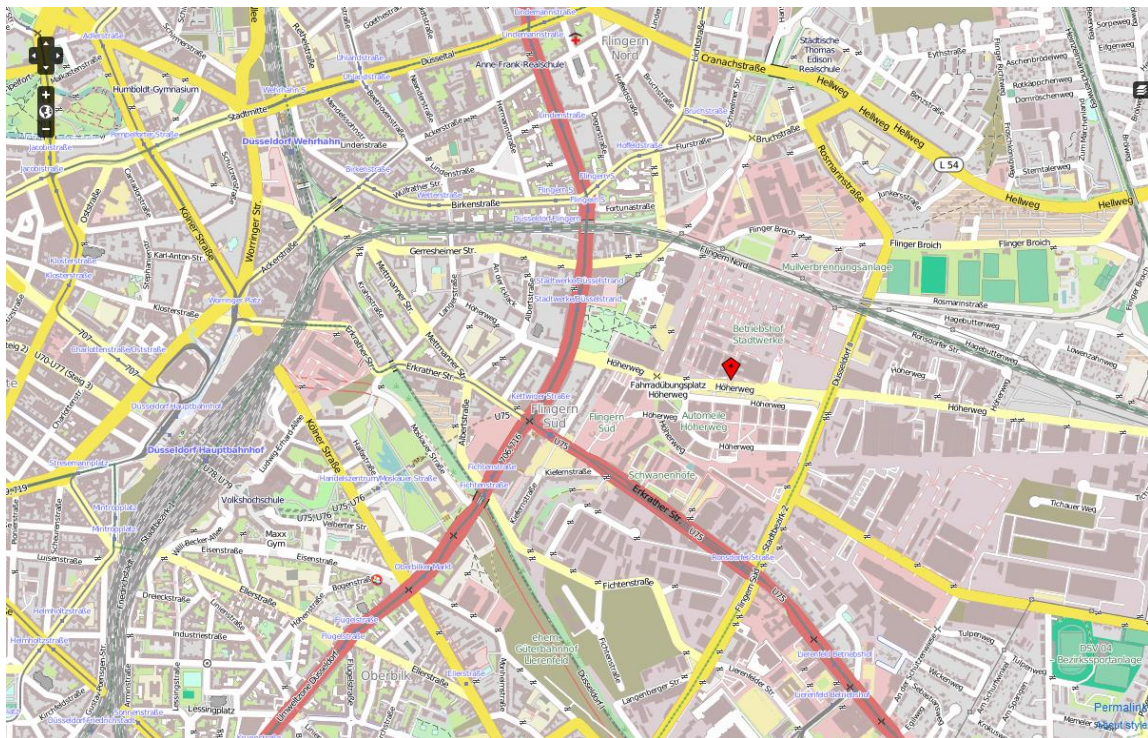
Figure 3-2: Location of the sampling site in Düsseldorf.
The red pin marks the sampling site on the ground of the Stadtwerke Düsseldorf in Düsseldorf Flingern (source http://www.openstreetmap.de (5.1.2016)).

Production of benzene, gas, coke and different tar oil components from 1893 until 1967 as well as the deconstruction of the plant in 1968 led to the release of mono- and polycyclic aromatic hydrocarbons into the aquifer (Anneser et al. 2008a). As a consequence, a contamination plume mainly consisting of BTEX, naphthalene and acenaphthalene developed (Wisotzky and Eckert 1997). After several remediation actions the BTEX plume extend 200 m x 40 m in dimension with a thickness of only $1 - 2$ m (Anneser et al. 2008a). A detailed description of the sampling site is provided elsewhere (Wisotzky and Eckert 1997, Anneser et al. 2008a).

For a detailed assessment of contamination degedration processes a high resolution multilevel well (HR-MLW) enabling a high vertical sampling resolution of down to 3 cm across the fringe and center of the contamination plume was installed (Anneser et al. 2008a). In short, groundwater samples were taken simultaneously through permanently installed high-density polyethylene (HDPE) tubes by peristaltic pumps at a rate of 1.5 mL min^{-1} to prevent mixing of waters from different depths. The sampling scheme using this HR-MLW was described in detail by Anneser et al. 2008a.

Thirty-two groundwater samples were taken in September 2013 with a vertical spatial resolution ranging from 3 cm in the plume core and fringes to 1 m in the non-contaminated deeper zone of the aquifer. Table 7-5 in the supplementary information contains the sampled depths during the sampling campaign in September 2013. The sampling volume was 250 mL (labeled with H) and 1 L (labeled with L).

3.3.2. Groundwater geochemistry and occurrence of (parent) contaminants[2]

The concentrations of aromatic hydrocarbons, i.e., BTEX and selected PAHs, were determined with a Trace DSQ GC-MS (Thermo Fisher Scientific, Waltham, USA) equipped with a Combi PAL autosampler (CTC Analytics, Zwingen, Switzerland) by the protocols described elsewhere (Anneser et al. 2008a). Basic physical-chemical parameters such as pH and redox potential (E_H) were determined in freshly collected groundwater samples with field sensors (WTW, Weilheim, Germany). Major ions, e.g., sulfate, were

---

[2] Measurements were predominantly performed by the collaboration partners from the Institute of Groundwater Ecology institute of ground water ecology of the Helmholtz Zentrum München Deutsches Forschungszentrum für Gesundheit und Umwelt (GmbH).

analyzed within 2 days by ion chromatography (Dionex DC-100, Idstein, Germany) from samples stored in the dark without headspace and cooled. Fe(II) concentrations were measured by the ferrozine assay (Stookey 1970). For sulfide determination, 200 µL of sample were fixed in duplicates in 1 mL of a 2% (w/v) zinc acetate solution and analyzed on-site following a modified protocol from Cline (Cline 1969). Total sulfur concentrations were measured by a CIROS VISION ICP-OES Spectrometer (Spectro Analytical Instruments Inc., Mahwah, Germany) from onsite 0.45 µm Millex-HV (Merck KGaA, Darmstadt, Germany) filtered and nitric acid stabilized water samples. The nitric acid (ROTIPURAN®, ≥65 %, p.a., Carl Roth GmbH & Co. KG, Karlsruhe, Germany) used for the stabilization of samples for ICP-OES analysis was purified by an IR-Subboiling-Apparatur BSB-939-IR (Berghof GmbH, Eningen, Germany).

3.3.3. Solid phase extraction of DOM

Prior to SPE the groundwater samples were filtered through 0.22 µm filter membranes. For the sample volume of 250 mL Durapore® filter membranes (MerckKGaA, Darmstadt, Germany) and for 1 L samples sterile Corning® bottle top vacuum filter units equipped with CA membranes (Corning Inc., Corning, USA) were used. Isolation of DOM was performed by an established SPE method described by Dittmar et al. (Dittmar et al. 2008). Briefly, the water samples were acidified to pH 2 with hydrochloric acid (32%, p.a., Merck KGaA, Darmstadt, Germany) and passed through Agilent Bond Elut PPL SPE cartridges (100 mg (for 250 mL sample volume) and 500 mg (for 1 L sample volume) with a flowrate of <4 mL min^{-1} and <10 mL min^{-1}, respectively). To prevent loss of organics caused by overloading of the first SPE cartridge, a second cartridge was attached below the first one. Then, the cartridges were rinsed with acidified (pH 2) purified water (MilliQ-Integral, Merck KGaA, Darmstadt, Germany) and dried under vacuum. The DOM was eluted with 2 mL and 10 mL methanol (Chromasolv® LC-MS grade methanol, Sigma Aldrich, Taufkirchen, Germany), respectively.

3.3.4. Ultrahigh resolution mass spectrometry

Ultrahigh resolution mass spectra were acquired with a SolariX Qe FT-ICR-MS (Bruker Daltonik GmbH, Bremen, Germany) equipped with a 12 T superconducting magnet. (–)ESI FT-ICR-MS analyses were performed with an Apollo II ESI source MS (Bruker Daltonik GmbH, Bremen, Germany). Prior to (–)ESI FT-ICR-MS analysis, the SPE-DOM samples were diluted 1:20 with methanol. Positive mode APPI experiments were

conducted with an Agilent G1971A APPI source adjusted and purchased from Bruker Daltonik GmbH (Bremen, Germany). The SPE-DOM extracts were diluted 1:20 with a solution of 90% methanol and 10% toluene as a dopant before the analysis. In order to prevent carry over and cross-contamination in (+)APPI FT-ICR-MS, the APPI source was rinsed thoroughly with a solution of 90% methanol and 10% toluene between the measurements.

The mass spectra were internally calibrated to known and high abundant masses of DOM with a mass accuracy of < 0.1 ppm. For both (−)ESI and (+)APPI FT-ICR-MS spectra, only singly charged molecular ions were found. The formula assignment of the mass spectra was performed with the in-house written FormCalc software tool and the NetCalc network approach described in (Tziotis et al. 2011). The mass accuracy window for the formula assignment was set to ±0.2 ppm. The assigned formulas were validated by setting sensible chemical constraints (N rule; O/C ratio ≤ 1; H/C ratio ≤ 2n+2 (C_nH_{2n+2}), double bond equivalents) in conjunction with isotope pattern comparison.

Hierarchical cluster analysis based on Pearson's correlations of assigned FT-ICR-MS peaks for both ionization modes were performed with Hierarchical Clustering Explorer Version 3.0 (Human-Computer Interaction Laboratory University of Maryland, College Park, USA) and R (Version 3.0.0). The assigned peaks were almost normally distributed; therefore, the usage of Pearson's correlation was adequate. This was further confirmed by hierarchical cluster analysis based on Spearman rank correlation, which led to analogous clustering results. To evaluate the molecular formulas explaining the main characteristics of each subcluster, formulas with a Pearson's correlation coefficient r > 0.9 were extracted for the individual subclusters. These molecular formulas are characteristic for the DOM chemistry in the specific depth region of the individual subclusters.

For MS/MS fragmentation, ions were accumulated in the first hexapole before they were pulsed through the quadrupole to the collision cell where they were fragmented by collision-induced dissociation (CID) using increasing voltage increments up to 30 V. Details on the parameters are given in the Appendix (Table 7–2).

3.3.5. EEM fluorescence spectroscopy and PARAFAC modeling

Excitation emission matrix fluorescence spectroscopy of SPE-DOM was measured using a Jobin Horiba Instruments (Kyoto, Japan) Aqualog spectro fluorometer. After

evaporation of the methanol from 100 μL SPE-DOM, the samples were dissolved in Barnstead™ Nanopure™ (Thermo Fisher Scientific, Waltham, USA) water whereby the concentration was adjusted to a maximum UV absorbance at 300 nm of 0.2. Excitation scans were conducted from 600 nm to 231 nm in 3 nm steps, and the emission wavelength ranged from 211.1 nm to 617.7 nm in ~3 nm increments. The integration time was set to 1 s. Inner filter effects and Rayleigh scattering were corrected by the Aqualog software. The spectra were normalized to a Starna® Scientific Ltd. (Hainault, UK) Quinine Sulfate Standard of 1 ppm. Fluorescence units were then given in quinine sulfate units (QSU).

Details on the PARAFAC modeling, which was performed by the drEEM MATLAB toolbox (Murphy et al. 2013), are given in the Appendix (7.2.1). Principal component analysis (PCA) of Fmax values was carried out with SIMCA-P 9.0 (Umetrics, Umeå, Sweden) to evaluate the influence of the components on the individual samples.

3.3.6. NMR spectroscopy

1D and 2D ^{1}H and ^{13}C NMR spectra were acquired with a Bruker (Bremen, Germany) AV III 800 spectrometer operating at $B_0 = 18.7$ T with Bruker standard pulse sequences and cryogenic detection. Five hundred microliters of methanolic DOM extract was dried and twice exchanged with 750 μL CD$_3$OD (Merck. 99.95% ^{2}H) each before dissolution in ~130 mg CD$_3$OD. The solution was transferred into eventually sealed 2.5 mm Bruker MATCH™ tubes. A detailed description of the NMR acquisition conditions is described in the Appendix (7.1.2).

3.3.7. Microbial community analysis

Microbial community analysis was performed by the collaboration partners Anna Róza Szalay and Dr. Tillmann Lueders from the Institute of Groundwater Ecology of the Helmholtz Zentrum München – Deutsches Forschungszentrum für Gesundheit und Umwelt (GmbH). Total DNA was extracted from water filters (Corning® bottle top vacuum filter units equipped with CA membranes (Corning Inc., Corning, USA)) from selected depths between 6.54 and 11.19 m bls by a protocol described in detail elsewhere (Lueders, Manefield and Friedrich 2004, Brielmann et al. 2009, Laban, Dao and Foght 2015) and 16S rRNA gene amplicon pyrosequencing was performed. A detailed description of the sequencing and data elaboration is given in the Appendix (7.2.3). The

matrix with the abundances of the operational taxonomic units (OTUs) was used for the multi-data correlation.

3.3.8. Multi-data correlation

Multi-data correlation of the individual DOM mass signals detected in (–)ESI FT-ICR-MS, OTUs from the microbial community analysis and the geochemical variables which included groundwater parameters, such as the pH value and redox potential, and the measured (parent) contaminants were done using SIMCA-P 13.0.3.0 (Umetrics, Umeå, Sweden) and RStudio (Version 0.99.896 – © 2009-2016 RStudio, Inc.). The mass signals were normalized by the sum of the intensities and the OTU abundances were normalized to a total sum of 100. For the integration, all the different datasets were aligned in one matrix and UV scaling was applied. The dataset included 462 OTUs and 15101 FT mass signals and 7 geochemical variables.

The data were examined with various techniques starting from unsupervised (PCA) to supervised techniques: orthogonal partial least squares analysis (OPLS) and orthogonal partial least squares discriminant analysis (OPLS-DA). The OPLS model investigated the possible relation between the 7 geochemical variables and the OTUs together with mass signals. And the OPLS-DA model investigated the relation between the 4 different zones and the OTUs together with the mass signals. Classification of the samples according to the four zones (Table 7-5) is based on the results from unsupervised statistical techniques and the previously described detailed knowledge on the distribution of the geochemical variables (Anneser et al. 2008b). The validity of both models was proven with 7 cross validations and with the cross validation analysis of variance (ANOVA). The possible overfitting of the models was excluded due to the goodness of the fit and prediction (Table 7-6). The 7 geochemical variables were extremely significant in the OPLS model indicted by the p-values of the model (Table 7-7).

In order to extrapolate the mass signals and the correlated OTUs, which are responsible for the discrimination of the investigated groups, the loadings of the OPLS-DA analysis were extracted. The threshold for the representative mass signals and correlated OTUs was adjusted individually for the groups and set when further extension did not result in a meaningful change in the van Krevelen diagram. Similarly, the correlating mass signals with the four major geochemical variables which define the ecosystem, were more appropriately extracted with the evaluation of the coefficients, of the OPLS. The

coefficients are related to the centered and scaled data (CoeffCS) and they are computed from all significant extracted components. They summarize the relationship between Y (geochemical variables) and the X matrix (mass signals and OTUs).

3.4. Results and discussion

3.4.1. Groundwater geochemistry and occurrence of (parent) contaminants

Biogeochemical gradients and distribution patterns of major contaminants provide critical information on the redox processes involved in transformation of contaminants and active biodegradation pathways (Meckenstock et al. 2015). Typically, biodegradation in organic contaminant plumes in porous aquifers is most pronounced at the plume fringes as repeatedly confirmed by (1) steep and opposing gradients of contaminants and electron acceptors such as sulfate, (2) peaking of the metabolic end products sulfide and Fe(II) from sulfate and iron reduction, respectively, and (3) bacterial cell counts and contaminant specific stable carbon isotope values at the plume fringes (Anneser et al. 2008a, Bauer et al. 2008, Meckenstock et al. 2015).

Water samples collected from the petroleum hydrocarbon contaminated aquifer in Düsseldorf Flingern showed steep small-scale gradients for BTEX and naphthalene as the major contaminants (Figure 3-3). The contaminant plume, at the time of sampling, was located at the groundwater table extending to 0.8 m beneath (6.51–7.31 m below land surface (bls)). According to the scheme of Anneser et al., the contaminant plume was subdivided into three compartments (Figure 3-3) (Anneser et al. 2008b). First, the upper plume fringe (6.51–6.61 m bls) was bound at the upper side by the groundwater table including the capillary fringe, which was located right above the groundwater table and only partially filled with water. Second, the plume core was defined as the zone exhibiting BTEX concentrations >50% of the observed maximum of 616 µmol L^{-1} (6.61–7.01 m bls). Third, the lower plume fringe located below the plume core, extended from 7.01–7.31 m bls. The depths below 7.31 m bls is referred to as the deep zone.
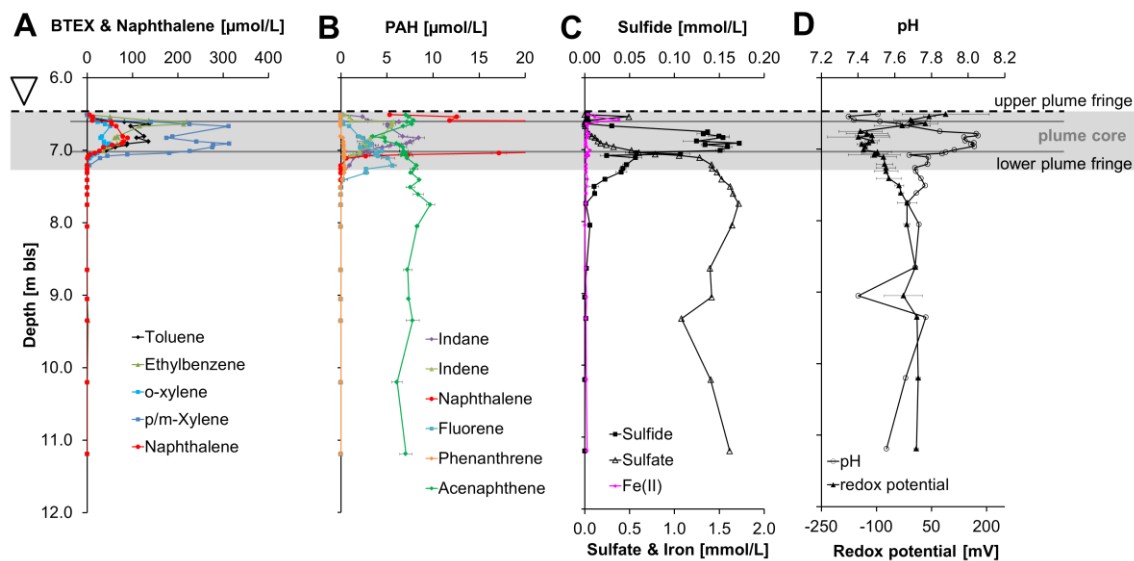
Figure 3-3: Vertical profiles of the main contaminants and hydrochemical parameters.
Vertical concentration profiles of main contaminants A) BTEX and B) PAHs, C) sulfide, sulfate and Fe(II) as well as D) the hydrochemical parameters pH and redox potential (depth in m below land surface (m bls)). The black dashed line depicts the groundwater table. Values represent single or means of duplicate and triplicate measurements (error bars depict standard deviations), respectively. The assumed contamination plume is highlighted in gray and the plume core defined by >50% of the maximal BTEX concentration is depicted by the solid gray line. Reprinted with permission from (Dvorski et al. 2016). Copyright (2016) American Chemical Society.

PAHs, in particular naphthalene, exhibited a high abundance (maximum of 89.5 µmol L^{-1} at 6.78 m bls) in the plume core (Figure 3-3A, B). The three-ring PAHs exhibited the highest abundances ~0.3 m deeper (Figure 3-3A, B). Acenaphthene was present at approximate concentrations of 7 µmol L^{-1} all along the sampled vertical profile (Figure 3-3B). Previous studies at this site had shown a comparable distribution of the major contaminants, however, with slightly different concentrations of the individual compounds (Anneser et al. 2008a, Anneser et al. 2008b).

Redox potentials between +89 mV at the groundwater table and −149 mV in the plume core indicated strictly anoxic conditions except for the capillary fringe (Figure 3-3D). The pH profile showed elevated values of up to pH 8.05 in the plume core (Figure 3-3D). Sulfate as the predominant electron acceptor was almost absent in the plume core and showed a steep counter gradient to the major contaminants at the lower plume fringe. Outside of the contaminant plume, sulfate exhibited a rather constant high concentration of approximately 1.5 mmol L^{-1} (Figure 3-3C). Hence, hydrocarbon degradation was sulfate-limited in the plume core. Sulfide peaked at concentrations of up to 0.17 mmol L^{-1} in the plume core and lower plume fringe, indicating a hot spot of sulfate reduction

between 6.75 and 7.21 m bls. The discrepancy between the amount of sulfate reduced within the contaminated area and the free sulfide detected in the water is explained by precipitation of reduced sulfur with iron as well as incorporation of reduced sulfur into DOM (see paragraphs 3.4.2.1and 3.4.3). As already shown in previous studies (Winderl et al. 2008, Anneser et al. 2008a, Anneser et al. 2008b, Anneser et al. 2010), sulfate reduction was the key redox process involved in biodegradation of organic contaminants in the Düsseldorf Flingern aquifer. However, in contrast to earlier surveys, sulfate, sulfide, and BTEX profiles indicated biodegradation by sulfate reduction taking place not only at the lower plume fringe but also in parts of the plume core. These changing patterns may be related to temporal dynamics of contaminant concentrations and biodegradation activities as evaluated by contaminant-specific stable isotope analysis (CSIA) and microbial community analysis (unpublished data). Extraordinary high Fe(II) concentrations of up to 0.38 mmol L^{-1} were found close to the groundwater table, thereby hinting, in accordance with previous studies (Anneser et al. 2008a), at iron reduction to be a relevant redox process at the upper plume fringe.

3.4.2. DOM characteristics in an petroleum hydrocarbon contaminated aquifer

For a comprehensive analysis of the petroleum hydrocarbon contaminants influence on DOM characteristics (–)ESI and (+)APPI FT-ICR-MS, NMR, and EEM fluorescence spectroscopy of SPE-DOM sampled spatilly highly resolved across the vertical plume transect was performed.

3.4.2.1. Ultrahigh resolution mass spectrometry of DOM

(–)ESI FT-ICR-MS of DOM

(–)ESI FT-ICR-MS spectra from SPE-DOM showed distinct compositional variation along the aquifer (Figure 6-4). However, this variation is hardly visible from the ring charts depicting the elemental composition (CHO, CHNO, CHOS and CHNOS), van Krevelen and m/z-resolved H/C atomic ratios of the (–)ESI FT-ICR-MS derived molecular formulas of four representative SPE-DOM samples from the four zones, i.e. upper plume fringe, plume core, lower plume fringe, and deep zone, introduced in paragraph 3.4.1. (Figure 6-5). Therefore, hierarchical cluster analysis was performed to group the samples according to their resemblance and to identify the major differences of the molecular DOM composition along the vertical plume transect. The analysis

confirmed that sample similarity followed spatial proximity and revealed three distinct subclusters, 6.51–6.64 m bls, 6.67–7.06 m bls, and 7.08–10.20 m bls (Figure 3-4A). The cluster formation resembles in the broadest sense the defined zones, although especially the lower plume fringe was not resolved by the hierarchical cluster analysis. The extensive chemical dissimilarity between the subclusters is depicted in Figure 3-4B. The van Krevelen diagrams and ring charts display the most representative molecular formulas (correlation coefficient r > 0.9) for each subcluster (cf. 3.3.4).
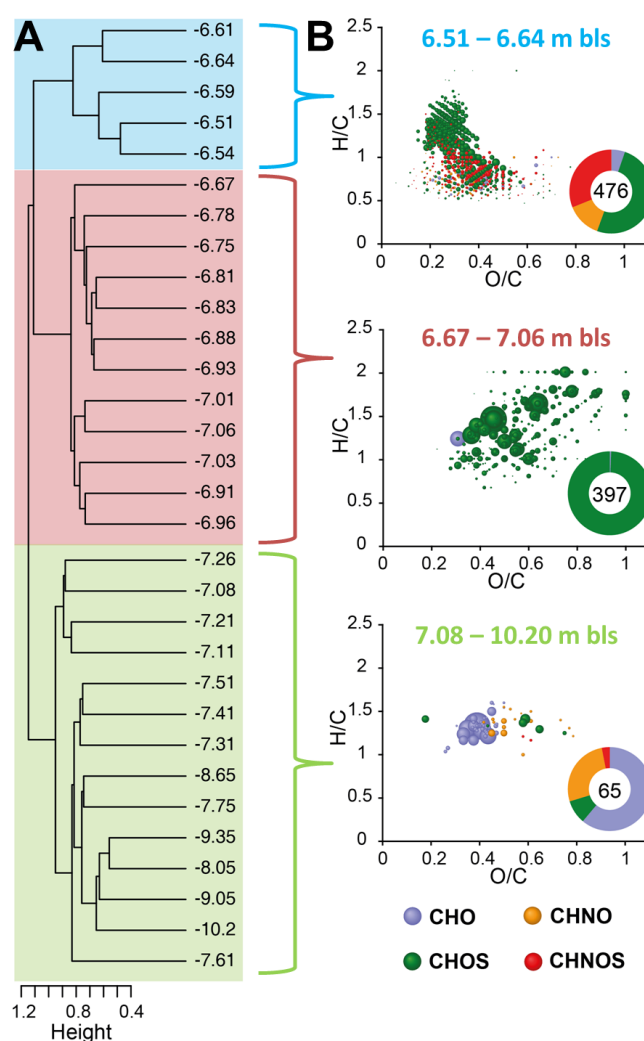
Figure 3-4: Characteristic (–)ESI FT-ICR-MS derived molecular formulas elaborated by hierarchical cluster analysis.
A) Hierarchical cluster analysis of the assigned (–)ESI FT-ICR-MS derived molecular formulas observed in SPE-DOM along the aquifer with samples named according to their sampling depth (bls = below land surface). B) Van Krevelen diagrams depict the most representative characteristic molecular formulas (correlation coefficient > 0.9; cf. 3.3.4) for the three main subclusters, representing the specific DOM chemistry. The bubble area depicts the mean mass peak intensity within the respective subcluster. Reprinted with permission from (Dvorski et al. 2016). Copyright (2016) American Chemical Society.

64

The differences between (–)ESI FT-ICR mass spectra of the SPE-DOM isolates corresponded to the respective prevailing and clearly distinct zone-dependent redox chemistry (Figure 3-3, Figure 6-4). The specific DOM chemistry in the upper part of the aquifer, including the upper plume fringe, plume core, and 5 cm of the lower plume fringe (cf. blue and red subcluster, Figure 3-4), was dominated by sulfur organic molecules. This was also shown by increased abundance of CHOS molecular formulas in a single nominal mass depicted in (Figure 6-7) and is in agreement with sulfate reduction being the major redox process in the plume and its fringes (Anneser et al. 2010). The samples from 6.67–7.06 m bls (red subcluster, Figure 3-4) were dominated by CHOS compounds with a contribution to the total intensity of assigned molecular formulas of up to 52% (Figure 3-5A). This was most likely a result of high sulfide concentrations in these depths generated by sulfate reduction (Figure 3-3C). The relative proportion of CHO compounds from 6.67–7.06 m bls decreased (Figure 3-5A), thus, indicating that CHOS compounds were formed from CHO compounds.

The characteristic mass peaks of SPE-DOM from the below 7.08 m bls showed mainly CHO and CHNO compounds in the polyphenolic region of the van Krevelen diagram (1.5 > H/C > 0.7 and 0.7 > O/C > 0.1) (Figure 3-4B). Hence, DOM characteristics of less contaminated deep zone groundwater showed similarities to previously published (–)ESI FT-ICR-MS results of groundwater DOM (Einsiedl et al. 2007, Longnecker and Kujawinski 2011). The comparably low number of characteristic mass peaks for deep zone SPE-DOM arose from the fact that these samples represented general DOM patterns of the sampling site, which was only marginally impacted by petroleum contaminants, degradation products, and intense sulfur redox chemistry.
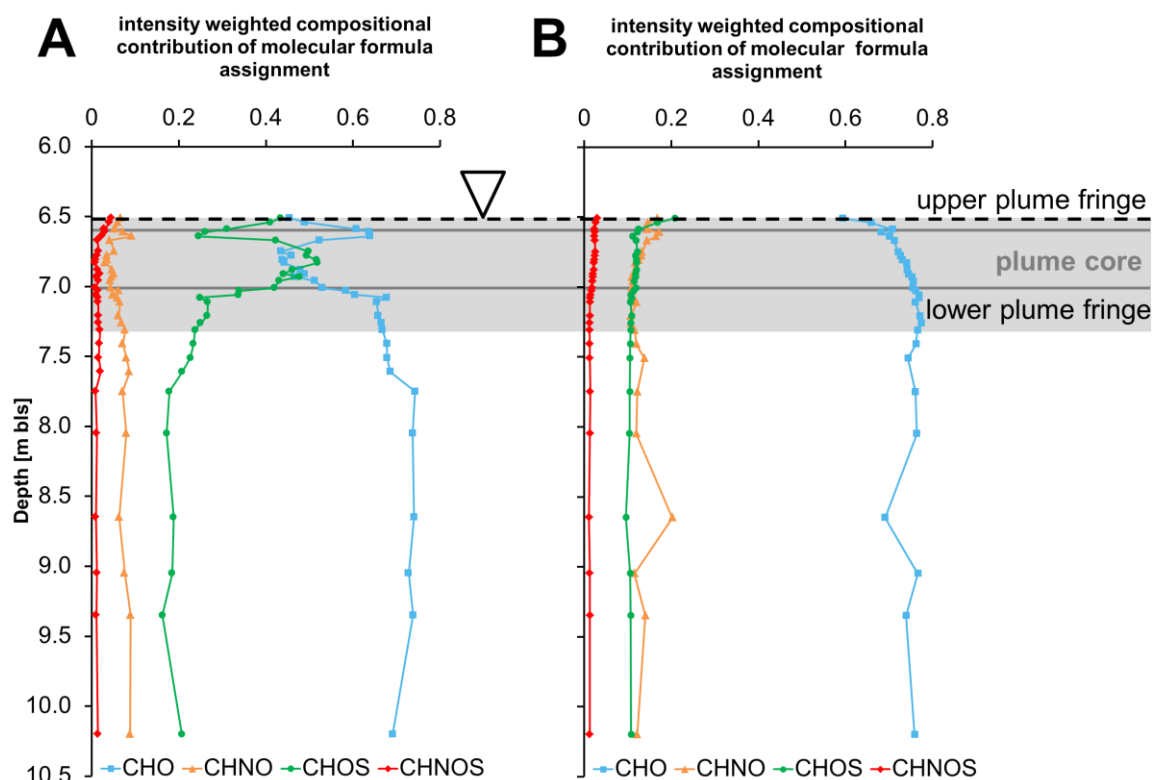
Figure 3-5: Vertical profile of FT-ICR-MS derived molecular formulas.
A) (–)ESI and (B) (+)APPI FT-ICR mass spectra derived intensity weighted compositions of assigned molecular formulas showed increased contribution of CHOS and decreased CHO compounds in the highly sulfidic region from 6.67–7.06 m bls in (–)ESI FT-ICR mass spectra. (+)APPI FT-ICR mass spectra did not show this trend, thereby suggesting that CHOS compounds were formed from highly functionalized CHO molecules of the natural DOM pool as a result of bacterial sulfate reduction. Reprinted with permission from (Dvorski et al. 2016). Copyright (2016) American Chemical Society.

Natural DOM, which is preferably characterized with (–)ESI FT-ICR-MS, was highly effected by bacterial sulfate reduction and the prevailing distinct zone-dependent redox chemistry. Therefore, further data elaboration and multi-data correlation based on the (–)ESI FT-ICR-MS derived molecular formulas from DOM, bacterial community data as well as geochemical and contamination properties was performed. This analysis, detailed in paragraph 3.4.3, enabled an enhanced discussion of the linkage between the abiotic and biotic processes contributing to the DOM characteristics of the specific zones.

(+)APPI FT-ICR-MS of DOM

(+)APPI is the method of choice for the detection of molecules with extended, conjugated π-electron systems such as petroleum contaminants and their degradation products (Sleighter and Hatcher 2011). As an effect of the sample preparation, which was not optimized for the extraction of nonpolar contaminants but for DOM extraction, a mere

6% of the annotated molecular formulas of the whole data set were oxygen-free molecules. Therefore, only the results of the oxygen containing CHNOS molecular formulas are presented and discussed.

Hierarchical cluster analysis of (+)APPI FT-ICR mass peaks and the associated van Krevelen diagrams of characteristic molecular formulas of the subclusters showed that all samples above 7.06 m bls were dominated by aromatic and even condensed aromatic molecules (low H/C and O/C ratios) (Figure 3-6B, C). These molecules are typically derived from petroleum, thus the segmentation of the cluster was clearly driven by the elevated contamination input in the top ~50 cm beneath the groundwater table (6.54 m bls). Furthermore, (+)APPI FT-ICR-MS showed that a large proportion of characteristic formulas were sulfur organic compounds, which was in accordance with the (−)ESI FT-ICR-MS results and the intensive bacterial sulfate reduction (Figure 3-6B, C) (Anneser et al. 2010, Einsiedl et al. 2015). However, the intensity-weighted contribution of assigned molecular formulas did not show any clear trend in the highly sulfidic region (Figure 3-5B). Thus, CHOS compounds formed as a result of bacterial sulfate reduction were proposed to derive from highly functionalized DOM molecules (i.e. carboxylic acids, carbonyl derivatives, alcohols,…), which have a greater (−)ESI ionization efficiency (Sleighter and Hatcher 2011).

On the contrary, SPE-DOM isolates from the deeper zone of the aquifer were characterized by a large combined abundance (greater 80% of the overserved characteristic mass peaks describing the overall diversity) of CHO and CHNO compounds with $1.5 > H/C > 1$ and $0.6 > O/C > 0.2$ (Figure 3-6C); therefore, corresponding to APPI FT-ICR mass spectra of DOM from previous studies (Hertkorn et al. 2008, D'Andrilli et al. 2010). This implied that DOM from the lower fringe and below was presumably not heavily affected by the contamination and its degradation products at the time of sampling.
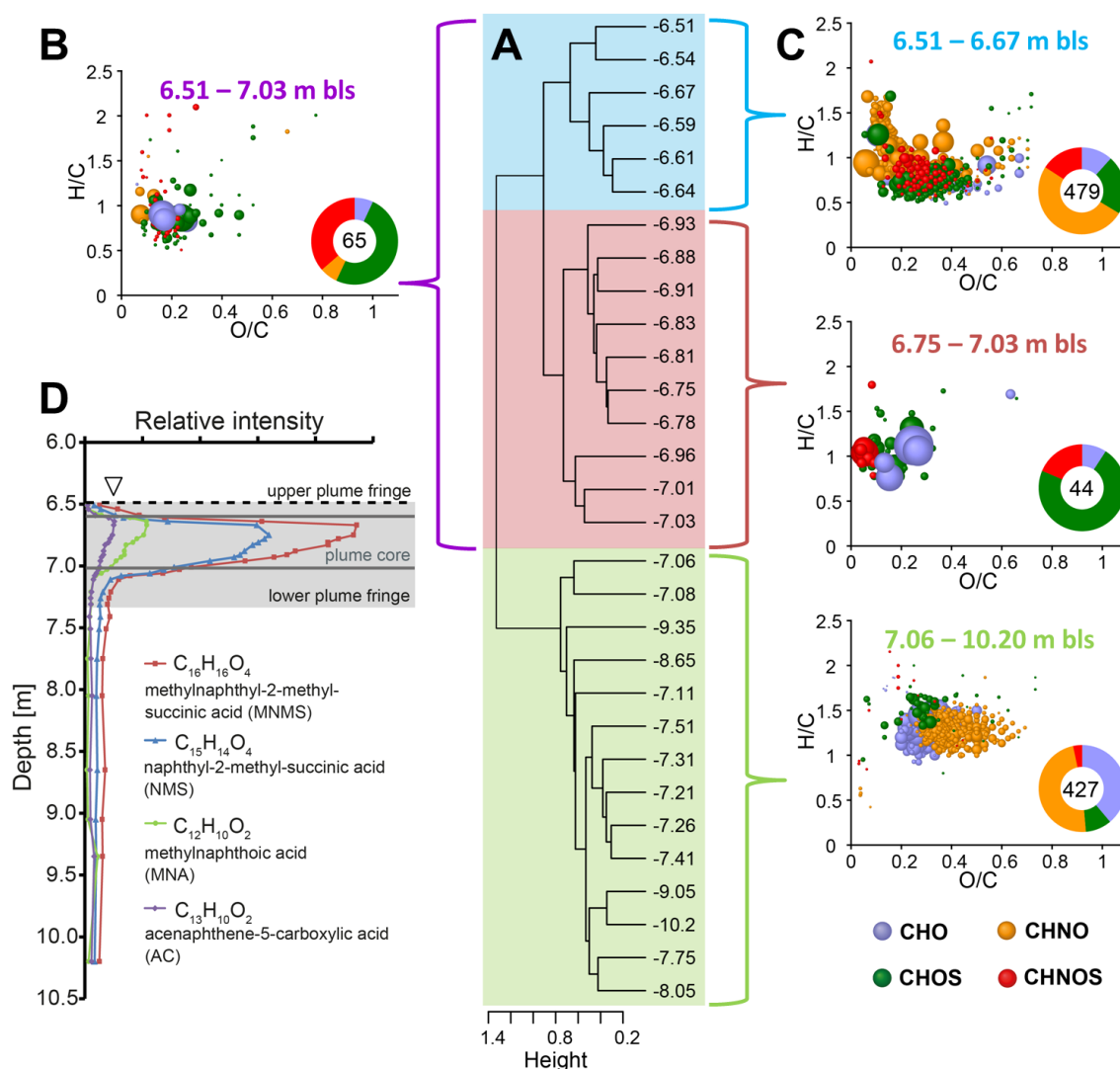
Figure 3-6: Characteristic (+)APPI FT-ICR-MS derived molecular formulas elaborated by hierarchical cluster analysis.
A) Hierarchical cluster analysis of the assigned (+)APPI FT-ICR-MS derived molecular formulas observed in SPE-DOM along the aquifer with samples named according to their sampling depth. B) Van Krevelen diagram of shared characteristic molecular formulas of the two upper subclusters, which were highly affected by the contamination plume and C) van Krevelen diagrams of the characteristic molecular formulas for the three main subclusters representing the specific SPE-DOM chemistry. The bubble area depicts the mean mass peak intensity within the respective subcluster. Note that the size of the three and four most abundant CHO (blue) bubbles of the purple B) and red subcluster (C) had to be down-sized because of their very high mass peak intensity. D) (+)APPI FT-ICR-MS derived abundance profile of main petroleum contamination degradation products. Reprinted with permission from (Dvorski et al. 2016). Copyright (2016) American Chemical Society.

Field and culture degradation studies of BTEX, PAHs and heteroatom PAHs at the same or similar conditions were able to identify typical degradation products (Annweiler, Michaelis and Meckenstock 2001, Martus and Puttmann 2003, Griebler et al. 2004, Safinowski, Griebler and Meckenstock 2006, Jobelius et al. 2011, Jarling et al. 2015). Due to the high accuracy in molecular formula annotation combined with the profound

68

literature knowledge, the respective mass peaks most probably derive from these known degradation products. Figure 3-6D shows the relative mass peak intensities for the four highest abundant putative degradation products originating from BTEX, PAHs and heteroatom PAHs as well as their methylated relatives methylnaphthyl-2-methylsuccinic acid (MNMS, $C_{16}H_{16}O_4$), naphthyl-2-methyl-succinic acid (NMS, $C_{15}H_{14}O_4$), methylnaphthoic acid (MNA, $C_{12}H_{10}O_2$), and acenaphthene-5-carboxylic acid (AC, $C_{13}H_{10}O_2$). The depth profile was in accordance with the distribution of plume marker compounds, hydrochemical parameters, and redox chemistry markers (Figure 3-3, Figure 3-6D). Moreover, MNMS, NMS, AC, and an unknown compound ($C_{15}H_{12}O_2$) represented the highly abundant characteristic masses of the 6.75 to 7.03 m bls subcluster (Figure 3-6C). Hence, the initial steps of biodegradation, which have been identified in previous degradation studies (Annweiler et al. 2001, Martus and Puttmann 2003, Griebler et al. 2004, Safinowski et al. 2006, Jobelius et al. 2011, Jarling et al. 2015), were mainly located in the lower part of the plume core where bacterial sulfate reduction was highly active.

3.4.2.2. EEM fluorescence spectroscopy of DOM

EEM-PARAFAC modeling was validated for a three component model and the relative contribution of each component was identified for the SPE-DOM samples taken along the aquifer (Figure 3-7, Figure 7-1, Figure 7-2). The first component (C1) showed an excitation/emission (Ex/Em) maximum at 237(288)/360 nm, which was similar to the PARAFAC components modeled in *Deepwater Horizon* oil spill studies (Zhou and Guo 2012, Zhou et al. 2013, Mendoza et al. 2013) resembling oil and its degradation products as well as BTEX- and PAH-like fluorescence (Table 6-4) . The second component (C2) identified at an Ex/Em maximum of 255(315)/420 nm, which was in accordance with humic-like fluorescence, has been found in many PARAFAC studies on organic matter (Coble 1996, Ishii and Boyer 2012, Huang et al. 2015). Also, PARAFAC studies on the *Deepwater Horizon* oil spill showed similar components, which are described as humic-like therein (Table 6-4) (Zhou and Guo 2012, Zhou et al. 2013, Mendoza et al. 2013, Bianchi et al. 2014). The third component (C3) exhibited its Ex/Em maximum at 255/333 nm matching previously published components that were reported as oil, BTEX, and PAH related (Table 6-4) (Zhou and Guo 2012, Mendoza et al. 2013).

High bacterial activity was expected to show protein-like fluorescence, however this signal was absent from zones of highly active sulfate reducing bacteria. In fact, the typical

protein-like fluorescence has never been observed under anoxic conditions from sulfate reducing bacteria but has often been associated with aerobic heterotrophic bacteria (Yang, Hur and Zhuang 2015). At this point, it is not clear why anaerobic conditions would prevent the release of water soluble proteins that contain tyrosine and/or tryptophan. Furthermore, Wang et al. showed significant quenching of tyrosine and tryptophan fluorescence as well as shift of the peak position in the presence of humic substances (Wang, Cao and Meng 2015).

To distinguish fluorescence spectra of SPE-DOM dominated by contamination-related versus typical DOM fluorescence, PCA of Fmax values of the components was performed (Figure 3-7). PCA revealed that SPE-DOM from 6.59–6.96 m bls were mainly driven by C1, which was annotated to oil, BTEX and, PAH, in addition to its degradation products. The samples from 7.01–7.21 m bls showed a strong correlation with C3, which was also described as oil, BTEX, PAH, and its degradation products. Therefore, C3 fluorescence most likely derived from further degraded products and three-ring PAHs that were more abundant in this region (Figure 3-3B). Samples in close vicinity of the groundwater table and the ones from the deep zone (highlighted in green, Figure 3-7B) were characterized by C2, showing that their fluorescence was humic-like and not strongly affected by the contamination. The ratios of C1/C2 and C3/C2, which indicated oil/humic contributions to SPE-DOM composition, were elevated for the samples ranging from 6.61–7.08 m bls. Therefore, EEM fluorescence spectroscopy also successfully differentiated SPE-DOM influenced by the contamination plume.
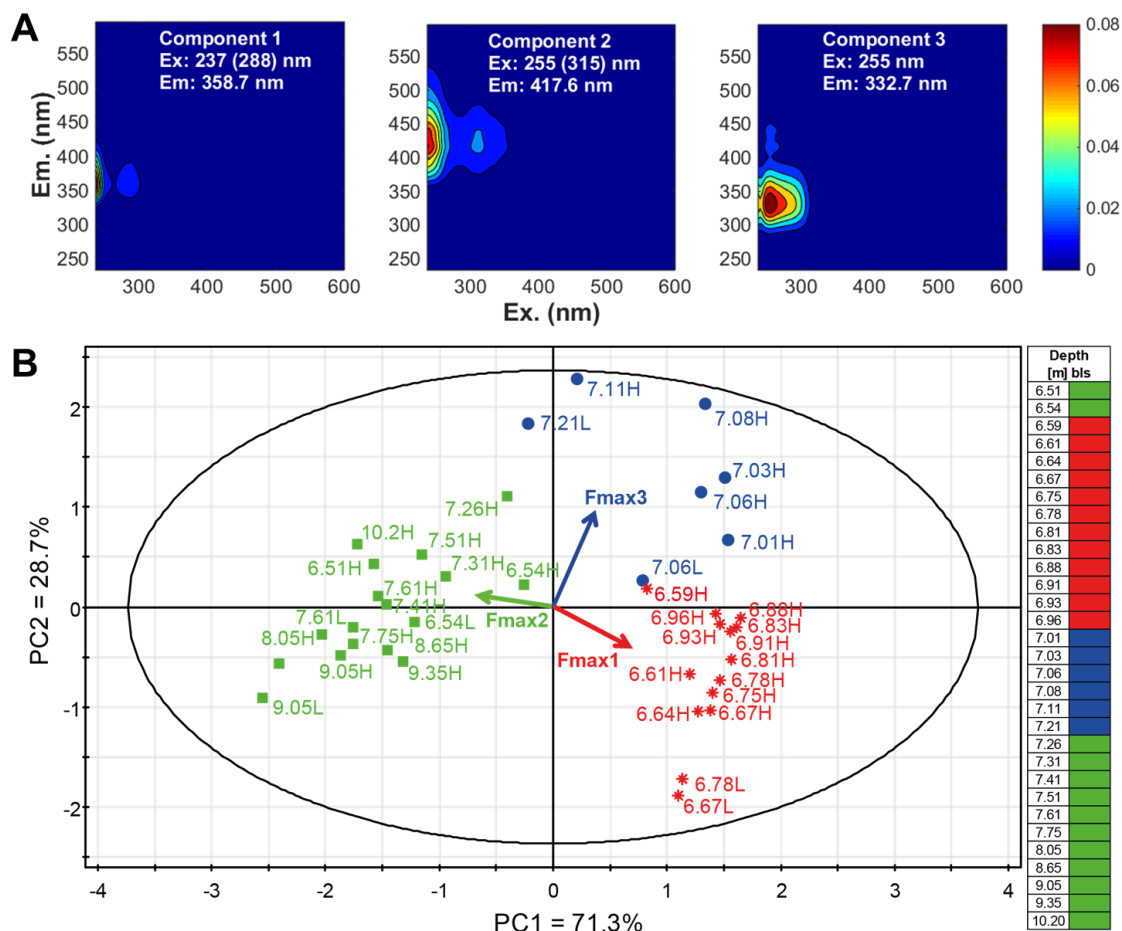
Figure 3-7: PARAFAC components and PCA.
A) EEM fluorescence spectra of three PARAFAC-derived components C1–C3. B) PCA of SPE-DOM along the aquifer based on the Fmax values of the PARAFAC components. Samples are labeled according to their sampling depth in m bls. H corresponds to 250 mL samples, and L corresponds to 1 L samples. Reprinted with permission from (Dvorski et al. 2016). Copyright (2016) American Chemical Society.

3.4.2.3. NMR spectroscopy of DOM

^{1}H NMR spectra (Figure 3-8A) of selected SPE-DOM sampling positions that were indicative of changing geochemical parameters and contamination levels provided detailed structural information and substantial variance according to zonation (Figure 3-3). These variations at first indicated variable contributions of common bulk DOM with broad NMR resonances and of petroleum degradation products showing sharp NMR resonances with well resolved splittings from J-couplings (Figure 3-8). The ^{1}H NMR section integrals according to DOM substructures depicted by the bar charts (Figure 3-8B) are also shown in Table 6-5 and Table 6-6. Furthermore, Table 6-7 encloses detailed description of key structural units of observed DOM and petroleum degradation products.
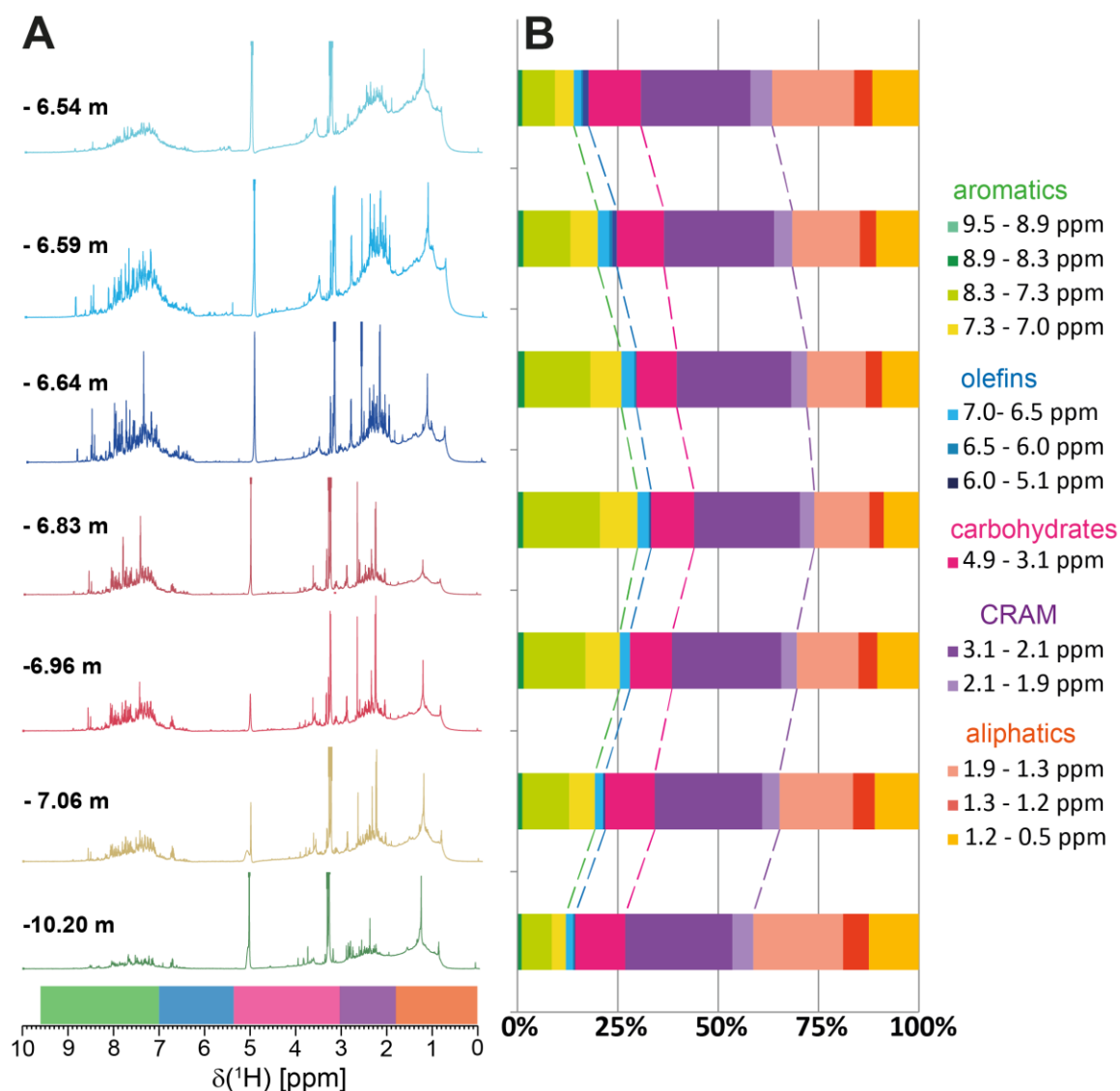
Figure 3-8: ^{1}H NMR spectra of selected SPE-DOM along the aquifer.
A) ^{1}H NMR spectra (800 MHz, CD$_3$OD) of selected SPE-DOM with depth provided and color coded according to similarity of contamination patterns and geochemical parameters. B) Bar charts indicate relative ^{1}H NMR section integrals according to substructures shown in Table 6-5 and Table 6-6, whereby the main structural sections are depicted with dotted lines. Reprinted (adapted) with permission from (Dvorski et al. 2016). Copyright (2016) American Chemical Society.

In general, the relative contribution of aromatic structures ($\delta(^1$H) = 9.5–7.0 ppm) ranged up to 30% in the plume core and fringes, while it was below 15% for SPE-DOM close to the groundwater table (6.64 m bls) and the deep zone (10.20 m bls) (Table 6-6). Figure 6-9 depicts overlaid ^{1}H NMR spectra adjusted to common amplitude of the aliphatic bulk DOM signature ($\delta(^1$H) = 0.8–2.0 ppm; Figure 6-9A) and alternatively area-normalized ^{1}H NMR spectra across the entire range of chemical shifts ($\delta(^1$H) = 0.5–9.5 ppm; Figure 6-9B). Hence, ^{1}H NMR spectra clearly showed a nearly constant but somewhat variable

background bulk DOM signature present in all SPE-DOM and highly variable proportions of PAH and its degradation products.

In particular, not only the ratios of aromatic protons ($\delta(^1H) > 7$ ppm) and those of HOOC-C$_\alpha$**H**-protons ($\delta(^1H) \sim 2.1$–2.7 ppm) differed quite substantially, but the line shapes within these sections of chemical shifts also greatly differed. This demonstrated a huge variance of PAH-degradation products present at each individual depth of sampling. As the petroleum contamination arose mainly from BTEX and naphthalene, only a very small percentage of the NMR total integral derived from multi (>3) ring condensed aromatics with $\delta(^1H) > 8.3$ ppm. Most of the aromatic structures were found in the chemical shift region $\delta(^1H) = 8.3$–7.3 ppm, which was indicative of single and two-ring aromatics, six membered N-heterocycles, and especially oxidized aromatics (i.e., mainly polycarboxylated). These types of structural features were in general matching the contaminants and their degradation products (Griebler et al. 2004, Jobelius et al. 2011). The two SPE-DOM from the top and bottom of the aquifer, while assumed representative of common groundwater DOM, nevertheless showed elevated proportions of petroleum derivatives compared to pristine DOM levels (Einsiedl et al. 2007). This background concentration was drastically increased in the plume core, and the co-occurrence of contaminants and their degradation products was confirmed by co-occurring sharp NMR resonances at $\delta(^1H) > 7$ ppm (aromatics) and $\delta(^1H) \sim 2.1$–2.7 ppm (aliphatic carboxylic acids). Additionally, J-resolved (JRES) and total correlation (TOCSY) spectroscopy indicated the presence of multiring polycyclic aromatic compounds. Most of them showed two rings (cf. Figure 6-10), in accordance with common composition of groundwater contamination by petroleum products (Anneser et al. 2008a, Anneser et al. 2010). Furthermore, aliphatic cross peaks in TOCSY and methylene-edited ^1H, ^{13}C distortion less enhanced by polarization transfer heteronuclear single quantum coherence (DEPT HSQC) NMR spectra showed typical DOM signatures as well as succinic acid side chains attached to aromatics (cf. Figure 6-11) that are typical for PAH degradation products such as NMS, which were also detected in the (+)APPI FT-ICR mass spectra (Figure 3-6D) (Griebler et al. 2004, Safinowski et al. 2006, Jarling et al. 2015, Jobelius et al. 2011). The proportion of non-functionalized monoaromatic structures ($\delta(^1H) = 7.3$–7.0 ppm) was lower but might be underestimated because of losses during the sample preparation as a consequence of their high volatility.

The region $\delta(^1H) = 7.0–6.5$ ppm of $C_{sp2}\underline{\textbf{H}}$ likely originated from OH and OR substituted aromatics of common SPE-DOM and partially indicated aromatics with fused alicyclic units, which are constituents of partly biodegraded mineral oil (Meckenstock et al. 2014). Otherwise, conjugated ($\delta(^1H) = 6.5–6.0$ ppm) and isolated double bonds ($\delta(^1H) = 6.0–5.1$ ppm) likely represented natural product derivatives present in groundwater SPE-DOM.

The slight depletion of carbohydrates ($\delta(^1H) = 4.9–3.1$ ppm) in SPE-DOM from depths with high contamination levels might be an artifact of the sample preparation as PPL cartridges discriminate against carbohydrates (Hertkorn et al. 2013). Also, the region of carboxyl-rich alicyclic molecules (CRAM) from $\delta(^1H) = 3.1–1.9$ ppm showed no clear trend because of the interference of CRAM and contamination degradation products.

Contaminant abundance and that of 'original' SPE-DOM signatures were inversely related across the aquifer (cf. Figure 6-9B, radar diagram). However, the region of non-functionalized aliphatics (CCC$\underline{\textbf{H}}$; $\delta(^1H) = 1.9–0.5$ ppm), a major contributor of common SPE-DOM (Hertkorn et al. 2013), maintained its core integrity with limited but clearly recognizable variance (Figure 3-8A) across the entire range of sampling.

3.4.3. Effects of petroleum hydrocarbon degradation by bacterial sulfate reduction on DOM

The above presented results demonstrated that the DOM characteristics were highly affected by bacterial sulfate reduction. Both (+)APPI FT-ICR-MS, which favors the detection of petroleum derived compounds, and (–)ESI FT-ICR-MS, which is preferably applied for the characterization of natural DOM and metabolites, revealed characteristic CHOS compounds at the depths where sulfate reduction is active. Organosulfur compounds were found by far more abundant in the (–)ESI FT-ICR mass spectra in which CHOS compounds represented >50% of the total mass peak intensity of the corresponding assigned molecular formulas in the zone with maximum sulfide concentrations (Figure 3-5). Thus, formation of sulfur compounds as result of bacterial sulfate reduction mainly occurred in the natural DOM pool (Figure 3-5). Hence, the molecular formulas from (–)ESI FT-ICR-MS were selected to study the correlation of the DOM characteristics, bacterial community data as well as the geochemical and contamination. This multi-data correlation enabled to study the effects of bacterial sulfate reduction on the DOM composition of the specific zones in detail.

3.4.3.1. Performance and results of the multi-data correlation

Unsupervised statistics (e.g. hierarchical cluster analysis cf. Figure 3-4) showed similar grouping of the samples according to the zones, i.e. upper fringe, plume core and lower fringe, defined by Anneser et al. (Anneser et al. 2008b) and introduced in paragraph 3.4.1., which was extend with the deep zone not particularly affected by the contaminants and their biodegradation (cf. 3.4.2). Hence, the classification of the OPLS-DA model was based on this zone definition (Table 7-5) and the samples in between zones, named transition, were not considered for the OPLS-DA model. By this OPLS-DA model the relation between the 4 different zones and the OTUs together with the mass signals was investigated.

The score plot of the OPLS-DA model revealed a clear separation of the samples according to the four distinct zones of the aquifer (Figure 3-9A, B). The extraction of the representative variables for the four zones was based on the CoeffCS (cf. methods section 3.3.8). The threshold was adapted individually for each group and set when further extension did not result in a meaningful change in the van Krevelen diagram. For the representative description of the characteristics of the upper fringe 10.3%, plume core 35.3%, lower fringe 3.2%, and deep zone 12.8% of all variables 15563 (462 OTUs and 15101 DOM mass signals; 15563) were necessary. The zone specific van Krevelen diagrams in conjunction with the ring charts depicting the molecular class (CHO, CHNO, CHOS, CHNOS) contributions are shown in Figure 3-9C-F. Furthermore, plots of the number of carbon, oxygen and hydrogen atoms vs. number of sulfur atoms of the zone specific characteristic CHOS molecular formulas illustrate the clear differences in their chemical composition. The combined loading and score plot including the names, if known in the literature, of the discriminating OTUs are depicted in the Supplementary Information (Figure 6-12).
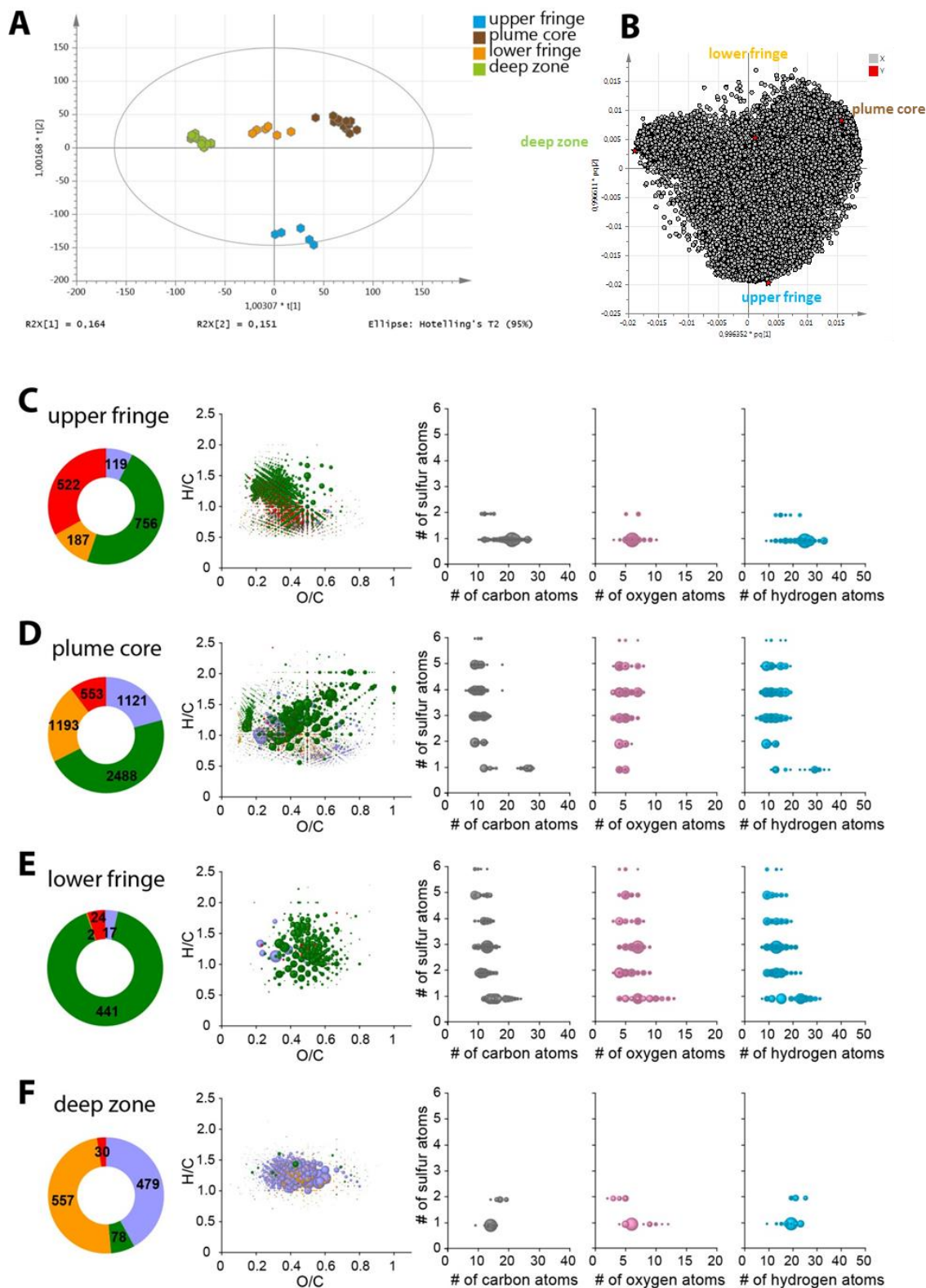
Figure 3-9: OPLS-DA model based on the zones, OTUs and mass signals.
A) Score and B) loading plot of the multi-data (DOM mass signals and OTUs) OPLS-DA model (x-variables: mass signals and OTUs; y-variables (classes): upper fringe, plume core, lower fringe, and deep zone; without transition samples). Representative molecular formulas related to the C) upper fringe, D) plume core, E) lower fringe, and F) deep zone are depicted by ring charts, van Krevelen diagrams and plots of the number of carbon, oxygen and hydrogen atoms vs. number of sulfur atoms of the CHOS molecular formulas.

However, particularly the DOM composition was dependent of the geochemical parameters. As a result of the overlapping presence of sulfide and contaminates (BTEX and PAH) in the plume core, one third of the data set was required to describe the devise characteristics of the plume core. Although the classification of the samples is based on the presented geochemical parameters (cf. paragraph 3.4.1., (Anneser et al. 2008b)), it was not possible to extract the variables particularly correlating with the individual geochemical parameters from the OPLS-DA model, because of the overlapping abundance of the geochemical parameters in the groups (cf. Figure 3-3). As depicted in Figure 3-3 and shown by previous studies (Anneser et al. 2008a, Anneser et al. 2008b, Anneser et al. 2010), it is possible to describe the major characteristic changes along the vertical profile in the contaminated aquifer with a few geochemical and contamination parameters, which were named in the following geochemical variables and were considered in the multi-data correlation. The geochemical variables were, (i) the concentration of the major contaminants, which was used as sum concentrations of BTEX and PAHs, (ii) the redox potential as an indicator for the oxygen saturation (iii) the concentration of dissolved sulfide which is coupled to the pH value, and (iv) the sulfate concentration which is coupled to the total sulfur concentration. PCA of the multi-data (DOM mass signals, OTUs and geochemical variables) already showed a clear separation of the variables depicted in the loading plot (Figure 3-10, left). However, the separation of the variables was further enhanced by the application of OPLS, whereby the geochemical variables were taken as y-variables (Figure 3-10, right). In particular, the OPLS model enabled, by the contribution of the second component, an increased differentiation between sulfate (and total sulfur) and the redox potential, as well as between sulfide (and pH value) and the BTEX (and PAH) geochemical variables (indicated by the arrows; Figure 3-10).
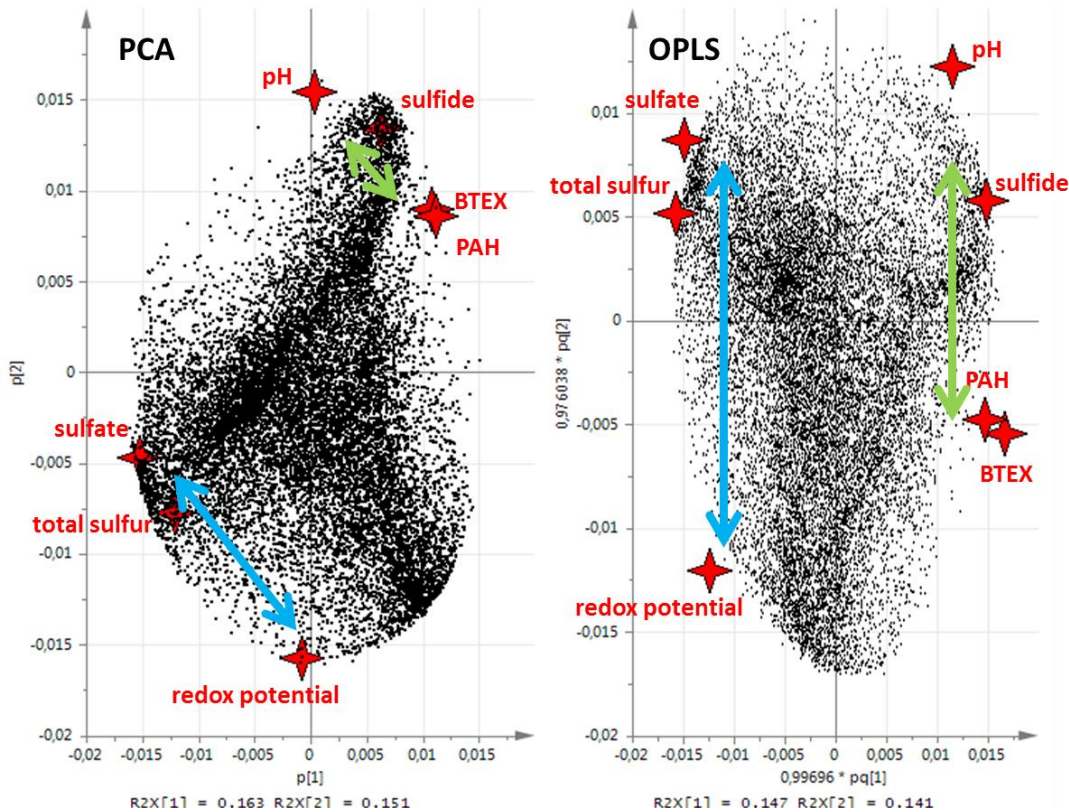
Figure 3-10: Enhanced separation of the variables by OPLS compared to PCA.
Loading plot of the multi-data (DOM mass signals, OTUs and geochemical variables) PCA and OPLS analysis with the increased differentiation between the variables indicated by arrows.

The performed OPLS model was used for the extraction of the representative DOM mass signals correlating with the four major geochemical variables defining the system, namely the redox potential, sulfide, BTEX and sulfate concentration (Figure 3-11B-E). Extraction of the characteristic masses was performed by considering the CoeffCS (cf. paragraph 3.3.8), whereby the characteristic mass signals for the individual geochemical variables represented about 10% of the total data set (redox potential 8.3%, sulfate 8.3%, sulfide 10.0%, and BTEX 9.0%). The score plot of the OPLS model (Figure 3-11A) indicated again the strong relation between the geochemical variables and the zones, since the samples are also separated by the zone considered in the OPLS-DA analysis.
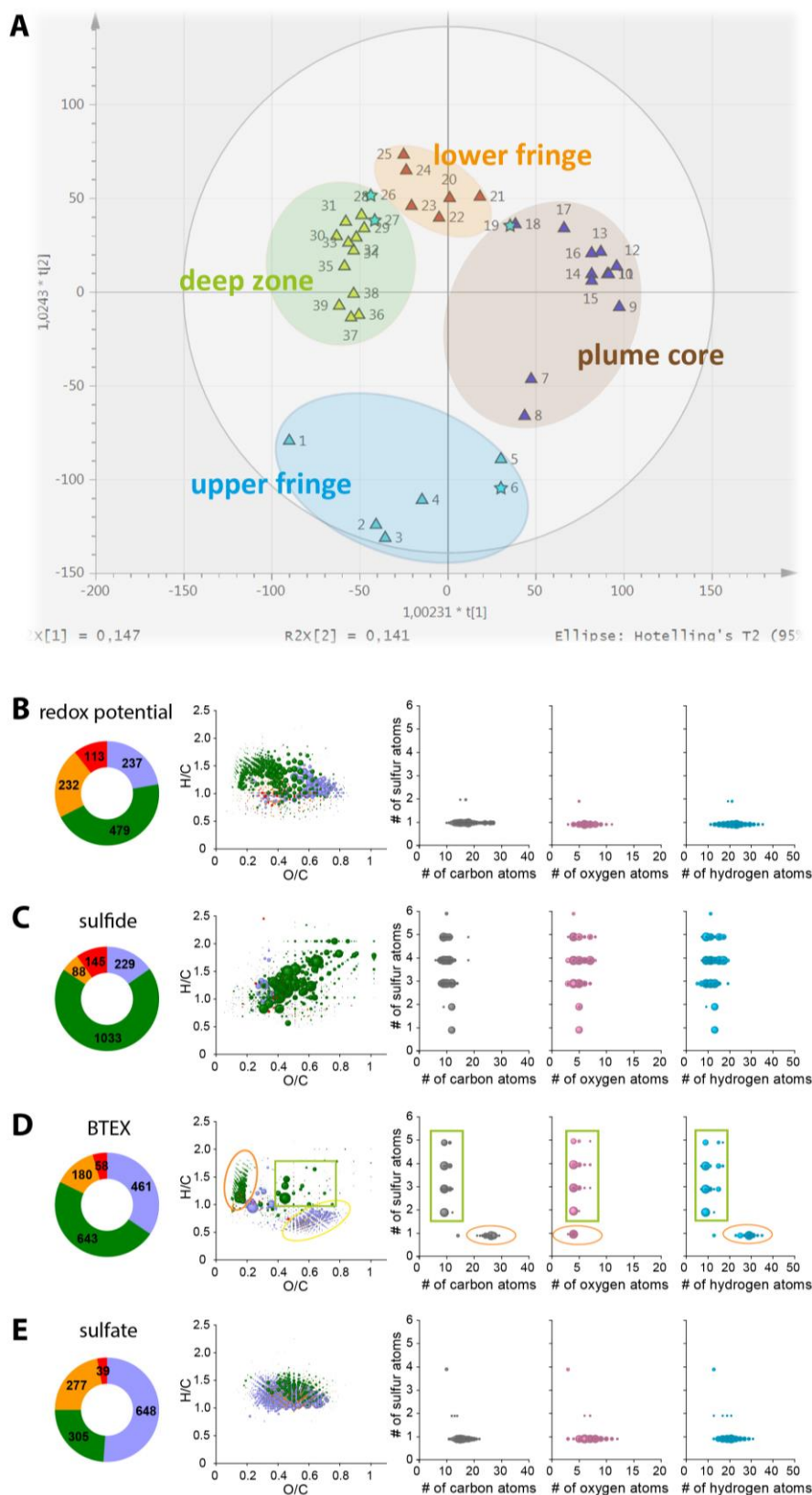
Figure 3-11: OPLS model based on the geochemical variables, OTUs and mass signals.
A) Score plot of the multi-data OPLS (x-variables: DOM mass signals and OTUs; y-variables: 7 geochemical variables). Representative molecular formulas correlating with the B) redox potential, C) sulfide, D) BTEX, and E) sulfate concentration are depicted by ring charts, van Krevelen diagrams and plots of the number of carbon, oxygen and hydrogen atoms vs. number of sulfur atoms of the CHOS molecular formulas.

3.4.3.2. Effects of bacterial sulfate reduction and its linked abiotic processes on DOM

The OPLS-DA model (Figure 3-9A, B) enabled a clear separation of the samples according to the four distinct zones of the aquifer that correspond to the prevailing redox chemistry in the respective zone (Figure 3-3, Figure 6-4).

DOM in the upper plume fringe and the relation to the redox potential

Sulfide concentrations in the upper plume fringe were low because of the supposed dynamic re-oxidation of sulfide to thiosulfate and sulfite close to the capillary fringe (Einsiedl et al. 2015). Indicative for the suboxic conditions were the positive values of redox potential (Figure 3-3D). Hence, the redox potential is most likely the major geochemical parameter influencing the DOM characteristics in the upper fringe. Furthermore, the Fe(II) concentration was elevated in the upper fringe (Figure 3-3C), which likely led to precipitation of sulfide with Fe(II) and implied a dominance of iron over sulfate reduction in this zone (Anneser et al. 2010). Apart from this, multi-data correlation identified bacteria known to be capable of oxidative sulfur cycling to be characteristic for the upper fringe (Figure 6-12). For example, the known sulfide oxidizers of the genera Beggiatoa (Dworkin and Gutnick 2012) or Sulfuritalea were present in the upper fringe, the latter is known to oxidize thiosulfate, elemental sulfur, and sulfite (Watanabe et al 2014). Thus, DOM chemistry in the upper fringe was affected differently compared to the plume core and lower fringe, where bacterial sulfate reduction was the dominant redox process involved in the contaminant degradation. Einsiedl et al. found elevated sulfite concentrations close to the capillary fringe; thus, characteristic CHOS compounds in the upper fringe (Figure 3-9C) potentially resulted from sulfonation reactions (Einsiedl et al. 2015). Sulfonation of organic matter with sulfite was verified by laboratory experiments with model compounds having activated double bonds, such as ethyl acrylate (Vairavamurthy et al. 1994). Indeed, primarily $CHOS_1$ compounds with low O/C ratios were characteristic for the upper plume fringe (Figure 3-9C) and correlated with the redox potential (Figure 3-11B). These compounds potentially derived from sulfonation of petroleum derived carboxylated alkene degradation products. This is corroborated by the MS/MS fragmentation pattern of the high abundant upper plume fringe marker compound $[C_{21}H_{25}O_6S]^-$ (Figure 3-12A, B) which showed the loss of H_2O and CO_2 typical for carboxylic acids and the loss of SO_3 and H_2SO_3 indicative for sulfonic acids (Gross 2011).

Furthermore, the influence of ionizable aromatic molecules (H/C < 1) was high in the upper fringe, thereby indicating fewer degraded contaminants present inside the upper plume fringe, which was likely due to the limited access to electron acceptors (Figure 3-3C) (Anneser et al. 2008a).
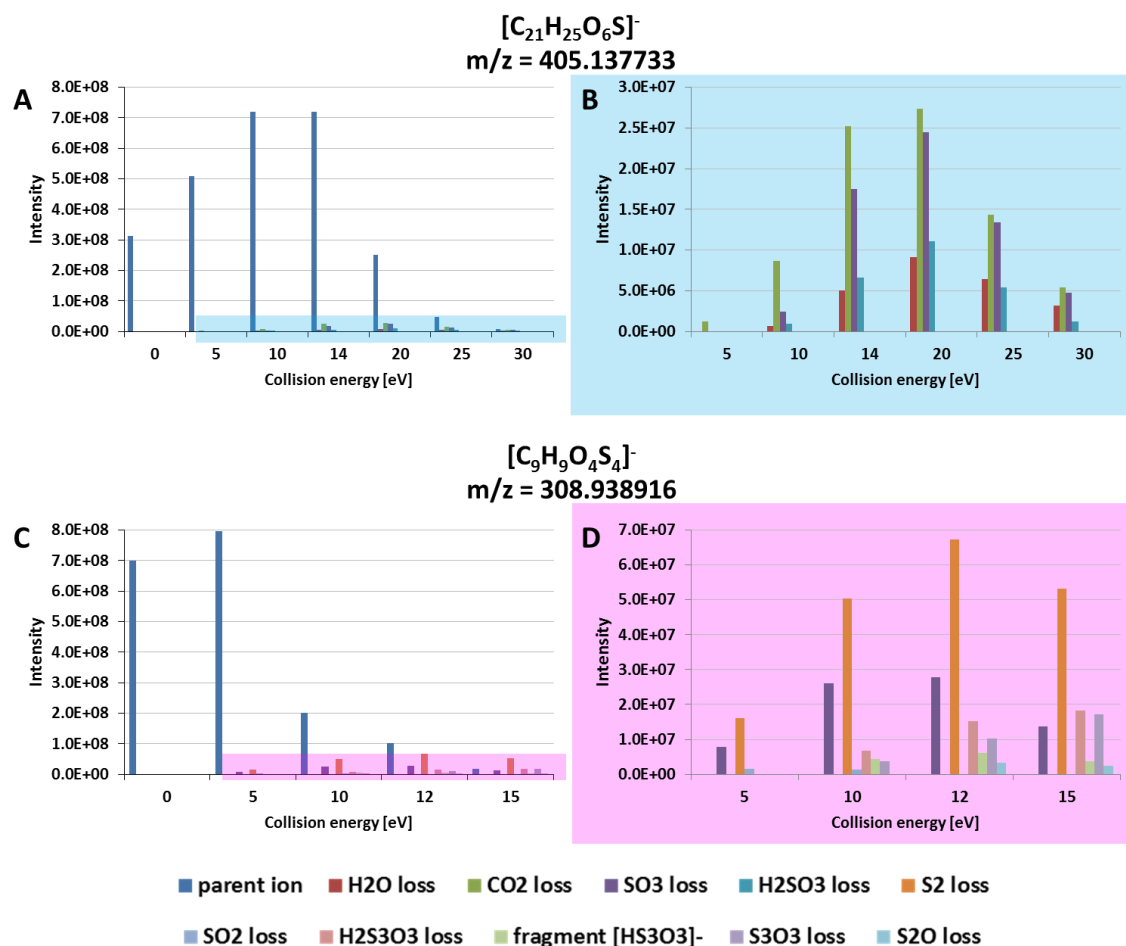
Figure 3-12: Fragment abundance in CID MS/MS spectra of maker compounds.
Bar charts depict fragments found in the CID MS/MS spectra of the highly abundant A, B) upper plume fringe marker compound $[C_{21}H_{25}O_6S]^-$ and C, D) plume core marker compound $[C_9H_9O_4S_4]^-$.

A substantial portion of characteristic CHNO and especially CHNOS compounds suggested significant nitrogen DOM chemistry in the upper plume fringe where dissolved sulfide was almost absent. Analogous to the (−)ESI FT-ICR-MS results, the proportion of characteristic CHNO and CHNOS compounds was greater in the upper plume fringe samples in the (+)APPI mass spectra, further corroborating the hypothesis that organic nitrogen chemistry played a role in this depth region (Figure 3-6C). In fact, nitrate was available as electron acceptor at the time of sampling (data not shown here, cf. (Müller et al. 2016)). Furthermore, multi-data correlation revealed the presence of typical nitrate

reduction coupled toluene degraders in the upper plume fringe, e.g., Azoarcus sp. which was already found during previous samplings at the site (Winderl et al 2007),

DOM in the plume core and lower plume fringe and the relation to BTEX and sulfide

As a result of the overlapping strong abundance of contaminants and sulfide resulting from bacterial sulfate reduction (Figure 3-3), one third of the data set was required to describe the diverse DOM characteristics of the plume core (Figure 3-9D). In agreement with the dominance (>50%) of CHOS compounds in the contribution to the total intensity of assigned molecular formulas (Figure 3-5A, Figure 6-7), also CHOS compounds were the most prominent contributors in the OPLS-DA derived characteristic mass signals in the plume core and lower plume fringe. These CHOS compounds were predominately polysulfurized (Figure 3-9D, E). The presence of such polysulfurized molecules was verified by isotopic pattern matching. This is exemplarily depicted in Figure 6-8 in the Supplementary Information for the mass signal of the molecular formula $[C_9H_9O_4S_4]^-$, a major marker compound of the plume core. However, CHOS ($1.0 <$ H/C < 1.5 and O/C $<$ 0.2) and CHO (H/C < 1 and O/C > 0.5) compounds most likely resulting from the degradation of petroleum hydrocarbons were also characteristic for the plume core DOM.

OPLS analysis enabled further elaboration which molecular formulas were derived from elevated sulfide concentration as a product of bacterial sulfate reduction and which were derived from the contamination, predominantly consisting of BTEX (Figure 3-11C, D). Because of the strong overlap of the two geochemical variables also a small proportion of molecular formulas partly overlapped between the characteristic mass signals, which are highlighted with the green box Figure 3-11D.

The majority of molecular formulas which correlated with the dissolved sulfide concentration were polysulfurized compounds, such as $[C_9H_9O_4S_4]^-$ (Figure 3-11C), with very low numbers of oxygen atoms testifying for the presence of reduced sulfur functionality in the molecules (detail discussed in paragraph 2.4.3.2). This was confirmed by the MS/MS fragmentation pattern of $[C_9H_9O_4S_4]^-$ (Figure 3-12C, D). The major fragment lost S_2 (depicted in orange) which is indicative for a terminal polythiol group (Gross 2011). Polythiol groups were most probably formed from sulfide or even polysulfide (unfortunately not analyzed), whose formation and presence is very likely under the prevalent pH conditions. The formation of sulfur organic compounds at elevated sulfide concentrations is a common biogeochemical process (Casagrande et al.

1979, Casagrande et al. 1980, Henneke et al. 1997, Heitmann et al. 2007) that has also been confirmed in several laboratory experiments with DOM and model organic compounds (Vairavamurthy and Mopper 1987, Perlinger et al. 2002, Heitmann and Blodau 2006, Yu et al. 2015b). Sulfide reacted with organic matter functionalities such as single and activated double bonds (Michael systems, Quinones) (Vairavamurthy and Mopper 1987, Perlinger et al. 2002, Heitmann and Blodau 2006, Yu et al. 2015b). Therefore, direct reaction of highly nucleophilic sulfide with DOM functional entities to result in CHOS molecules is anticipated in the plume core and lower fringe.

Additionally, the loss of $H_2S_3O_3$ (depicted in light red), as well as the lost fragment S_3-polysulfane monosulfuric acid (depicted in light green) itself, was present (Figure 3-12). Hence, polysulfurized molecules may also be formed by the reaction of intermediate oxidation state polysulfur to form polysulfur sulfonic acids ($R-S_xO_3H$). Indeed, polythionates and polysulfane monosulfuric acids were detected in the (–)ESI FT-ICR mass spectra of SPE-DOM (cf. 2.4.3.3) and their vertical profile followed the sulfide concentration (Figure 3-13).

The presence of intermediate sulfur species was also suggested by the characteristic OTUs of the plume core. Desulfocapsa is associated with sulfur disproportionation and found to tolerate higher hydrogen sulfide concentrations while it is not associated with sulfate reduction (Frederiksen and Finster 2004) and Sulfuricurvum contributes to the oxidation of sulfides, elemental sulfur, polysulfides or thiosulfate (Handley et al 2014) (Figure 6-12). Although abiotic reactivity of sulfur species with DOM is likely the prominent formation process of CHOS compounds, it cannot be excluded that CHOS compounds were also formed directly during bacterial sulfur cycling.

The molecular formulas related to the BTEX concentrations were CHOS compounds with $1.0 < H/C < 1.5$ and $O/C < 0.2$ as well as CHO compounds with $H/C < 1$ and $O/C > 0.5$. The sulfur organic compounds were depleted in oxygen $CHOS_1$ molecules in the van Krevelen region of unsaturated hydrocarbons (Ohno et al. 2010), hence, resembling to typical sulfur containing naphthalene derivatives which were already detected in water droplets in oil (Meckenstock et al. 2014). The characteristic CHO compounds were oxidized condensed aromatic structures (Ohno et al. 2010, Meckenstock et al. 2014), most likely carboxylated PAHs which were also detected in the NMR spectra (cf. 3.4.2.3). Carboxylation of PAHs was shown to occur during the initial steps of PAH degradation

(Griebler et al. 2004, Meckenstock, Safinowski and Griebler 2004, Safinowski et al. 2006, Jobelius et al. 2011)
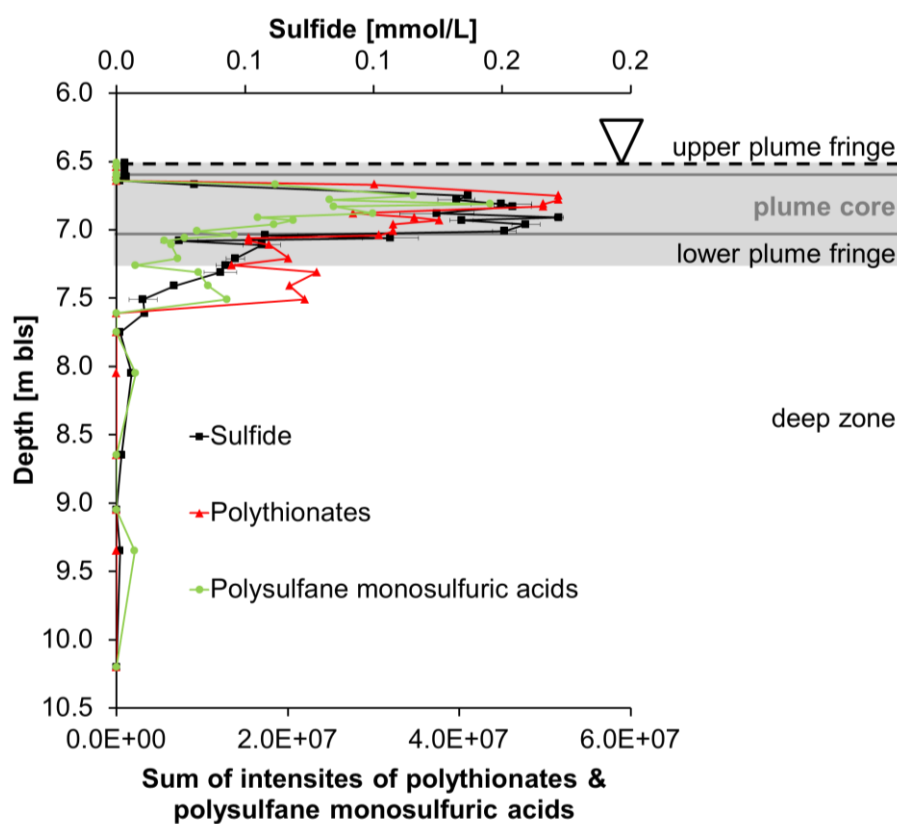
Figure 3-13: Vertical profile of inorganic sulfur species.
Vertical profile of the sulfide concentration and the sum abundances of polythionates and polysulfane monosulfuric acids in (–)ESI FT-ICR mass spectra from SPE-DOM (cf. abundances of the individual polysulfur intermediates are displayed in Figure 6-6).

DOM in the deep zone and the relation with sulfate

The characteristic mass signals of the deep zone showed mainly CHO and CHNO compounds in the polyphenolic region of the van Krevelen diagram ($1.5 > H/C > 0.7$ and $0.7 > O/C > 0.1$) (Figure 3-9F). Hence, DOM characteristics of less contaminated deep zone groundwater showed similarities to previously published (–)ESI FT-ICR-MS results of groundwater DOM (Einsiedl et al. 2007, Longnecker and Kujawinski 2011).

In the deep zone sulfate concentrations were at constant high levels (Figure 3-3C) and the number of CHOS compounds was increased compared to a pristine groundwater (Figure 6-7). However, CHOS compounds were not characteristic of that zone. Also correlation of the sulfate concentration did not reveal CHOS compounds to be of particular importance. This corroborates the general believe of sulfate not being involved in the formation of sulfur organic compounds. The molecules correlating with sulfate were

$CHOS_1$ compounds in the lignin region of the van Krevelen diagram. Hence, were similar to typical CHOS compounds reported in diverse aquatic systems (Herzsprung et al. 2010, Sleighter et al. 2014, Gonsior et al. 2016).

3.5. Summary and conclusions

To capture the prevailing steep and distinct biogeochemical gradients and associated redox processes in porous aquifers, high resolution sampling in the centimeter range is needed. At a petroleum hydrocarbon contaminated aquifer, the installation of a high-resolution multi-level well (HR-MLW) revealed the fringes of the contamination plume to be hot spots of biodegradation via bacterial sulfate reduction (Anneser et al. 2008a, Anneser et al. 2008b, Anneser et al. 2010, Einsiedl et al. 2015).

Spatially high resolution sampling was combined with non-targeted high resolution analytics to study the interaction of the petroleum hydrocarbon degradation by bacterial sulfate reduction with DOM. Moreover, multi-data correlation based on the DOM molecular formulas, bacterial community data as well as the major geochemical and contaminant properties defining the plume zones, i.e. upper fringe, plume core, lower fringe, and deep zone, enabled to study the effects of bacterial sulfate reduction on the DOM composition of the specific zones in detail. This approach revealed DOM signatures from petroleum contaminants and specific degradation products as well as signatures derived from elevated sulfide concentrations originating from bacterial sulfate reduction.

Contaminant signatures in the DOM were primarily present in the plume and most prominently in the plume core. (+)APPI FT-ICR-MS, which favors the detection of non-polar petroleum derived compounds, showed that samples in the plume core and its fringes were characterized by aromatic and even condensed aromatic molecules (Figure 3-6). Additionally, degradation products associated with initial steps of biodegradation (Annweiler et al. 2001, Martus and Puttmann 2003, Griebler et al. 2004, Safinowski et al. 2006, Jobelius et al. 2011, Jarling et al. 2015) were mainly located in the lower part of the plume core where bacterial sulfate reduction was highly active. Furthermore, (−)ESI FT-ICR-MS (Figure 3-11D), which is selective towards DOM molecules containing carboxylic acids and other polar functional groups, revealed the presence of oxygen depleted sulfur organic compounds resembling sulfur containing naphthalene derivatives

(Meckenstock et al. 2014). Furthermore, oxidized condensed aromatic structures (Ohno et al. 2010, Meckenstock et al. 2014), most likely carboxylated PAHs which were also detected in the NMR spectra (cf. 3.4.2.3), were present in the contaminant plume. NMR spectroscopy also evaluated variable contribution of common bulk DOM and petroleum contaminants and its degradation products (Figure 3-8). Additionally, EEM fluorescence spectroscopy in combination with PARAFAC modeling attributed DOM samples to specific contamination traits typical for the plume zonation (Figure 3-7).

DOM characteristics were highly affected by bacterial sulfate reduction, the major redox process involved in the contaminant biodegradation (Anneser et al. 2008a, Anneser et al. 2010). Both (+)APPI and (−)ESI FT-ICR-MS revealed characteristic CHOS compounds at the depths where sulfate reduction is active. Organosulfur compounds were found to be far more abundant in the (−)ESI FT-ICR mass spectra (Figure 3-4, Figure 3-5, Figure 3-6). CHOS compounds represented >50% of the total mass peak intensity of the corresponding assigned molecular formulas derived from (−)ESI FT-ICR mass spectra in the zone with maximum dissolved sulfide concentrations (Figure 3-3C, Figure 3-5A). Thus, reduced sulfur mainly reacted with the natural DOM pool and particularly with CHO compounds (Figure 3-5A).

Multi-data correlation enabled a detailed study of the correspondence between (−)ESI FT-ICR-MS derived molecular formulas, bacterial community data as well as the distinct zone-dependent redox chemistry. A summary of the observed formation of sulfur organic compounds due to the intensive sulfur cycling is depicted in Figure 3-14.
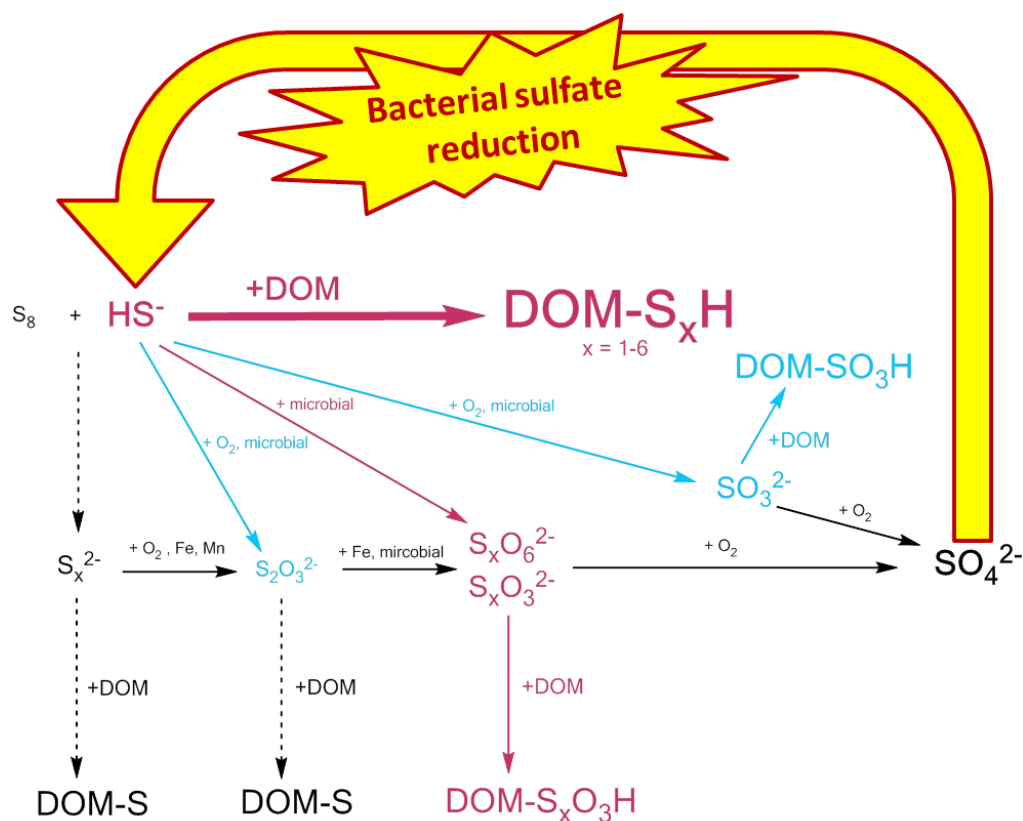
Figure 3-14: Reaction scheme of the formation of sulfur organic compounds in the aquifer. Formation of reduced sulfur organic compounds occurred predominantly in the plume core and lower plume fringe where sulfate reduction was the key redox process, resulting in dissolved sulfide as well as intermediate oxidation state polysulfur compounds (depicted in red). In the upper plume fringe abiotic and biotic oxidation of sulfide resulted most likely in the formation sulfite, which reacted with DOM by sulfonic acid formation (depicted in blue).

The upper plume fringe was characterized by suboxic conditions and biodegradation was shifted towards iron and nitrate reduction. Besides bacteria involved in oxidative sulfur cycling were found to be characteristic for that zone and previous studies showed the presence of sulfite resulting from the oxidation of sulfide (Einsiedl et al. 2015). The DOM signature was characterized by $CHOS_1$ compounds formed by sulfonation of petroleum derived carboxylated alkene degradation products as well as fewer degraded contaminants (Figure 3-9C, Figure 3-11B). The presence of less degraded contaminants most likely resulted from the limited access to electron acceptors (Figure 3-3C) (Anneser et al. 2008a).

Both the plume core and lower plume fringe were characterized by polysulfurized CHOS molecules, which correlated with the prevailing elevated sulfide concentrations resulting from bacterial sulfate reduction (Figure 3-9D, E and Figure 3-11C). The reduced sulfur organics were most likely polythiols and polysulfur sulfonic acids ($R-S_xO_3H$) which were

formed from the reaction of sulfide, polysulfide and intermediate polysulfur species (Figure 3-13, Figure 3-12, Figure 6-12) with organic matter functionalities, such as single and activated double bonds, as shown in laboratory experiments (Vairavamurthy and Mopper 1987, Perlinger et al. 2002, Heitmann and Blodau 2006, Yu et al. 2015b).

DOM characteristics of less contaminated deep zone groundwater (Figure 3-9F) showed similarities to previously published (–)ESI FT-ICR-MS results of groundwater DOM (Einsiedl et al. 2007, Longnecker and Kujawinski 2011). Furthermore, multi-data correlation confirmed that sulfate is not involved in the formation of sulfur organic compounds (Figure 3-11E).

The approach enabled a comprehensive molecular level understanding of natural DOM and its role in petroleum hydrocarbon bioremediation. DOM was shown to directly react with sulfide resulting from bacterial sulfate reduction to form stable sulfur organic compounds. Hence, DOM acts as a sulfide sink. This has beneficial effects on the petroleum hydrocarbon biodegradation, since elevated sulfide concentrations may even further decelerate biodegradation at low sulfate concentrations; indeed, high concentrations of sulfide are toxic to many microbes (Muyzer and Stams 2008). In this context, natural DOM may act as a beneficial key player in the mediation of sulfide resulting from bacterial sulfate reduction. In consequence, natural DOM may be applied in bioremediation.

4. Abiotic reactivity of inorganic sulfur species with dissolved organic matter
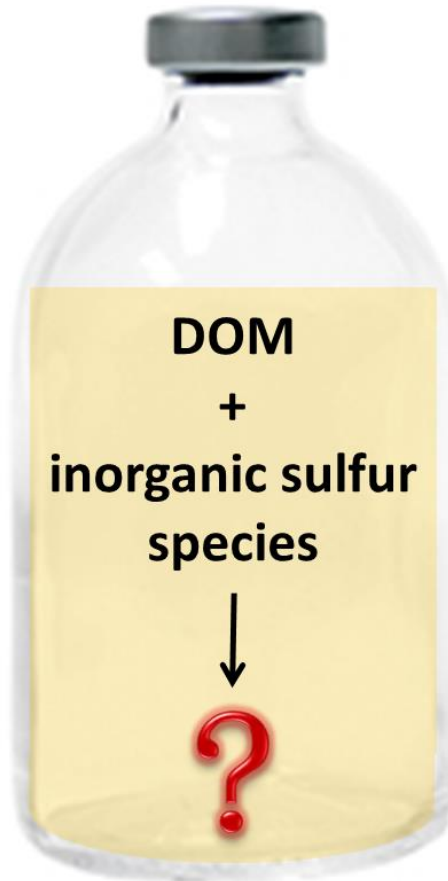
4.1. Introduction

Assimilatory and dissimilatory sulfur cycling leads to the formation of sulfur organic compounds in ecosystems (Brown 1982, Vairavamurthy and Mopper 1987, Aizenshtat et al. 1995, Bailey et al. 2002, Henneke et al. 1997, Amrani 2014). It is known that a variety of biotic and abiotic pathways are involved in the formation of sulfur organic compounds (Amrani 2014). The reactions range from the biosynthesis of primary metabolites, such as cysteine, to abiotic sulfurization including the formation of S cross-linked polymers (Amrani et al. 2007, Amrani 2014).

Although intensive sulfur cycling is present in diverse ecosystems, research was primarily focused on sediments and the associated petroleum generation, which has been reviewed recently (Amrani 2014). Many studies concluded that the formation of sulfur organic compounds is related to early steps of diagenesis (Vairavamurthy and Mopper 1987, Sinninghe Damsté et al. 1988, Sinninghe Damsté et al. 1989, Sinninghe Damsté and De Leeuw 1990, Hebting et al. 2006, Schmidt et al. 2009, Seidel et al. 2014). Besides the incorporation of sulfur into wetland DOM (Sleighter et al. 2014) and particularly the field studies of this thesis proofed the formation of CHOS compounds in ground and lake water DOM at aquatic sites with intensive sulfur cycling (cf. chapter 2 and 3). Independent from the ecosystem, the formation of sulfur organic molecules in sulfur enriched organic matter pool is believed to be primarily abiotic (Sinninghe Damsté and De Leeuw 1990, Amrani 2014, Sleighter et al. 2014).

4.1.1. Inorganic sulfur species

An overview of the major inorganic sulfur species and their oxidation state ranging from +6 to –2 is given in Figure 4-1. The scheme summarizes the reaction pathway from the most reduced sulfur species sulfide (S^{2-}), to the most oxidized sulfur species sulfate (SO_4^{2-}). Polysulfides (S_x^{2-}), thiosulfate ($S_2O_3^{2-}$) and sulfite (SO_3^{2-}) are intermediate products of the sulfide oxidation (Vairavamurthy et al. 1994). Polysulfides (S_x^{2-}) are formed through the oxidation of sulfide at the suboxic interfaces (Ferdelman, Church and Luther III 1991), sulfide oxidation with iron or dissolved organic matter (Filley et al. 2002, Heitmann and Blodau 2006), as well as the reaction of HS^- and elemental sulfur (Aizenshtat and Amrani 2004). In aquatic media at pH 7 – 9 the most abundant S_x^{2-} species are S_4^{2-}, S_5^{2-}, S_6^{2-} (Aizenshtat and Amrani 2004, Kamyshny et al. 2004). While sulfide, e.g. resulting from bacterial sulfate reduction, is often enriched in anoxic

environments, intermediate sulfur species are primarily found in suboxic environments. For example in Cinder Pool, a Yellowstone hot spring, thiosulfate and polythionates were detected besides sulfide and sulfate (Xu et al. 2000). And in the contaminated aquifer in Düsseldorf Flingern (chapter 3), where bacterial sulfate reduction is the dominant redox process, thiosulfate and sulfite were found (Einsiedl et al. 2015). And also polysulfides have been reported for diverse oxic and anoxic environments (Luther, Giblin and Varsolona 1985, Rozan, Theberge and Luther III 2000, Gun et al. 2000).
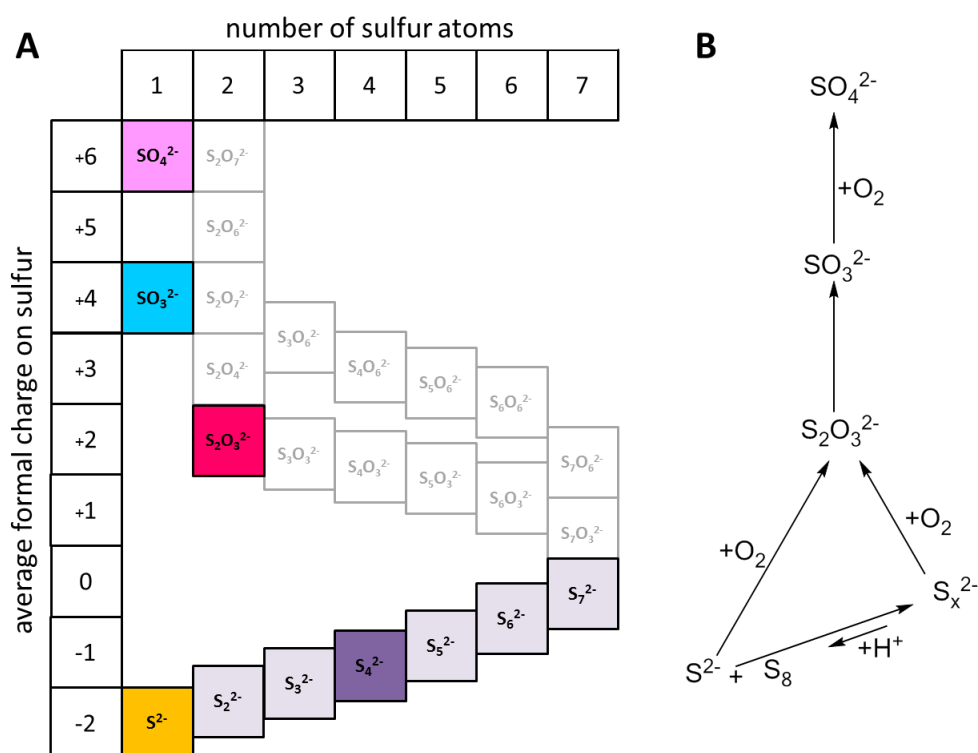
Figure 4-1: Overview of inorganic sulfur species.
A) Scheme of the inorganic sulfur species sorted according to the number of sulfur atoms and the formal charge (oxidation state) of the sulfur atoms (adjusted from (Aizenshtat and Amrani 2004)). Due to their major abundances in nature, the reactivity of the colored sulfur species with DOM was tested in this thesis. The color code for sulfate (pink), sulfite (blue), polysulfide (purple), and sulfide (orange) is consistently used in this chapter. B) Summary of the reaction pathway from the reduced (bottom) to the oxidized inorganic sulfur (top).

4.1.2. Reactivity of inorganic sulfur species with organic matter

The sulfurization of organic matter in sulfide enriched environments is a common biogeochemical process (Casagrande et al. 1979, Casagrande et al. 1980, Francois 1987, Henneke et al. 1997, Heitmann et al. 2007). Many field studies showed that also polysulfide is of importance in the incorporation of sulfur into organic matter (Kohnen et al. 1989, Boulegue, Lord III and Church 1982, Kohnen et al. 1991b, Aizenshtat and

Amrani 2004, Kohnen et al. 1991a). Sulfur incorporation into organic matter requires (1) the presence of reactive inorganic sulfur species, (2) functional groups in the organic molecules which are receptive to inorganic sulfur species and (3) low concentrations of competing reaction partners, such as iron, which reacts faster with reduced sulfur species than organic matter (Berner and Westrich 1985). Laboratory experiments with the reduced sulfur species sulfide and polysulfide have shown the addition of thiol and polythiol functionalities on model compounds with carbonyl, i.e. aldehydes, ketones, monosaccharides (Schouten et al. 1993, Schouten et al. 1994, van Dongen et al. 2003), α,β-unsaturated carbonyls (LaLonde et al. 1987, Perlinger et al. 2002, Amrani and Aizenshtat 2004b, Amrani et al. 2007), and even isolated double bonds (Sinninghe Damsté et al. 1989, De Graaf et al. 1992, Schouten et al. 1994) leading to low-molecular weight or macromolecular organosulfur compounds. Sequences of H_2S/HS^- additions and elimination reactions also cause double bond isomerizations and desulfurization (Sinninghe Damsté et al. 1989, Hebting et al. 2003, Hebting et al. 2006). Photochemical studies also proofed that radical reactions are involved in the formation of thiophens and polysulfur cross-linked macromolecules (Adam et al. 1998, Amrani and Aizenshtat 2004a).

Batch experiments, under anoxic conditions similar to those found e.g. in wetlands, reacting complex humic acid (HA) mixtures (Pahokee Peat Reference Humic Acid (1R103H, IHSS) and HA purchased from Sigma Aldrich) with sulfide confirmed the formation of sulfurized DOM (Heitmann and Blodau 2006, Yu et al. 2015a, Yu et al. 2015b).

So far only less attention has been paid on the reactivity of the further oxidized sulfur species thiosulfate and sulfite. But they are considered as sulfurization agents at oxic-anoxic interfaces, since sulfonic acid formation at α,β-unsaturated carbonyls was shown in laboratory experiments (Vairavamurthy et al. 1994).

4.2. Objectives

So far the majority of previous laboratory studies were limited on the formation of sulfur organic compounds at individual compounds with (poly)sulfide and double bonds. Additionally, only a few of the experiments were performed at conditions resembling to those in nature.

Thus, the goal of this study was the performance of model reactions of complex DOM mixtures with a variety of reactive inorganic sulfur species under conditions resembling typical environmental settings (Figure 4-2). Due to its unique capability of CHO and CHOS differentiation in complex organic mixtures, FT-ICR-MS was utilized to characterize the changes in DOM resulting from the formation of sulfur organic compounds. To evaluate the influence of the DOM characteristics experiments were performed with two different DOM: First, the abiotically and biotically processed Suwannee River fulvic acid (SRFA) 2S101F which was used as a standard reference material for the comparison of DOM composition from field sites (Gonsior et al. 2011, Cortés-Francisco and Caixach 2013) and even for studies on the influence and behavior of DOM (Wenk et al. 2015, Harris et al. 2015). Second, a pine needle extract was used representing plant litter, a typical representative for a fresh water DOM source.[3] The performance of experiments with the most reduced to the most oxidized inorganic sulfur species, allowed a direct comparison of the reactivity behavior of the sulfur species. Furthermore, these experiments enable the review of the reactivity, which is generally believed to be high for the reduced sulfur species. Furthermore, differences in the reaction behavior of inorganic sulfur species with DOM as a result of the prevalent pH conditions were investigated. Since reduced sulfur species are sensitive towards oxidation and sulfur cycling is often occurring at the interface of anoxic and oxic water layers, the influence of the oxygen saturation in the experimental solution was also evaluated.

The overall aim of the experiments was to enable a direct comparison of the abiotic formation of sulfur organic compounds in the laboratory with the formation found at field sites with intensive sulfur cycling, such as the hypolimnic water DOM from the meromictic lake Hechtsee (cf. chapter 2) and the bacterial sulfate reduction hotspot at the petroleum hydrocarbon contaminated groundwater system in Düsseldorf Flingern (cf. chapter 3) as well as hydrothermal springs (e.g. Yellowstone National Park).

---

[3] Pine needles were chosen since pine tree litter is believed to be a major contributor to DOM of sulfur species rich hydrothermal springs in Yellowstone National Park (YNP). The characterization of DOM from YNP thermal springs is not subject of this thesis, but the investigations were performed during the same period, and showed distinct CHOS chemistry depending on spring type and the prevailing inorganic sulfur species present.
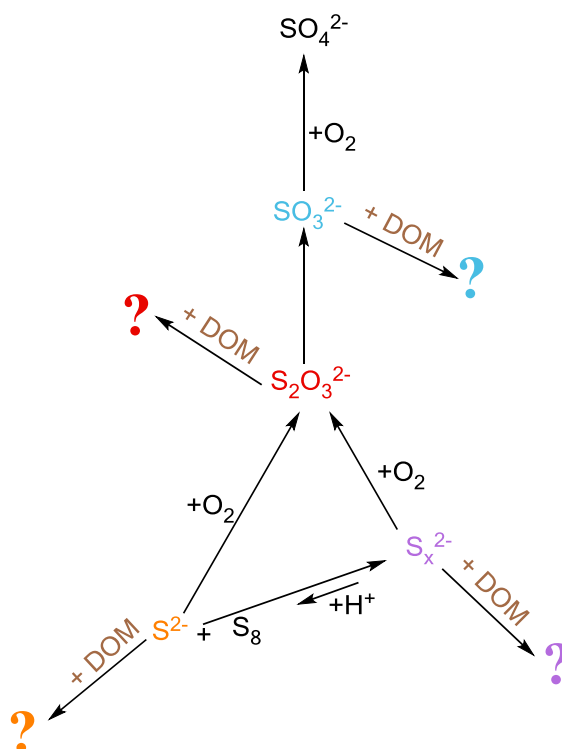
Figure 4-2: Supposed reactive inorganic sulfur species.
Scheme of the supposedly reactive inorganic sulfur species, i.e. sulfide (S^{2-}), polysulfide (S_x^{2-}), thiosulfate ($S_2O_3^{2-}$) and sulfite (SO_3^{2-}), with DOM.

4.3. Materials and methods – Development of the experimental setup

4.3.1. Preparation of the pine needle extract

A 1 L glass bottle was filled with 20.5 g of pine needles litter and a small pine cone from Yellowstone National Park. 1 L 0.1 M hydrochloric acid (prepared with purified water (Barnstead™ GenPure™ xCAD Plus Ultrapure Water Purification System, Thermo Fisher Scientific Inc., Waltham, MA, USA) was added and the bottle was closed. The extraction was performed in a 60 °C warm water bath for 18 h. After that the solution was cooled down in the water bath. The pH of the solution was adjusted to pH 2 by addition of 5 M sodium hydroxide solution. The extract was filtered through 0.22 µm nitrocellulose membranes (Millipore, Billerica, MA, USA) with a glass filter unit, because of blockage the filter had to be exchanged after about 40 mL of the extract.

To concentrate the extract SPE by an established method described by Dittmar et al. was performed (Dittmar et al. 2008). Briefly, a 5 g Agilent (Agilent Technologies, Santa Clara, CA, USA) Bond Elut PPL SPE cartridge was rinsed with 6 mL of methanol (Chromasolv® LC-MS grade methanol, Sigma Aldrich) followed by 6 mL of acidified

(pH 2) purified water. The sample was gravity fed through the cartridge. Afterwards the cartridge was rinsed with 15 mL acidified (pH 2) purified water and thoroughly dried. The pine needle DOM was eluted with 20 mL methanol.

For the estimation of the DOM concentration of the methanolic extract, it was dried thoroughly under a gentle stream of nitrogen and diluted in purified water at various ratios. The DOC concentrations of the dilutions were measured (vario TOC cube, Elementar, Hanau, Germany). The DOM concentration of the methanolic extract was calculated by taking the measured DOC concentrations of the different dilutions as well as a mean molecular composition of 50% carbon under consideration. The DOM concentration of the methanolic extract was 12.3 mg mL^{-1}.

4.3.2. Reaction of DOM with inorganic sulfur species

The experiments were performed in triplicates in 10 mL serum bottles. Purified water (MilliQ-Integral, Merck KGaA, Darmstadt, Germany) was used for the preparation of the solutions. For pH 6 and 8 conditions 0.1 M potassium hydrogen phosphate (puriss. p.a., >99.5%, Fluka) and for pH 10 conditions 0.05 M sodium bicarbonate (p.a., >99%, Merck) buffer was used. The pH of the buffers was adjusted with 0.1 M sodium hydroxide (reagent grade, >=98%, Sigma Aldrich) and 10 mM sodium chloride (puriss. p.a., >=99.5%, Sigma Aldrich) as electrolyte for cyclic voltammetry was added. DOM was added to a final concentration of 0.5 mg Suwannee River fulvic acid (SRFA) (International Humic Substances Society, 2S101F) and 0.44 mg PN per 10 mL. Both OM were added in the form of high concentrated aquatic solutions, whereby the PN extract was dried under a gentle stream of nitrogen before dilution in purified water. It was assumed that DOM molecules consist to approximately 50 w% accounts from carbon and that the average molecular weight of the molecules is for SRFA 400 g mol^{-1} and for PN 350 g mol^{-1}. According to the chosen estimates the DOM concentration equals approximately 0.125 mM. Anaerobic experimental solutions were purged with nitrogen for 8 min in order to establish fully anoxic conditions prior the addition of inorganic sulfur species. High concentrated stock solutions of inorganic sulfur species, i.e. sulfide (sodium sulfide nonahydrate, >99.99%, Sigma Aldrich), sodium tetrasulfide (synthesized in the laboratory of the collaboration partners after an adapted method from Rosen and Tegman, for further details please see the Appendix (Rosen and Tegman 1971)), thiosulfate (sodium thiosulfate, 99%, Sigma Aldrich), sulfite (sodium sulfite, ≥98%,

Sigma Aldrich) and sulfate (sodium sulfate anhydrous, p.a., >99%, Merck), were prepared freshly in nitrogen purged anoxic purified water and added to the experimental solution to a final concentration of 1.25 mM. The reaction solutions were sealed with a crimped butyl rubber stopper and wrapped in aluminum foil to prevent the samples from light and gently shaken at 22 °C for 6 d and 24 d, respectively. The pH (Electrode Gel; Deutsche Metrohm GmbH & Co. KG, Filderstadt, Germany) was checked directly after the sulfur species addition and directly before DOM extraction and sulfur speciation. Blanks only containing DOM or inorganic sulfur species were processed similarly.

4.3.3. Sulfur speciation

Sulfur speciation was performed by the collaboration partners Fotios-Christos A. Kafantaris and Dr. Gregory K. Druschel from the Indiana University – Purdue University Indianapolis. The results are not shown in detail in this thesis. However, striking results are mentioned in the results and discussion section of this chapter.

The electrochemical analyses gave quick information regarding the speciation of sulfur in the system without the chemical alteration of the system. Electrochemical measurements were carried out using a Princeton Applied Research (Oak Ridge, TN , USA) dropping mercury electrode (DME) system that was coupled to an Analytical Instruments, Inc. (Ringoes, NJ, USA) DLK-100 potentiostat, operated via desktop computer. The samples were placed in an electrochemical cell where the working, reference and control electrodes were submerged. Ultrahigh purity nitrogen was supplied to the DME and the headspace above the electrochemical cell to flush the sample prior to analysis. Cyclic Voltammetry was performed from –0.1V to –1.8V and back to –0.1V, using Ag/AgCl as a reference electrode and Pt wire as a counter electrode.

Chromatographic determination of the sulfite, thiosulfate, elemental sulfur and polysulfide was performed as described in paragraph 2.3.2 (Zopfi et al. 2004, Rethmeier et al. 1997, Kamyshny et al. 2007, Kamyshny et al. 2009).

4.3.4. DOM characterization

4.3.4.1. Isolation of DOM from experimental solution

Isolation of DOM was performed by an adjusted established SPE method (Dittmar et al. 2008). Briefly, 100 mg Bond Elut PPL SPE were rinsed with methanol and purified water adjusted to pH 2 with formic acid (for mass spectrometry, ~98%, Sigma Aldrich). The

experimental solution was acidified to pH 2 with formic acid and fed through the Bond Elut PPL SPE cartridge. After that, the cartridge was rinsed with acidified purified water and dried under vacuum. The DOM was eluted with 1 mL methanol. In the case of the anoxic experimental solutions, all used solutions and equipment was flushed with nitrogen prior usage to maintain the anoxic conditions. The SPE-DOM samples were stored at –20°C. The recovery of the SPE isolation was determined by measuring the TOC concentrations of SPE-DOM after vaporization of the methanol with a Shimadzu (Duisburg, Germany) TOC-5000A TOC analyzer. A slight pH dependency was found for the DOC recovery rate of the SPE procedure, which was a little lower for pH 10 with the sodium bicarbonate buffer, than for pH 6 and 8 with the potassium hydrogen phosphate buffer (Figure 4-3). The overall DOC recovery rate was around 70%.
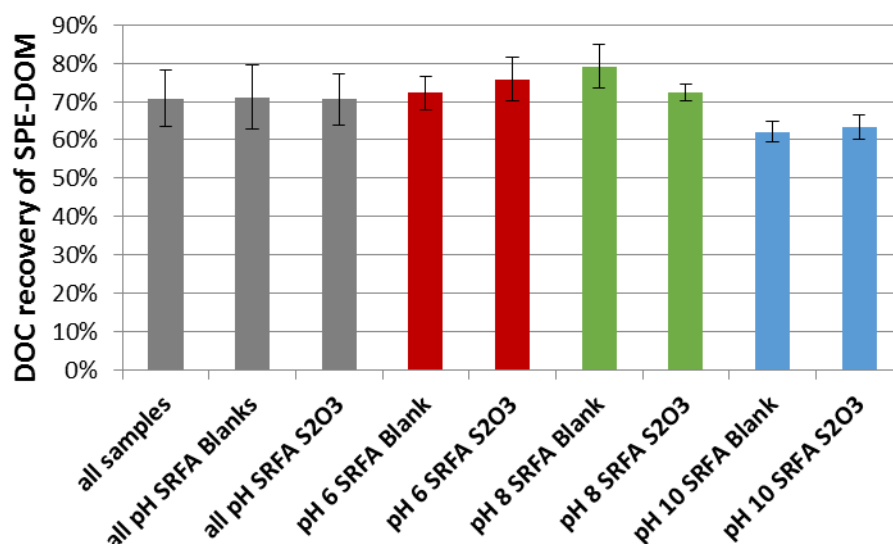
Figure 4-3: Recovery of DOM by SPE.
DOC recovery rates of the SPE-DOM isolation method at pH 6, 8 and 10 with and without inorganic sulfur species in the solution.

4.3.4.2. FT-ICR-MS analysis

(–)ESI FT-ICR mass spectra were acquired with a SolariX Qe FT-ICR-MS (Bruker Daltonik GmbH, Bremen, Germany) as described in 2.3.4. For detailed information on the FT-ICR-MS parameters see Appendix 7.1.1 (Table 7-1). For MS/MS fragmentation, ions were accumulated in the first hexapole before they were pulsed through the quadrupole to the collision cell where they were fragmented by collision-induced dissociation (CID) using increasing voltage increments up to 30 V. Details on the parameters are given in the Appendix (Table 7–2). Mass spectral data processing was performed similar as described in 2.3.4. The following brief description highlights the differences. The mass spectra of

the DOM containing experiments were internally calibrated to known and high abundant masses of DOM and the sulfur species blanks to ubiquitous fatty acid masses with a mass accuracy of < 0.1 ppm. After export and alignment of the mass spectra a mass defect filter was applied and singly abundant masses were eliminated. Molecular formula were assigned via a network approach (Tziotis et al. 2011) with the mass accuracy window set to ±0.1 ppm. Molecular formula were validated (cf. 2.3.4) and classified into molecular groups containing CHO, CHNO, CHOS, or CHNOS. Although for pH 6 and 8 conditions potassium hydrogen phosphate buffer was used, phosphorous containing organic molecules were nearly not abundant in any of the experiments and therefore not taken under consideration. Ubiquitous masses highly abundant in the respective sulfur species blanks were eliminated from further analysis; also DOM blanks were corrected for ubiquitous masses. To evaluate the formed CHOS compounds from the reaction of DOM with inorganic sulfur species, only masses present in two of the triplicates having a C_f((DOM + inorganic sulfur species)/DOM Blank) >3 (Liger-Belair et al. 2009) were taken under consideration. Hierarchical cluster analysis based on Spearman rank correlation and average linkage was performed with R (Version 3.0.0) and TM4-Multi Experiment Viewer (MeV) based on the normalized (sum intensity) of the assigned molecular formulas. Heat maps depicting the covariation between the molecular formulas and respective subclusters were generated with the MeV software (Saeed et al. 2003). Based on this approach, characteristic molecular formulas for the subclusters which represent specific experimental conditions were extracted to distinguish formed CHOS compounds most reprehensive and characteristic for the respective conditions.

4.3.4.3. NMR
^{1}H NMR spectra were acquired with a Bruker (Bremen, Germany) AV III 800 spectrometer operating at B_0 = 18.7 T with Bruker standard pulse sequences and cryogenic detection. Methanolic DOM extract was dried and twice exchanged with CD_3OD (Merck. 99.95% [2]H) each before final dissolution in CD_3OD. A detailed description of the NMR acquisition conditions is described in the Appendix (7.1.2).

4.3.5. Optimization of the experimental setup

4.3.5.1. Solid phase extraction and buffers
In the first place sulfur species reactivity with DOM was tested in unbuffered aquatic solution. The reaction solution was directly measured by means of (–)ESI FT-ICR-MS

after 1:1 dilution with methanol. Figure 4-4 displays the mass spectra of SRFA in water (pH 6.5) in comparison with SRFA in water with the pH adjusted to 10 with sodium hydroxide and SRFA with polysulfide (sodium tetrasulfide) with a natural pH of 9. The two alkaline samples show sodium adduct peaks, which are highlighted in pink. Similar sodium adduct formation has already been found in (–)ESI spectra of aromatic carboxylic acids and is described as deprotonated dimer ion pair with sodium [2M–2H$^+$Na] (Schug and McNair 2002, Schug and McNair 2003). The substructure units of DOM resemble to the model compounds in the two studies of Schug and McNair, hence it is very likely that formation of such sodium-bridged dimer ions occurs. Unfortunately, their molecular mass is very similar to CHOS compounds with low O/C and H/C ratios, resulting in false annotations of CHOS compounds and a shift of the CHO molecular masses in the van Krevelen space (cf. van Krevelen diagram in Figure 4-4). Thus, alkaline sodium salt containing solutions have to be desalinated prior their analysis with (–)ESI FT-ICR-MS. Due to its comparably low cost and the possibility to handle multiple samples similarly in short time SPE was chosen as sample preparation.
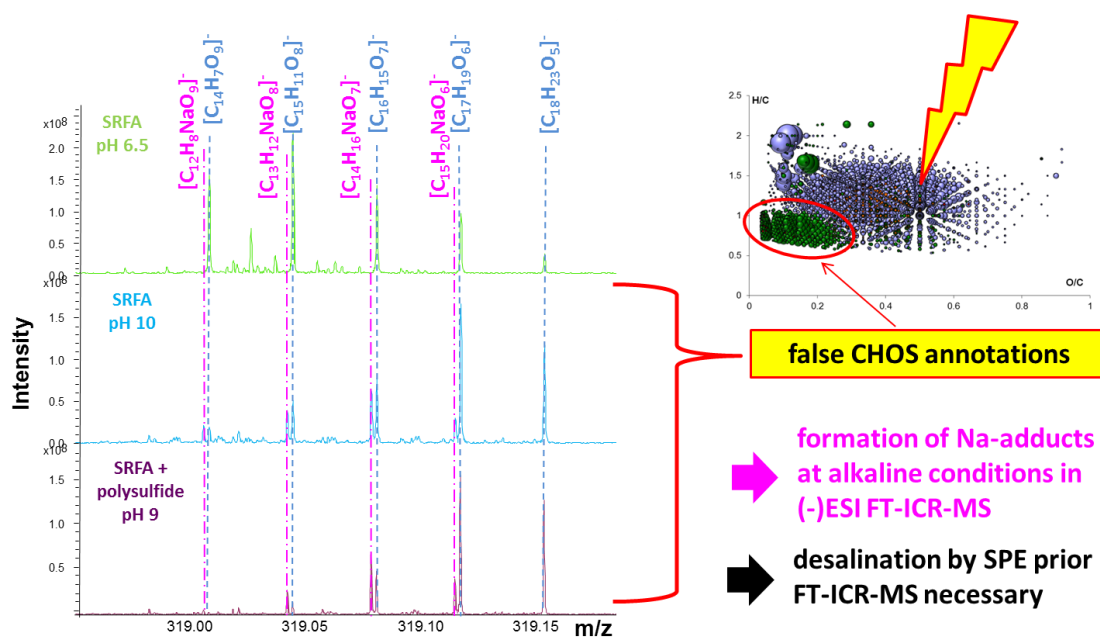
Figure 4-4: Na-adducts in (–)ESI FT-ICR mass spectra of alkaline DOM solutions.
Nominal mass 319 of the (–)ESI FT-ICR-MS of SRFA-DOM at pH 6.5 and 10 as well as pH 9 after polysulfide addition with the assigned Na-adducts in alkaline solutions (50:50 water : methanol). The van Krevelen diagram displays the falsely annotated CHOS molecular formulas, which are caused by the Na-adducts, in the alkaline samples.

In order to allow experiments at different pH values under constantly controlled conditions it is necessary to use buffers. Considering the aim, to investigate the reaction

of DOM with inorganic sulfur species, the usage of inorganic buffers is absolutely necessary. Otherwise the extraordinary high concentration of a single organic buffer compound could possibly suppress the reaction with natural DOM and especially would cause suppression in the mass spectrometric characterization of natural DOM. Nevertheless, inorganic buffer salts would also cause ion suppression during (–)ESI mass spectrometry. Hence, SPE extraction of DOM is utterly necessary prior mass spectrometric analysis. The application of SPE prior DOM characterization has the advantage, that DOM and inorganic sulfur speciation by cyclic voltammetry, which requires the presence of electrolyte salts, can be performed from a single reaction solution.

4.3.5.2. Concentration and duration

Initial experiments were performed under anoxic conditions with different molar ratios of DOM molecules to inorganic sulfur species (10:1; 1:1 and 1:10, considering the approximations discussed in 4.3.2). Experiments were performed in buffered solutions at pH 6, 8 and 10 or without buffer at pH 7 were the pH was adjusted with hydrochloric acid. In summary, these experiments revealed that the reaction between inorganic sulfur species and DOM does not occur and result immediately (within minutes) in the formation of CHOS. Especially, with SRFA-DOM formation of CHOS compounds was almost absent also after 24 h under equimolar conditions and even at excess of supposedly reactive sulfide. On the contrary the pine needle DOM showed reaction with sulfur species already after 24 h. In order to allow direct comparison of the reactivity with different DOM sources 6 d were chosen as experiment duration to ensure also the formation of CHOS compounds with SRFA as DOM source. The findings, also suggested that CHOS formation is more likely, when inorganic sulfur species is present in excess. Moreover, at natural sites of intensive sulfur cycling particularly e.g. sulfide occurs often in higher concentrations than DOM and especially specific molecules of the complex DOM mixture (cf. 2.4.1). Hence, inorganic sulfur species were used in 10-fold excess for the experiments discussed in the following.

Additionally, inorganic sulfur speciation showed that anoxic conditions in the sealed serum bottles remained for more than 6 days. After 24 days, supposedly as a result of air diffusion through the stopper into the serum bottles, partial oxidation occurred in the nitrogen purged sulfide blank (corresponds to anoxic experimental conditions). Hence, all

the SRFA-DOM experiments with 24 d duration are at least partly taking place under oxic conditions and are therefore excluded from the following discussion.

4.4. Results and Discussion

4.4.1. Comparison of Suwannee River Fulvic Acid and pine needle DOM

It is crucial to employ DOM with low pristine CHOS levels for the evolution of CHOS formation from DOM and reactive sulfur species. SRFA is especially suitable due to its low sulfur concentration of only 0.46% (Perdue 2013). Also FT-ICR-MS analysis revealed sulfur organic compounds, with only 7% of the molecular formula assignments and especially only 1.27% of the total assigned mass peak intensity (Table 6-8 and Figure 4-5), as minor constituent of SRFA. The majority of the molecules, with >94.43% of the total intensity of assigned mass peaks (Table 6-8), were CHO compounds. Although 22% of the assigned mass peaks were CHNO compounds, they only made up 4.27% of the total mass peak intensity. The present CHNOS compounds were negligible (Table 6-8 and Figure 4-5). In agreement with previous studies on the composition of Suwannee River humic substances decomposing vegetation is believed to be the primary DOM source (Averett et al. 1994, Haiber et al. 2001, Kujawinski, Hatcher and Freitas 2002, Stenson, Marshall and Cooper 2003, Leenheer and Rostad 2004, Hertkorn et al. 2007) and SRFA is predominantly composed from lignin and tannin derived molecules (cf. van Krevelen diagram in Figure 4-5). The share of functional group entities investigated by ^{1}H NMR spectroscopy showed that the majority of molecules are carboxylic-rich alicyclic (CRAM) and aliphatic molecules (Figure 4-6; cf. Table 7-4). The section integrals of aromatic and olefin (characterized by double bonds) substructures were of minor abundance in SRFA. These findings are in agreement with previously published NMR spectra of SRFA (Haiber et al. 2001, Hertkorn et al. 2007). CRAM likely represents highly processed products of ultimately terpenoids origin and has been identified as a major constituent of organic matter and particularly also of SRFA (MacCarthy 2001, Hertkorn et al. 2007). The high abundance of CRAM implies that SRFA consists of well metabolized and processed molecules, thus indicates that many SRFA constituents are recalcitrant.
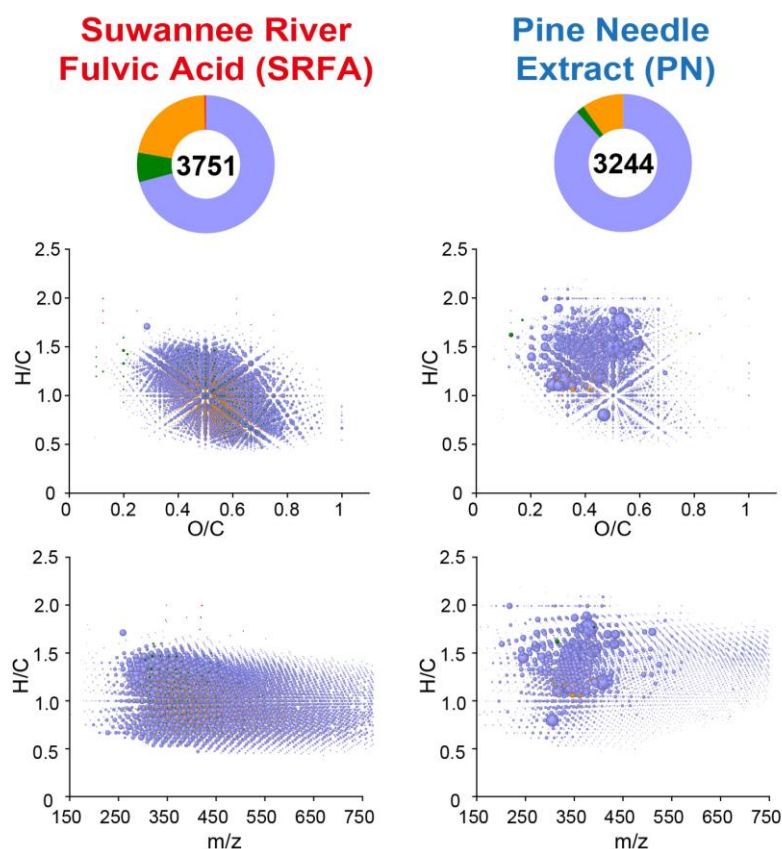
Figure 4-5: FT-ICR-MS derived molecular formula of SRFA and pine needle extract.
Van Krevelen diagrams and m/z-resolved H/C ratios of the assigned molecular formula from FT-ICR mass spectra of Suwannee River Fulvic Acid (SRFA) and pine needle extract (PN). The ring charts display the count of assigned elemental compositions classified into molecular groups containing CHO (blue), CHNO (orange), CHOS (green), or CHNOS (red).

In contrast to DOM, which has been subject to intensive biotic and abiotic degradation, the pine needle extract (PN) is representative for fresh plant litter derived organic matter. The contribution of sulfur containing molecules was, with 1.75% of formula assignments and < 1% of the total mass peak intensity of assigned molecular formulas (Table 6-8 and Figure 4-5), very low. Additionally, CHNO compound contribution was little so that the vast majority of the molecular composition was CHO molecules. Therefore, also the PN is very suitable for the investigations on the formation of CHOS.

In comparison to the SRFA, the van Krevelen diagram of the PN is dominated by less aromatic (H/C > 1) and less oxidized compounds (O/C < 0.6) indicative for primary and secondary plant metabolite and structural materials, such as lignins. The molecular weight and intensity distributed was less continuous than for SRFA (Table 6-8 and Figure 4-5), suggesting an enrichment of specific lower molecular weight compounds. Also the sharp signals in the ^{1}H NMR spectrum of PN indicate an increased abundance of specific

compounds (Figure 4-6, blue spectrum). Based on the ^{1}H NMR section integrals aliphatic and carbohydrate functional groups are predominant. The high abundance of carbohydrate functional entities was most likely caused by structure molecules such as cellulose. In agreement with the FT-ICR-MS derived van Krevelen diagrams, the contribution of aromatic compounds was lower than for SRFA. But the olefin section integral was almost doubled. This confirmed the presence of secondary pine tree metabolites, such as resin acids and odorous substances, which are terpenoids. The strong abundance of double bonds is in line with PN being fresh, non-processed organic matter, since double bonds are reactive organic functional groups, e.g. with sulfide (Vairavamurthy and Mopper 1987, Perlinger et al. 2002, Heitmann and Blodau 2006, Yu et al. 2015b). Hence, the PN is an ideal model DOM to study the formation of sulfur organic compounds. In general, considering the different sample preparations used, the PN ^{1}H NMR spectra are in consense with those from other studies (Bastone et al. 2016, Skakovskii et al. 2006, Parfitt and Newman 2000)
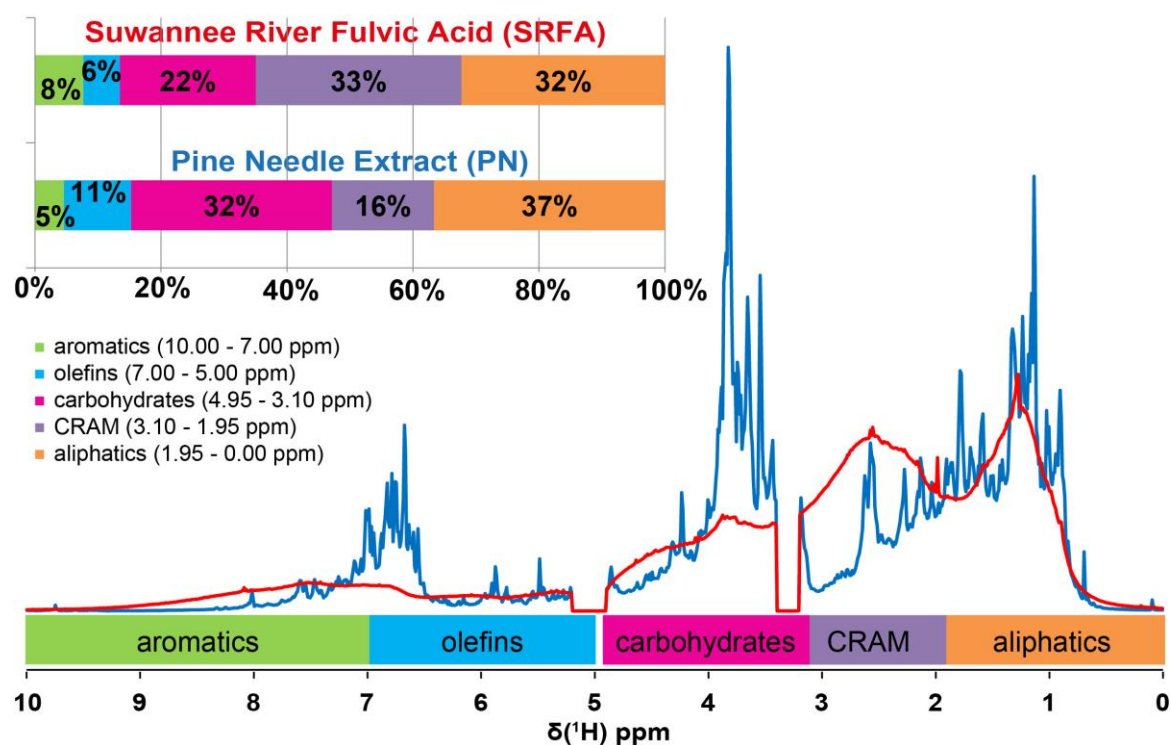
Figure 4-6: ^{1}H NMR spectra of SRFA and pine needle extract.
^{1}H NMR spectra (800 MHz, CD$_3$OD) of Suwannee River Fulvic Acid (SRFA) (depicted in red) and pine needle extract (PN) DOM (depicted in blue). Bar charts indicate ^{1}H NMR section integrals according to main substructures: aromatics (green), olefins (blue), carbohydrates (pink), CRAM (purple) and aliphatics (orange).

4.4.2. Overview of the reactivity of inorganic sulfur species with dissolved organic matter

In order to obtain comprehensive knowledge on the reactivity of reduced to oxidized sulfur species a great variety of experiments under conditions resembling typical ecosystem settings were performed (Figure 4-7). The formation of sulfur organic compounds was observed after 6 d for the reduced to intermediate inorganic sulfur species under all tested conditions. On the contrary, no reaction was observed with DOM and completely oxidized sulfate even after 24 d. Generally, sulfate is very stable under natural conditions and is a major ion in natural waters with average concentrations of 1.2 mmol kg^{-1} in rivers and 0.053 mmol kg^{-1} in the ocean (Bailey et al. 2002). Sulfur organic molecules are typically not major constituent of DOM (Lechtenfeld et al. 2011, Pohlabeln and Dittmar 2015, Wagner et al. 2015b, Gonsior et al. 2016), hence, abiotic reaction of organic molecules with sulfate was not very likely to be involved in the formation of sulfur organic molecules. This was confirmed with the performed laboratory experiments, in which no formation of sulfur organic molecules was found. Therefore, the following paragraphs only include reactions with reduced and intermediate oxidation state inorganic sulfur species. To increase the readability of the following paragraphs, they are referred to as all sulfur species.
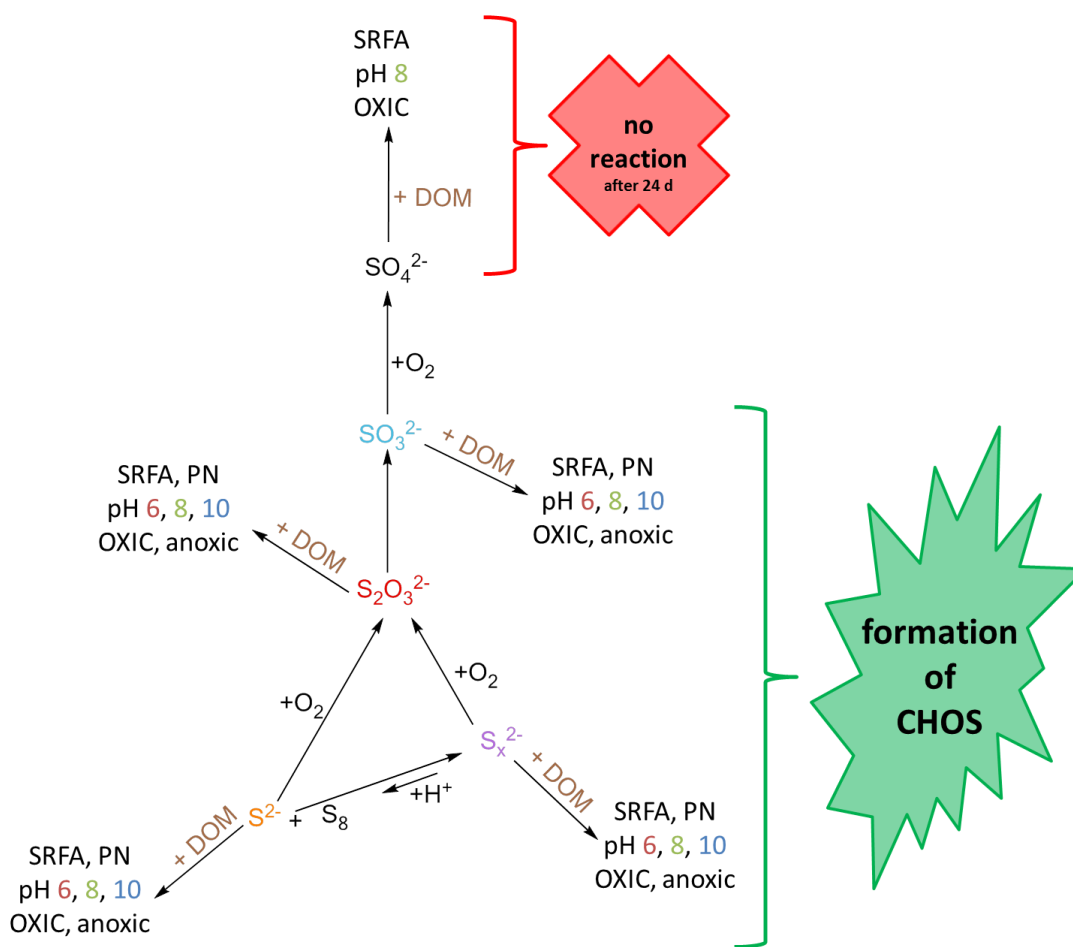
Figure 4-7: Overview of performed experimental conditions.
Scheme of the experimental conditions performed to assess the reactivity of inorganic sulfur species, i.e. sulfide (S^{2-}), polysulfide (S_x^{2-}), thiosulfate ($S_2O_3^{2-}$), sulfite (SO_3^{2-}) and sulfate (SO_4^{2-}), with DOM.

The formation of sulfur organic compounds, based on the number of assigned molecular formulas and the intensity weighted compositional contribution of the individual compound classes, for the reaction of SRFA-DOM with thiosulfate and sulfite is summarized in Table 6-9 and with sulfide and polysulfide in Table 6-10. The summaries for the reactions with PN-DOM are given in Table 6-11 and Table 6-12. Independently of the organic matter and inorganic sulfur species almost exclusively CHO compounds reacted in the formation of sulfur organic compounds, since only the number of CHOS molecular formulas and their intensity contribution increased significantly. The number of assigned CHO molecular formula was constant for the great majority of experimental conditions. Formation of nitrogen and sulfur containing compounds CHNOS were of minor abundance for all experiments. Hence, inorganic sulfur species preferentially react with non-nitrogen containing compounds. Important to note here is that this finding might be partly biased, since CHNO compounds are generally less abundant in organic matter,

105

especially analyzed with (–)ESI FT-ICR-MS, which favors the detection of acidic functional groups (Sleighter and Hatcher 2011).

Since only CHOS compounds varied decisively, hierarchical cluster analysis based on the CHOS compounds was performed to evaluate the similarity between the different experimental conditions (Figure 4-8). The analysis verified the reproducibility of the experimental setup (Figure 4-8A), because replicate experiments clustered together. The two hierarchical cluster analysis for PN and SRFA-DOM mostly resemble each other. This indicated that the general reaction behavior of the different inorganic sulfur species is independent of the DOM. In both clusters the experiments with thiosulfate (pH 6 and 8) resembled most to the CHOS already present in the DOM blanks. The experiments with sulfite were clearly separated from those with the reduced sulfur species.
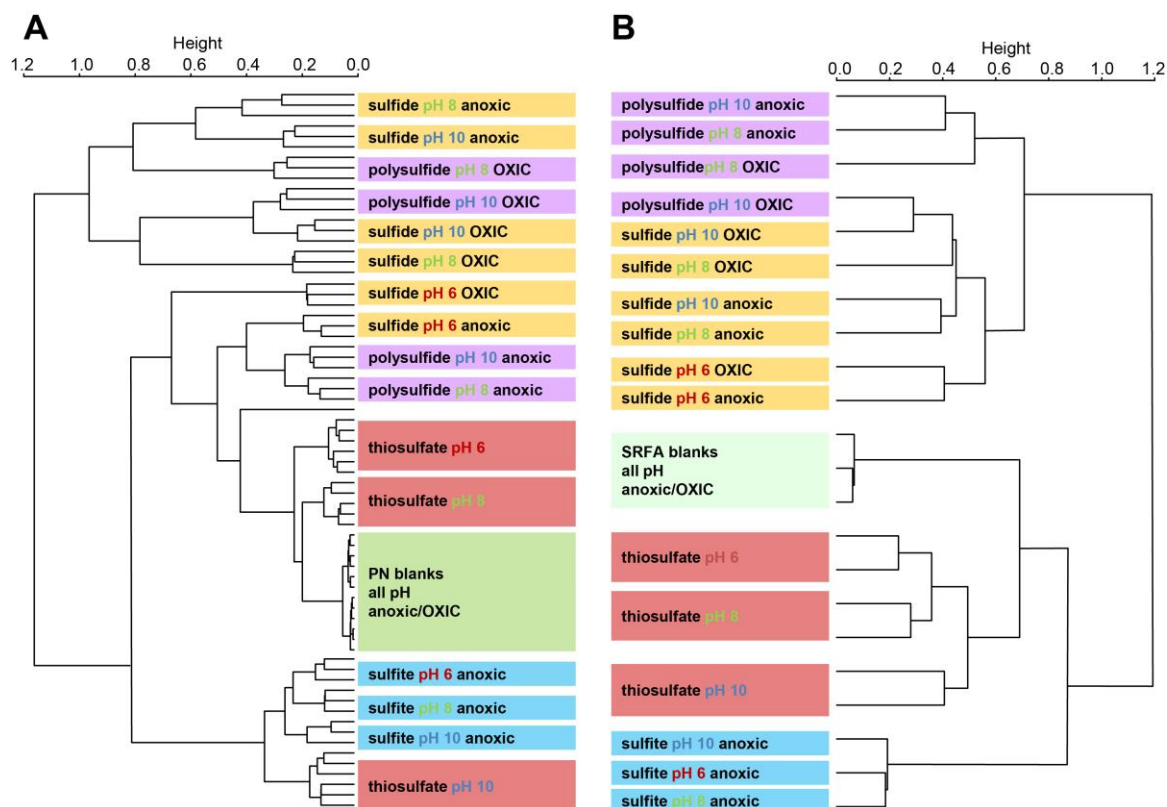
Figure 4-8: Hierarchical cluster analysis of the CHOS compound formation.
Hierarchical cluster analysis (Spearman rank correlation, average linkage) of the assigned CHOS compounds with and without addition of sulfide, polysulfide, thiosulfate and sulfite at pH 6, 8 and 10 under oxic and anoxic conditions from the experiments with A) pine needle extract (based on all replicates) and B) Suwannee River Fulvic Acid (based on mean intensities of peaks abundant in two out of three replicates).

Furthermore, the analysis revealed that both the pH and the oxygen saturation of the reaction solution have an influence on the formed CHOS compounds. Both findings were expected, due to the variations of the protonation state of the inorganic sulfur species according to their pK_a values and their stability at the different pH values, as well as their oxidation sensitivity. A detailed discussion on the respective behaviors is given below for the individual sulfur species.

In order to give a general overview of the sulfur organic compounds formed by the reaction of DOM and inorganic sulfur species, Figure 4-9 depicts the CHOS formed at pH 8 under anoxic conditions for all sulfur species and the two tested DOM. These conditions were chosen for the exemplary depiction due to their great resemblance to those found in natural aquatic ecosystems with intensive sulfur cycling, e.g. Hechtsee (chapter 2; Table 2−1) and the contaminated groundwater site in Düsseldorf Flingern (chapter 3; Figure 3-3), where CHOS compounds enriched DOM was found. Please see the Supplementary

Information for the detailed results of all the other experimental conditions (Figure 6-13, Figure 6-14, Figure 6-15, Figure 6-16, Figure 6-17 and Figure 6-18).

In consent with the similar pattern of the hierarchical cluster analysis, also the general reactivity of the inorganic sulfur species was similar for the experiments with PN and SRFA-DOM. In the following only the major characteristics of the formed CHOS compounds are summarized. The detailed discussion of the individual sulfur species reactivity is given below in individual paragraphs. Sulfite addition experiments resulted almost exclusively in the formation of $CHOS_1$ compounds. The addition of thiosulfate led to the formation of $CHOS_2$, and in the case of SRFA-DOM also $CHOS_4$, however, also to a great extend in the formation of $CHOS_1$. Surprisingly, a vast majority of the CHOS compounds formed in the experiments with polysulfide only carried one sulfur atom. Experiments with the most reduced sulfur species sulfide also led primarily to the formation of $CHOS_1$ compounds. A considerable number of molecules with more than one sulfur atom were formed, comparable to characteristic CHOS molecular formulas found at the two investigated field sites. Taken the general differences between PN and SRFA-DOM in the coverage of the van Krevelen chemical space of the CHO precursor compounds into consideration, the formed CHOS compounds with the different inorganic sulfur species also resemble.
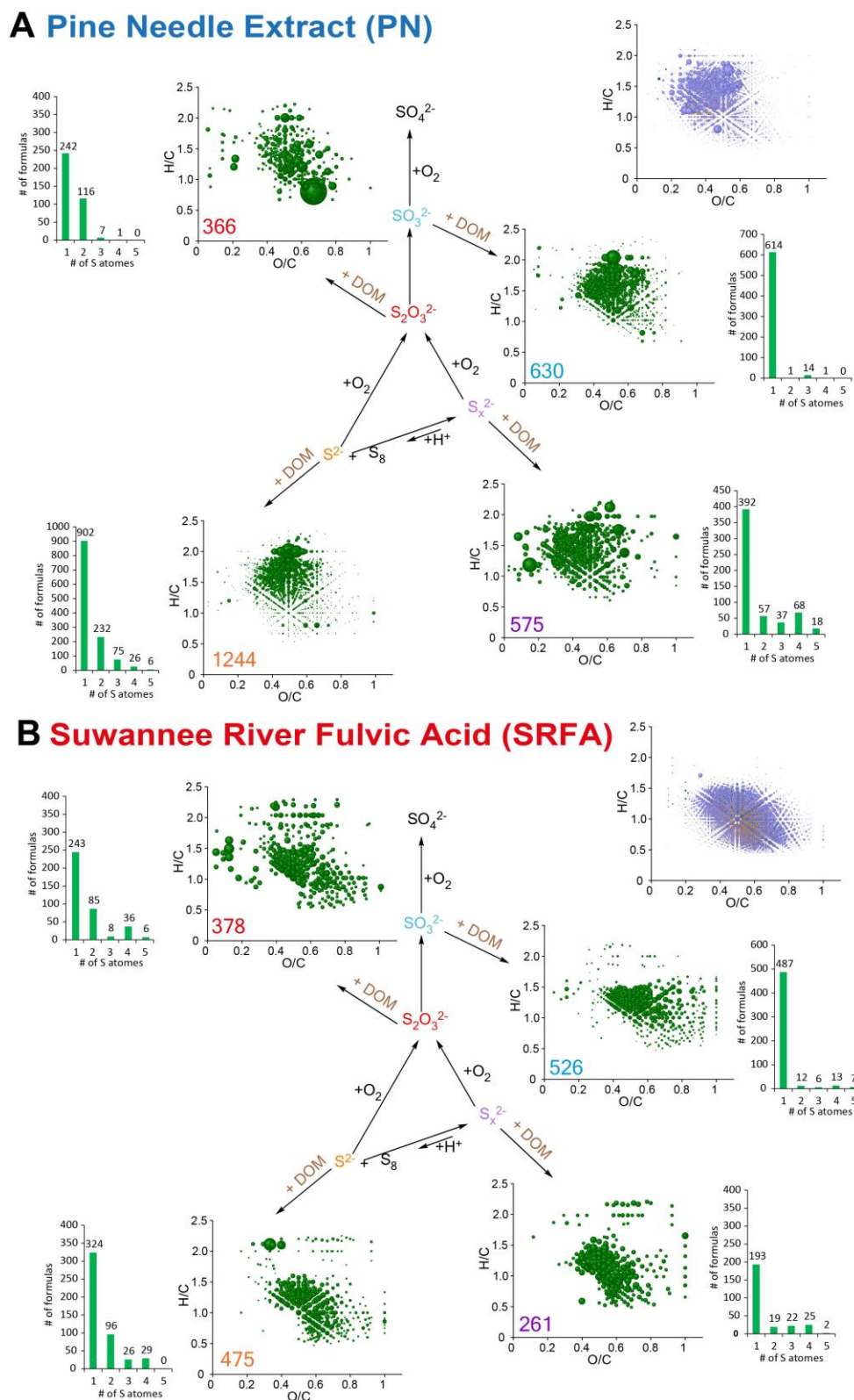
Figure 4-9: Formed CHOS compounds with the different inorganic sulfur species.
Van Krevelen diagrams and bar charts of the number of sulfur atoms incorporated in the formed CHOS compounds after the reaction of A) pine needle extract (PN) and B) Suwannee River Fulvic Acid (SRFA) with sulfide (S^{2-}), polysulfide (S_x^{2-}), thiosulfate ($S_2O_3^{2-}$) and sulfite (SO_3^{2-}) at pH 8 under anoxic conditions.

4.4.2.1. Comparison of the CHOS formation capacity of SRFA and PN

Clear differences in the CHOS formation capability of the two selected DOM was not only observed for the exemplarily depicted anoxic conditions at pH 8 (Figure 4-9), but for all experimental conditions. This is depicted by a broad overview of the reaction behavior of SRFA-DOM and PN-DOM in Figure 4-10, where the mean values of the number of assigned molecular formulas and the intensity weighted compositional contribution of the individual compound classes (CHO, CHOS, CHOS, CHNOS) for similar, according to the results of the hierarchical cluster analysis (Figure 4-8), experimental conditions are displayed. The number of CHOS molecules as well as their intensity weighted compositional contribution (% of intensity) was in total higher for the sulfur species addition experiments with PN-DOM than for those with SRFA-DOM. Interestingly, this trend was only predominantly pronounced for the reactions with the further reduced inorganic sulfur species, i.e. sulfide and polysulfide. This implied that the reaction of reduced sulfur species with OM occur at functional groups, which are preferentially present in fresh OM, which is less processed than the recalcitrant SRFA-DOM, whereas sulfite and thiosulfate react with molecular features present in both types of organic matter. The selectivity of reaction sites involved in the formation of CHOS compounds are discussed in detail in the individual paragraphs of the sulfur species.

4.4.2.2. Relation of the sulfur species nucleophilicity and CHOS formation

The nucleophilicity is a measure for the reactivity with positively polarized functional groups, such as carbonyls, in organic molecules. In order to evaluate the relation between the nucleophilicity of the inorganic sulfur species and the formation of sulfur organic compounds only the number of CHOS molecular formulas can be taken in consideration. The peak intensities might be biased for the different experimental settings, since acidic functional groups, such as sulfonic acids have higher ionization efficiencies than e.g. thiols in (–)ESI mass spectra (Sleighter and Hatcher 2011). Since the capacity of the CHOS formation with sulfide and polysulfide was comparably low for SRFA-DOM, but in a similar range for thiosulfate and sulfite, only the results of the reaction with PN-DOM can be taken under consideration (Figure 4-10B). Additionally, only the anoxic experiments can be contemplated, since the oxic experiments of sulfide and polysulfide include mixtures of inorganic sulfur species due to their oxidation (ascertained by inorganic sulfur speciation, data not shown). The number of formed CHOS follows with the trend of the nucleophilicity of the inorganic sulfur species (Suzuki 1999):

$$HS^- > RS^- > CN^- > SO_3^{2-} > OH^- > S_8 > S_2O_3^{2-} > S_4O_6^{2-} > SCN^- > Cl^-$$
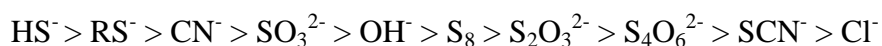
The polysulfide nucleophilicity is often reported to be even higher than the one of sulfide, but thorough literature research revealed contradictory statements, even when only nucleophilicity was discussed in relation to polysulfide chain length (Luther III 1990, Ahrika et al. 1999, Kleinjan, de Keizer and Janssens 2005). The here presented comprehensive investigations on the reactivity of equimolar levels of sulfide and polysulfide (predominantly synthesized Na_2S_4) with DOM, showed less formation of sulfur organic compounds with polysulfide. This implies that the nucleophilicity of polysulfides is often overestimated. However, it is important to note that the nucleophilicity is depending on the pH value and the state protonation of the sulfur species. Hence, this observation might not be generalizable. Furthermore, other factors such as steric hindrance and the abundance of reactive functional sites are also influencing the reactivity.
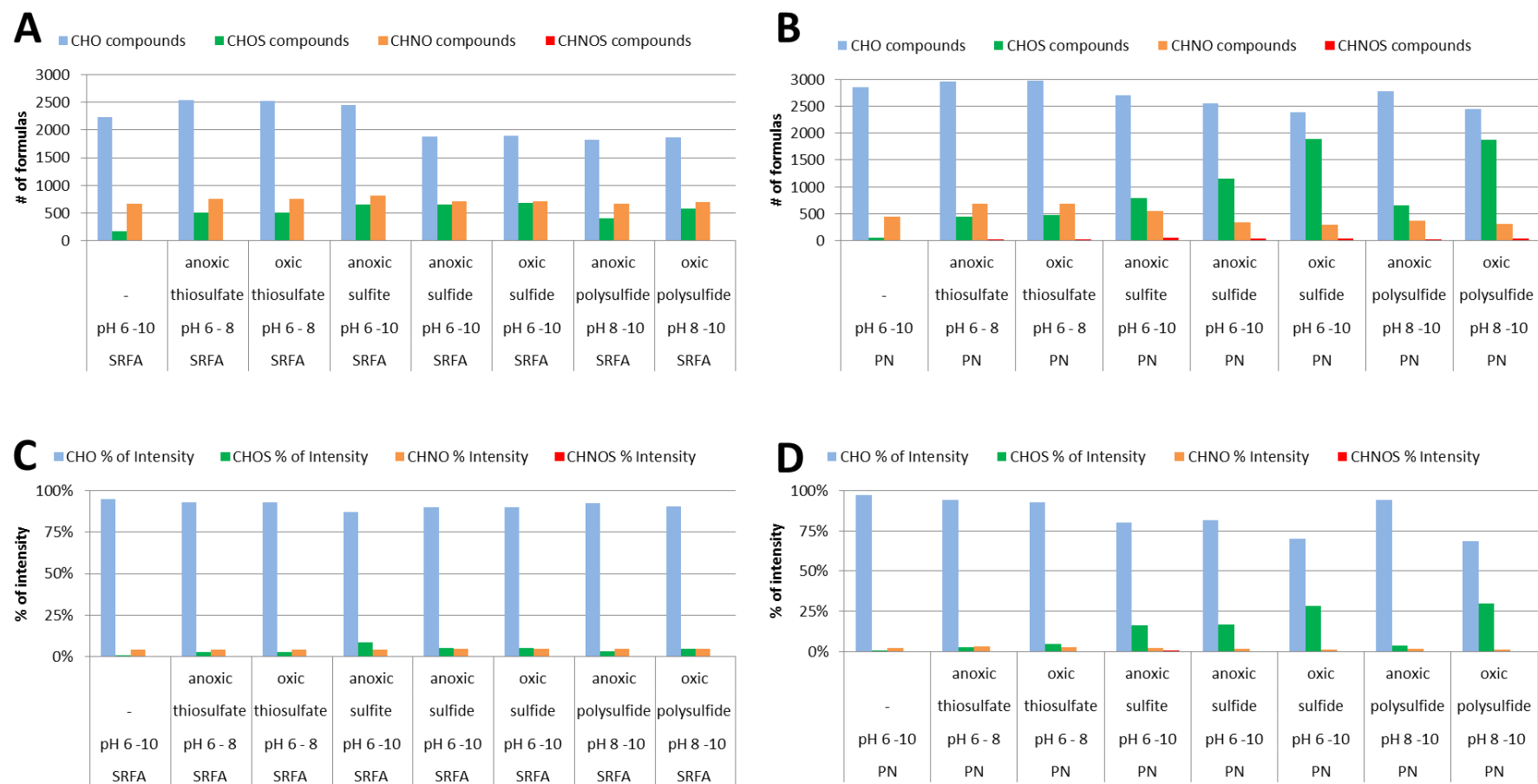
Figure 4-10: Comparison of the CHOS formation capacity.
Mean value of the number of annotated molecular formulas of similar experimental conditions with A) Suwannee River Fulvic Acid (SRFA) and B) pine needle extract (PN). Mean values of the intensity weighted compositional contribution of the individual compound classes (% of intensity) of similar experimental conditions with C) Suwannee River Fulvic Acid (SRFA) and D) pine needle extract (PN).

4.4.2.3. Comparison of the oxic and anoxic reaction conditions

The comparison of the reactivity under oxic and anoxic conditions is of special interest for the reduced sulfur species, which are prone to oxidation in the presence of oxygen. The major oxidation product of sulfide and polysulfide in oxic water is thiosulfate (Chen and Morris 1972, O'Brien and Birkner 1977, Zhang and Millero 1993, Rickard 2012). Also in the oxic experiments with sulfide and polysulfide, thiosulfate was detected as major oxidation product (data not shown). Furthermore, the experiments with polysulfide at pH 8 under anoxic conditions resulted, besides the precipitation of elemental sulfur, in the formation of thiosulfate (data not shown). Polysulfides are very stable in alkaline solutions, but their stability is limited at lower pH values (Kamyshny et al. 2004, Rickard and Luther III 2007, Rickard 2012). Furthermore, DOM was reported to be involved in the oxidation of sulfide (Heitmann and Blodau 2006, Yu et al. 2015a, Yu et al. 2015b). However, inorganic sulfur speciation of the anoxic experiments did not show considerable amounts of oxidation products within 6 days.

Since the CHOS formation was higher with PN than SRFA-DOM, the following analysis was focused for an enhanced comprehension on the experiments with PN-DOM. The hierarchical cluster analysis (Spearman rank correlation) in conjunction with the corresponding heat maps enabled the extraction of characteristic masses for individual experimental conditions and groups of conditions, which led to the formation of the same sulfur organic compounds (Figure 4-11, Figure 4-12). The hierarchical cluster analysis of the anoxic model experiments (Figure 4-11) can be considered for comparison with anaerobic field sites, which show an enrichment of sulfur organic compounds, such as the hypolimnic water DOM from the meromictic lake Hechtsee (cf. chapter 2) and the bacterial sulfate reduction hotspot at the petroleum hydrocarbon contaminated groundwater system in Düsseldorf Flingern (cf. chapter 3). For the evaluation of the formation of sulfur organic compounds under oxic conditions, such as specific hydrothermal springs (e.g. Elk Geyser in Yellowstone National Park) the hierarchical cluster analysis of the oxic model experiments (Figure 4–12) can be considered for comparison.
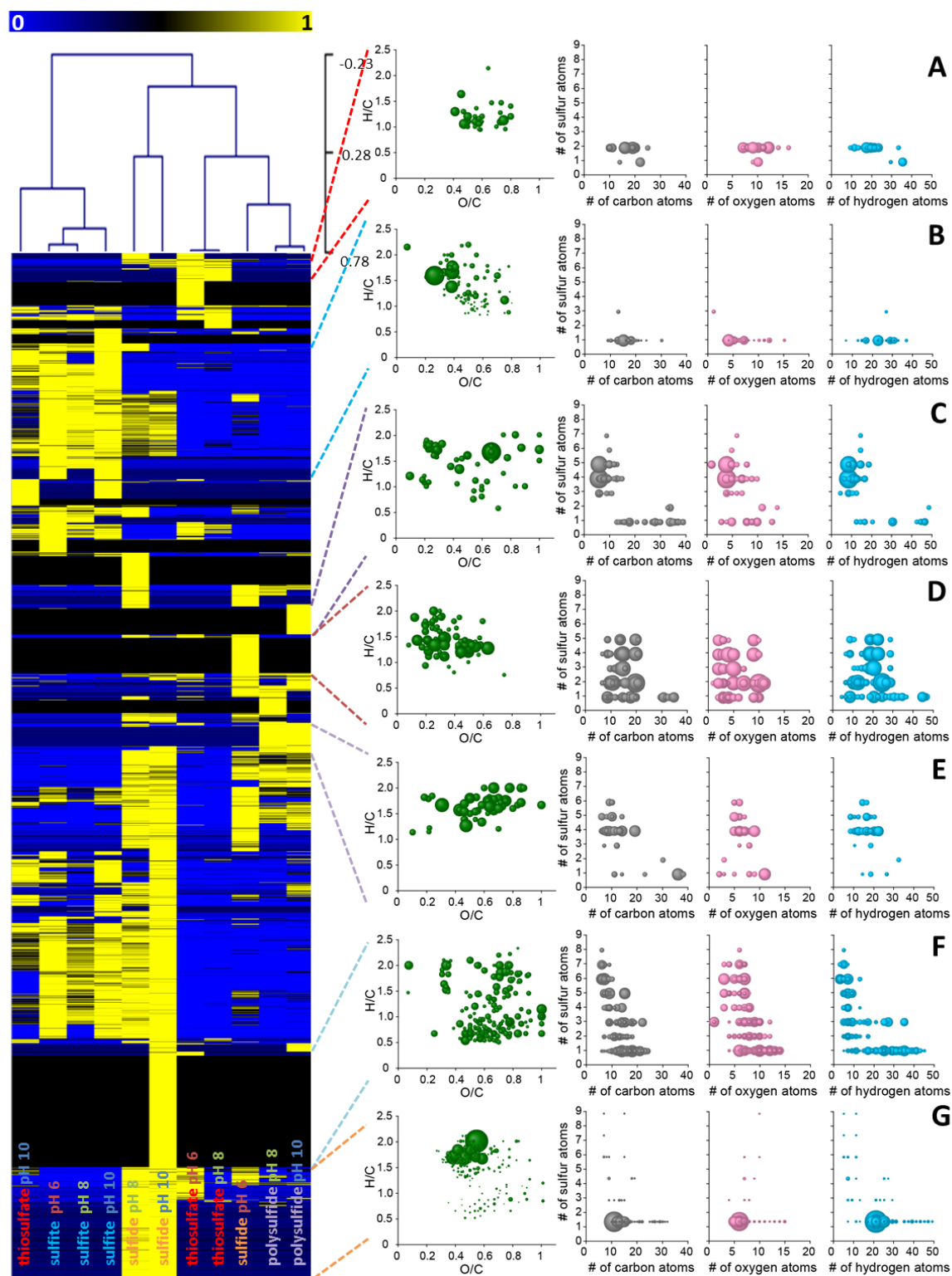
Figure 4-11: Hierarchical cluster of CHOS compounds formed at anoxic conditions.
Hierarchical cluster analysis (Spearman rank correlation) of the formed CHOS compounds after reaction of PN-DOM with sulfide, polysulfide, thiosulfate and sulfite at pH 6, 8 and 10 at anoxic conditions. The heat map, van Krevelen diagrams and sulfur vs. carbon, oxygen and hydrogen plots (bubble areas represent the abundance) depict the characteristic molecular masses for individual experimental conditions and groups of conditions.
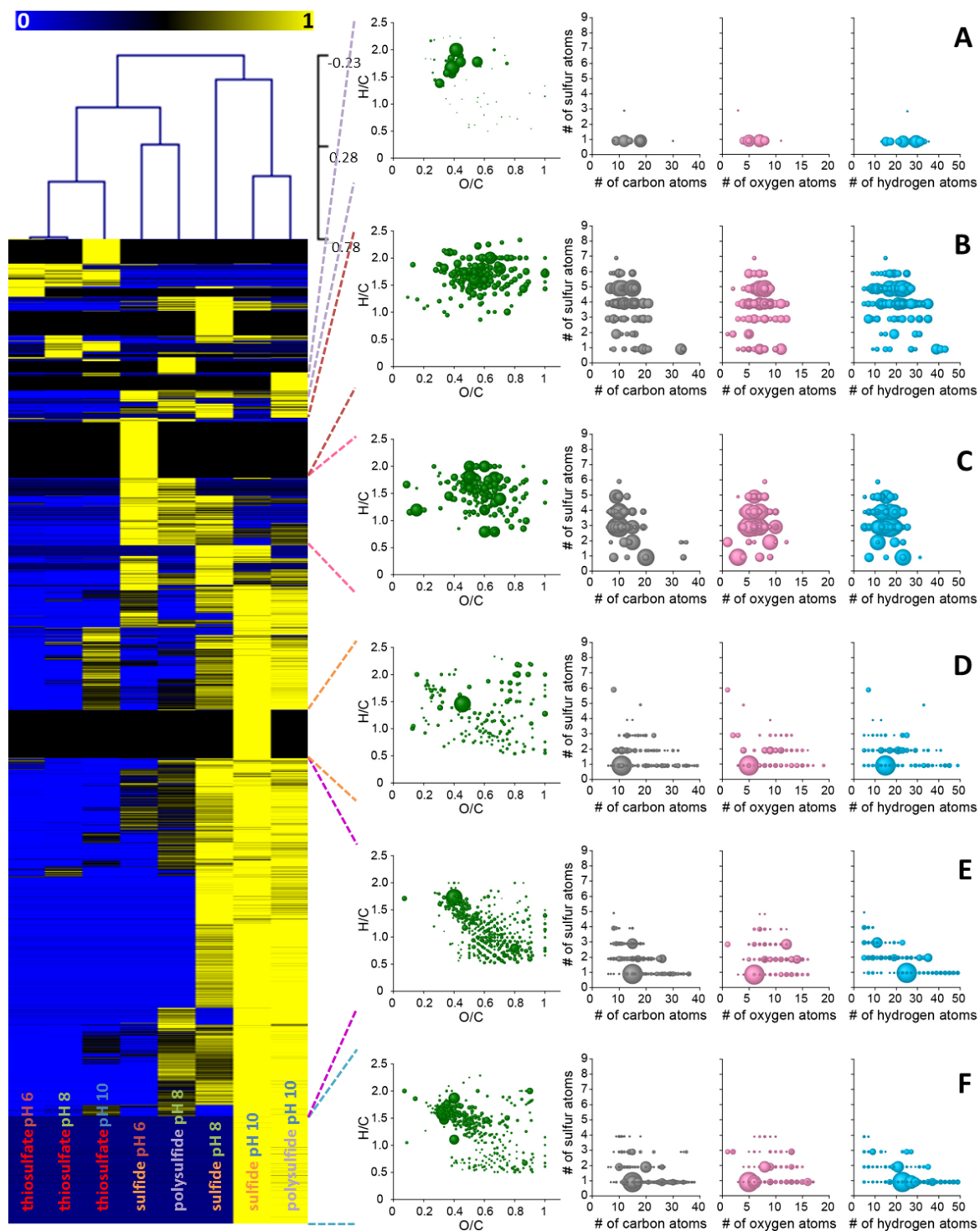
Figure 4-12: Hierarchical cluster of CHOS compounds formed at oxic conditions.
Hierarchical cluster analysis (Spearman rank correlation) of the formed CHOS compounds after reaction of PN-DOM with sulfide, polysulfide and thiosulfate at pH 6, 8 and 10 at oxic conditions. The heat map, van Krevelen diagrams and sulfur vs. carbon, oxygen and hydrogen plots (bubble areas represent the abundance) depict the characteristic molecular masses for individual experimental conditions and groups of conditions.

The direct comparison of the characteristic CHOS formed by the reaction of the further reduced sulfur species sulfide and polysulfide is substantially different under oxic and anoxic conditions. As a result of progressing sulfur species oxidation, CHOS formed under oxic conditions had generally higher O/C values. However, also under anoxic conditions at pH 8 and 10 CHOS compounds with O/C > 0.5 are formed in experiments with reduced sulfur species. These molecules typically have multiple sulfur atoms. This is in agreement, with the observed characteristic CHOS compounds of sulfide rich field sites (cf. chapter 2 and 3). An in depth discussion of the characteristic CHOS formed at the individual experimental conditions is given in the following paragraphs, whereby the reactivity of sulfite is discussed first, followed by thiosulfate and topped off with sulfide and polysulfide.

4.4.3. Details on the reactivity of the individual sulfur species

4.4.3.1. Reactivity of sulfite with DOM

Sulfite is readily oxidized to sulfate by O_2, thus reactivity was exclusively studied under anoxic conditions (Holleman, Wiberg and Wiberg 2007). Hierarchical cluster analysis showed similar reaction behavior of sulfite independent of the pH value (Figure 4-8). Important to note here is that sulfite samples cluster together with thiosulfate experiments performed at pH 10, because of hydrolysis of thiosulfate (Holleman et al. 2007).

Independent of the pH almost exclusively $CHOS_1$ molecules, like exemplarily shown for pH 8 in Figure 4-9, were formed (Figure 6-17 and Figure 6-18). Further elaboration by cluster analysis in conjunction with the extraction of characteristic masses for the individual sulfur species also proofed characteristic molecular formulas after reaction with sulfite were all $CHOS_1$ compounds (Figure 4-11 B).

The intensity weighted compositional contribution of CHOS was similar or higher for the experiments with sulfite compared to those with sulfide under anoxic conditions, while the number of assigned molecular formulas was in the same range or even lower (Figure 4-10; Table 6-9, Table 6-10, Table 6-11, Table 6-12). This is a clear indication that sulfonic acids were formed, which have increased ionization efficiencies in (–)ESI. This is in agreement, with previous laboratory studies with sulfite and α,β-unsaturated organic compounds (e.g., ethyl acrylate), that resulted in the formation of sulfonic acids $R\text{-}SO_3^-$ (Vairavamurthy et al. 1994). Sulfonation reactions entail an increase of the O/C ratio

which is illustrated by the van Krevelen diagrams of the CHOS compounds and their putative CHO precursor molecules (Figure 4-13). For the formation of $C_xH_yO_{z+3}S$ molecular formulas 82% of the precursor $C_xH_yO_z$ molecular formulas were present in the PN-DOM blank. Again corroborating that sulfonation reactions are most likely occurring.

Figure 4-13: Putative CHO precursor molecules from the incorporation of sulfite.
Van Krevelen diagrams of the putative CHO precursor molecules present in the PN-DOM blank and the formed $CHOS_1$ compounds resulting from the incorporation of sulfite at pH 6.

Sulfite reactivity based on the number of reaction products (Figure 4-10 A, B) was only slightly increase and the intensities were doubled for PN-DOM compared with SRFA-DOM (Figure 4-10 C, D). This implies that sulfite preferentially reacts with functional groups more abundant in fresh DOM such as double bonds (cf. ^{1}H NMR spectra Figure 4-6). However, the aliphatic section integrals were comparable for the two DOM (32% and 37%) and in conjunction with their distinct coverages of the source CHO (Figure 4-5) and formed CHOS compounds van Krevelen chemical space (Figure 4-9), hinted that sulfite had a tendency for the reaction with more aliphatic compounds.

4.4.3.2. Reactivity of thiosulfate with DOM

The reactivity of thiosulfate is best to be investigated under pH 6 conditions, due to its hydrolysis in alkaline solutions (Holleman et al. 2007). Therefore, the experiments with thiosulfate at pH 10 resembled those with sulfite (see above) and the most $CHOS_2$ compounds were found at pH 6 conditions were thiosulfate hydrolysis is not occurring.

The reactivity of thiosulfate was independent of the oxygen saturation of the experimental solution, because of the stability of thiosulfate towards O_2. Comparably low numbers and intensity weighted compositional contribution of CHOS compounds formed with

thiosulfate were found for both types of DOM (Figure 4-10). Furthermore, experiments with thiosulfate clustered with the CHOS present in the DOM blanks (Figure 4-8). Formation of sulfur organic compounds has also been shown in laboratory studies with α,β-unsaturated organic compounds (e.g., ethyl acrylate), that resulted in the formation of sulfonic acids (R-SO_3^-), proposed to be generated from disproportionation of organic thiosulfates R-$S_2O_3^-$ (Vairavamurthy et al. 1994). However, in the experiments with PN and SRFA-DOM the formation of $CHOS_2$ was observed (Figure 4-9) and almost exclusively $CHOS_2$ compounds were identified by hierarchical cluster analysis as characteristic masses for the thiosulfate reactivity with DOM (Figure 4-11A). For the formation of $C_xH_yO_{z+3}S_2$ molecular formulas 79% of the precursor $C_xH_yO_z$ molecular formulas were present in the PN-DOM blank. This indicated that the incorporation of thiosulfate function entities in organic molecules is very likely occurring and that disproportionation postulated by Vairavamurthy et al. might in fact only play a minor role (Vairavamurthy et al. 1994). The formed $CHOS_2$ compounds clearly have lower H/C and higher O/C ratios then the $CHOS_1$ compounds formed from sulfite (Figure 4-13). Since hydrogen and oxygen numbers are changing in the same way for sulfite and thiosulfate incorporation to organic molecules, organic thiosulfates are formed from further oxidized and more aromatic types of molecules than sulfonic acids. The low abundance of CHOS compounds in the experiments with DOM and thiosulfate, is most likely explained by the low nucleophilicity of thiosulfate (Suzuki 1999). This also suggests that nucleophilic attack is of minor importance to the thiosulfate reactivity.

Figure 4-14: Putative CHO precursor molecules from the incorporation of thiosulfate.
Van Krevelen diagrams of the putative CHO precursor molecules present in the PN-DOM blank and the formed $CHOS_2$ compounds resulting from the incorporation of sulfite at pH 6.

4.4.3.3. Reactivity of sulfide and polysulfide with DOM

Previous studies already showed the incorporation of sulfide (Vairavamurthy and Mopper 1987, Sinninghe Damsté et al. 1989, De Graaf et al. 1992, Perlinger et al. 2002, Hebting et al. 2006) and polysulfides (LaLonde et al. 1987, Schouten et al. 1994, Amrani and Aizenshtat 2004b, Amrani et al. 2007, Schouten et al. 1993) at double bonds and especially α,β-unsaturated carbonyls. Based on the above discussed strong nucleophilicity of sulfide, most sulfur organic compounds were formed in the reactions with sulfide (Figure 4-10). The reactivity of polysulfide with SRFA and PN-DOM was lower (Figure 4-10), although polysulfide has been claimed to be the most reactive inorganic sulfur species with organic matter (Aizenshtat and Amrani 2004). A direct comparison of polysulfide and sulfide reactivity showed that polysulfide is especially more reactive towards activated unsaturated molecules having a terminal carboxyl group (e.g. acrylic acid, cinnamic acid) and thus formation of thiols by Michael addition (Vairavamurthy and Mopper 1989). In agreement with the above cited literature, reduced sulfur species preferentially reacted with double bonds, which had an increased abundance in the fresh PN-DOM (olefin section integral of ^{1}H NMR spectrum, Figure 4-6).

Overview of the presence of oxidation products from reduced sulfur species

The reaction was also clearly influenced by the oxygen saturation of the experimental solution and the resulting oxidation products that also reacted with DOM. A clear evidence for this was the increased number and especially intensity weighted compositional contribution of CHOS compounds (increased ionization efficiency of oxidized sulfur organic functionalities), which were both higher for the oxic experiments, especially for the reactions with PN-DOM (Figure 4-10). For both, sulfide and polysulfide, thiosulfate was the major oxidation product, which was only detectable in the oxic experiments (data not shown). Furthermore, polythionates, polysulfane monosulfuric acids and polysulfanes have been almost exclusively identified in some FT-ICR mass spectra of the SPE-DOM from the experiments with sulfide and polysulfide (Figure 4-15). Polythionates and polysulfane monosulfuric acids are important intermediates of the abiotic sulfur redox transformations (Takano and Watanuki 1988, Suzuki 1999, Xu et al. 2000, Druschel et al. 2003c) and are formed by the reaction, e.g. of sulfur dioxide with hydrogen sulfide (Schmidt and Heinrich 1958, Druschel et al. 2003a). Polythionate and polysulfane monosulfuric acids were most abundant in the oxic experiments with polysulfide and PN-DOM, suggesting polysulfide oxidation was enhanced in the presence

of DOM. Furthermore, S_6-polysulfane was detected and confirmed by isotopic pattern comparison (Figure 6-19) in the polysulfide blank under alkaline and anoxic conditions. This showed that polysulfide is under the given conditions even stable over 6 days in aqueous solution and even during the SPE sample preparation method.

Additionally, to O_2 based oxidation of reduced sulfur species, other studies observed the oxidation of sulfide by electron transfer from DOM resulting in the formation of thiosulfate (Heitmann and Blodau 2006, Yu et al. 2015a, Yu et al. 2015b). Therefore, it is crucial to elaborate which sulfur organic compounds were characteristically or even exclusively formed by the reaction with sulfide and polysulfide for a correct evaluation of their reactivity. This was performed by means of hierarchical cluster analysis of the CHOS compounds formed under anoxic (Figure 4-11) and oxic (Figure 4–12) conditions. Furthermore, the analysis enabled the distinction of CHOS compounds based on the pH dependency of the reactivity.
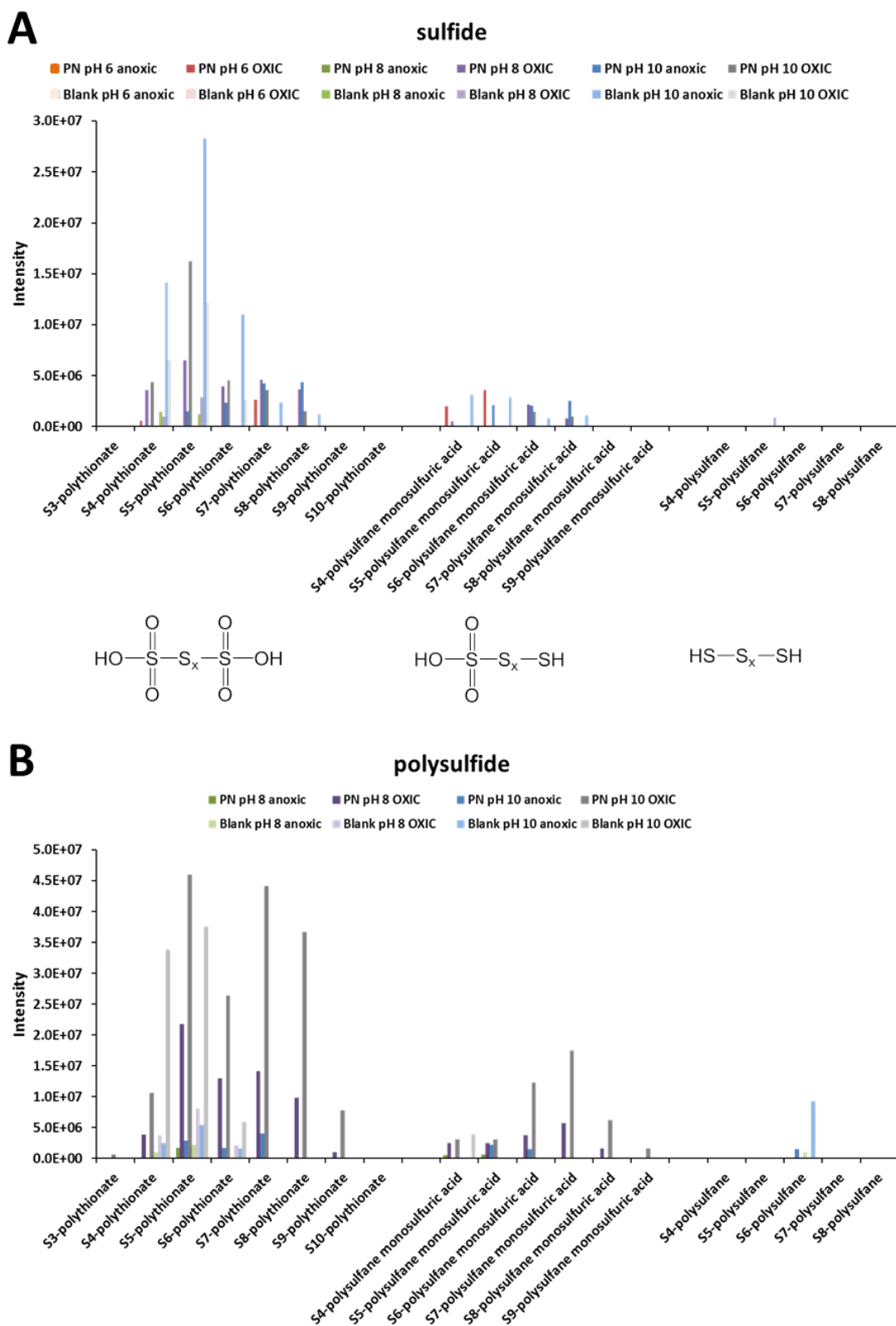
Figure 4-15: FT-ICR-MS based inorganic polysulfur speciation of the experiments with pine needle DOM.
Polythionates, polysulfane monosulfuric acids and polysulfane present in the FT-ICR mass spectra of experiments with A) sulfide and B) polysulfide and PN-DOM and the respective sulfur species blanks.

Reactivity of sulfide with DOM at anoxic conditions

Sulfide reactivity at anoxic conditions was dominated by the formation of $CHOS_1$ compounds for all pH values. Formation of primarily $CHOS_1$ was also reported for the reaction of monosaccharides with sulfide and elemental sulfur (resulting in a mixture of sulfide and polysulfide, cf. Figure 4-2) in aqueous solutions (van Dongen et al. 2003).

Sulfide was most reactive at pH 10 where the dominating sulfide species is very nucleophilic HS^- and least reactive at pH 6 where the dominating sulfide species is less nucleophilic H_2S (Figure 6-13, Table 6-12) (Suzuki 1999, Rickard 2012). Thus, decreased formation of sulfur organic compounds at lower pH values most likely resulted from less dissolved sulfide in solution because H_2S gas was also in the head space above the reaction solution as well as a decreased occurrence of nucleophilic addition reactions. The formation of $C_xH_{y+2}O_zS$ compounds by the incorporation of hydrogen sulfide into CHO is illustrated exemplarily for pH 10 in Figure 4-16, whereby 79% of the precursor $C_xH_yO_z$ molecular formulas were present in the PN-DOM blank. 25% of the precursor CHO (depicted in dark blue) were completely absent after reaction with sulfide and additional 29% (depicted in gray) were considerably reduced (C_F((Intensity PN Blank)/(Intensity PN + Sulfide)) > 1.5 (Liger-Belair et al. 2009)), further corroborating the pronounced reactivity of sulfide, which leads to a slightly increased H/C ratio of the CHOS. The molecules which were only reduced after reaction of sulfide (depicted in gray) resemble in SRFA-DOM in the coverage of the of van Krevelen space. Hence, explaining the lower abundance of CHOS formed with SRFA-DOM than with PN-DOM.
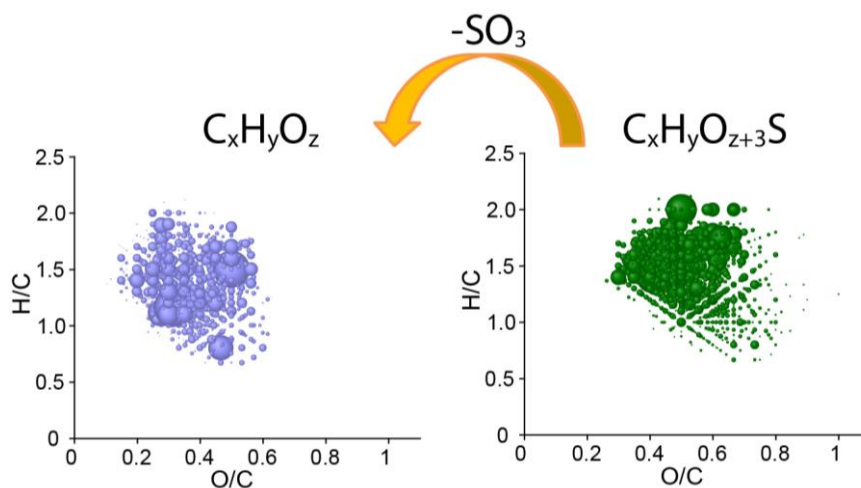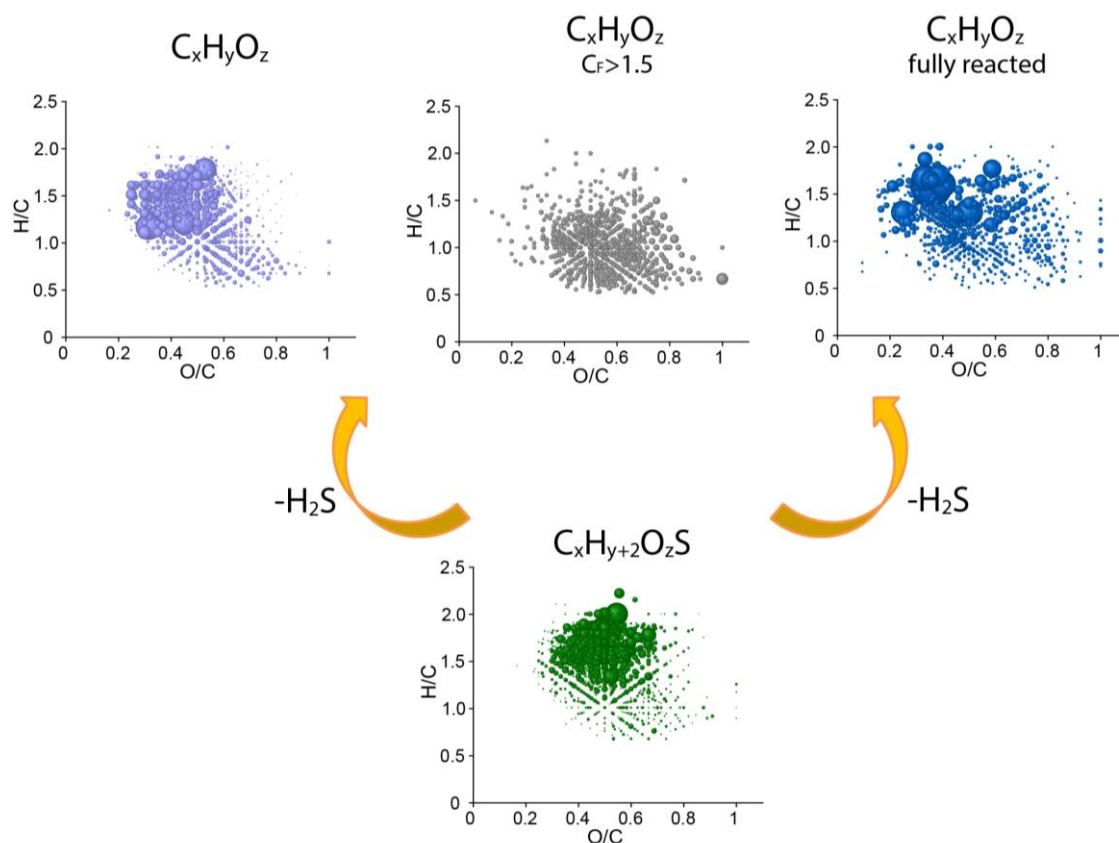
Figure 4-16: Putative CHO precursor molecules from the incorporation of hydrogen sulfide. Van Krevelen diagrams of the putative CHO precursor molecules present in the PN-DOM blank and the formed $CHOS_1$ compounds resulting from the incorporation of hydrogen sulfide at pH 10 under anoxic conditions.

Hierarchical cluster analysis enabled the extraction of characteristic molecular formulas formed at the different pH values (Figure 4-11). The characteristic molecular formulas formed at pH 6 were more saturated molecules ($H/C > 1$) and less oxidized ($O/C < 0.6$, low number of oxygen atoms in the molecules), hence the carbon oxidation state of these molecules was quite reduced (Figure 4-11D). Molecules like that are unlikely to undergo nucleophilic addition reaction but more probably undergo electrophilic addition of hydrogen sulfide. This is in agreement with the protonation state and thus reduced nucleophilicity of sulfide at pH 6 and electrophilic additions occurring preferentially under acid catalysis (cf. addition of water to alkenes which requires acid catalysis). Based on the low number of oxygen atoms in combination with the incorporation of multiple sulfur atoms, sulfur functionalities in these molecules had to be at least in parts of reduced type (cf. chapter 2.4.3.2). Some of the generally dominating $CHOS_1$ compounds, with medium range O/C rations were found to be especially occurring at pH 8 and 10 (Figure 4-11G). The further oxidized carbon oxidation state of these molecules result in an

123

increased carbon electrophilicity and thus these molecules are expected to undergo nucleophilic addition reactions, which is favored at alkaline pH values. This is in agreement with the sulfur organic molecules formed at pH 10, where sulfurization of even further oxidized compounds (O/C high and H/C also low) occurred (Figure 4-11F). Additionally, polysulfurized molecules with low numbers of oxygen, again testified for the presence of reduced sulfur species in the organic molecules (cf. chapter 2.4.3.2), were characteristic at pH 10. These $CHOS_x$ molecules were comparable to those exclusively formed in the experiments with polysulfide (see below).

Reactivity of polysulfide with DOM at anoxic conditions

Polysulfide is not stable at pH 6 and very stable in alkaline solutions with pH $\geq$ 10 (Kamyshny et al. 2004). Thus, experiment with polysulfide were not performed at pH 6 condition and also at pH 8 polysulfide was partly oxidized to thiosulfate and elemental sulfur immediately after addition to the DOM solution (formation of precipitate, sulfur speciation data).

Like the sulfide, also the polysulfide reactivity at anoxic conditions was dominated by the formation of $CHOS_1$ compounds independently of the pH value. This is in agreement with the findings of primarily $CHOS_1$ from the reaction of monosaccharides with sulfide and elemental sulfur (resulting in a mixture of sulfide and polysulfide, cf. Figure 4-2) in aqueous solution (van Dongen et al. 2003). Furthermore, primarily $CHOS_1$ formation showed that only minor part of polysulfide is incorporated directly as S_x into the organic molecules. Hence, the reaction of polysulfide with DOM is not only characterized by the addition of polysulfide chains to double bonds, like it has been shown in laboratory experiments (LaLonde et al. 1987, Schouten et al. 1994, Amrani and Aizenshtat 2004b, Amrani et al. 2007, Schouten et al. 1993), but also by the disproportionation of polysulfide. The latter is very likely comparable to the oxidation of sulfur species by organic matter like it was reported for sulfide (Heitmann and Blodau 2006, Yu et al. 2015b, Yu et al. 2015a).

However, reaction of polysulfide with DOM also resulted in the formation polysulfurized organic molecules. Since tetrasulfide was used in the experiments particularly $CHOS_4$ compounds were formed (Figure 4-9, Figure 6-15 and Figure 6-16). For the formation of $C_xH_{y+2}O_zS_4$ molecular formulas 70% of the precursor $C_xH_yO_z$ molecular formulas were present in the PN-DOM blank (Figure 4-17). This indicated that the incorporation of

tetrasulfide function entities in organic molecules very likely occurred. MS/MS fragmentation of the polysulfurized PN-DOM confirmed the incorporation of tetrasulfide into DOM, since only the loss of H_2S_4 was detected from the parent ion identified as $[C_{10}H_{11}O_6S_4]^-$ (Figure 4-18).
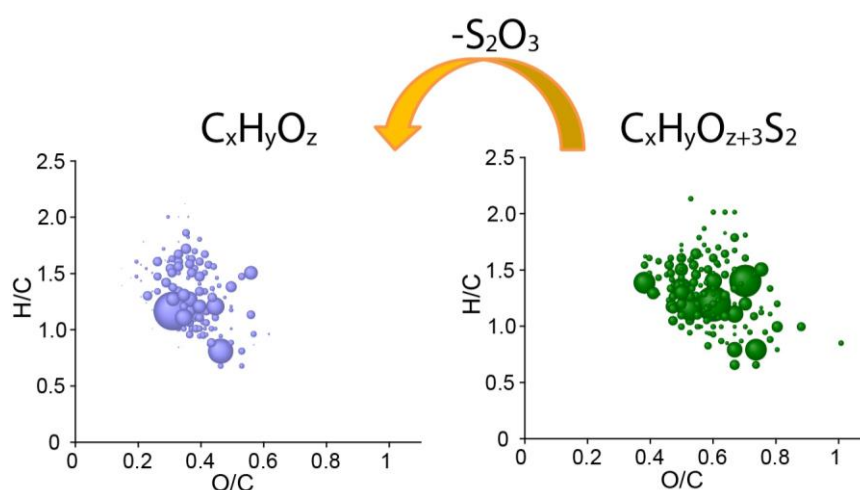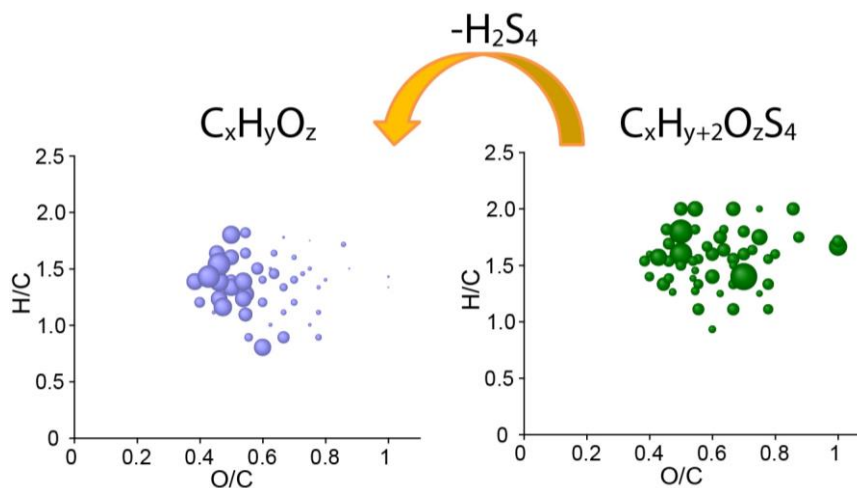

Figure 4-17: Putative CHO precursor molecules from the incorporation of polysulfide.
Van Krevelen diagrams of the putative CHO precursor molecules present in the PN-DOM blank and the formed $CHOS_1$ compounds resulting from the incorporation of polysulfide at pH 10 under anoxic conditions.

Hierarchical cluster analysis confirmed the formation of $CHOS_x$ exclusively formed by the reaction of DOM with polysulfide (Figure 4-11E). The low numbers of oxygen atoms present in these molecules testified for the presence of reduced sulfur species in the organic molecules (cf. chapter 2.4.3.2) which was even verified by MS/MS fragmentation (Figure 4-18). As a result of the increased stability of polysulfide in alkaline solutions and the favorable conditions for nucleophilic addition reactions more unique polysulfurized molecules were found at pH 10 (Figure 4-11C).
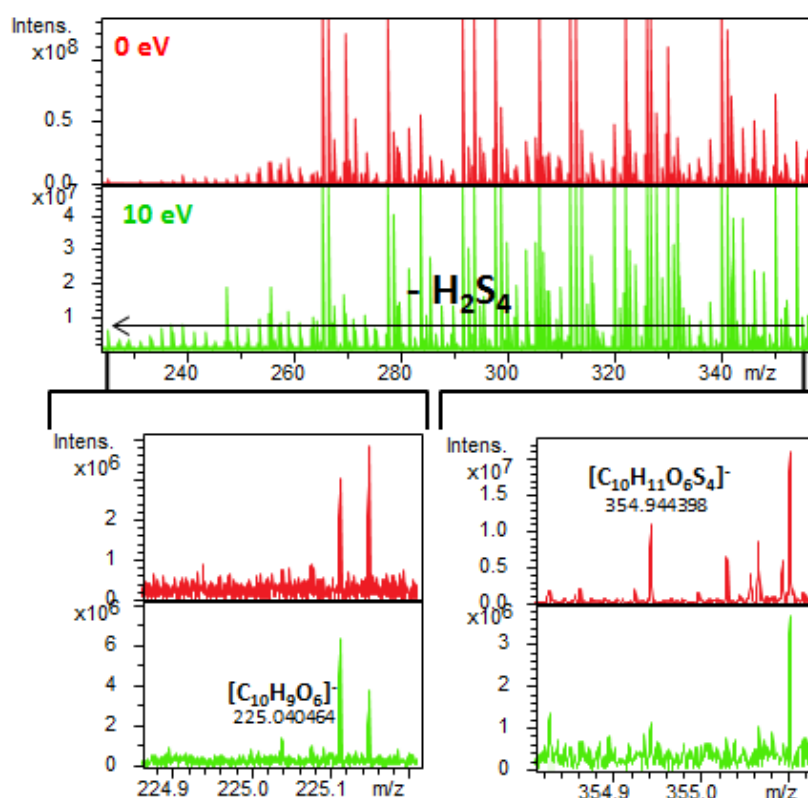
Figure 4-18: CID MS/MS spectrum of PN-DOM reacted with polysulfide.
CID MS/MS spectrum (m/z = 290 ± 55) of PN-DOM reacted with polysulfide at pH 10 (anoxic) conditions. The m/z 354.944398 has the molecular formula $[C_{10}H_{11}O_6S_4]^-$ (validated by the isotopic pattern). Only the loss of H_2S_4 was detected in the MS/MS spectra (collision energy 10 and 20 eV). Other typical losses from oxidized sulfur functionalities, such as SO_3 and SO_2 were not detected.

Reactivity of sulfide and polysulfide with DOM at oxic conditions

In the presence of oxygen the reactivity was not only based on the original reduced sulfur species but also on their oxidation products, such as thiosulfate (major oxidation product) and polythionates. Generally, this mixed reactivity of reduced to oxidized sulfur species resulted in an increased formation of sulfur organic compounds with multiple sulfur atoms (Figure 6-13, Figure 6-14, Figure 6-15 and Figure 6-16).

Hierarchical cluster analysis of the experiments at oxic conditions revealed similar reaction behavior of sulfide (pH 8 and 10) and polysulfide at pH 10 (Figure 4–12). The characteristically formed sulfur organic compounds were oxidized with low H/C and high O/C ratios (Figure 4–12E). This coverage of the van Krevelen chemical space was not observed for the direct reaction with the oxidized sulfur species thiosulfate and sulfite (Figure 4-9, Figure 4-11A, B). Hence, these oxidized CHOS compounds were directly formed from intermediate oxidation state sulfur species such as polythionates and

polysulfane monosulfonic acids, which were in particular present in the oxic experiments with polysulfide (Figure 4-15), and/or oxidation products of polysulfurized organic molecules. As a result of the above discussed increased reactivity of sulfide and polysulfide at pH 10, also more sulfur organic compounds were exclusively formed at pH 10 (Figure 4−12 A, D, F). Whereby an increased formation of $CHOS_1$ compounds, which resembled those formed from DOM and sulfite (Figure 4-11B), was particularly found for the polysulfide experiments (Figure 4−12A). However, it is unclear whether sulfite resulting from the oxidation of polysulfide reacted or the sulfonic acids were formed from the oxidation of thiol functionalities.

Further, sulfide at pH 6 and polysulfide at pH 8 showed similar reaction behavior (Figure 4−12). These reactions resulted in the formation of polysulfurized CHOS compounds, where sulfur functionalities were at least partially present in reduced form due to the low number of oxygen atoms present in the molecules (cf. chapter 2.4.3.2, Figure 4−12C). Analogous to the pH 6 reactions with sulfide at anoxic condition (Figure 4-11D), an increased number of $CHOS_X$ compounds was found in the corresponding oxic experiments (Figure 4−12B). These molecules of the oxic experiments with the increased number of oxygen atoms in the molecules, may have resulted from the oxidation of the compounds present at anoxic conditions and/or were formed from the reaction of intermediate polysulfur species, such as the polysulfane monosulfuric acids which were particularly present in the pH 6 oxic experiments with sulfide (Figure 4-15A).

4.5. Summary and conclusions

The abiotic reactivity of inorganic sulfur species from the most reduced sulfide to the most oxidized sulfate with DOM under conditions resembling typical ecosystem (pH 6, 8, 10; anoxic and oxic conditions) settings proofed the formation of sulfur organic compounds with the reduced to intermediate inorganic, i.e. sulfide, polysulfide, thiosulfate and sulfite, sulfur species under all tested conditions (Figure 4-7). Independently of the organic matter and inorganic sulfur species almost exclusively CHO compounds reacted in the formation of sulfur organic compounds. The formation of sulfur organic compounds did not occur immediately and was dependent on the DOM characteristics. Furthermore, the CHOS formation capacity was particularly increased for the reactions with sulfide and polysulfide and fresh DOM, represented by PN-DOM,

compared to the reaction capacity of biotically and abiotically processed DOM, represented by SRFA-DOM. This is in agreement with the laboratory studies that showed the incorporation of sulfide (Sinninghe Damsté et al. 1989, De Graaf et al. 1992, Perlinger et al. 2002, Hebting et al. 2006) and polysulfides (LaLonde et al. 1987, Schouten et al. 1994, Amrani and Aizenshtat 2004b, Amrani et al. 2007, Schouten et al. 1993) at double bonds, which were more abundant in fresh PN-DOM (Figure 4-6, olefin section integral of ^{1}H NMR spectrum). Nevertheless, the general reaction behavior of the different inorganic sulfur species was independent of the DOM and followed overall the nucleophilicity trend of the inorganic sulfur species. Thus, the summarized reactivity trend was sulfide (S^{2-}) > sulfite (SO_3^{2-}) > thiosulfate ($S_2O_3^{2-}$). The comprehensive investigations on the reactivity of equimolar levels of sulfide and polysulfide with DOM, showed less formation of sulfur organic compounds with polysulfide. This implies that the nucleophilicity of polysulfides was often overestimated as being the highest.

The sulfite (and thiosulfate pH 10) reactivity was independent of the pH and lead almost exclusively to the formation of $CHOS_1$ molecules. In agreement with the studies from Vairavamurthy et al., sulfonation leads to the formation of sulfonic acids preferentially occurring at double bonds (Vairavamurthy et al. 1994).

The reactivity of thiosulfate was independent of the oxygen saturation status of the experimental solution. Although thiosulfate reactivity was low, the formation of $CHOS_2$ most likely present as organic thiosulfate groups, with PN and SRFA-DOM was observed. Hence, disproportionation of organic thiosulfate groups postulated by Vairavamurthy et al. might in fact only play a minor role.

Sulfide and polysulfide experiments were clearly influenced by the oxygen saturation of the experimental solution and the resulting oxidation products. Sulfide reactivity at anoxic conditions was dominated by the formation of $CHOS_1$ compounds for all pH values. The highest reactivity of sulfide was at pH 10, at which the dominating sulfide species is very nucleophilic HS^- and lowest at pH 6, at which the dominating sulfide species is less nucleophilic H_2S. Furthermore, the carbon oxidation state of the characteristic molecular formulas formed at pH 6 was more reduced, thus were most probably formed by electrophilic addition of H_2S, while the carbon oxidation state was higher for the characteristic formulas formed at pH 8 and 10, hence most probably formed by nucleophilic addition, which is favored at alkaline pH values.

The formation of polysulfurized molecules with low number of oxygen atoms in the molecules, which verifies the presence of reduced sulfur species in the organic molecules, was shown for reaction of sulfide under anoxic conditions. Thus, the presence of polysulfides is not required for the formation polysulfurized molecules. However, polysulfide reactions lead to the formation of unique polysulfurized molecules at pH 10, at which polysulfide is very stable. But it was also shown that polysulfide reactivity at anoxic conditions was dominated by the formation of $CHOS_1$ compounds independently of the pH value. Thus, only a minor part of polysulfide is incorporated directly as S_x into the organic molecules which clearly indicated disproportionation of polysulfide by the reaction with DOM.

In oxygen saturated experiments with sulfide and polysulfide, the mixed reactivity of reduced to oxidized sulfur species resulted in an increased formation of sulfur organic compounds with multiple sulfur atoms and very oxidized sulfur organic molecules. Additionally, increased abundance of intermediate oxidation state inorganic polysulfur molecules were observed. The formation of oxidized CHOS compounds could occur via direct formation with intermediate oxidation state sulfur species and/or the oxidation of reduced sulfur organic molecules. However, polysulfurized CHOS compounds, where sulfur functionalities were at least partially present in reduced form due to the low number of oxygen atoms present in the molecules, were also present in the oxic experiments.

The performed laboratory experiments proofed the individual formation of sulfur organic compounds under a variety of conditions resembling typical ecosystems of intensive sulfur cycling. Hence, the obtained details on the CHOS formation can be considered as a library for the formation of sulfur organic compounds. In particular, the hierarchical cluster analysis of the anoxic model experiments (Figure 4-11) can be considered for comparison with anaerobic field sites, such as the hypolimnic water DOM from the meromictic lake Hechtsee (cf. chapter 2) and the bacterial sulfate reduction hotspot at the petroleum hydrocarbon contaminated groundwater system in Düsseldorf Flingern (cf. chapter 3). For the evaluation of the formation of sulfur organic compounds under oxic conditions, such as specific hydrothermal springs (e.g. Elk Geyser, Octopus Spring, Rabbit Creek in Yellowstone National Park) the hierarchical cluster analysis of the oxic model experiments (Figure 4–12) can be considered for comparison. Additionally, oxic conditions were identified as hotspots for the formation of sulfur organic compounds. All

in all, the obtained results of the formation of sulfur organic compounds enhance the understanding of the linkage of the carbon and sulfur cycle in the environment.

To further improve the knowledge on the formation of sulfur organic compounds, future work should perform additional characterization by means of XANES spectroscopy for the quantification of the present sulfur functionalities in the organic matter. This would enhance the differentiation of the sulfur oxidation state of $CHOS_1$ compounds which were predominately formed by all sulfur species. Their specification is very tedious (MS/MS fragmentation and derivatization) and also not absolutely reliable by means of FT-ICR-MS in such complex mixtures such as DOM. Also the performance of experiments with individual compounds having different organic functionalists would be beneficial for this. Additionally, these experiments enable to obtain an in depth knowledge on the reactivity of sulfur species, besides the reactivity with double bonds. Furthermore, kinetic studies would enhance the knowledge on competing reactions and it would be possible to understand whether oxidized sulfur organics are formed from oxidized inorganic sulfur species or from the oxidation of thiol groups in oxic experiments.

5. Overall summary and conclusions

Two freshwater aquatic ecosystems with intensive sulfur cycling were studied: the hypolimnic (sulfide-rich) water of the meromictic lake Hechtsee (chapter 2) and the petroleum hydrocarbon contaminated groundwater, where bacterial sulfate reduction is the key redox process involved in the contaminant biodegradation (Düsseldorf Flingern, chapter 3). At both field sites a distinct enrichment of sulfur organic compounds was found in samples with reactive inorganic sulfur, especially dissolved sulfide. In DOM from sulfide-rich water samples polysulfurized CHOS compounds with low numbers of oxygen atoms were found testifying the presence of reduced sulfur functionalities in the molecules. This was confirmed by low abundances in (–)ESI FT-ICR mass spectra in the hypolimnic water from Hechtsee. Additionally, MS/MS fragmentation of high abundant marker compounds from the Düsseldorf Flingern aquifer confirmed the formation of polythiols as well as polysulfur sulfonic acids (R-S_xO_3H), as an intermediate oxidation state, polysulfur species (polythionates, polysulfane monosulfuric acids) were overlapping with the abundance of sulfide. Furthermore, formation of sulfonic acids occurred in the suboxic zone of the Düsseldorf Flingern aquifer. At both field sites, sulfur organic formation was likely to be abiotically, however, biotic formation cannot be entirely excluded, particularly in the Düsseldorf Flingern aquifer with intensive microbial activity.

For the comparison of the findings from field sites, laboratory experiments on the abiotic formation of sulfur organic compounds by reaction of DOM with inorganic sulfur species (sulfide, polysulfide, thiosulfate, sulfite, and sulfate) under similar conditions as found in ecosystems (pH 6, 8, 10; anoxic and oxic) were performed (chapter 4). These experiments, revealed especially sulfide and sulfite to be involved in the formation of sulfur organic compounds. Furthermore, the presence of polysulfides was not required to form polysulfurized molecules. In oxygen saturated experiments with sulfide and polysulfide, the mixed reactivity of reduced to oxidized sulfur species resulted in an enhanced formation of sulfur organic compounds with multiple sulfur atoms and very oxidized sulfur organic molecules. Additionally, increased abundances of intermediate oxidation state inorganic polysulfur molecules (polythionates, polysulfane monosulfuric acids) were observed under oxic conditions. The obtained details on the CHOS formation can be considered as a library for the formation of sulfur organic compounds in aquatic

ecosystems. Therefore, the two field site investigations and laboratory experiments are set into relation in the following.

In the field and laboratory predominantly CHO compounds were the precursor molecules to react with inorganic sulfur species to form CHOS compounds.

Sulfate was confirmed to be not involved in the formation of sulfur organic compounds in the field, as well as in the laboratory experiments (cf. paragraph 3.4.3.2, Figure 3-11E and paragraph 4.4.2).

Sulfite reactivity is of special interest in suboxic regions such as the saturated/unsaturated interface (capillary fringe) of the Düsseldorf Flingern aquifer. In these samples, taken directly beneath the groundwater table (referred to as upper plume core), bacterial sulfate reduction was not the dominating redox process (cf. paragraph 3.4.3.2) and oxidation to sulfite occurred (Einsiedl et al. 2015). The DOM signature of the upper plume fringe was characterized by $CHOS_1$ compounds formed by sulfonation of carboxylated alkene degradation products (anthropogenic) (Figure 3-9, Figure 3-11). These sulfonic acids, considering the fact that in the laboratory allochthonous DOM was used, resemble to the characteristic $CHOS_1$ sulfonic acids formed in the laboratory experiments (Figure 4-11B, Figure 4-13). Also the laboratory experiments resulted in the exclusive formation of $CHOS_1$ compounds (paragraph 4.4.3.1).

Thiosulfate reactivity is of interest in suboxic and oxic environments with hydrogen sulfide inputs, such as hydrothermal springs and especially acid sulfate systems, e.g., Elk spring and Cinder pool (Yellowstone National Park), where oxidation of sulfide leads to the formation of thiosulfate (Xu et al. 2000). As a result of the low thiosulfate reactivity, confirmed by the laboratory experiments, specific thiosulfate reaction products were not observed in the upper fringe samples of the Düsseldorf Flingern aquifer, where thiosulfate has been detected (Einsiedl et al. 2015).

Polysulfide concentrations were very low within the sulfidic water of the meromictic lake Hechtsee (cf. paragraph 2.4.1.1) and unfortunately not analyzed in the groundwater aquifer with intensive bacterial sulfate reduction. However, the model reactions confirmed that the presence of polysulfide is not necessary for the formation of $CHOS_x$. Even so, the laboratory experiments showed unique $CHOS_x$ formed in the reactions with polysulfides. The laboratory experiments with DOM and sulfide revealed formation of

polysulfurized CHOS compounds similar to those found in the sulfide-rich water from the meromictic lake Hechtsee (cf. paragraph 3.4.3.2, Figure 2-7, Figure 2-8) and the groundwater aquifer plume core and lower plume fringe (cf. paragraph 3.4.3.2, Figure 3-9D, E and Figure 3-11C). Thus, polysulfurized molecules in sulfide enriched aquatic ecosystems were formed by the abiotic reaction of sulfide with the DOM. In the laboratory experiments the reactivity, particularly with reduced sulfur species, was higher with the fresh pine needle derived organic matter compared to the processed DOM from Suwannee River. This clearly indicated that sulfurization primarily occurred at double bonds and activated double bonds as it was previously shown (Vairavamurthy and Mopper 1987, Perlinger et al. 2002, Hebting et al. 2003). In agreement with this, also sulfurization of DOM was higher in the Düsseldorf Flingern aquifer. Herein an increased input of unsaturated organic compounds was present (cf. paragraph 3.4.2), but lower dissolved sulfide concentrations (maximum 170 µmol L^{-1}), compared to DOM from the hypolimnic water of Hechtsee (sulfide concentration 920 µmol L^{-1}) which was indicated to be further degraded and humified (cf. paragraph 2.4.2.2).

Furthermore, it is very likely that oxidation intermediates such as polythionates and polysulfane monosulfuric acids, which were also present in the sulfidic samples of the field sites (Figure 2-10, Figure 3-13) are involved in the formation of CHOS$_x$. Hence, strong resemblance of CHOS formation products was found between the oxic experiment of sulfide and polysulfide at pH 6 to 8 (Figure 4−12C, Figure 4-15) and the characteristic polysulfur sulfonic acids particularly found in the plume core and lower plume fringe of the Düsseldorf Flingern aquifer.

Additionally, the characteristic CHOS compounds found in the laboratory experiments under oxic conditions (Figure 4−12) resembled the sulfur organics found in oxygen enriched hydrothermal springs of YNP, e.g., Elk Geyser, Rabbit Creek and Octopus Spring, which were not subject of this thesis, but the investigations were performed during the same period, and showed distinct CHOS chemistry depending on spring type and the prevailing inorganic sulfur species present.

The formation of sulfur organic compounds in ecosystems with distinct sulfur chemistry again testified for the unique DOM capacity to reflect key ecosystem characteristics. Moreover, the formation of sulfur organic compounds confirmed a decisive linkage of the aquatic carbon and sulfur cycle. The great accordance of the field and laboratory

investigations corroborated that formation of sulfur organic compounds in DOM is predominantly an abiotic process.

6. Supplementary Information

6.1. Effects of the inorganic sulfur chemistry on the DOM of a meromictic lake – Chapter 2
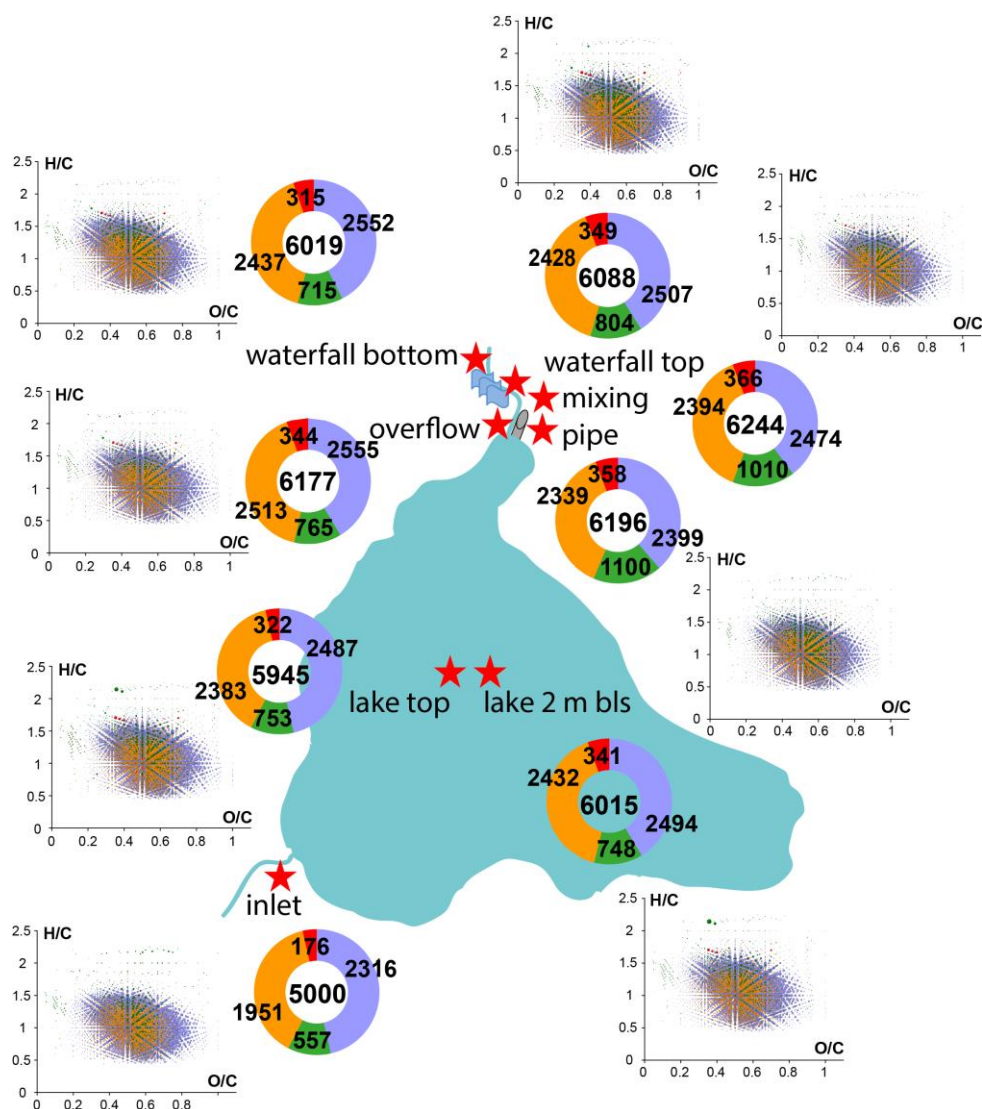
Figure 6-1: FT-ICR-MS assigned elemental compositions of Hechtsee SPE-DOM.
Sketch of Hechtsee with red stars as indicators for the sampling sites. Van Krevelen diagrams and ring charts display the assigned elemental compositions classified into molecular groups containing CHO (blue), CHNO (orange), CHOS (green), or CHNOS (red).

Table 6-1: Molecular formula characteristics of Hechtsee SPE-DOM.
Summary of the (–)ESI FT-ICR-MS derived molecular formula characteristics of the Hechtsee SPE-DOM.

Members of molecular series	inlet (IN)	lake top (LT)	lake 2 m bls (L2m)	overflow (OF)	pipe (PIPE)	mixing (MIX)	waterfall top (WFT)	waterfall bottom (WFB)
CHO compounds	2316	2487	2494	2555	2399	2474	2507	2552
CHOS compounds	557	753	748	765	1100	1010	804	715
CHNO compounds	1951	2383	2432	2513	2339	2394	2428	2437
CHNOS compounds	176	322	341	344	358	366	349	315
total number assigned mass peaks	5000	5945	6015	6177	6196	6244	6088	6019
average mass	444.30	417.14	416.66	413.34	425.98	418.79	415.57	417.06
average H [%]	4.81	5.02	5.03	5.09	4.93	4.97	5.00	5.09
average C [%]	54.44	54.48	54.51	54.64	54.45	54.31	54.44	54.74
average O [%]	39.92	39.46	39.49	39.30	39.41	39.64	39.45	39.12
average N [%]	0.52	0.66	0.63	0.65	0.65	0.64	0.70	0.70
average S [%]	0.30	0.37	0.35	0.32	0.55	0.44	0.41	0.35
computed H/C ratio	1.06	1.11	1.11	1.12	1.09	1.10	1.10	1.12
computed O/C ratio	0.55	0.54	0.54	0.54	0.54	0.55	0.54	0.54
computed N/C ratio	0.0696	0.0744	0.0745	0.0749	0.0742	0.0745	0.0746	0.0749
computed S/C ratio	0.0921	0.0814	0.0821	0.0805	0.0884	0.0863	0.0778	0.0737
$(DBE)_w$	10.57	9.58	9.56	9.42	9.94	9.66	9.58	9.54
$(DBE/O)_w$	0.98	0.95	0.95	0.95	0.97	0.95	0.96	0.96
$(\#C)_w$	20.20	18.98	18.97	18.86	19.37	18.99	18.89	19.06
$(\#H)_w$	21.42	21.00	20.99	21.07	21.07	20.87	20.83	21.27
$(\#O)_w$	11.11	10.31	10.30	10.18	10.52	10.40	10.27	10.22
$(\#N)_w$	0.17	0.20	0.19	0.19	0.20	0.19	0.21	0.21
$(\#S)_w$	0.04	0.05	0.05	0.04	0.07	0.06	0.05	0.05
CHO % of Int	85.34%	82.40%	83.40%	83.42%	81.11%	82.45%	81.09%	81.82%
CHOS % of Int	2.30%	3.08%	2.83%	2.63%	4.48%	3.52%	3.54%	2.91%
CHNO % Int	12.05%	13.92%	13.19%	13.42%	13.78%	13.42%	14.70%	14.72%
CHNOS % Int	0.30%	0.59%	0.58%	0.53%	0.63%	0.61%	0.67%	0.55%

Table 6-2: CHOS molecular formula characteristics from pipe water SPE-DOM.
Characteristic CHOS molecular formulas of pipe water SPE-DOM separated into $CHOS_1$ to $CHOS_6$ class with average number of carbon, oxygen and hydrogen atoms in the molecules. The percentage of formulas containing reduced sulfur functionality was calculated by considering that 3 oxygen compounds are required to form a sulfonic acid functional group.

	$CHOS_1$	$CHOS_2$	$CHOS_3$	$CHOS_4$	$CHOS_5$	$CHOS_6$
number of formulas	73	66	103	75	35	9
average number of carbon atoms	20.56	12.89	12.30	10.88	8.97	8.33
average number of oxygen atoms	10.93	7.95	8.15	7.28	6.59	6.56
average number of hydrogen atoms	18.51	12.55	12.73	13.69	11.91	11.89
percentage of formulas containing reduced sulfur functionalities	0.0%	18.2%	16.5%	98.7%	97.1%	100.0%
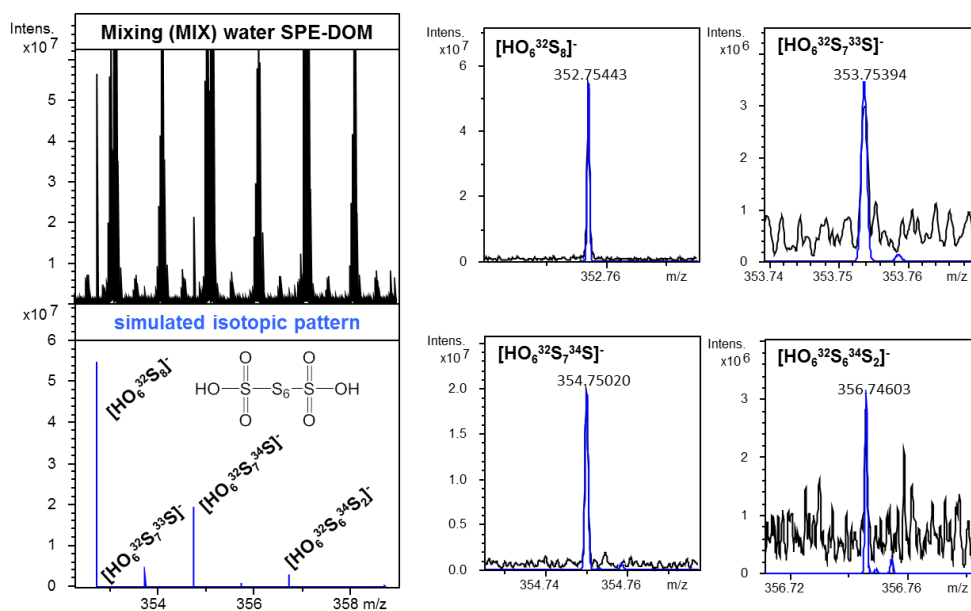
Figure 6-2: Isotopic pattern of S_8-polythionate.
Isotopic pattern of S_8-polythionate ($H_2S_8O_6$) matches m/z 352.75443 in Hechtsee SPE-DOM.
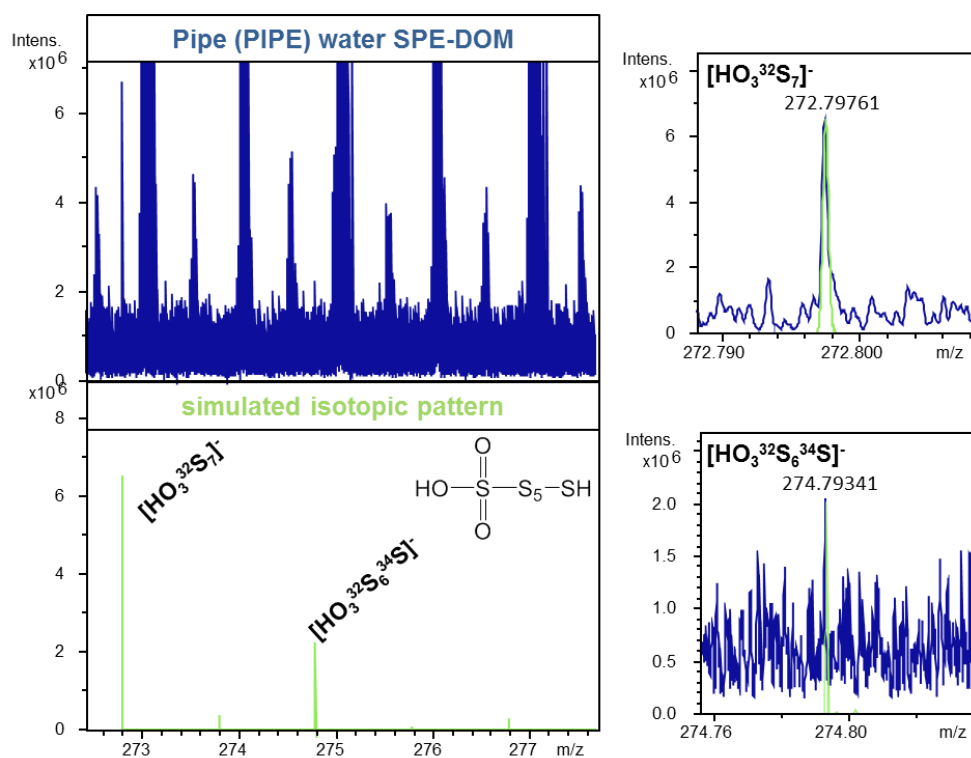
Figure 6-3: Isotopic pattern of S_7-polysulfane monosulfuric acid.
Isotopic pattern of S_7-polysulfane monosulfuric acid ($H_2S_7O_3$) matches m/z 272.79761 in Hechtsee SPE-DOM.

Table 6-3: Summary of DOS and DOC measures.
Summary of the SPE extractable DOS and DOC concentrations, DOC SPE extraction efficiency, molar DOS/DOC ratios, number and total mass peak intensities of assigned CHO and CHOS (including identified inorganic polysulfur species) compounds.

	inlet (IN)	lake top (LT)	lake 2 m bls (L2m)	overflow (OF)	pipe (PIPE)	mixing (MIX)	waterfall top (WFT)	waterfall bottom (WFB)
# CHO compounds	2316	2487	2494	2555	2399	2474	2507	2552
# CHOS* compounds	557	753	748	765	1107	1020	805	715
# CHOS* / (#CHO + #CHOS*)	19.39%	23.24%	23.07%	23.04%	31.57%	29.19%	24.31%	21.89%
CHO % of Intensity	85.34%	82.40%	83.40%	83.42%	81.10%	82.41%	81.09%	81.82%
CHOS* % of Intensity	2.30%	3.08%	2.83%	2.63%	4.49%	3.56%	3.54%	2.91%
CHOS* % of Intensity / (CHOS*+CHO % of Intensity)	2.63%	3.61%	3.28%	3.06%	5.25%	4.14%	4.18%	3.44%
DOC [mmol L^{-1}] extract	23.39	26.90	26.90	28.26	22.37	25.95	26.19	27.39
DOC extraction efficiency	51.45%	43.77%	37.65%	43.72%	48.18%	34.96%	42.96%	35.53%
DOS [mmol L^{-1}] extract	0.1138	0.1276	0.1257	0.1319	0.2710	0.2280	0.1575	0.1444
DOS/DOC	0.0049	0.0047	0.0047	0.0047	0.0121	0.0088	0.0060	0.0053

* number of assigned CHOS molecules (# CHOS) and CHOS intensity include the count and intensities of the identified polythionates and polysulfane monosulfidic acids

6.2. Bacterial sulfate reduction and its effect on dissolved organic matter – Chapter 3
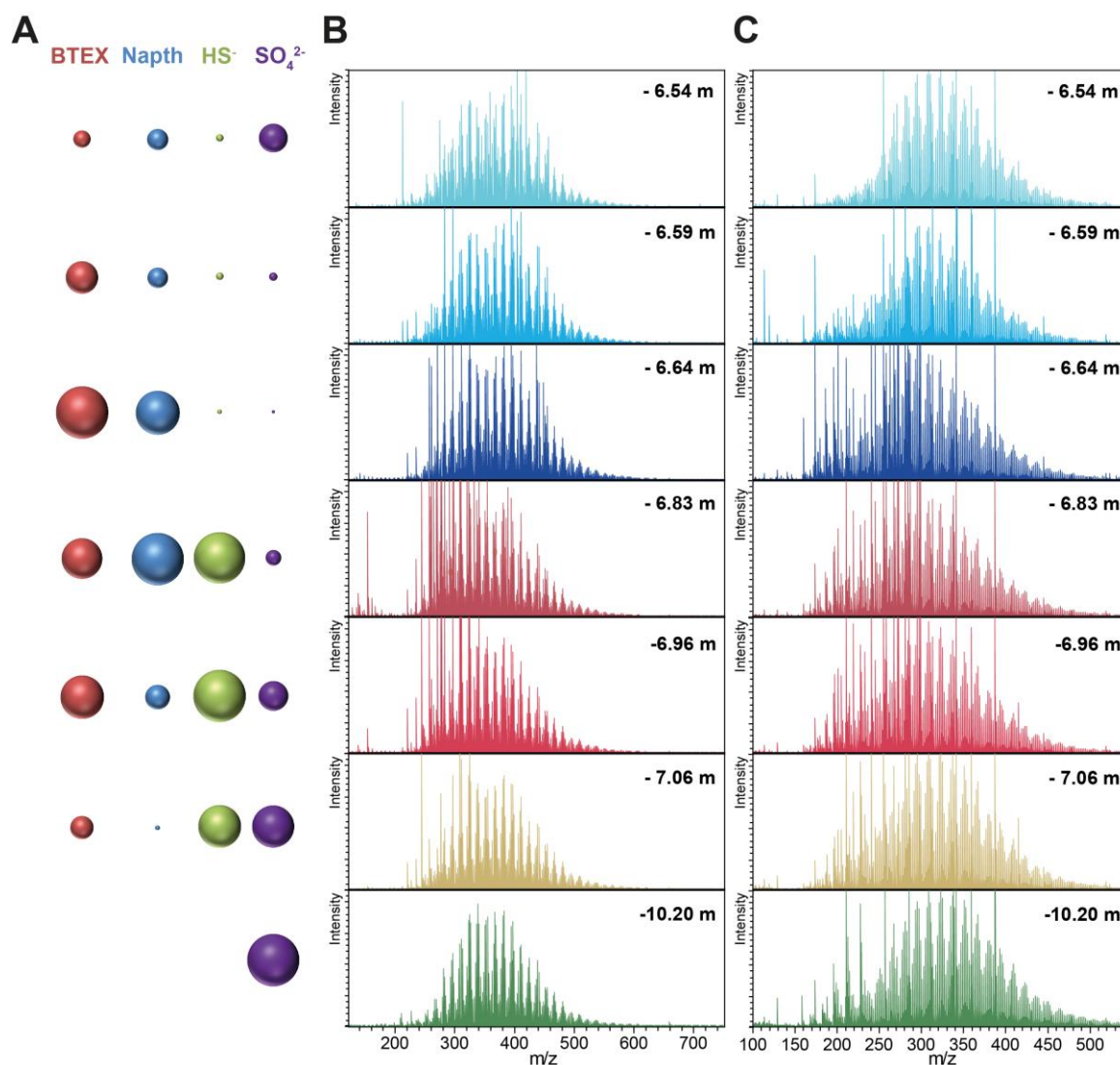
Figure 6-4: Geochemical parameters and FT-ICR mass spectra at selected depths.
A) The bubbles display the BTEX (red), naphthalene (blue), hydrogen sulfide (light green), and sulfate (purple) concentrations in the groundwater. B) (–)ESI FT-ICR mass spectra from m/z 123–750 and C) (+)APPI FT-ICR mass spectra from m/z 100–550 of selected SPE-DOM samples along the aquifer. Reprinted with permission from (Dvorski et al. 2016). Copyright (2016) American Chemical Society.
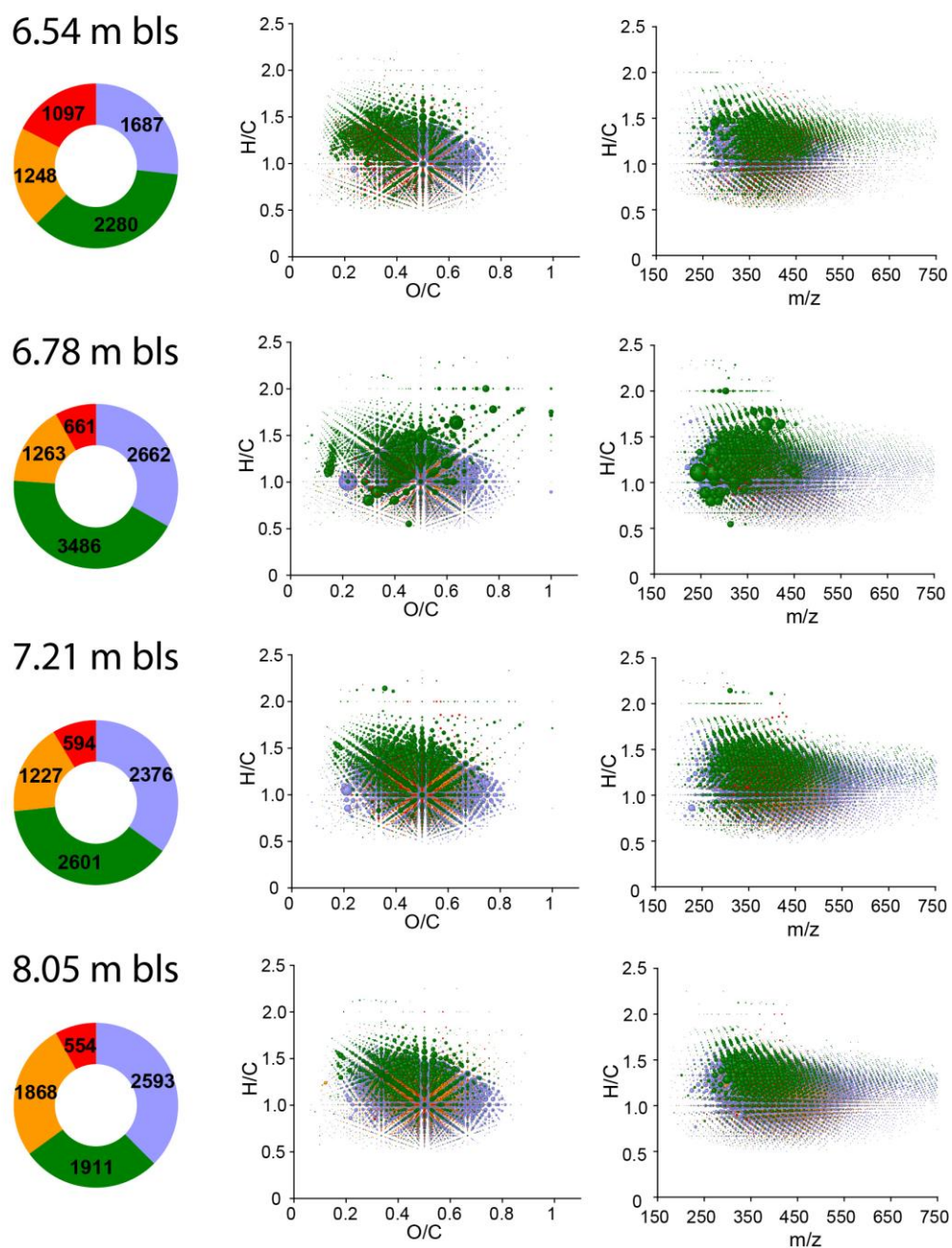
Figure 6-5: Molecular formulas representative for the zones.
Ring charts, van Krevelen and m/z-resolved H/C atomic ratios of the (–)ESI FT-ICR-MS derived molecular formulas of four representative SPE-DOM samples (6.54 m bls = upper plume fringe, 6.78 m bls = plume core, 7.21 m bls = lower plume fringe, and 8.05 m bls = deep zone).
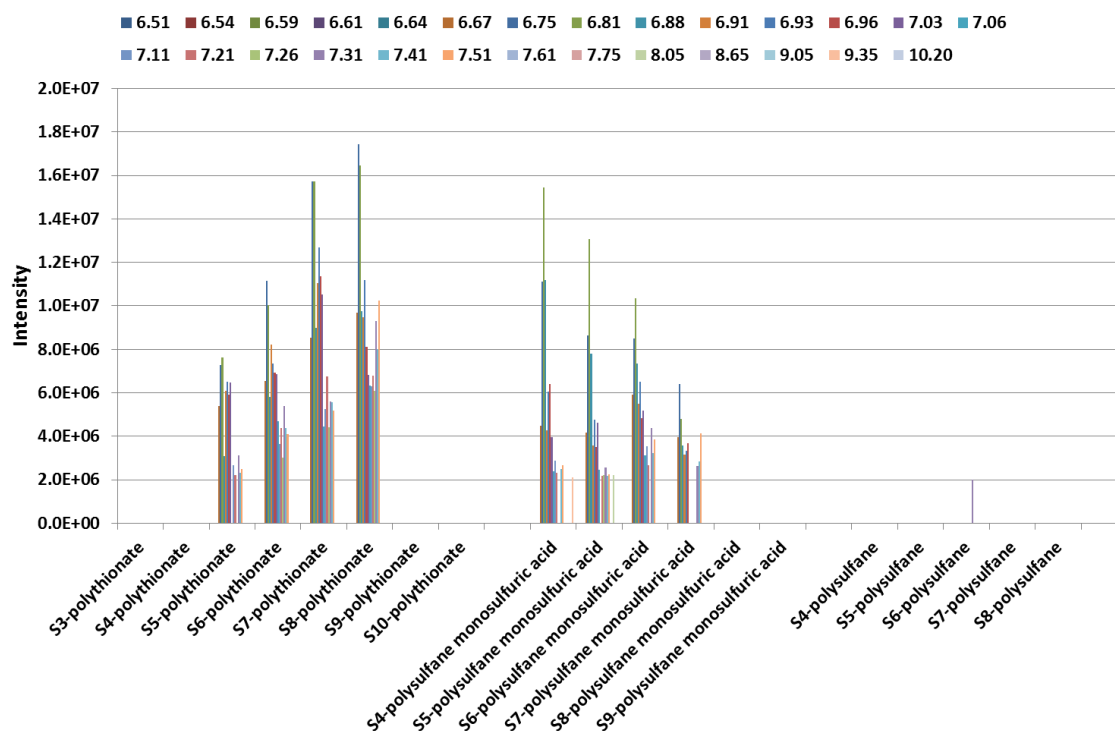
Figure 6-6: FT-ICR-MS based inorganic polysulfur speciation along the aquifer.
Polythionates, polysulfane monosulfuric acids, and polysulfanes present in the FT-ICR mass spectra SPE-DOM along the vertical aquifer profile.
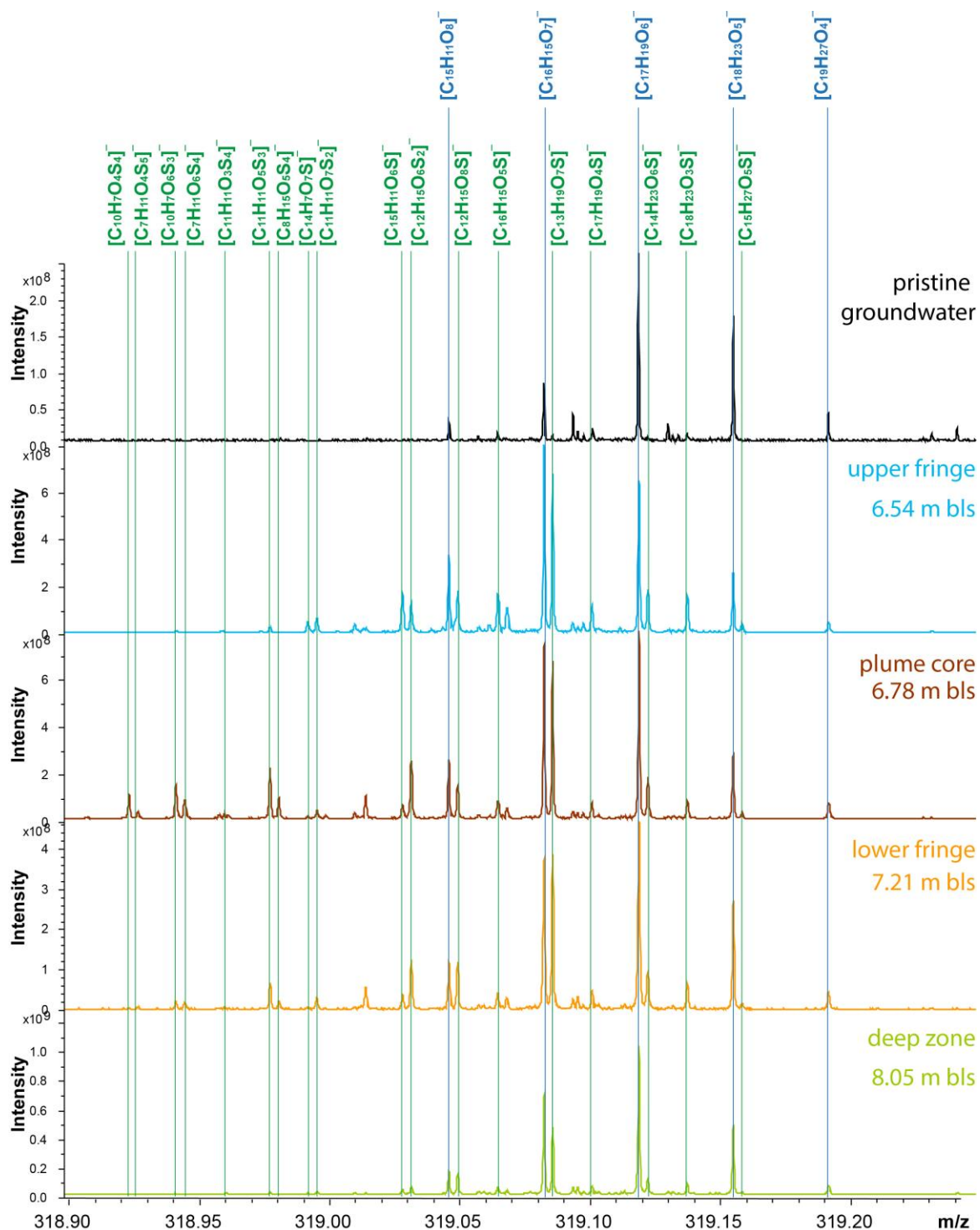
Figure 6-7: Nominal mass 319 of representative samples from the zones.
Expansion of nominal mass 319 from (–)ESI FT-ICR mass spectra of representative samples from the upper fringe (blue), plume core (brown), lower fringe (orange), and deep zone (green) in comparison with SPE-DOM from a pristine groundwater sampled on the campus of the Helmholtz Zentrum München. The enhanced relative intensity of CHOS (Figure 3-5) as well as the high abundance of CHOS annotations in a single nominal mass (m/z 318.9–319.2) indicates that CHOS molecules are discriminating the samples where bacterial sulfate reduction is active.
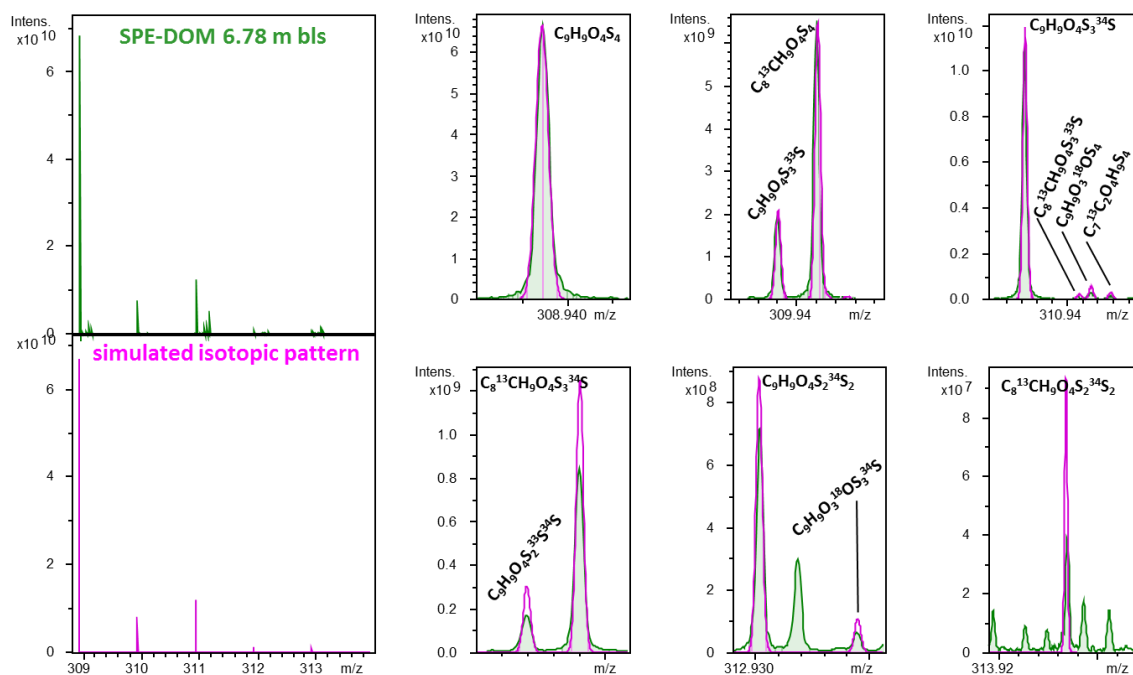
Figure 6-8: Isotopic pattern verification of a plume core marker compound.
Isotopic pattern of highest abundant plume core marker compound $[C_9H_9O_4S_4]^-$ in SPE-DOM from 6.78 m bls (green) in comparison to the simulated isotopic pattern.

Table 6-4: Comparison of PARAFAC model results.
EEM fluorescence spectroscopy in combination with PARAFAC modeling results compared to other studies. Reprinted with permission from (Dvorski et al. 2016). Copyright (2016) American Chemical Society.

component	Ex λ [nm]	Em λ [nm]	description	Zhou et al. 2012	Mendoza et al. 2013	Zhou et al. 2013	Bianchi et al. 2014
				Comp: Ex/Em (nm) (description)			
C1	237 (288)	358.7	oil, BTEX, PAH and its degradation products	C3: 232/346 (oil)	C4 & C6: 225, 270, 280/340 (naphthalene-like enriched, benzene/arene-like)	C2: 236/350 (oil - related, degradation product)	
C2	255 (315)	417.6	humic-like	C4: 248/446 (humic like)	C3 250/440 (humic-like)	C3: 256 (340)/460 (terrestrial humic substance, and chemically dispersed oil)	C1: 240/400-436 (terrestrial humic substance-like)
C3	255	332.8	oil, BTEX, PAH and its degradation products	C2: 264/234 (oil)	C2: 220, 255, 270/330, (benzene/arene-like enriched, naphthalene-like)		

Table 6-5: ^{1}H NMR section integrals for selected samples.
^{1}H NMR section integrals derived from total area-normalized ^{1}H NMR spectra integrals with main structures provided for selected samples along the aquifer, according to sampling depth. Reprinted with permission from (Dvorski et al. 2016). Copyright (2016) American Chemical Society.

structure	key structures	$\delta(^1H)$ [ppm]	6.54 [m bls]	6.59 [m bls]	6.64 [m bls]	6.83 [m bls]	6.96 [m bls]	7.06 [m bls]	10.2 [m bls]
aromatics	$\underline{H}_{ar}$	9.5 - 7.0	14.1	20.1	25.9	29.9	25.5	19.3	12.1
olefins	$\underline{H}C=C$, $\underline{H}CO_2$	7.0 - 5.1	3.6	4.7	3.8	3.4	2.5	2.6	2.3
carbohydrates	$\underline{H}CO$	4.9 - 3.1	13.0	11.8	10.0	10.7	10.4	12.3	12.4
CRAM	$\underline{H}CCX$	3.1 - 1.9	32.7	32.0	32.5	29.9	31.1	31.2	31.9
aliphatics	$\underline{H}CCC$	1.9 - 0.5	36.5	31.5	27.8	26.0	30.4	34.7	41.2

Table 6-6: Details of the ^{1}H NMR section integrals for selected samples.
^{1}H NMR section integrals derived from total area-normalized ^{1}H NMR spectra integrals with main structures provided for selected samples along the aquifer, according to sampling depth (cf. Table S5 for attribution of δ_H section integrals). Reprinted with permission from (Dvorski et al. 2016). Copyright (2016) American Chemical Society.

structure		$\delta(^1H)$ [ppm]	6.54 [m bls]	6.59 [m bls]	6.64 [m bls]	6.83 [m bls]	6.96 [m bls]	7.06 [m bls]	10.2 [m bls]
aromatics $\underline{H}_{ar}$	a	9.5 - 8.9	0.2	0.3	0.2	0.1	0.2	0.2	0.1
	b	8.9 - 8.3	1.0	1.2	1.6	1.4	1.4	1.1	0.9
	c	8.3 - 7.3	8.1	11.7	16.4	19.1	15.4	11.7	7.5
	d	7.3 - 7.0	4.7	6.9	7.7	9.3	8.5	6.4	3.5
olefins $\underline{H}C=C$, $\underline{H}CO_2$	e	7.0 - 6.5	1.8	2.8	3.2	2.8	2.5	2.1	1.7
	f	6.5 - 6.0	0.5	0.8	0.4	0.3	0.0	0.1	0.4
	g	6.0 - 5.1	1.4	1.1	0.2	0.4	0.0	0.5	0.2
carbohydrates $\underline{H}CO$	h	4.9 - 3.1	13.0	11.8	10.0	10.7	10.4	12.3	12.4
CRAM $\underline{H}CCX$	i	3.1 - 2.1	27.3	27.4	28.6	26.4	27.2	26.8	26.7
	j	2.1 - 1.9	5.4	4.6	3.9	3.6	3.9	4.4	5.2
aliphatics $\underline{H}CCC$	k	1.9 - 1.3	20.4	16.8	14.6	13.7	15.4	18.3	22.4
	l	1.3 - 1.2	4.5	4.0	4.0	3.6	4.7	5.4	6.4
	m	1.2 - 0.5	11.6	10.6	9.1	8.7	10.3	11.0	12.4

Table 6-7: ^{1}H NMR key structural units of DOM and PAH degradation products.
Description of ^{1}H NMR key structural units of DOM and PAH degradation products observed in this study. Reprinted with permission from (Dvorski et al. 2016). Copyright (2016) American Chemical Society.

	$\delta(^1\text{H})$ [ppm]	key structural units of DOM and PAH degradation products observed in this study
a*	9.5–8.9	multi (≥4) ring condensed aromatics
b*	8.9–8.3	multi (≥3) ring condensed aromatics
c*	8.3–7.3	single and two-ring aromatics; six-membered N-heterocycles; oxidized aromatics, i.e., mainly (poly)carboxylated aromatics
d*	7.3–7.0	alkylated and non-substituted monoaromatic rings
e*	7.0–6.5	aromatics with oxygenated substituents (OH, OR); alkylated aromatics with fused alicyclic units attached
f	6.5–6.0	conjugated double bonds: =C-C=C$\underline{\text{H}}$; five membered ring heterocycles (O, N, S)
g	6.0–5.1	isolated double bonds: =C$\underline{\text{H}}$; anomerics in carbohydrates: O$_2$C$\underline{\text{H}}$
h	4.9–3.1	OC$\underline{\text{H}}$ oxygenated aliphatics (e.g., carbohydrates, esters, ethers)
i*	3.1–2.1	remotely functionalized aliphatics: OCC$_\beta$$\underline{\text{H}}$, HOOC-C$_\alpha$$\underline{\text{H}}$-C (aliphatic carboxylic acids); $\delta_\text{H} > 2.5$ ppm: C$_\text{ar}$-C$\underline{\text{H}}$-C$\underline{\text{H}}$-COOH, -C-C$\underline{\text{H}}$-NH
j	2.1–1.9	acetate, remotely functionalized aliphatics: OCCC$\underline{\text{H}}$
k	1.9–1.3	OCCC$\underline{\text{H}}$, branched aliphatics, fused alicyclic rings
l	1.3–1.2	(C$\underline{\text{H}}_2$)$_n$ polymethylene; certain branched aliphatics, alicyclic rings
m	1.2–0.5	certain branched aliphatics: CCCC$\underline{\text{H}}$, C$\underline{\text{H}}_3$ groups, certain alicyclic rings

* occurrence of PAH and its degradation products; other NMR resonances mainly comprise SPE-DOM structures
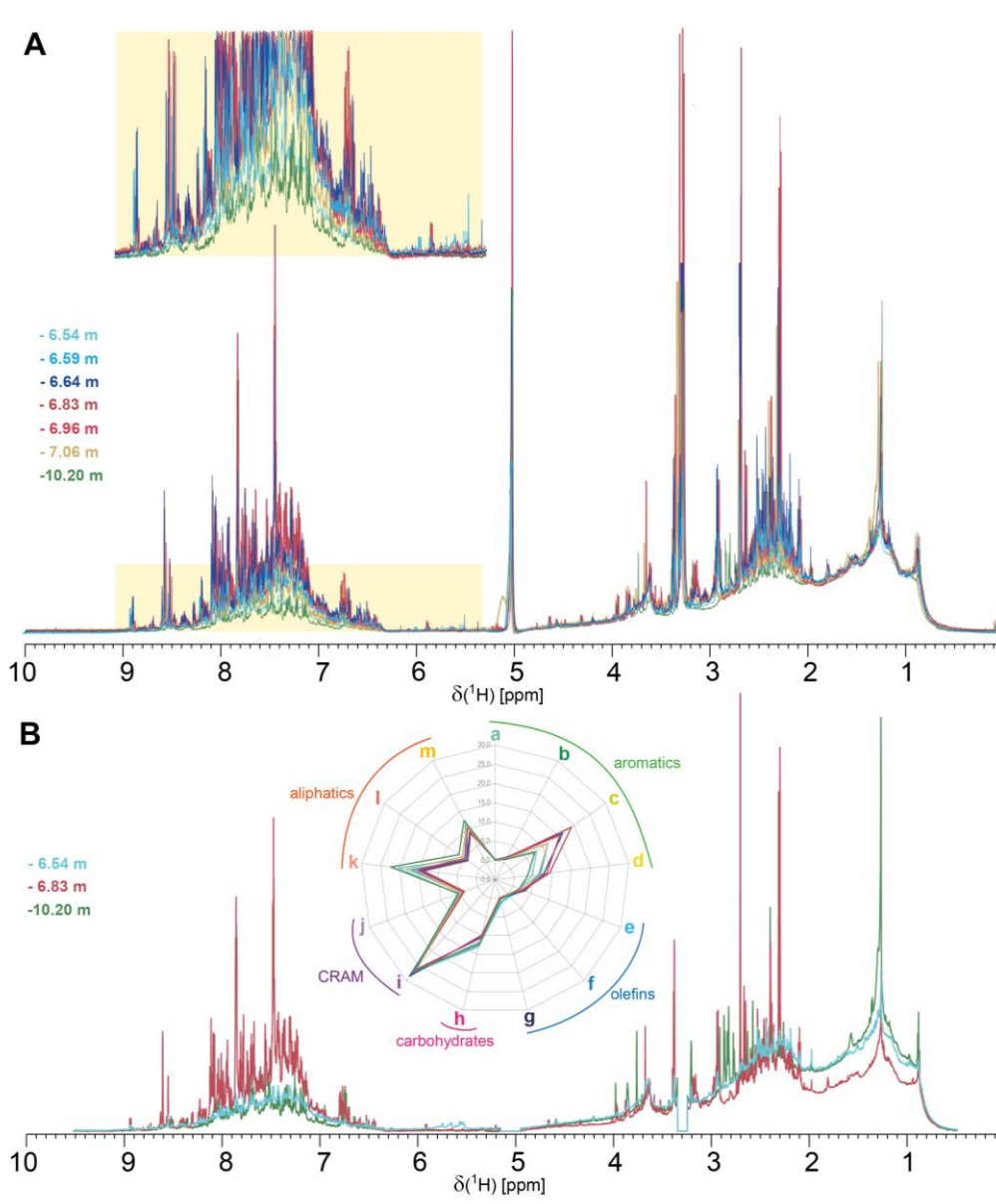
Figure 6-9: Overlay of ^{1}H NMR spectra of SPE-DOM along the aquifer.
Overlay of ^{1}H NMR spectra of SPE-DOM (800 MHz, CD$_3$OD). A) Visual overlay according to the common intensity of 'pure' aliphatics (CCCH; δ_H = 0.5–1.9 ppm) revealed the limited variance of the DOM bulk signature even in the case of highly petroleum contaminated SPE-DOM. B) Overlay of selected ^{1}H NMR spectra, which were normalized to the total integral area, that show the increased integral area in the aromatic region for contaminated SPE-DOM (6.83 m bls) compared to the increased integral of the aliphatic region for lesser petroleum contaminated SPE-DOM from the very top (6.54 m bls) and bottom (10.20 m bls) of the aquifer. The radar diagram of the ^{1}H NMR section integrals, derived from total area-normalized ^{1}H NMR spectra integrals according to structural zones, points out the increased aromatic proportion for contaminated SPE-DOM compared to increased aliphatic integral proportion for less petroleum contaminated SPE-DOM. Reprinted with permission from (Dvorski et al. 2016). Copyright (2016) American Chemical Society.
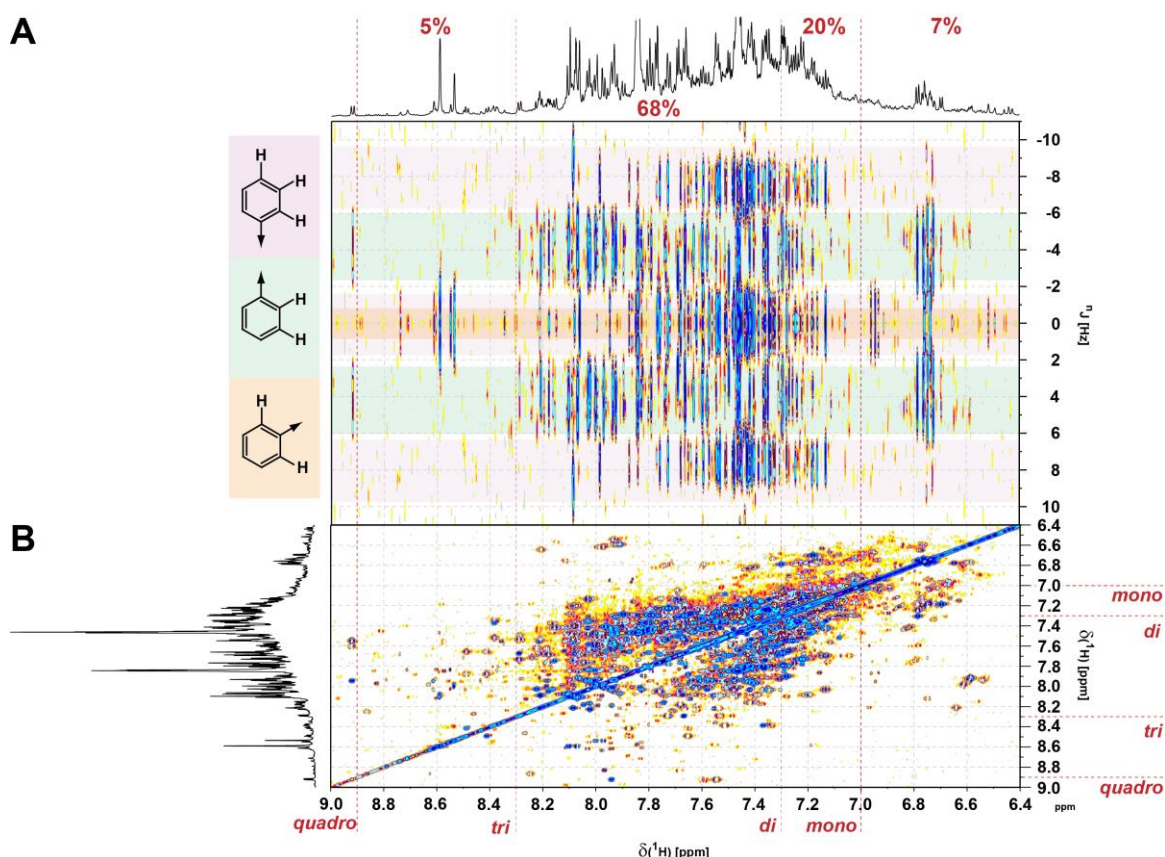
Figure 6-10: JRES and TOCSY NMR spectra of SPE-DOM taken at 6.83 m bls.
A) JRES, and B) TOCSY NMR spectra (800 MHz, CD_3OD) of SPE-DOM taken at 6.83 m bls. Joint positioning of δ_H and $^nJ_{HH}$ indicated the absence of olefin protons in accordance with negligible ^1H NMR integral at $\delta_H \sim 5.15$–6.3 ppm (Figure 3-8, Figure 6-9 and Table 6-6). An increased ring count in alkylated polycyclic hydrocarbons induced progressive downfield chemical shift, while cumulative carboxylation behaved analogously. The projection NMR spectrum is provided with aromatic NMR section integral (sum = 100%) for various fused ring arrangements (cf. Table 6-5). Panel A: Triplett splittings with $^3J_{HH} \approx 8$ Hz indicated HC_{ar}-**H**C_{ar}-**H**C_{ar} groups (purple shade; 1,2,3 and 1,2,3,4-substitution); dublett splittings with $^3J_{HH} \approx 8$ Hz indicated isolated ortho C_q-**H**C_{ar}-**H**C_{ar}-C_q groups (green shade), and complex splittings with $^4J_{HH} < 3$ Hz indicated isolated meta protonated **H**C_{ar}-C_q-**H**C_{ar} groups (orange shade). Panel B: TOCSY cross peaks from vicinal intra aromatic correlations (**H**C_{ar}-**H**C_{ar} : $^3J_{HH} \approx 8$ Hz) with chemical shift ranges for singly ($\delta_H > 7.0$ ppm), doubly ($\delta_H > 7.3$ ppm), and higher fused aromatic systems ($\delta_H > 8.3$ ppm) indicated in color. Alicyclic rings condensed with aromatic rings caused the latter to resonate below 7 ppm ($\delta_H < 7$ ppm); likewise, oxygenated aromatics did the same. However, the latter are at best very marginal contributors and will not account for the appreciable NMR cross peak integral observed here. The observed ^1H NMR chemical shift and cross peak distribution suggested the presence of mostly substituted single and doubly fused aromatic rings. Reprinted with permission from (Dvorski et al. 2016). Copyright (2016) American Chemical Society.
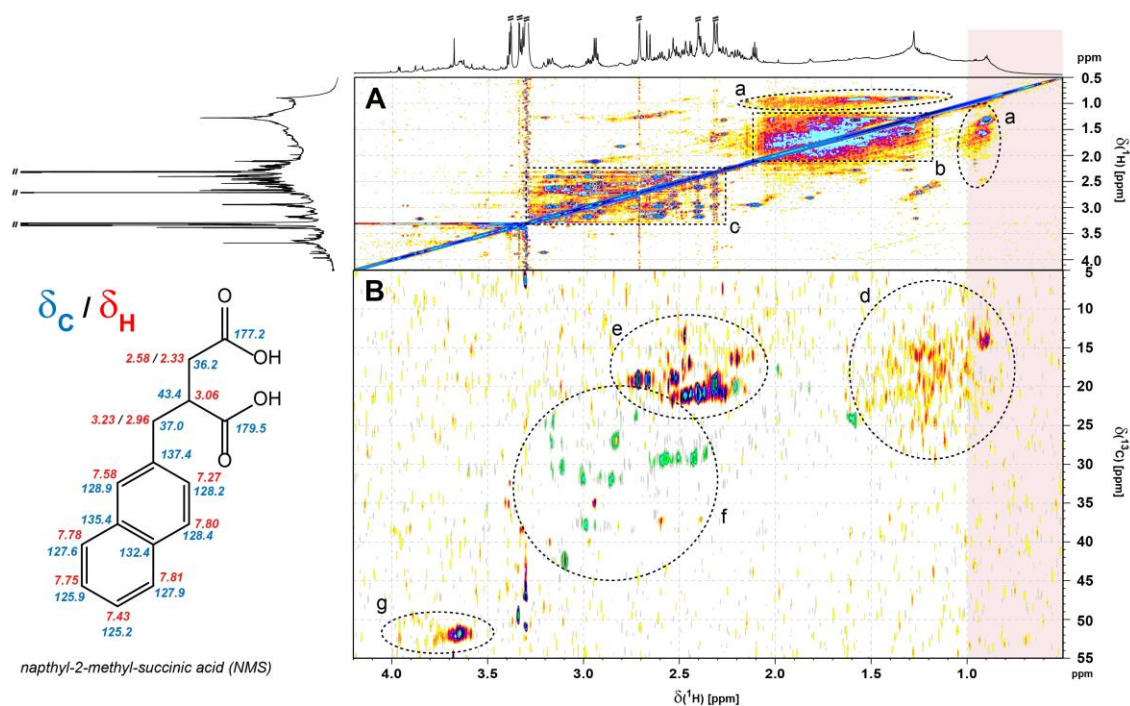
Figure 6-11: TOCSY and methylene-edited ^{1}H, ^{13}C HSQC NMR spectra of SPE-DOM taken at 6.83 m bls.

A) TOCSY and B) methylene-edited ^{1}H, ^{13}C HSQC NMR spectra (800 MHz, CD$_3$OD) of aliphatic ^{1}H chemical shift region (δ_H = 0.5–4.2 ppm) from SPE-DOM sample taken at 6.83 m bls. Panel A: section a: C-CH-C**H**$_3$ cross peaks; section b: intra-aliphatic C-**CH**-C$_n$-**CH**-C cross peaks (n = 0, 1), section c: C$_{ar}$-**CH**-C$_n$-**CH**-COOH cross peaks (n = 0, 1). Panel B: (B) general colors of cross peaks: CH$_3$, CH: red, and CH$_2$: green. Section d: C-**CH$_3$** cross peaks; section e: C$_{ar}$-**CH$_3$** cross peaks; section f: C$_{ar}$-**CH$_2$**-C and C$_{al}$-**CH$_2$**-COOH cross peaks; section g: methyl esters **H$_3$C**O-C(=O)-C-. Cross peaks at δ_H = 2.0–3.25 ppm were indicative for protons in α-positons to carboxylic groups (**H**Cα-COOH) and those attached to aromatic groups **H**Cα-C$_{ar}$. Both TOCSY and ^{1}H, ^{13}C DEPT HSQC spectra of aliphatic spin systems indicated the presence of structural subunits as found in common PAH degradation products such as succinic acid derivatives like NMS (shown in the insert with $\delta_{H/C}$ as computed from ACD Labs software) (Griebler et al. 2004, Jobelius et al. 2011, Jarling et al. 2015). Reprinted with permission from (Dvorski et al. 2016). Copyright (2016) American Chemical Society.
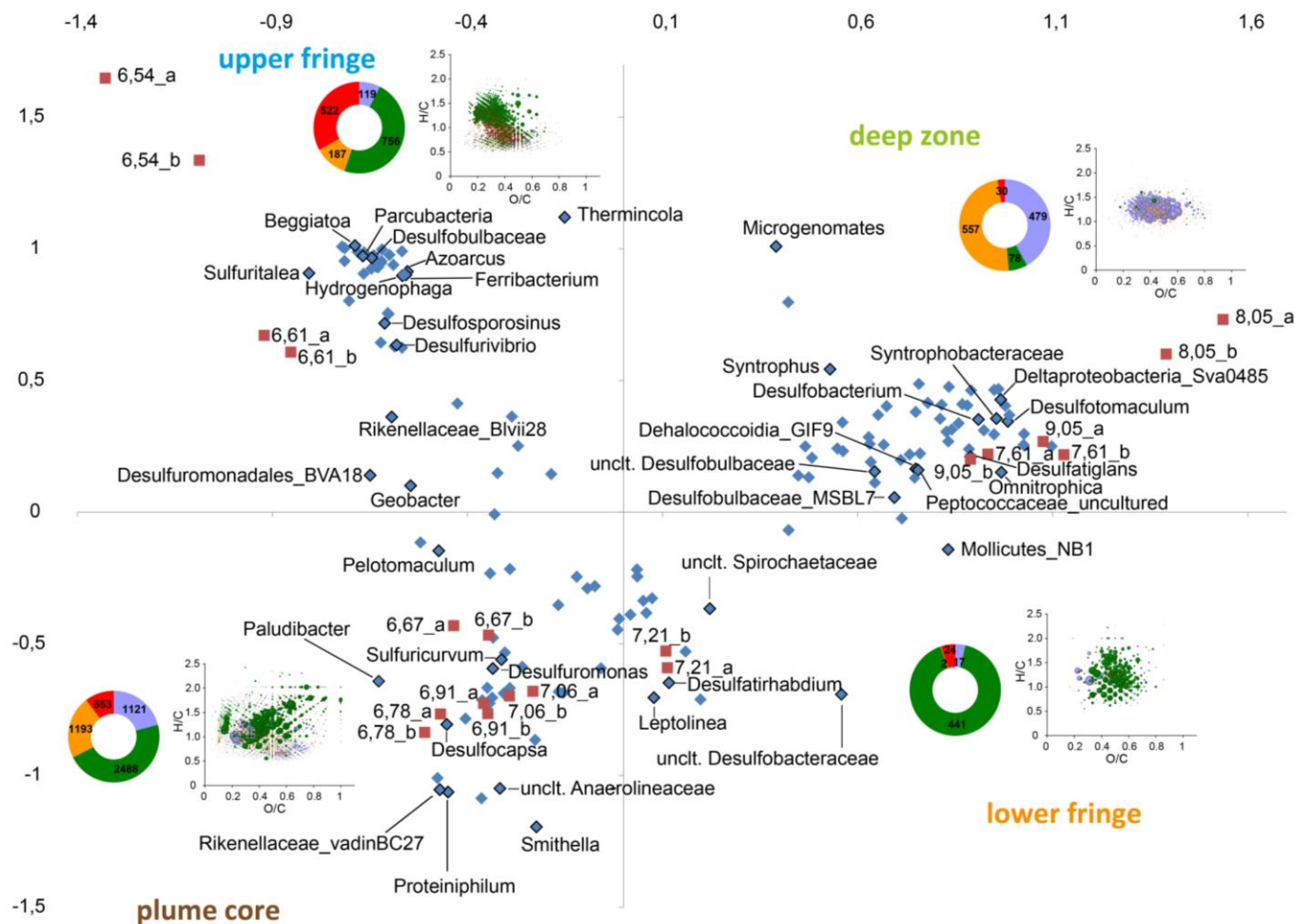
Figure 6-12: Combined score and loading plot of the multi-data OPLS-DA model.
Combined score and loading plot of the multi-data (DOM mass signals and OTUs) OPLS-DA model. The samples are depicted by red squares and the OTUs by blue diamonds and named according to the literature if known. The ring charts and van Krevelen diagrams depict the characteristic DOM mass signals of the individual zones.

6.3. Abiotic reactivity of inorganic sulfur species with DOM – Chapter 4

Table 6-8: Molecular formula characteristics of SRFA and pine needle extract.
Summary of the (–)ESI FT-ICR-MS derived molecular formula characteristics of Suwannee River Fulvic Acid (SRFA) and the pine needle extract (PN) DOM

Members of molecular series	Suwannee River Fulvic Acid (SRFA)	Pine Needle Extract (PN)
CHO compounds	2661	2867
CHOS compounds	255	57
CHNO compounds	828	319
CHNOS compounds	7	1
total number assigned mass peaks	3751	3244
average mass	428.49	388.90
average H [%]	4.84	6.83
average C [%]	55.68	59.21
average O [%]	39.20	33.83
average N [%]	0.15	0.09
average S [%]	0.13	0.04
computed H/C ratio	1.04	1.38
computed O/C ratio	0.53	0.43
computed N/C ratio	0.0575	0.0906
computed S/C ratio	0.0812	0.0850
$(DBE)_w$	10.56	6.94
$(DBE/O)_w$	1.02	0.90
$(\#C)_w$	19.92	19.23
$(\#H)_w$	20.78	26.61
$(\#O)_w$	10.52	8.24
$(\#N)_w$	0.05	0.03
$(\#S)_w$	0.02	0.01
CHO % of Intensity	94.43%	97.91%
CHOS % of Intensity	1.27%	0.36%
CHNO % Intensity	4.27%	1.73%
CHNOS % Intensity	0.03%	0.00%

Table 6-9: Molecular formulas of the experiments with the SRFA DOM and thiosulfate and sulfite.
Summary of the (–)ESI FT-ICR-MS derived molecular formulas of the experiments with the Suwannee River Fulvic Acid (SRFA) and thiosulfate ($S_2O_3^{2-}$) and sulfite (SO_3^{2-}). Only molecular formulas abundant in two out of three replicates are taken in consideration. The intensity weighted compositional contribution of the individual compound classes is based on the mean values.

DOM	SRFA	SRFA	SRFA	SRFA	SRFA	SRFA	SRFA	SRFA	SRFA	SRFA	SRFA	SRFA
pH	6	8	10	6	6	6	8	8	8	10	10	10
sulfur species	-	-	-	$S_2O_3^{2-}$	$S_2O_3^{2-}$	SO_3^{2-}	$S_2O_3^{2-}$	$S_2O_3^{2-}$	SO_3^{2-}	$S_2O_3^{2-}$	$S_2O_3^{2-}$	SO_3^{2-}
conditions				anoxic	oxic	anoxic	anoxic	oxic	anoxic	anoxic	oxic	anoxic
CHO compounds	2564	2573	2543	2519	2502	2402	2562	2532	2413	2517	2512	2542
CHOS compounds	230	184	190	480	466	692	538	546	626	662	570	630
CHNO compounds	660	645	618	729	740	840	793	759	778	752	760	844
CHNOS compounds	4	3	4	9	5	10	9	3	13	8	7	13
CHO % of Intensity	94.52%	94.89%	94.96%	93.20%	93.30%	85.44%	92.76%	92.36%	87.47%	75.60%	92.09%	88.79%
CHOS % of Intensity	1.36%	1.08%	1.12%	2.62%	2.44%	9.99%	2.97%	3.49%	8.28%	20.98%	3.76%	6.92%
CHNO % Intensity	4.10%	4.00%	3.89%	4.15%	4.24%	4.51%	4.25%	4.14%	4.17%	3.36%	4.13%	4.22%
CHNOS % Intensity	0.01%	0.02%	0.02%	0.03%	0.02%	0.07%	0.03%	0.01%	0.08%	0.06%	0.02%	0.06%

Table 6-10: Molecular formulas of the experiments with the SRFA DOM and sulfide and polysulfide.
Summary of the (–)ESI FT-ICR-MS derived molecular formulas of the experiments with the Suwannee River Fulvic Acid (SRFA) and sulfide (S^{2-}) and polysulfide (S_x^{2-}). Only molecular formulas abundant in two out of three replicates are taken in consideration. The intensity weighted compositional contribution of the individual compound classes is based on the mean values.

DOM	SRFA	SRFA	SRFA	SRFA	SRFA	SRFA	SRFA	SRFA	SRFA	SRFA	SRFA	SRFA	SRFA
pH	6	8	10	6	6	8	8	8	8	10	10	10	10
sulfur species	-	-	-	S^{2-}	S^{2-}	S^{2-}	S^{2-}	S_x^{2-}	S_x^{2-}	S^{2-}	S^{2-}	S_x^{2-}	S_x^{2-}
conditions				anoxic	oxic	anoxic	oxic	anoxic*	oxic*	anoxic	oxic	anoxic	oxic
CHO compounds	1869	1940	1869	1862	1862	1880	1929	1755	1817	1882	1875	1897	1909
CHOS compounds	159	150	144	689	735	646	689	351	502	619	643	464	662
CHNO compounds	662	753	654	706	706	733	746	619	655	705	675	705	739
CHNOS compounds	0	0	0	11	7	13	16	6	6	12	12	9	15
CHO % of Intensity	94.38%	94.35%	94.56%	90.60%	90.18%	89.53%	90.65%	92.04%	90.93%	90.35%	89.45%	92.21%	89.70%
CHOS % of Intensity	0.80%	0.67%	0.75%	4.67%	5.19%	5.72%	4.55%	3.16%	4.34%	5.06%	6.09%	3.11%	5.49%
CHNO % Intensity	4.82%	4.97%	4.69%	4.70%	4.61%	4.71%	4.75%	4.77%	4.71%	4.55%	4.42%	4.64%	4.71%
CHNOS % Intensity	0.00%	0.00%	0.00%	0.03%	0.02%	0.03%	0.04%	0.03%	0.03%	0.04%	0.04%	0.03%	0.10%

* single measurements

Table 6-11: Molecular formulas of the experiments with the pine needle DOM and thiosulfate and sulfite.
Summary of the (–)ESI FT-ICR-MS derived molecular formulas of the experiments with the pine needle extract (PN) and thiosulfate ($S_2O_3^{2-}$) and sulfite (SO_3^{2-}). Only molecular formulas abundant in two out of three replicates are taken in consideration. The intensity weighted compositional contribution of the individual compound classes is based on the mean values.

DOM	PN	PN	PN	PN	PN	PN	PN	PN	PN	PN	PN	PN
pH	6	8	10	6	6	6	8	8	8	10	10	10
sulfur species	-	-	-	$S_2O_3^{2-}$	$S_2O_3^{2-}$	SO_3^{2-}	$S_2O_3^{2-}$	$S_2O_3^{2-}$	SO_3^{2-}	$S_2O_3^{2-}$	$S_2O_3^{2-}$	SO_3^{2-}
conditions				anoxic	oxic	anoxic	anoxic	oxic	anoxic	anoxic	oxic	anoxic
CHO compounds	2910	2861	2874	3016	3026	2634	2914	2920	2745	2916	2929	2750
CHOS compounds	49	31	47	494	402	851	383	536	642	774	808	864
CHNO compounds	396	868	457	394	607	331	980	762	867	423	488	436
CHNOS compounds	3	4	3	24	22	62	15	17	39	30	28	58
CHO % of Intensity	97.14%	95.53%	96.17%	95.46%	92.99%	77.31%	92.67%	91.86%	85.02%	85.98%	87.21%	78.33%
CHOS % of Intensity	0.63%	0.34%	1.35%	2.62%	4.49%	20.28%	2.58%	5.34%	11.14%	12.05%	10.58%	18.10%
CHNO % Intensity	2.21%	4.11%	2.47%	1.83%	2.44%	1.75%	4.71%	2.72%	3.57%	1.83%	2.12%	2.03%
CHNOS % Intensity	0.02%	0.02%	0.02%	0.09%	0.08%	0.66%	0.05%	0.08%	0.27%	0.14%	0.09%	1.54%

Table 6-12: Molecular formulas of the experiments with the pine needle DOM and sulfide and polysulfide.
Summary of the (–)ESI FT-ICR-MS derived molecular formulas of the experiments with the pine needle extract (PN) and sulfide (S^{2-}) and polysulfide (S_x^{2-}). Only molecular formulas abundant in two out of three replicates are taken in consideration. The intensity weighted compositional contribution of the individual compound classes is based on the mean values.

DOM	PN	PN	PN	PN	PN	PN	PN	PN	PN	PN	PN	PN	PN
pH	**6**	**8**	**10**	**6**	**6**	**8**	**8**	**8**	**8**	**10**	**10**	**10**	**10**
sulfur species	-	-	-	S^{2-}	S^{2-}	S^{2-}	S^{2-}	S_x^{2-}	S_x^{2-}	S^{2-}	S^{2-}	S_x^{2-}	S_x^{2-}
conditions				anoxic	oxic	anoxic	oxic	anoxic	oxic	anoxic	oxic	anoxic	oxic
CHO compounds	2673	2867	2957	2633	2567	2558	2441	2755	2672	2448	2134	2802	2227
CHOS compounds	62	57	35	758	1287	1254	1981	608	1450	1437	2400	701	2310
CHNO compounds	306	319	362	347	309	341	301	348	312	322	292	379	298
CHNOS compounds	3	1	4	8	12	58	35	14	27	46	67	24	58
CHO % of Intensity	97.55%	97.91%	97.41%	92.07%	87.92%	78.03%	70.12%	94.97%	80.99%	73.98%	52.49%	93.72%	56.40%
CHOS % of Intensity	0.60%	0.36%	0.33%	6.06%	10.32%	19.86%	28.30%	3.16%	17.46%	24.31%	45.85%	4.16%	41.99%
CHNO % Intensity	1.84%	1.73%	2.25%	1.83%	1.69%	1.67%	1.41%	1.81%	1.44%	1.49%	1.33%	1.91%	1.31%
CHNOS % Intensity	0.01%	0.00%	0.01%	0.03%	0.06%	0.44%	0.16%	0.06%	0.10%	0.22%	0.33%	0.21%	0.29%
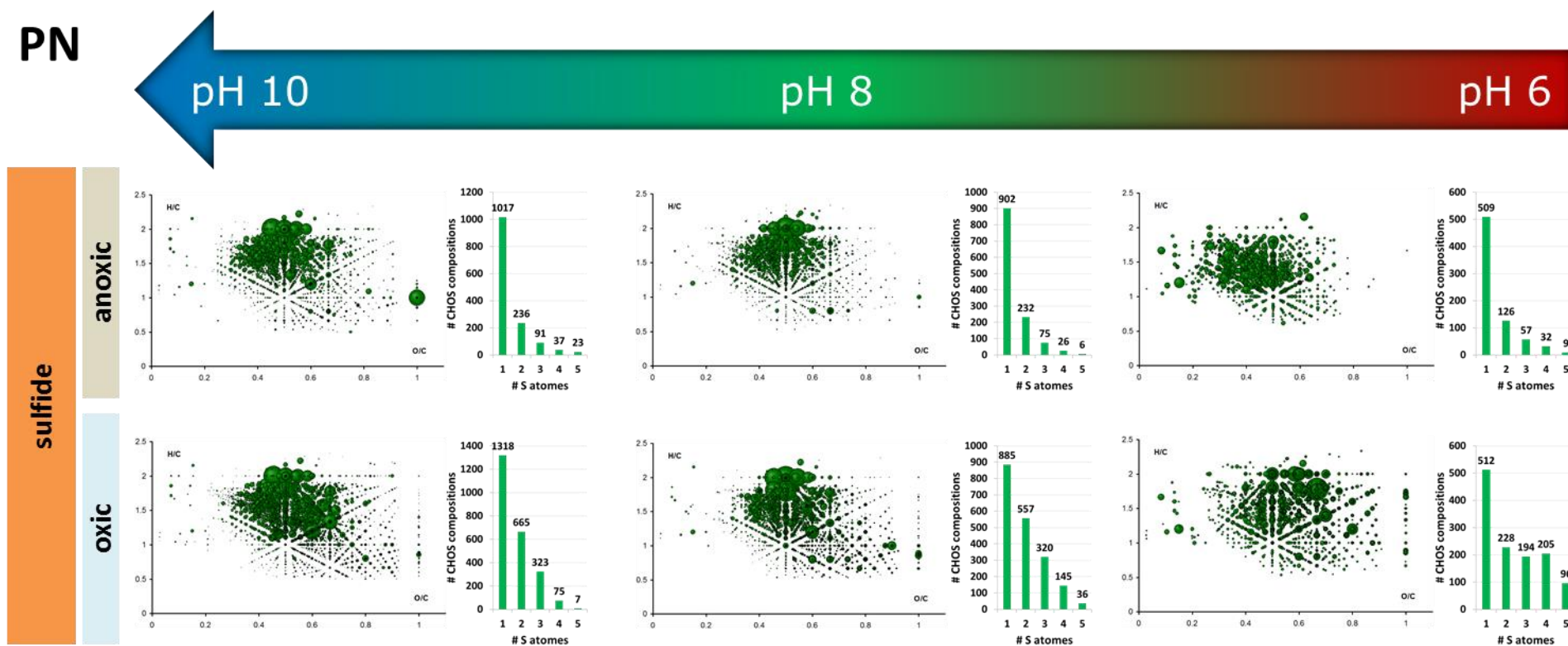
Figure 6-13: CHOS compounds formed the reaction of pine needle DOM with sulfide.
Van Krevelen diagrams and bar charts depicting the number of sulfur atoms distribution of the formed CHOS compounds by the reaction of pine needle (PN) DOM with sulfide.
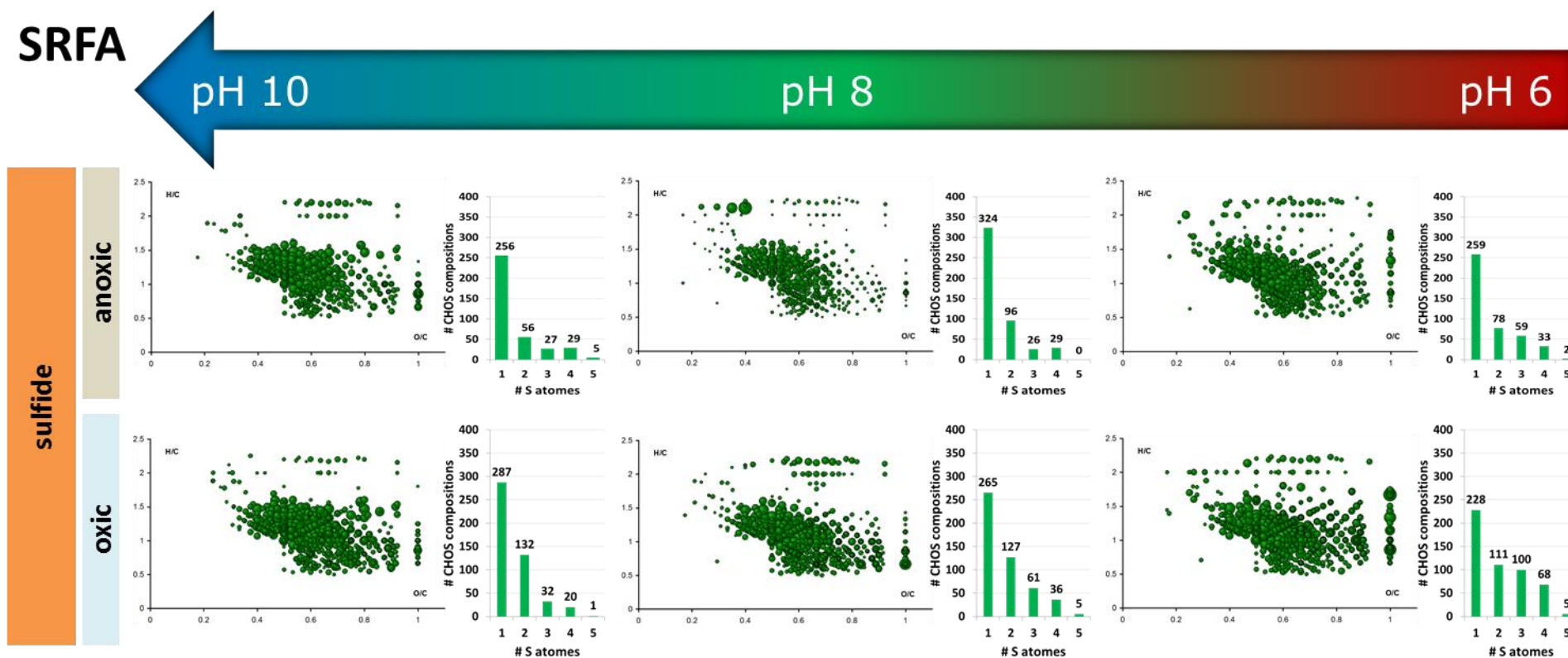
Figure 6-14: CHOS compounds formed the reaction SRFA DOM with sulfide.
Van Krevelen diagrams and bar charts depicting the number of sulfur atoms distribution of the formed CHOS compounds by the reaction of SRFA DOM with sulfide.
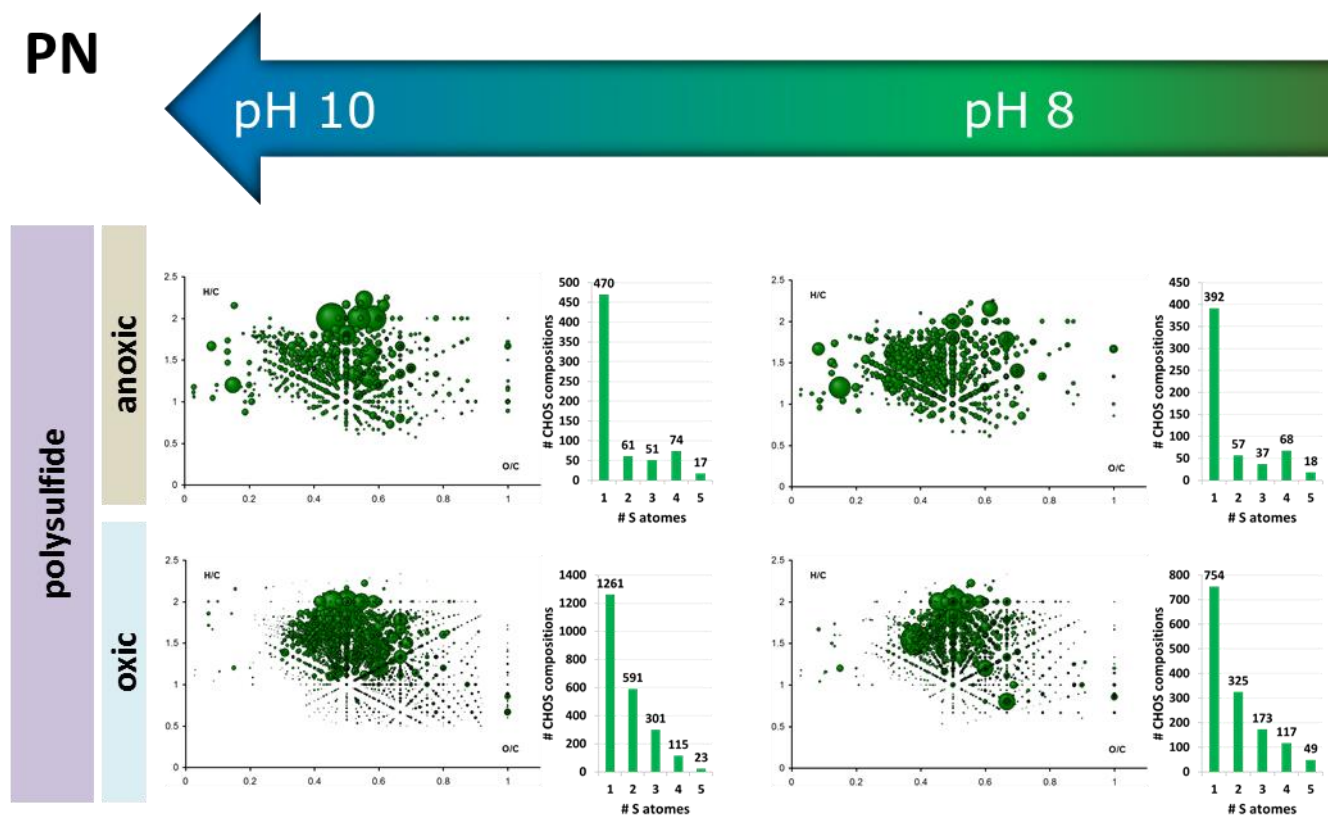
Figure 6-15: CHOS compounds formed the reaction of pine needle DOM with polysulfide.
Van Krevelen diagrams and bar charts depicting the number of sulfur atoms distribution of the formed CHOS compounds by the reaction of pine needle (PN) DOM with polysulfide.
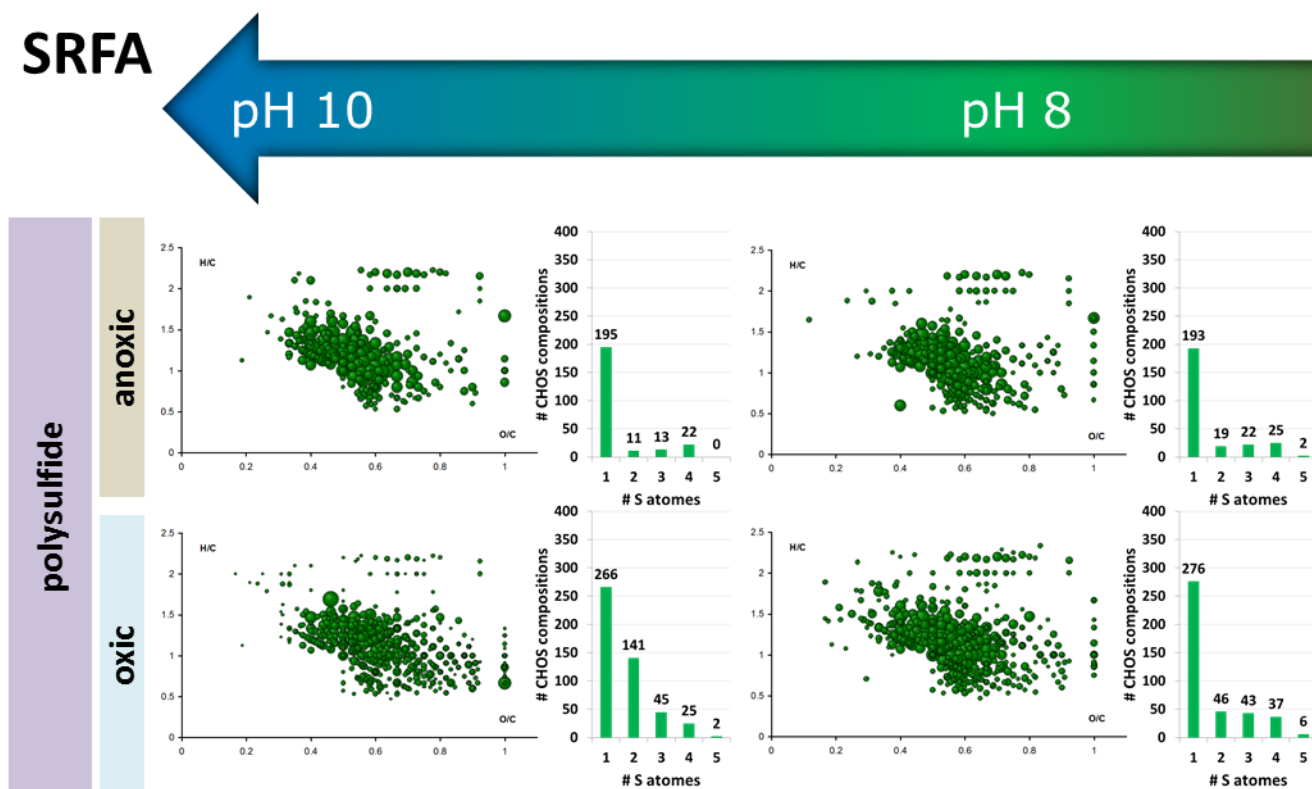
Figure 6-16: CHOS compounds formed the reaction of SRFA DOM with polysulfide.
Van Krevelen diagrams and bar charts depicting the number of sulfur atoms distribution of the formed CHOS compounds by the reaction of SRFA DOM with polysulfide.
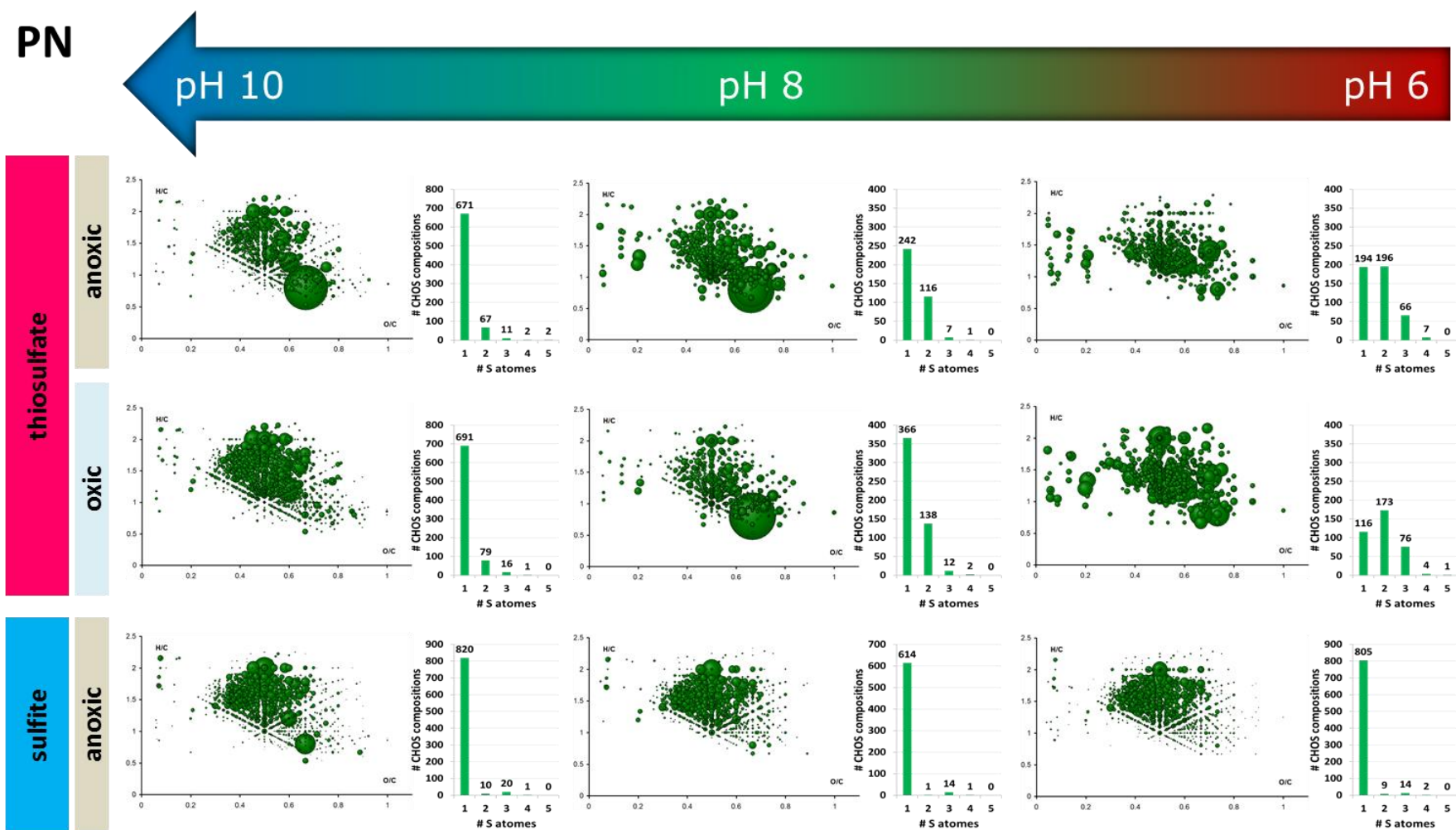
Figure 6-17: CHOS compounds formed the reaction of pine needle DOM with thiosulfate and sulfite.
Van Krevelen diagrams and bar charts depicting the number of sulfur atoms distribution of the formed CHOS compounds by the reaction of pine needle (PN) DOM with thiosulfate and sulfite.
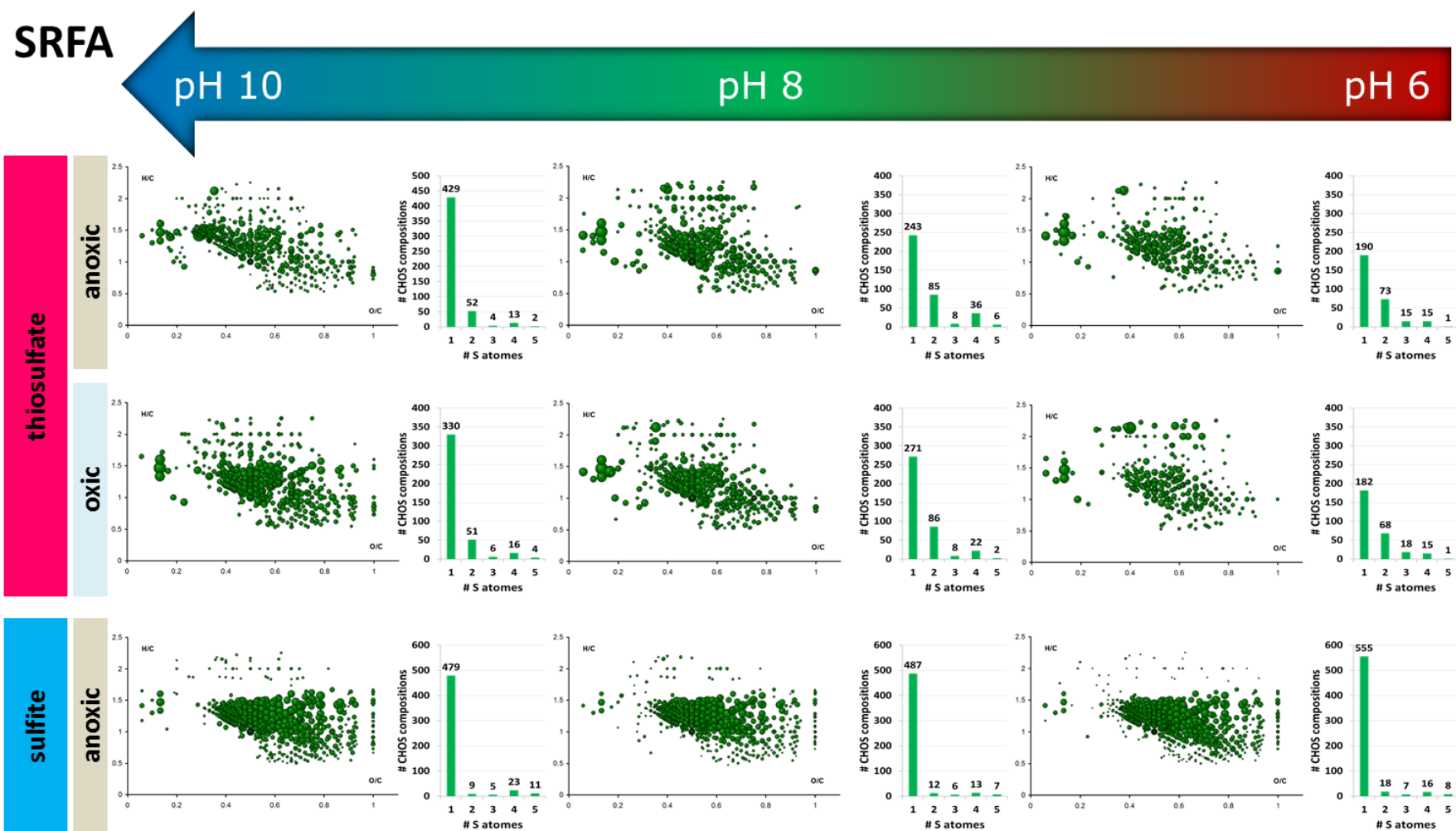
Figure 6-18: CHOS compounds formed the reaction of SRFA DOM with thiosulfate and sulfite.
Van Krevelen diagrams and bar charts depicting the number of sulfur atoms distribution of the formed CHOS compounds by the reaction of SRFA DOM with thiosulfate and sulfite.
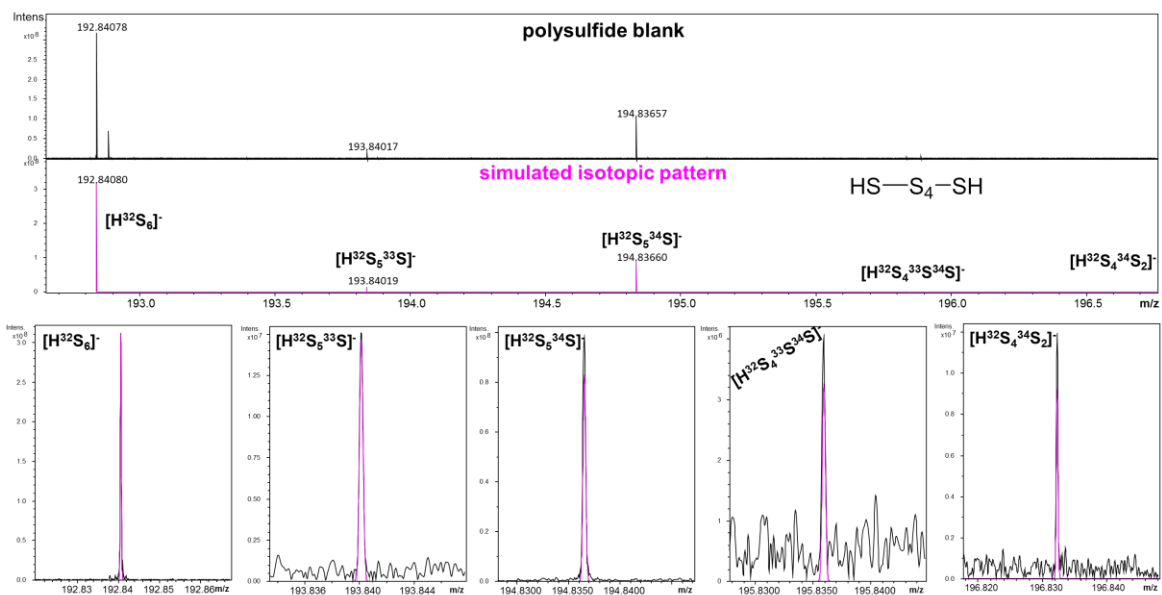
Figure 6-19: Isotopic pattern verification of S$_6$-polysulfane in the polysulfide solution.
Isotopic pattern of S$_6$-polysulfane (H$_2$S$_6$) detected in the polysulfide blank solution (black) in comparison to the simulated isotopic patte

7. Appendix

7.1. General materials and methods

7.1.1. Ultrahigh resolution mass spectrometry

Table 7-1: Parameters of the FT-ICR-MS measurements.
(cf. 2.3.4, 3.3.4 and 4.3.4.2)

Parameter	Hechtsee	Düsseldorf		Model Experiments
	(–)ESI	(–)ESI	(+)APPI	(–)ESI
Flow rate [µL/h]	120	120	1000	120
Mass range [Da]	150 – 1000	123 – 1000	100 – 1000	100 – 1000
Time of flight [ms]	0.7	0.6	0.6	0.7
Ion accumulation time [s]	0.3	0.1	0.2	0.3
Acquired scans	500	500	500	300
Collision voltage [V]	4	3	-2	4
Capillary voltage [V]	3600	3600	2000	3600
Drying gas flow rate [L/min]	4	4	3	4
Drying gas temperature [C°]	180	180	250	180
Nebulizer gas flow rate [bar]	2.2	2.2	2.0	2.2
Spray shield [V]	-500	-500	-500	-500
Time domain [MW]	4	4	4	4

Table 7-2: Parameters of the MS/MS FT-ICR-MS measurements.
(cf. 3.3.4 and 4.3.4.2)

Parameter	Düsseldorf (–)ESI FT-ICR-MS	Model Experiments (–)ESI FT-ICR-MS
Flow rate [µL/h]	120	120
Isolation mass range [Da]	0.5 – 2	± 55
Time of flight [ms]	0.6	0.7
Ion accumulation time [s]	0.1	2
Acquired scans	50	150
Collision voltage [V]	3	4
Collision voltage collision cell [eV]	0 – 30	0 – 30
Capillary voltage [V]	3600	3600
Drying gas flow rate [L/min]	4	4
Drying gas temperature [C°]	180	180
Nebulizer gas flow rate [bar]	2.2	2.2
Spray shield [V]	-500	-500
Time domain [MW]	2	2

7.1.2. NMR spectroscopy

1D and 2D ^{1}H and ^{13}C NMR spectra were acquired from re-dissolved DOM in CD_3OD at 283 K with a Bruker (Karlsruhe, Germany) AV III 800 spectrometer operating at B_0 = 18.7 Tesla with Bruker standard pulse sequences and cryogenic detection.

1D ^{1}H NMR spectra were recorded with a spin-echo sequence (10 µs delay) to allow for high-Q probe ringdown and classical presaturation to attenuate residual water present "*noesypr1d*" (typically 4–16 k scans with 5 s acquisition time, 5 s relaxation delay, 1 ms mixing time; 1 Hz exponential line broadening). Integration of the spectra was performed in the chemical shift range δ_H = 0.5–9.5 ppm with the exclusion of residual water (δ_H = 4.9–5.1 ppm) and methanol (δ_H = 3.25–3.35 ppm) NMR resonances by means of AMIX-based bucket analysis (0.1 ppm uniform width, normalized total ^{1}H NMR integral = 100%). The integrals were further grouped according to their specific chemical regions of aromatics (δ_H = 7.0–9.5 ppm, green), olefinics (δ_H = 5.1–7.0 ppm, blue), carbohydates (δ_H = 4.9–3.1 ppm, pink), CRAM (δ_H = 3.1–1.9 ppm, purple), and aliphatics (δ_H = 0.5–1.9 ppm, orange) (cf. Figure 5, Table S3 and also Tables S4 and S5, with more detailed attribution of key substructures to δ_H ranges).

The one bond coupling constant ^{1}J(CH) used in 2D ^{1}H,^{13}C DEPT-HSQC spectra (*hsqcedetgpsisp2.2*) was set to 145 Hz; other conditions were as follows: ^{13}C 90 degree decoupling pulse, GARP (70 µs); 50 kHz WURST 180 degree ^{13}C inversion pulse (Wideband, Uniform, Rate, and Smooth Truncation; 1.2 ms); F2 (^{1}H): spectral width of 5981 Hz (11.96 ppm); 1.25 s relaxation delay; F1 (^{13}C): SW = 17607 Hz (140 ppm). Absolute value JRES and echo-antiecho TOCSY spectra (with solvent suppression: *jresgpprqf*, *dipsi2etgpsi19*) used a spectral width of 5498 Hz [JRES (F1) = 50 Hz] and were computed to a 16384 × F1 matrix [JRES/TOCSY (F1) = 128/4096]. Other NMR acquisition conditions are given Table 7-3.

Table 7-3: Parameters of the NMR measurements.
Acquisition conditions for NMR spectra provided in Figures 5 and S7-8. PK: NMR probehead used, 8Q: 800 MHz 5 mm cryogenic inverse quaternary ^{1}H/^{13}C/^{15}N/^{31}P; NS: number of scans (for 2D NMR: F2); AQ: acquisition time [ms]; D1: relaxation delay [ms]; NE: number of F1 increments in 2D NMR spectra; WDW1, WDW2: apodization functions in F1/F2 (EM exponential line broadening factor [Hz]; SI: sine bell); PR1, PR2: coefficients used for windowing functions WDW1, WDW2, EM is given in [Hz], SI derived functions indicate shift by π/n. Total NMR acquisition time AQ_Σ is computed as follows: AQ_Σ = NS × (D1 + AQ) × NE, with NE = 1 for 1D NMR spectra.

Experiment	PK	NS	AQ [ms]	D1 [ms]	NE	WDW1	WDW2	PR1	PR2
^{1}H	8Q	480--15616	5000	5000	/	/	EM	-	1
JRES	8Q	2048	1000	500	64	QS	QS	0	0
TOCSY	8Q	160	1000	500	2243	QS	EM	6	2.5
DEPT-HSQC	8Q	2048	250	1250	317	QS	EM	2.5	2.5

Table 7-4: ^{1}H NMR section integrals and main structures.
^{1}H NMR section integrals derived from total area-normalized ^{1}H NMR spectra integrals with main structures provided.

structure	key structures	δ(^{1}H) [ppm]
aromatics	$\underline{\mathbf{H}}_{ar}$	10 - 7.0
olefins	$\underline{\mathbf{H}}C=C$, $\mathbf{H}CO_2$	7.0 - 5.0
carbohydrates	$\underline{\mathbf{H}}CO$	4.9 - 3.1
CRAM	$\underline{\mathbf{H}}CCX$	3.1 - 1.9
aliphatics	$\underline{\mathbf{H}}CCC$	1.9 - 0

7.1.3. Synthesis of polysulfide salts

Sodium tetrasulfide salts were synthesized using methods adapted from Rosen and Tegman (Rosen and Tegman 1971). Anhydrous sodium sulfide and elemental sulfur salts (Thermo Fisher Scientific Inc., Waltham, MA, USA) were mixed at appropriate stoichiometry, crushed and placed in glass tubes under a dry anoxic N_2 atmosphere by the use of an anaerobic chamber (Coy Laboratory Products Inc., Grass Lake, MI, USA). The tubes were evacuated in a vacuum line after being frozen due to submersion in liquid N_2, so to avoid volatilization of elemental sulfur. Tubes were sealed using a propane torch. Synthesis took place through melting and reaction for 12 h at 210 °C, followed by an annealing step for about half an hour at 350 °C. The product was removed and re-grinded under N_2 atmosphere, placed in another tube, liquid N_2-frozen and vacuum-sealed, whereas the melting and reaction steps were repeated. The whole synthesis included three cycles of the aforementioned procedure, in order to enhance the solid-state reaction through the whole solid material. The salts were then washed with hexane to remove residual elemental sulfur impurities, resealed under vacuum, and kept in the anaerobic chamber until used in the kinetics experiments and as standards in voltammetric analysis.

7.2. *Extended materials and methods section of chapter 3*

7.2.1. List of samples

Table 7-5: List of sampled depths in September 2013.

port	depth [m] bls	sampling volume for SPE-DOM extraction 250 mL = H, 1 L = L	classes in OPLS-DA
C28	6.51	H	upper fringe
C29	6.54	H, L	upper fringe
C31	6.59	H	upper fringe
C32	6.61	H	upper fringe
C33	6.64	H	transition
C34	6.67	H, L	plume core
D1	6.75	H	plume core
D2	6.78	H, L	plume core
D3	6.81	H	plume core
D4	6.83	H	plume core
D6	6.88	H	plume core
D7	6.91	H	plume core
D8	6.93	H	plume core
D9	6.96	H	plume core
D11	7.01	H	plume core
D12	7.03	H	transition
D13	7.06	H, L	lower fringe
D14	7.08	H	lower fringe
D15	7.11	H	lower fringe
D19	7.21	H, L	lower fringe
D21	7.26	H	transition
D23	7.31	H	transition
D27	7.41	H	deep zone
D31	7.51	H	deep zone
D35	7.61	H, L	deep zone
E1	7.75	H	deep zone
E4	8.05	H, L	deep zone
E10	8.65	H	deep zone
F4	9.05	H, L	deep zone
F7	9.35	H	deep zone
G2	10.20	H	deep zone
H2	11.19		

7.2.2. PARAFAC modeling of EEM fluorescence spectra

PARAFAC modeling was performed by the drEEM MATLAB toolbox (Murphy et al. 2013). A total of 45 EEM spectra were visually investigated, and outliers were removed. To reduce concentration effects during modeling, the samples were normalized to unit variance. After model completion, the normalization was reversed. The model evaluation and final assignment were performed as described in Murphy et al. by taking into account the following criteria: 1) residual analysis, 2) spectral loading, and 3) split-half validation (Figure 7-1, Figure 7-1)Fmax values describing the fluorescence intensity at the maximum for each component were exported.
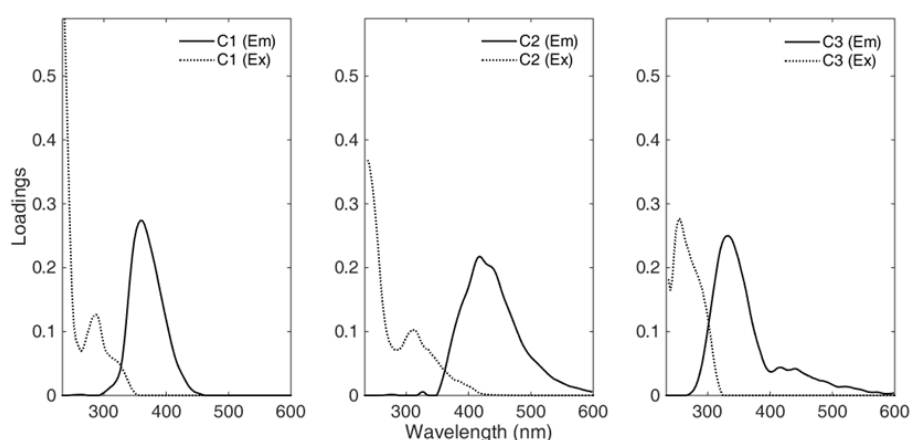
Figure 7-1: PARAFAC model excitation and emission loadings
Excitation and emission loadings of the three components modeled with PARAFAC. Reprinted with permission from (Dvorski et al. 2016). Copyright (2016) American Chemical Society.
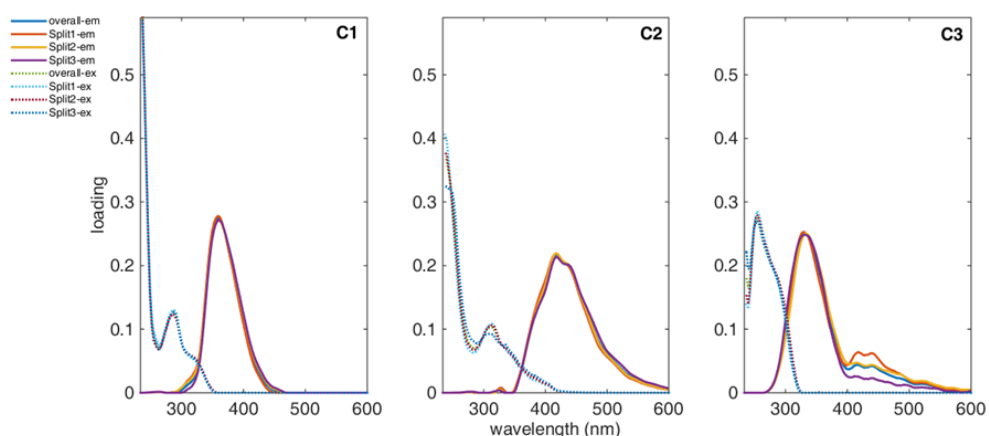
Figure 7-2: Split-half validation of PARAFAC model
Split-half validation results for the three component PARAFAC model. Reprinted with permission from (Dvorski et al. 2016). Copyright (2016) American Chemical Society.

PARAFAC Model Report

Info

      Toolbox   drEEM 0.1.0
      Date   16.07.2015 13:54

Preprocessing

      nSample - full dataset 45
      nSample - modeled dataset   42
      No. excluded samples 3
      Excluded samples -indices   23
      Scatter Removal   24
      Zapped (Samples,EmRange,ExRange)   33
      Fluorescence unit   35
      ScalingNormalised to unit variance in sample mode

PARAFAC model

      No. PARAFAC components 3
      No. Ex wavelengths   122
      No. Em wavelengths   112

Validation

      Split_Style   random then combine
      Split_NumBeforeCombine   3
      Split_NumAfterCombine   3
      Split_Combinations   1 2   1 3   2 3
      Split_nSample 28   28   28
      Split_AnalRuns   1   1   1
      Split_PARAFAC_options   0.000001   0   0   0   0   0
      Split_PARAFAC_constraints 2   2   2
      Split_PARAFAC_convgcrit 0.000001   0.000001   0.000001

      Split_PARAFAC_Initialise   SVD
      Val_ModelName   Model3
      Val_Source   Model3it_5
      Val_Err   10679.84415
      Val_It 48
      Val_Result   Overall Result= Validated for all comparisons

      Val_Splits   AB   AC   BC
      Val_Comparisons   AB vs AC,   AB vs BC,   AC vs BC,
      Val_ConvgCrit   0.00000001
      Val_Constraints   nonnegativity
      Val_Initialise random
Core consist   Val_Core   89.69881479
      Val_PercentExpl   98.32132604
      Val_CompSize   63.54726548 39.62173401 28.4657282
      Val_Preprocess   Reversed normalisation to recover true scores

7.2.3. Microbial community analysis

DNA extraction

Total DNA was extracted from water filters (no replicate extractions) and sediment samples (in triplicates) from selected depth between 6.54 and 11.19 m bls and is described in details elsewhere (Lueders et al. 2004, Laban et al. 2015, Brielmann et al. 2009)

Amplicon library preparation

Bacterial 16S rRNA gene amplicon pyrosequencing was performed using a unidirectional sequencing approach. Barcoded amplicons for multiplexing were prepared using the primers Ba27f (5'-aga gtt tga tcm tgg ctc ag-3') and Ba907r (5'-ccg tca att cmt ttr agt t-3') extended with the respective AL or BL adapters, key sequence and a multiplex identifier (MID) as on the forward primer as recommended for the 454 GS FLX+ chemistry protocol (Roche). Technical duplicate amplicon libraries were prepared for each water sample, biological triplicate libraries from each sediment samples. PCR amplification conditions were the same as described before (Karwautz and Lueders 2014). Amplicons were visualized with gel electrophoresis in a 1.5% agarose gel. Cleanup of the amplicons was done with a PCRextract kit (5Prime, Hamburg, Germany) according to the manufacturer's protocol. Quality of single amplicons was checked for primer dimer contamination and correct fragment size using the Bioanalyzer2100 (Agilent, USA) loading High Sensitivity DNA assay chips (Agilent, USA), as described by the manufacturer. Two multiplexed amplicon pools (consisting of 22 libraries from the water samples or 17 amplicons from sediments) were prepared in equimolar amounts ($5*10^9$ molecules μl^{-1}) of barcoded amplicons as quantified by the Quant-iT PicoGreen dsDNA quantification kit (Invitrogen, Paisley, UK). Each amplicon pool then underwent a second purification step with Agencourt AMPure-XP beads (Beckman Coulter, Brea, CA) using an adapted heat-denaturation protocol (Roche). Emulsion PCR and emulsion breaking were performed following protocols of Roche and pyrosequencing was performed on a 454 GS FLX+ sequencer by IMGM Laboratories, Planegg, Germany.

Sequence data handling

Initial quality filtering of the raw pyrosequencing reads was done by using the automated amplicon pipeline of the GS Run Processor with the LongAmplicon3 filter (Roche). Sequences were then de-multiplexed to separate MID barcodes (Pilloni et al. 2012), initial quality trimming was done in GREENGENES; using the TRIM function with the default settings (DeSantis et al. 2006). Trimmed sequences were uploaded and analyzed via the NGS analysis pipeline of the SILVA rRNA gene database project (SILVAngs 1.3) (Quast et al. 2013). Reads were aligned using the SILVA Incremental Aligner (SINA SINA v1.2.10 for ARB SVN (revision 21008)) (Pruesse, Peplies and Glöckner 2012) against the SILVA SSU rRNA SEED and quality controlled (Quast et al. 2013). Reads shorter than 50 aligned nucleotides or below 40 alignment score, reads with more than 2% of ambiguities or more than 2% of homopolymers were excluded from the downstream processing. Dereplication and clustering of the unique reads into operational taxonomic units (OTUs) was done by using cd-hit-est (version 3.1.2) (Li and Godzik 2006) running in accurate mode, ignoring overhangs, and applying identity criteria of 1.00 and 0.98, respectively. The classification of the OTUs was performed by a local nucleotide BLAST search against the non-redundant version of the SILVA SSU Ref dataset (release 123; http://www.arb-silva.de) using blastn (version 2.2.30) with standard settings (Camacho et al. 2009). Weak BLAST hits (below 93%) or reads without any BLAST hits remained unclassified and were assigned to the metagroup "No Relative".

7.2.4. Validation of the multi-data correlation

Table 7-6: Validation of the OPLS and OPLS-DA model.

Model	R²(Y) (cum)	Q²(cum)	CV-Anova (p-values)
			values in
OPLS	0,926	0,852	Table 7-7
OPLS-DA	0,93	0,808	9.88E-18

Table 7-7: OPLS model parameters.

M1(Untitled)	Sum of Squares (SS)	Degree of Freddom (F)	Mean Squares (MS)	F-test (F)	p-values (p)	Standard deviation (SD)
VAR_2 redox potential						
Total corr	40	40	1			1
Regression	333,419	10	333,419	15,023	4.11E-04	182,598
Residual	665,815	30	0,221938			0,471103
VAR_3 pH						
Total corr	40	40	1			1
Regression	304,615	10	304,615	958,056	6.47E-02	174,532
Residual	953,852	30	0,317951			0,563871
VAR_5 sulfide						
Total corr	40	40	1			1
Regression	328,773	10	328,773	138,477	1.07E-04	181,321
Residual	712,265	30	0,237422			0,487259
VAR_14 sulfate						
Total corr	39	39	1			1
Regression	362,391	10	362,391	38,065	5.54E-10	190,366
Residual	276,089	29	0,0952032			0,30855
VAR_25 BTEX						
Total corr	37	37	1			1
Regression	327,946	10	327,946	210,551	3.08E-05	181,093
Residual	420,542	27	0,155756			0,39466
VAR_39 total sulfur						
Total corr	39	39	1			1
Regression	343,447	10	343,447	21,395	8.85E-06	185,323
Residual	465,529	29	0,160527			0,400658
VAR_50 PAH						
Total corr	40	40	1			1
Regression	330,515	10	330,515	14,27	7.54E-04	181,801
Residual	694,847	30	0,231616			0,481265

References

Adam, P., E. Philippe & P. Albrecht (1998) Photochemical Sulfurization of Sedimentary Organic Matter: A Widespread Process Occurring at Early Diagenesis in Natural Environments? *Geochimica et Cosmochimica Acta,* 62**,** 265-271.

Aeschbacher, M., D. Vergari, R. P. Schwarzenbach & M. Sander (2011) Electrochemical Analysis of Proton and Electron Transfer Equilibria of the Reducible Moieties in Humic Acids. *Environmental Science & Technology,* 45**,** 8385-8394.

Ahrika, A., J. Robert, M. Anouti, J. Paris, Z.-H. Jiang, S.-P. Yan, G.-L. Wang, X.-K. Yao, H.-G. Wang, J. P. Tuchagues & M. Ögren (1999) Nucleophilic Substitution of Alkyl Halides by Electrogenerated Polysulfide Ions in N,N-dimethylacetamide. *Acta Chemica Scandinavica,* 53**,** 513-520.

Aigner, G. 2015. Badegewässerprofil Hechtsee, Strandbad. ed. B. f. Gesundheit. Wien.

Aiken, G. R., D. M. McKnight, R. L. Wershaw & P. MacCarthy. 1986. *Humic Substances in Soil, Sediment, and Water: Geochemistry, Isolation, and Characterization.* New York: John Wiley & Sons Ltd.

Aiken, G. R., E. M. Thurman, R. L. Malcolm & H. F. Walton (1979) Comparison of XAD macroporous resins for the concentration of fulvic acid from aqueous solution. *Analytical Chemistry,* 51**,** 1799-1803.

Aizenshtat, Z. & A. Amrani. 2004. Significance of δ34S and evaluation of its imprint on sedimentary sulfur rich organic matter: I. The role of resuced sulfur species in the diagenetic stage: A concenptual review. In *Geochemical Investigations in Earth and Space Science: A Tribute to Isaac R. Kaplan,* eds. R. J. Hill, J. Leventhal, Z. Aizenshtat, M. J. Baedecker, G. Claypool, R. Eganhouse, M. Goldhaber & K. Peters, 15–33. Amsterdam: Elsevier.

Aizenshtat, Z., E. B. Krein, M. A. Vairavamurthy & T. P. Goldstein. 1995. Role of Sulfur in the Transformations of Sedimentary Organic Matter: A Mechanistic Overview. In *Geochemical Transformations of Sedimentary Sulfur,* eds. M. A. Vairavamurthy, M. A. A. Schoonen, T. I. Eglington, G. W. Luther III & B. Manowitz, 16-37. Washington, DC: American Chemical Society.

Amon, R. M. W. & R. Benner (1996a) Bacterial utilization of different size classes of dissolved organic matter. *Limnology and Oceanography,* 41**,** 41-51.

Amon, R. M. W. & R. Benner (1996b) Photochemical and microbial consumption of dissolved organic carbon and dissolved oxygen in the Amazon River system. *Geochimica et Cosmochimica Acta,* 60**,** 1783-1792.

Amrani, A. (2014) Organosulfur compounds: Molecular and isotopic evolution from biota to oil and gas. *Annual Review of Earth and Planetary Sciences,* 42**,** 733-768.

Amrani, A. & Z. Aizenshtat (2004a) Photosensitized oxidation of naturally occurring isoprenoid allyl alcohols as a possible pathway for their transformation to thiophenes in sulfur rich depositional environments. *Organic Geochemistry,* 35**,** 693-712.

Amrani, A. & Z. Aizenshtat (2004b) Reaction of polysulfide anions with α,β unsaturated isoprenoid aldehydes in aquatic media: Simulation of oceanic conditions. *Organic Geochemistry,* 35**,** 909-921.

Amrani, A., J. W. Turner, Q. Ma, Y. Tang & P. G. Hatcher (2007) Formation of sulfur and nitrogen cross-linked macromolecules under aqueous conditions. *Geochimica et Cosmochimica Acta,* 71**,** 4141-4160.

Anneser, B., F. Einsiedl, R. U. Meckenstock, L. Richters, F. Wisotzky & C. Griebler (2008a) High-resolution monitoring of biogeochemical gradients in a tar oil-contaminated aquifer. *Applied Geochemistry,* 23**,** 1715-1730.

Anneser, B., G. Pilloni, A. Bayer, T. Lueders, C. Griebler, F. Einsiedl & L. Richters (2010) High Resolution Analysis of Contaminated Aquifer Sediments and Groundwater - What Can be Learned in Terms of Natural Attenuation? *Geomicrobiology Journal,* 27**,** 130-142.

Anneser, B., L. Richters & C. Griebler. 2008b. Application of High-Resolution Groundwater Sampling in a Tar Oil-Contaminated Sandy Aquifer, Studies on Small-Scale Abiotic Gradients. In *Advances in Subsurface Pollution of Porous Media - Indicators, Processes and Modelling: IAH selected papers, volume 14,* eds. J. L. Candelad, I. Vadillo & F. J. Elorza, 107-122. Leiden: CRC Press/Balkema.

Annweiler, E., W. Michaelis & R. U. Meckenstock (2001) Anaerobic cometabolic conversion of benzothiophene by a sulfate-reducing enrichment culture and in a tar-oil-contaminated aquifer. *Applied and Environmental Microbiology,* 67**,** 5077-5083.

Averett, R. C., J. A. Leenheer, D. M. McKnight & K. A. Thorn (1994) Humic Substances in the Suwannee River, Georgia: Interactions, Properties, and Proposed Structures. *USGS Water-Supply Paper,* 2373.

Azam, F., T. Fenchel, J. G. Field, J. S. Gray, L. A. Meyer-Reil & F. Thingstad (1983) The Ecological Role of Water-Column Microbes in the Sea. *Marine Ecology - Progress Series,* 10**,** 257-263.

Bailey, R. A., H. M. Clark, J. P. Ferris, S. Krause & R. L. Strong. 2002. 10 - The environmental chemistry of some important elements. In *Chemistry of the Environment (Second Edition),* 347-414. San Diego: Academic Press.

Bak, F. & H. Cypionka (1987) A novel type of energy metabolism involving fermentation of inorganic sulphur compounds. *Nature,* 326**,** 891-892.

Bak, F. & N. Pfennig (1987) Chemolithotrophic growth of Desulfovibrio sulfodismutans sp. nov. by disproportionation of inorganic sulfur compounds. *Archives of Microbiology,* 147**,** 184-189.

Bastone, S., A. Spinella, D. F. Chillura Martino, S. Tusa & E. Caponetti (2016) More insight into characterization of the waterlogged wooden part of Acqualadroni Roman Rostrum by solid-state NMR. *Microchemical Journal,* 124**,** 831-836.

Battin, T. J., S. Luyssaert, L. A. Kaplan, A. K. Aufdenkampe, A. Richter & L. J. Tranvik (2009) The boundless carbon cycle. *Nature Geoscience,* 2**,** 598-600.

Bauer, R. D., P. Maloszewski, Y. Zhang, R. U. Meckenstock & C. Griebler (2008) Mixing-controlled biodegradation in a toluene plume--results from two-dimensional laboratory experiments. *Journal of Contaminant Hydrology,* 96**,** 150-168.

Berggren, M., H. Laudon & M. Jansson (2009) Hydrological control of organic carbon support for bacterial growth in boreal headwater streams. *Microbial Ecology,* 57**,** 170-178.

Berner, R. A. & J. T. Westrich (1985) Bioturbation and the early diagenesis of carbon and sulfur. *American Journal of Science,* 285**,** 193-206.

Bianchi, T. S., C. Osburn, M. R. Shields, S. Yvon-Lewis, J. Young, L. Guo & Z. Zhou (2014) Deepwater horizon oil in gulf of Mexico waters after 2 years: transformation into the dissolved organic matter pool. *Environmental Science & Technology,* 48**,** 9288-9297.

Blough, N. V. & R. Del Vecchio. 2002. Chapter 10 - Chromophoric DOM in the Coastal Environment A2 - Carlson, Dennis A. HansellCraig A. In *Biogeochemistry of Marine Dissolved Organic Matter*, 509-546. San Diego: Academic Press.

Boulegue, J., C. J. Lord III & T. M. Church (1982) Sulfur speciation and associated trace metals (Fe, Cu) in the pore waters of Great Marsh, Delaware. *Geochimica et Cosmochimica Acta,* 46**,** 453-464.

Boyer, J. N., S. K. Dailey, P. J. Gibson, M. T. Rogers & D. Mir-Gonzalez (2006) The role of dissolved organic matter bioavailability in promoting phytoplankton blooms in Florida Bay. *Hydrobiologia,* 569**,** 71-85.

Bracchini, L., S. Loiselle, A. M. Dattilo, S. Mazzuoli, A. Cózar & C. Rossi (2004) The Spatial Distribution of Optical Properties in the Ultraviolet and Visible in an Aquatic Ecosystem. *Photochemistry and Photobiology,* 80**,** 139-149.

Brendel, P. J. & G. W. Luther, III (1995) Development of a Gold Amalgam Voltammetric Microelectrode for the Determination of Dissolved Fe, Mn, O2, and S(-II) in Porewaters of Marine and Freshwater Sediments. *Environmental Science & Technology,* 29**,** 751-761.

Brielmann, H., C. Griebler, S. I. Schmidt, R. Michel & T. Lueders (2009) Effects of thermal energy discharge on shallow groundwater ecosystems. *FEMS Microbiology Ecology,* 68**,** 273-286.

Brown, K. A. (1982) Sulphur in the environment: A review. *Environmental Pollution Series B, Chemical and Physical,* 3**,** 47-80.

Camacho, C., G. Coulouris, V. Avagyan, N. Ma, J. Papadopoulos, K. Bealer & T. L. Madden (2009) BLAST+: architecture and applications. *BMC Bioinformatics,* 10**,** 1-9.

Casagrande, D. J., K. Gronli & N. Sutton (1980) The distribution of sulfur and organic matter in various fractions of peat: origins of sulfur in coal. *Geochimica et Cosmochimica Acta,* 44**,** 25-32.

Casagrande, D. J., G. Idowu, A. Friedman, P. Rickert, K. Siefert & D. Schlenz (1979) H2S incorporation in coal precursors: origins of organic sulphur in coal. *Nature,* 282**,** 599-600.

Chen, K. Y. & J. C. Morris (1972) Kinetics of oxidation of aqueous sulfide by oxygen. *Environmental Science & Technology,* 6**,** 529-537.

Chen, M., S. Kim, J.-E. Park, H. S. Kim & J. Hur (2016) Effects of dissolved organic matter (DOM) sources and nature of solid extraction sorbent on recoverable DOM

composition: Implication into potential lability of different compound groups. *Analytical and Bioanalytical Chemistry*, 1-11.

Cline, J. D. (1969) Spectrometric Determination of Hydrogen Sulfide in Natural Waters. *Limnology and Oceanography,* 14**,** 454-458.

Coble, P. G. (1996) Characterization of marine and terrestrial DOM in seawater using excitation-emission matrix spectroscopy *Marine Chemistry,* 51**,** 325-346.

Coble, P. G., J. Lead, A. Baker, D. M. Reynolds & G. M. Spencer. 2014. *Aquatic Organic Matter Fluorescence*. New York: Cambridge University Press.

Cole, J. J., Y. T. Prairie, N. F. Caraco, W. H. McDowell, L. J. Tranvik, R. G. Striegl, C. M. Duarte, P. Kortelainen, J. A. Downing, J. J. Middelburg & J. Melack (2007) Plumbing the Global Carbon Cycle: Integrating Inland Waters into the Terrestrial Carbon Budget. *Ecosystems,* 10**,** 172-185.

Cook, R. L. 1992. Sulphur Cycling and Fluxes in Temperate Dimictic Lakes. In *Sulphur Cycling on the Continents - Wetlands, Terrestrial Ecosystems, and Associated Water Bodies,* eds. R. W. Howarth, J. W. B. Stewart & M. V. Ivanov, 125-144. Chinester: John Wiley & Sons Ltd.

Cooke, G. D., E. B. Welch, S. Peterson & S. A. Nichols. 2005. *Restoration and Management of Lakes and Reservoirs*. Boca Raton: CRC Press Taylor & Francis Group.

Cortés-Francisco, N. & J. Caixach (2013) Molecular Characterization of Dissolved Organic Matter through a Desalination Process by High Resolution Mass Spectrometry. *Environmental Science & Technology,* 47**,** 9619-9627.

Cory, R. M. (2010) Effect of instrument-specific response on the analysis of fulvic acid fluorescence spectra. *Limnology and Oceanography: Methods,* 8**,** 67-78.

Cory, R. M. & D. M. McKnight (2005) Fluorescence spectroscopy reveals ubiquitous presence of oxidized and reduced quinones in dissolved organic matter. *Environmental Science & Technology,* 39**,** 8142-8149.

D'Andrilli, J., T. Dittmar, B. P. Koch, J. M. Purcell, A. G. Marshall & W. T. Cooper (2010) Comprehensive characterization of marine dissolved organic matter by Fourier transform ion cyclotron resonance mass spectrometry with electrospray and atmospheric pressure photoionization. *Rapid Communications in Mass Spectrometry,* 24**,** 643-650.

De Graaf, W., J. S. S. Damsté & J. W. de Leeuw (1992) Laboratory simulation of natural sulphurization: I. Formation of monomeric and oligomeric isoprenoid polysulphides by low-temperature reactions of inorganic polysulphides with phytol and phytadienes. *Geochimica et Cosmochimica Acta,* 56**,** 4321-4328.

Derenne, S. & T. T. Nguyen Tu (2014) Characterizing the molecular structure of organic matter from natural environments: An analytical challenge. *Comptes Rendus Geoscience,* 346**,** 53–63.

DeSantis, T. Z., P. Hugenholtz, N. Larsen, M. Rojas, E. L. Brodie, K. Keller, T. Huber, D. Dalevi, P. Hu & G. L. Andersen (2006) Greengenes, a chimera-checked 16S rRNA gene database and workbench compatible with ARB. *Applied and Environmental Microbiology,* 72**,** 5069-5072.

Devkota, S., Y. Wang, M. W. Musch, V. Leone, H. Fehlner-Peach, A. Nadimpalli, D. A. Antonopoulos, B. Jabri & E. B. Chang (2012) Dietary-fat-induced taurocholic acid promotes pathobiont expansion and colitis in Il10-/- mice. *Nature,* 487**,** 104-108.

Dittmar, T., B. Koch, N. Hertkorn & G. Kattner (2008) A simple and efficient method for the solid-phase extraction of dissolved organic matter (SPE-DOM) from seawater. *Limnology and Oceanography: Methods,* 6**,** 230-235.

Druschel, G. K., R. J. Hamers & J. F. Banfield (2003a) Kinetics and mechanism of polythionate oxidation to sulfate at low pH by O2 and Fe3+. *Geochimica et Cosmochimica Acta,* 67**,** 4457-4469.

Druschel, G. K., R. J. Hamers, G. W. Luther & J. F. Banfield (2003b) Kinetics and mechanism of trithionate and tetrathionate oxidation at low pH by hydroxyl radicals. *Aquatic Geochemistry,* 9**,** 145-164.

Druschel, G. K., M. A. A. Schoonen, D. K. Nordstrom, J. W. Ball, Y. Xu & C. A. Cohn (2003c) Sulfur geochemistry of hydrothermal waters in Yellowstone National Park, Wyoming, USA. III. An anion-exchange resin technique for sampling and preservation of sulfoxyanions in natural waters. *Geochemical Transactions,* 4**,** 12-19.

Dubinenkov, I., R. Flerus, P. Schmitt-Kopplin, G. Kattner & B. P. Koch (2014) Origin-specific molecular signatures of dissolved organic matter in the Lena Delta. *Biogeochemistry,* 123**,** 1-14.

Durham, B. P., S. Sharma, H. Luo, C. B. Smith, S. A. Amin, S. J. Bender, S. P. Dearth, B. A. S. Van Mooy, S. R. Campagna, E. B. Kujawinski, E. V. Armbrust & M. A. Moran (2015) Cryptic carbon and sulfur cycling between surface ocean plankton. *Proceedings of the National Academy of Sciences,* 112**,** 453-457.

Dvorski, S. E.-M., M. Gonsior, N. Hertkorn, J. Uhl, H. Müller, C. Griebler & P. Schmitt-Kopplin (2016) Geochemistry of Dissolved Organic Matter in a Spatially Highly Resolved Groundwater Petroleum Hydrocarbon Plume Cross-Section. *Environmental Science & Technology,* 50**,** 5536–5546.

Eberhardt, C. & P. Grathwohl (2002) Time scales of organic contaminant dissolution from complex source zones: coal tar pools vs. blobs. *Journal of Contaminant Hydrology,* 59**,** 45–66.

Egeberg, P. K. & S. O. Bergli (2002) Fingerprinting of natural organic matter by capillary zone electrophoresis using organic modifiers and pattern recognition analysis. *Journal of Chromatography A,* 950**,** 221-231.

Einsiedl, F., N. Hertkorn, M. Wolf, M. Frommberger, P. Schmitt-Kopplin & B. P. Koch (2007) Rapid biotic molecular transformation of fulvic acids in a karst aquifer. *Geochimica et Cosmochimica Acta,* 71**,** 5474-5482.

Einsiedl, F., G. Pilloni, B. Ruth-Anneser, T. Lueders & C. Griebler (2015) Spatial distributions of sulphur species and sulphate-reducing bacteria provide insights into sulphur redox cycling and biodegradation hot-spots in a hydrocarbon-contaminated aquifer. *Geochimica et Cosmochimica Acta,* 156**,** 207–221.

Fasching, C., B. Behounek, G. A. Singer & T. J. Battin (2014) Microbial degradation of terrigenous dissolved organic matter and potential consequences for carbon cycling in brown-water streams. *Scientific Reports,* 4**,** 1-7.

Ferdelman, T. G., T. M. Church & G. W. Luther III (1991) Sulfur enrichment of humic substances in a Delaware salt marsh sediment core. *Geochimica et Cosmochimica Acta,* 55**,** 979-988.

Filley, T. R., K. H. Freeman, R. T. Wilkin & P. G. Hatcher (2002) Biogeochemical controls on reaction of sedimentary organic matter and aqueous sulfides in holocene sediments of Mud Lake, Florida. *Geochimica Et Cosmochimica Acta,* 66**,** 937-954.

Finster, K., W. Liesack & B. Thamdrup (1998) Elemental sulfur and thiosulfate disproportionation by Desulfocapsa sulfoexigens sp. nov., a new anaerobic bacterium isolated from marine surface sediment. *Applied and Environmental Microbiology,* 64**,** 119-125.

Fitts, C. R. 2012. *Groundwater Science (Second Edition).* Amsterdam: Elsevier.

Foght, J. (2008) Anaerobic biodegradation of aromatic hydrocarbons: pathways and prospects. *Journal of Molecular Microbiology and Biotechnology,* 15**,** 93-120.

Francois, R. (1987) A study of sulphur enrichment in the humic fraction of marine sediments during early diagenesis. *Geochimica et Cosmochimica Acta,* 51**,** 17-27.

Gaspar, A., M. Harir, N. Hertkorn & P. Schmitt-Kopplin (2010) Preparative free-flow electrophoretic offline ESI-Fourier transform ion cyclotron resonance/MS analysis of Suwannee River fulvic acid. *Electrophoresis,* 31**,** 2070-2079.

Gonsior, M., B. M. Peake, W. T. Cooper, D. Podgorski, J. D'Andrilli & W. J. Cooper (2009) Photochemically Induced Changes in Dissolved Organic Matter Identified by Ultrahigh Resolution Fourier Transform Ion Cyclotron Resonance Mass Spectrometry. *Environmental Science & Technology,* 43**,** 698-703.

Gonsior, M., P. Schmitt-Kopplin & D. Bastviken (2013) Depth-dependent molecular composition and photo-reactivity of dissolved organic matter in a boreal lake under winter and summer conditions. *Biogeosciences,* 10**,** 6945-6956.

Gonsior, M., J. Valle, P. Schmitt-Kopplin, N. Hertkorn, D. Bastviken, J. Luek, M. Harir, W. Bastos & A. Enrich-Prast (2016) Chemodiversity of Dissolved Organic Matter in the Amazon Basin. *Biogeosciences Discussions,* 13**,** 4279–4290.

Gonsior, M., M. Zwartjes, W. J. Cooper, W. Song, K. P. Ishida, L. Y. Tseng, M. K. Jeung, D. Rosso, N. Hertkorn & P. Schmitt-Kopplin (2011) Molecular characterization of effluent organic matter identified by ultrahigh resolution mass spectrometry. *Water Research,* 45**,** 2943-2953.

Green, N. W. & E. M. Perdue (2015) Fast Graphically Inspired Algorithm for Assignment of Molecular Formulae in Ultrahigh Resolution Mass Spectrometry. *Analytical Chemistry,* 87**,** 5086-5094.

Griebler, C. & T. Lueders (2009) Microbial biodiversity in groundwater ecosystems. *Freshwater Biology,* 54**,** 649-677.

Griebler, C., M. Safinowski, A. Vieth, H. Richow & R. U. Meckenstock (2004) Combined Application of Stable Carbon Isotope Analysis and Specific Metabolites Determination for Assessing In Situ Degradation of Aromatic Hydrocarbons in a Tar Oil-Contaminated Aquifer. *Environmental Science & Technology,* 38**,** 617–631.

Gross, J. H. 2011. Tandem Mass Spectrometry. In *Mass Spectrometry: A Textbook,* ed. H. J. Gross, 415-478. Berlin, Heidelberg: Springer Berlin Heidelberg.

Gun, J., A. Goifman, I. Shkrob, A. Kamyshny, B. Ginzburg, O. Hadas, I. Dor, A. D. Modestov & O. Lev (2000) Formation of Polysulfides in an Oxygen Rich Freshwater Lake and Their Role in the Production of Volatile Sulfur Compounds in Aquatic Systems. *Environmental Science & Technology,* 34**,** 4741-4746.

Haiber, S., H. Herzog, P. Burba, B. Gosciniak & J. Lambert (2001) Two-Dimensional NMR Studies of Size Fractionated Suwannee River Fulvic and Humic Acid Reference. *Environmental Science & Technology,* 35**,** 4289-4294.

Hansell, D. A. & C. A. Carlson (2001) Marine dissolved organic matter and the carbon cycle. *Oceanography,* 14**,** 41-49.

Hardisty, D. S., G. A. Olyphant, J. B. Bell, A. P. Johnson & L. M. Pratt (2013) Acidophilic sulfur disproportionation. *Geochimica et Cosmochimica Acta,* 113**,** 136-151.

Harris, B. D., T. A. Brown, J. L. McGehee, D. Houserova, B. A. Jackson, B. C. Buchel, L. C. Krajewski, A. J. Whelton & A. C. Stenson (2015) Characterization of Disinfection By-Products from Chromatographically Isolated NOM through High-Resolution Mass Spectrometry. *Environmental Science & Technology,* 49**,** 14239-14248.

Hebting, Y., P. Adam & P. Albrecht (2003) Reductive Desulfurization of Allylic Thiols by HS-/H2S in Water Gives Clue to Chemical Reactions Widespread in Natural Environments. *Organic Letters,* 5**,** 1571-1574.

Hebting, Y., P. Schaeffer, A. Behrens, P. Adam, G. Schmitt, P. Schneckenburger, S. M. Bernasconi & P. Albrecht (2006) Biomarker Evidence for a Major Preservation Pathway of Sedimentary Organic Carbon. *Science,* 312**,** 1627-1631.

Hedges, J. I. (1992) Global biogeochemical cycles: progress and problems. *Marine Chemistry,* 39**,** 67-93.

Heitmann, T. & C. Blodau (2006) Oxidation and incorporation of hydrogen sulfide by dissolved organic matter. *Chemical Geology,* 235**,** 12-20.

Heitmann, T., T. Goldhammer, J. Beer & C. Blodau (2007) Electron transfer of dissolved organic matter and its potential significance for anaerobic respiration in a northern bog. *Global Change Biology,* 13**,** 1771-1785.

Hellige, K., K. Pollok, P. Larese-Casanova, T. Behrends & S. Peiffer (2012) Pathways of ferrous iron mineral formation upon sulfidation of lepidocrocite surfaces. *Geochimica et Cosmochimica Acta,* 81**,** 69-81.

Helms, J. R., A. Stubbins, J. D. Ritchie, E. C. Minor, D. J. Kieber & K. Mopper (2008) Absorption spectral slopes and slope ratios as indicators of molecular weight, source, and photobleaching of chromophoric dissolved organic matter. *Limnology and Oceanography,* 53**,** 955-969.

Henneke, E., G. W. Luther III, G. J. De Lange & J. Hoefs (1997) Sulphur speciation in anoxic hypersaline sediments from the eastern Mediterranean Sea. *Geochimica et Cosmochimica Acta,* 61**,** 307-321.

Hertkorn, N. (2014) Environmental NMR: Solution-State Methods. *eMagRes,* 3**,** 55-74.

Hertkorn, N., R. Benner, M. Frommberger, P. Schmitt-Kopplin, M. Witt, K. Kaiser, A. Kettrup & J. I. Hedges (2006) Characterization of a major refractory component of marine dissolved organic matter. *Geochimica et Cosmochimica Acta,* 70**,** 2990-3010.

Hertkorn, N., H. Claus, P. Schmitt-Kopplin, E. M. Perdue & Z. Filip (2002) Utilization and Transformation of Aquatic Humic Substances by Autochthonous Microorganisms. *Environmental Science & Technology,* 36**,** 4334-4345.

Hertkorn, N., M. Frommberger, M. Witt, B. P. Koch, P. Schmitt-Kopplin & E. M. Perdue (2008) Natural Organic Matter and the Event Horizon of Mass Spectrometry. *Analytical Chemistry,* 80**,** 8908-8919.

Hertkorn, N., M. Harir, K. M. Cawley, P. Schmitt-Kopplin & R. Jaffé (2016) Molecular characterization of dissolved organic matter from subtropical wetlands: a comparative study through the analysis of optical properties, NMR and FTICR/MS. *Biogeosciences,* 13**,** 2257-2277.

Hertkorn, N., M. Harir, B. P. Koch, B. Michalke & P. Schmitt-Kopplin (2013) High-field NMR spectroscopy and FTICR mass spectrometry: powerful discovery tools for the molecular level characterization of marine dissolved organic matter. *Biogeosciences,* 10**,** 1583-1624.

Hertkorn, N., C. Ruecker, M. Meringer, R. Gugisch, M. Frommberger, E. M. Perdue, M. Witt & P. Schmitt-Kopplin (2007) High-precision frequency measurements: indispensable tools at the core of the molecular-level analysis of complex systems. *Analytical and Bioanalytical Chemistry,* 389**,** 1311-1327.

Herzsprung, P., N. Hertkorn, K. Friese & P. Schmitt-Kopplin (2010) Photochemical degradation of natural organic sulfur compounds (CHOS) from iron-rich mine pit lake pore waters – an initial understanding from evaluation of single-elemental formulae using ultra-high-resolution mass spectrometry. *Rapid Communications in Mass Spectrometry,* 24**,** 2909-2924.

Herzsprung, P., W. von Tümpling, N. Hertkorn, M. Harir, O. Büttner, J. Bravidor, K. Friese & P. Schmitt-Kopplin (2012) Variations of DOM Quality in Inflows of a Drinking Water Reservoir: Linking of van Krevelen Diagrams with EEMF Spectra by Rank Correlation. *Environmental Science & Technology,* 46**,** 5511-5518.

Hiriart-Baer, V. P. & R. E. H. Smith (2005) The effect of ultraviolet radiation on freshwater planktonic primary production: The role of recovery and mixing processes. *Limnology and Oceanography,* 50**,** 1352-1361.

Holleman, A. F., E. Wiberg & N. Wiberg. 2007. *Lehrbuch der Anorganischen Chemie.* Berlin: Walter de Gruyter & Co.

Huang, S., Y. Wang, Lei Tong, T. Ma, Y. Wang, C. Liu & L. Zhao (2015) Linking groundwater dissolved organic matter to sedimentary organic matter from a fluvio-lacustrine aquifer at Jianghan Plain, China by EEM-PARAFAC and hydrochemical analyses. *Science of the Total Environment,* 529**,** 131-139.

Huguet, A., L. Vacher, S. Relexans, S. Saubusse, J. M. Froidefond & E. Parlanti (2009) Properties of fluorescent dissolved organic matter in the Gironde Estuary. *Organic Geochemistry,* 40**,** 706-719.

Ishii, S. K. L. & T. H. Boyer (2012) Behavior of Reoccurring PARAFAC Components in Fluorescent Dissolved Organic Matter in Natural and Engineered Systems: A Critical Review. *Environmental Science & Technology,* 46**,** 2006–2017.

Jaffé, R., J. N. Boyer, X. Lu, N. Maie, C. Yang, N. M. Scully & S. Mock (2004) Source characterization of dissolved organic matter in a subtropical mangrove-dominated estuary by fluorescence analysis. *Marine Chemistry,* 84**,** 195-210.

Jaffé, R., K. M. Cawley & Y. Yamashita (2014) Applications of Excitation Emission Matrix Fluorescence with Parallel Factor Analysis (EEM-PARAFAC) in Assessing Environmental Dynamics of Natural Dissolved Organic Matter (DOM) in Aquatic Environments: A Review. 1160**,** 27-73.

Jarling, R., S. Kuhner, E. Basilio Janke, A. Gruner, M. Drozdowska, B. T. Golding, R. Rabus & H. Wilkes (2015) Versatile transformations of hydrocarbons in anaerobic bacteria: substrate ranges and regio- and stereo-chemistry of activation reactions. *Frontiers in Microbiology,* 6**,** 1-14.

Jobelius, C., B. Ruth, C. Griebler, R. U. Meckenstock, J. Hollender, A. Reineke, F. H. Frimmel & C. Zwiener (2011) Metabolites indicate hot spots of biodegradation and biogeochemical gradients in a high-resolution monitoring well. *Environmental Science & TechnologyEnviron,* 45**,** 474-481.

Jørgensen, B. B. (1977) Bacterial sulfate reduction within reduced microniches of oxidized marine sediments. *Marine Biology,* 41**,** 7-17.

Jørgensen, B. B. (1982) Mineralization of organic matter in the sea bed - the role of sulphate reduction. *Nature,* 296**,** 643-645.

Jørgensen, B. B. (1990) The sulfur cycle of freshwater sediments: Role of thiosulfate. *Limnology and Oceanography,* 35**,** 1329-1342.

Kamyshny, A., C. G. Borkenstein & T. G. Ferdelman (2009) Protocol for Quantitative Detection of Elemental Sulfur and Polysulfide Zero-Valent Sulfur Distribution in Natural Aquatic Samples. *Geostandards and Geoanalytical Research,* 33**,** 415-435.

Kamyshny, A., A. Goifman, J. Gun, D. Rizkov & O. Lev (2004) Equilibrium Distribution of Polysulfide Ions in Aqueous Solutions at 25 °C: A New Approach for the Study of Polysulfides' Equilibria. *Environmental Science & Technology,* 38**,** 6633-6644.

Kamyshny, A., J. Gun, D. Rizkov, T. Voitsekovski & O. Lev (2007) Equilibrium Distribution of Polysulfide Ions in Aqueous Solutions at Different Temperatures by Rapid Single Phase Derivatization. *Environmental Science & Technology,* 41**,** 2395-2400.

Kappler, A., M. Benz, B. Schink & A. Brune (2004) Electron shuttling via humic acids in microbial iron(III) reduction in a freshwater sediment. *FEMS Microbiology Ecology,* 47**,** 85-92.

Karwautz, C. & T. Lueders (2014) Impact of Hydraulic Well Restoration on Native Bacterial Communities in Drinking Water Wells. *Microbes and Environments,* 29**,** 363-369.

Kelly, P. D. (1999) Thermodynamic aspects of energy conservation by chemolithotrophic sulfur bacteria in relation to the sulfur oxidation pathways. *Archives of Microbiology,* 171**,** 219-229.

Kemker, C. (2013) pH of Water. Fundamentals of Environmental Measurements. http://www.fondriest.com/environmental-measurements/parameters/water-quality/ph/ (last accessed 9 Apr. 2016).

Kiefersfelden, G. (2009) Gemeinderat trifft kinderfreundliche Entscheidungen - Aus der Sitzung des Gemeinderats vom 29. April. *Kieferer Nachrichten* 150**,** 2.

Kim, D., J. M. Jin, Y. Cho, E.-H. Kim, H.-K. Cheong, Y. H. Kim & S. Kim (2015) Combination of ring type HPLC separation, ultrahigh-resolution mass spectrometry, and high field NMR for comprehensive characterization of crude oil compositions. *Fuel,* 157**,** 48–55.

Kim, S., L. A. Kaplan & P. G. Hatcher (2006) Biodegradable dissolved organic matter in a temperate and a tropical stream determined from ultra-high resolution mass spectrometry. *Limnology and Oceanography,* 51**,** 1054-1063.

Kim, S., R. W. Kramer & P. G. Hatcher (2003a) Graphical Method for Analysis of Ultrahigh-Resolution Broadband Mass Spectra of Natural Organic Matter, the Van Krevelen Diagram. *Analytical Chemistry,* 75**,** 5336-5344.

Kim, S., A. J. Simpson, E. B. Kujawinski, M. A. Freitas & P. G. Hatcher (2003b) High resolution electrospray ionization mass spectrometry and 2D solution NMR for the analysis of DOM extracted by C18 solid phase disk. *Organic Geochemistry,* 34**,** 1325-1335.

Kind, T. & O. Fiehn (2007) Seven Golden Rules for heuristic filtering of molecular formulas obtained by accurate mass spectrometry. *BMC Bioinformatics,* 8**,** 1-20.

Klapper, H. (1980) Experience with lake and reservoir restoration techniques in the German Democratic Republic. *Hydrobiologia,* 72**,** 31-41.

Kleinjan, W. E., A. de Keizer & A. J. H. Janssens (2005) Kinetics of the Reaction between Dissolved Sodium Sulfide and Biologically Produced Sulfur. *Industrial & Engineering Chemistry Research,* 44**,** 309-317.

Klupfel, L., A. Piepenbrock, A. Kappler & M. Sander (2014) Humic substances as fully regenerable electron acceptors in recurrently anoxic environments. *Nature Geoscience,* 7**,** 195-200.

Koch, B. P. & T. Dittmar (2006) From mass to structure: an aromaticity index for high-resolution mass data of natural organic matter. *Rapid Communications in Mass Spectrometry,* 20**,** 926-932.

Koch, B. P., T. Dittmar, M. Witt & G. Kattner (2007) Fundamentals of Molecular Formula Assignment to Ultrahigh Resolution Mass Data of Natural Organic Matter. *Analytical Chemistry,* 79**,** 1758-1763.

Koch, B. P., M. Witt, R. Engbrodt, T. Dittmar & G. Kattner (2005) Molecular formulae of marine and terrigenous dissolved organic matter detected by electrospray ionization Fourier transform ion cyclotron resonance mass spectrometry. *Geochimica et Cosmochimica Acta,* 69**,** 3299-3308.

Kohnen, M. E. L., J. S. S. Damsté, H. L. Ten Haven & J. W. De Leeuw (1989) Early incorporation of polysulphides in sedimentary organic matter. *Nature,* 341**,** 640-641.

Kohnen, M. E. l., J. S. Sinninghe Damsté, A. c. Kock-van Dalen & W. D. L. Jan (1991a) Di- or polysulphide-bound biomarkers in sulphur-rich geomacromolecules as revealed by selective chemolysis. *Geochimica et Cosmochimica Acta,* 55**,** 1375-1394.

Kohnen, M. E. L., J. S. Sinninghe Damsté, H. L. Ten Haven, A. C. kock.-Van Dalen, S. Schouten & J. W. De Leeuw (1991b) Identification and geochemical significance of cyclic di-and trisulphides with linear and acyclic isoprenoid carbon skeletons in immature sediments. *Geochimica et Cosmochimica Acta,* 55**,** 3685-3695.

Kördel, W., M. Dassenakis, J. Lintelmann & S. Padberg (1997) The importance of natural organic material for environmental processes in waters and soils. *Pure and Applied Chemistry* 69**,** 1571-1600.

Kruger, B. R., B. J. Dalzell & E. C. Minor (2011) Effect of organic matter source and salinity on dissolved organic matter isolation via ultrafiltration and solid phase extraction. *Aquatic Sciences,* 73**,** 405-417.

Kujawinski, E. B. & M. D. Behn (2006) Automated Analysis of Electrospray Ionization Fourier Transform Ion Cyclotron Resonance Mass Spectra of Natural Organic Matter. *Analytical Chemistry,* 78**,** 4363-4373.

Kujawinski, E. B., P. G. Hatcher & M. A. Freitas (2002) High-Resolution Fourier Transform Ion Cyclotron Resonance Mass Spectrometry of Humic and Fulvic Acids: Improvements and Comparisons. *Analytical Chemistry,* 74**,** 413-419.

Kujawinski, E. B., K. Longnecker, N. V. Blough, R. D. Vecchio, L. Finlay, J. B. Kitner & S. J. Giovannoni (2009) Identification of possible source markers in marine dissolved organic matter using ultrahigh resolution mass spectrometry. *Geochimica et Cosmochimica Acta,* 73**,** 4384-4399.

Laban, N. A., A. Dao & J. Foght (2015) DNA stable-isotope probing of oil sands tailings pond enrichment cultures reveals different key players for toluene degradation under methanogenic and sulfidogenic conditions. *FEMS Microbiology Ecology,* 91**,** 1-12.

LaLonde, R. T., L. M. Ferrara & M. P. Hayes (1987) Low-temperature, polysulfide reactions of conjugated ene carbonyls: A reaction model for the geologic origin of S-heterocycles. *Organic Geochemistry,* 11**,** 563-571.

Lam, B., A. Baer, M. Alaee, B. Lefebvre, A. Moser, A. Williams & A. J. Simpson (2007) Major Structural Components in Freshwater Dissolved Organic Matter. *Environmental Science & Technology,* 41**,** 8240-8247.

Lavonen, E. E., D. N. Kothawala, L. J. Tranvik, M. Gonsior, P. Schmitt-Kopplin & S. J. Kohler (2015) Tracking changes in the optical properties and molecular composition of dissolved organic matter during drinking water production. *Water Research,* 85**,** 286-294.

Lechtenfeld, O. J., B. P. Koch, W. Geibert, K. U. Ludwichowski & G. Kattner (2011) Inorganics in organics: quantification of organic phosphorus and sulfur and trace element speciation in natural organic matter using HPLC-ICPMS. *Analytical Chemistry,* 83**,** 8968-8974.

Leenheer, J. A. & J.-P. Croué (2003) Peer Reviewed: Characterizing Aquatic Dissolved Organic Matter. *Environmental Science & Technology,* 37**,** 18A-26A.

Leenheer, J. A. & C. E. Rostad (2004) Tannins and Terpenoids as Major Precursors of Suwannee River Fulvic Acid. *USGS Scientific Investigations Report,* 5276.

Li, W. & A. Godzik (2006) Cd-hit: a fast program for clustering and comparing large sets of protein or nucleotide sequences. *Bioinformatics,* 22**,** 1658-1659.

Liger-Belair, G., C. Cilindre, R. D. Gougeon, M. Lucio, I. Gebefügi, P. Jeandet & P. Schmitt-Kopplin (2009) Unraveling different chemical fingerprints between a champagne wine and its aerosols. *Proceedings of the National Academy of Sciences,* 106**,** 16545-16549.

Lin, V. S. (2015) Research highlights: challenges in the characterization, storage, and isolation of natural organic matter. *Environmental Science: Processes & Impacts,* 17**,** 2002-2005.

Lønborg, C., X. A. Álvarez-Salgado, K. Davidson, S. Martínez-García & E. Teira (2010) Assessing the microbial bioavailability and degradation rate constants of dissolved organic matter by fluorescence spectroscopy in the coastal upwelling system of the Ría de Vigo. *Marine Chemistry,* 119**,** 121-129.

Longnecker, K. & E. B. Kujawinski (2011) Composition of dissolved organic matter in groundwater. *Geochimica et Cosmochimica Acta,* 75**,** 2752-2761.

Lovley, D. R., J. D. Coates, E. L. Blunt-Harris, E. J. P. Phillips & J. C. Woodward (1996) Humic substances as electron acceptors for microbial respiration. *Nature,* 382**,** 445-448.

Lueders, T., M. Manefield & M. W. Friedrich (2004) Enhanced sensitivity of DNA- and rRNA-based stable isotope probing by fractionation and quantitative analysis of isopycnic centrifugation gradients. *Environmental Microbiology,* 6**,** 73-78.

Luther, G. W., A. E. Giblin & R. Varsolona (1985) Polarographic analysis of sulfur species in marine porewaters. *Limnology and Oceanography,* 30**,** 727-736.

Luther III, G. W. 1990. The frontier molecular orbital theory approach in geochemical processes. In *Aquatic Chemical Kinetics: Reaction Rates of Processes in Natural Waters,* ed. W. Stumm, 173-198. New York: Wiley.

Luther III, G. W. & T. M. Church. 1992. An Overview of the Environmental Chemistry of Sulphur in Wetland Systems. In *Sulphur Cycling on the Continents - Wetlands, Terrestrial Ecosystems, and Associated Water Bodies,* eds. R. W. Howarth, J. W. B. Stewart & M. V. Ivanov, 125-144. Chinester: John Wiley & Sons Ltd.

Luther III, G. W., B. T. Glazer, L. Hohmann, J. I. Popp, M. Taillefert, T. F. Rozan, P. J. Brendel, S. M. Theberge & D. B. Nuzzio (2001) Sulfur speciation monitored with solid state gold amalgam voltammetric microelectrodes: polysulfides as a special case in sediments, microbial mats and hydrothermal vent waters. *Journal of Environmental Monitoring,* 3**,** 61-66.

Lyons, T. W., D. A. Fike & A. Zerkle (2015) Emerging Biogeochemical Views of Earth's Ancient Microbial Worlds. *Elements,* 11**,** 415-421.

MacCarthy, P. (2001) The Principles of Humic Substances. *Soil Science,* 166**,** 738-751.

Maier, R. M. 2009. Biogeochemical Cycling. In *Environmental Microbiology (Second Edition),* eds. I. L. Pepper, C. P. Gerba, T. Gentry & R. M. Maier, 287-318. San Diego: Academic Press.

Marshall, A. G., C. L. Hendrickson & G. S. Jackson (1998) Fourier transform ion cyclotron resonance mass spectrometry: A primer. *Mass Spectrometry Reviews,* 17**,** 1-35.

Martus, P. & W. Puttmann (2003) Formation of alkylated aromatic acids in groundwater by anaerobic degradation of alkylbenzenes. *Science of the Total Environment,* 307**,** 19-33.

Matilainen, A., E. T. Gjessing, T. Lahtinen, L. Hed, A. Bhatnagar & M. Sillanpaa (2011) An overview of the methods used in the characterisation of natural organic matter (NOM) in relation to drinking water treatment. *Chemosphere,* 83**,** 1431-1442.

Mazzei, P. & A. Piccolo (2015) Interactions between natural organic matter and organic pollutants as revealed by NMR spectroscopy. *Magnetic Resonance in Chemistry,* 53**,** 667-678.

McKnight, D. M., E. W. Boyer, P. K. Westerhoff, P. T. Doran, T. Kulbe & D. T. Andersen (2001) Spectrofluorometric characterization of dissolved organic matter for indication of precursor organic material and aromaticity. *Limnology and Oceanography,* 46**,** 38-48.

Meckenstock, R. U., M. Elsner, C. Griebler, T. Lueders, C. Stumpp, J. Aamand, S. N. Agathos, H. J. Albrechtsen, L. Bastiaens, P. L. Bjerg, N. Boon, W. Dejonghe, W. E. Huang, S. I. Schmidt, E. Smolders, S. R. Sorensen, D. Springael & B. M. van Breukelen (2015) Biodegradation: Updating the Concepts of Control for Microbial Cleanup in Contaminated Aquifers. *Environmental Science & Technology,* 49**,** 7073-7081.

Meckenstock, R. U., M. Safinowski & C. Griebler (2004) Anaerobic degradation of polycyclic aromatic hydrocarbons. *FEMS Microbiology Ecology,* 49**,** 27-36.

Meckenstock, R. U., F. von Netzer, C. Stumpp, T. Lueders, A. M. Himmelberg, N. Hertkorn, P. Schmitt-Kopplin, M. Harir, R. Hosein, S. Haque & D. Schulze-Makuch (2014) Water droplets in oil are microhabitats for microbial life. *Science,* 345**,** 673-676.

Mendoza, W. G., D. D. Riemer & R. G. Zika (2013) Application of fluorescence and PARAFAC to assess vertical distribution of subsurface hydrocarbons and dispersant during the Deepwater Horizon oil spill *Environmental Science: Processes & Impacts,* 15**,** 1017-1030.

Meyer, B. & M. Ospina (1982) Raman Spectrometric Study of the Thermal Decomposition of Aqueous Tri-and Tetrathionate. *Phosphorus and Sulfur and the Related Elements,* 14**,** 23-36.

Miller, P. L. & Y.-P. Chin (2005) Indirect Photolysis Promoted by Natural and Engineered Wetland Water Constituents: Processes Leading to Alachlor Degradation. *Environmental Science & Technology,* 39**,** 4454-4462.

Milucka, J., T. G. Ferdelman, L. Polerecky, D. Franzke, G. Wegener, M. Schmid, I. Lieberwirth, M. Wagner, F. Widdel & M. M. M. Kuypers (2012) Zero-valent sulphur is a key intermediate in marine methane oxidation. *Nature,* 491**,** 541-546.

Minor, E. C., M. Swenson, B. M. Mattson & A. R. Oyler (2014) Structural characterization of dissolved organic matter: a review of current techniques for isolation and analysis. *Environmental Science: Processes & Impacts,* 16**,** 2064-2079.

Mitchell, P. J., A. J. Simpson & M. J. Simpson. 2014. Dissolved Organic Matter. In *NMR Spectroscopy: A Versatile Tool for Environmental Research,* eds. M. J. Simpson & A. J. Simpson, 177-192. Chichester: John Wiley & Sons, Ltd.

Moeckel, C., D. T. Monteith, N. R. Llewellyn, P. A. Henrys & M. G. Pereira (2014) Relationship between the Concentrations of Dissolved Organic Matter and Polycyclic Aromatic Hydrocarbons in a Typical U.K. Upland Stream. *Environmental Science & Technology,* 48**,** 130–138.

Mopper, K., A. Stubbins, J. D. Ritchie, H. M. Bialk & P. G. Hatcher (2007) Advanced Instrumental Approaches for Characterization of Marine Dissolved Organic Matter: Extraction Techniques, Mass Spectrometry, and Nuclear Magnetic Resonance Spectroscopy. *Chemical Reviews,* 107**,** 419-442.

Morris, D. P., H. Zagarese, C. E. Williamson, E. G. Balseiro, B. R. Hargreaves, B. Modenutti, R. Moeller & C. Queimalinos (1995) The attenuation of solar UV radiation in lakes and the role of dissolved organic carbon. *Limnology and Oceanography,* 40**,** 1381-1391.

Mostofa, K. M. G., F. Wu, C.-Q. Liu, W. L. Fang, J. Yuan, W. L. Ying, L. Wen & M. Yi (2009) Characterization of Nanming River (southwestern China) sewerage-impacted pollution using an excitation-emission matrix and PARAFAC. *Limnology,* 11**,** 217-231.

Mostofa, K. M. G., T. Yoshioka, E. Konohira & E. Tanoue (2007) Photodegradation of fluorescent dissolved organic matter in river waters. *Geochemical Journal,* 41**,** 323-331.

Mostofa, K. M. G., T. Yoshioka, A. Mottaleb & D. Vione. 2013. *Photobiogeochemistry of Organic Matter: Principles and Practices in Water Environments*. Heidelberg: Springer.

Müller, H., J. Bosch, C. Griebler, L. R. Damgaard, L. P. Nielsen, T. Lueders & R. U. Meckenstock (2016) Long-distance electron transfer by cable bacteria in aquifer sediments. *ISME Journal,* 10**,** 2010-2019.

Murphy, K. R., C. A. Stedmon, D. Graeber & R. Bro (2013) Fluorescence spectroscopy and multi-way techniques. PARAFAC. *Analytical Methods,* 5**,** 6557–6882.

Muyzer, G. & A. J. Stams (2008) The ecology and biotechnology of sulphate-reducing bacteria. *Nature Reviews Microbiology,* 6**,** 441-454.

Nebbioso, A. & A. Piccolo (2013) Molecular characterization of dissolved organic matter (DOM): a critical review. *Analytical and Bioanalytical Chemistry,* 405**,** 109-124.

Nikolaev, E. N., Y. I. Kostyukevich & G. N. Vladimirov (2014) Fourier transform ion cyclotron resonance (FT ICR) mass spectrometry: Theory and simulations. *Mass Spectrometry Reviews,* 35**,** 219–258.

Nürnberg, G. K. (1987) Hypolimnetic withdrawal as a lake restoration technique. *Journal of Environmental Engineering,* 113**,** 1006-1017.

Nürnberg, G. K. (2007) Lake responses to long-term hypolimnetic withdrawal treatments. *Lake and Reservoir Management,* 23**,** 388-409.

O'Brien, D. J. & F. B. Birkner (1977) Kinetics of oxygenation of reduced sulfur species in aqueous solution. *Environmental Science & Technology,* 11**,** 1114-1120.

Oduro, H., A. Kamyshny, A. L. Zerkle, Y. Li & J. Farquhar (2013) Quadruple sulfur isotope constraints on the origin and cycling of volatile organic sulfur compounds in a stratified sulfidic lake. *Geochimica et Cosmochimica Acta,* 120**,** 251-262.

Ohno, T., Z. He, R. L. Sleighter, C. W. Honeycutt & P. G. Hatcher (2010) Ultrahigh Resolution Mass Spectrometry and Indicator Species Analysis to Identify Marker Components of Soil- and Plant Biomass-Derived Organic Matter Fractions. *Environmental Science & Technology,* 44**,** 8594-8600.

Oliver, B. G., E. M. Thurman & R. L. Malcolm (1983) The contribution of humic substances to the acidity of colored natural waters. *Geochimica et Cosmochimica Acta,* 47**,** 2031-2035.

Olszewski, P. (1961) Versuch einer Ableitung des hypolimnischen Wassers aus einem See. *Verhandlungen des Internationalen Verein Limnologie,* 14**,** 855-861.

Overmann, J., T. J. Beatty, K. R. H. & K. J. Hall (1996) The sulfur cycle in the chemocline of a meromictic salt lake *Limnology and Oceanography,* 41**,** 147-156.

Pace, M. L., S. R. Carpenter, J. J. Cole, J. J. Coloso, J. F. Kitchell, J. R. Hodgson, J. J. Middelburg, N. D. Preston, C. T. Solomon & B. C. Weidel (2007) Does terrestrial organic carbon subsidize the planktonic food web in a clear-water lake? *Limnology and Oceanography,* 52**,** 2177-2189.

Parfitt, R. L. & R. H. Newman (2000) 13C NMR study of pine needle decomposition. *Plant and Soil,* 219**,** 273-278.

Parlanti, E., K. Wörz, L. Geoffroy & M. Lamotte (2000) Dissolved organic matter fluorescence spectroscopy as a tool to estimate biological activity in a coastal zone submitted to anthropogenic inputs. *Organic Geochemistry,* 31**,** 1765-1781.

Pechlaner, R. (1978) Erfahrungen mit Restaurierungsmassnahmen an eutrophen Badeseen Tirols. *Österreichische Wasserwirtschaft,* 30**,** 112-119.

Perdue, E. M. 2013. Standard and Reference Samples of Humic Acids, Fulvic Acids, and Natural Organic Matter from the Suwannee River, Georgia: Thirty Years of Isolation and Characterization. In *Functions of Natural Organic Matter in Changing Environment,* eds. J. Xu, J. Wu & Y. He, 85-88. Dordrecht: Springer Netherlands.

Perdue, E. M., N. Hertkorn & A. Kettrup (2007) Substitution Patterns in Aromatic Rings by Increment Analysis. Model Development and Application to Natural Organic Matter. *Analytical Chemistry,* 79**,** 1010-1021.

Perdue, E. M. & J. D. Ritchie. 2003. Dissolved Organic Matter in Freshwaters. In *Treatise on Geochemistry Volume 5: Surface and Ground Water, Weathering, and Soils,* eds. K. K. Holland & H. D. Turekian, 273-318. Oxford: Pergamon.

Perlinger, J. A., V. M. Kalluri, R. Venkatapathy & W. Angst (2002) Addition of Hydrogen Sulfide to Juglone. *Environmental Science & Technology,* 36**,** 2663-2669.

References

Pfeffer, C., S. Larsen, J. Song, M. Dong, F. Besenbacher, R. L. Meyer, K. U. Kjeldsen, L. Schreiber, Y. A. Gorby, M. Y. El-Naggar, K. M. Leung, A. Schramm, N. Risgaard-Petersen & L. P. Nielsen (2012) Filamentous bacteria transport electrons over centimetre distances. *Nature,* 491**,** 218–221.

Pilloni, G., M. S. Granitsiotis, M. Engel & T. Lueders (2012) Testing the Limits of 454 Pyrotag Sequencing: Reproducibility, Quantitative Assessment and Comparison to T-RFLP Fingerprinting of Aquifer Microbes. *PLoS ONE,* 7**,** 1-7.

Pohlabeln, A. M. & T. Dittmar (2015) Novel insights into the molecular structure of non-volatile marine dissolved organic sulfur. *Marine Chemistry,* 168**,** 86-94.

Poser, A., R. Lohmayer, C. Vogt, K. Knoeller, B. Planer-Friedrich, D. Sorokin, H.-H. Richnow & K. Finster (2013) Disproportionation of elemental sulfur by haloalkaliphilic bacteria from soda lakes. *Extremophiles,* 17**,** 1003-1012.

Pruesse, E., J. Peplies & F. O. Glöckner (2012) SINA: Accurate high-throughput multiple sequence alignment of ribosomal RNA genes. *Bioinformatics,* 28**,** 1823-1829.

Quast, C., E. Pruesse, P. Yilmaz, J. Gerken, T. Schweer, P. Yarza, J. Peplies & F. O. Glöckner (2013) The SILVA ribosomal RNA gene database project: improved data processing and web-based tools. *Nucleic Acids Research,* 41**,** 590-596.

Ravichandran, M. (2004) Interactions between mercury and dissolved organic matter - a review. *Chemosphere,* 55**,** 319-331.

Raymond, P. A., J. Hartmann, R. Lauerwald, S. Sobek, C. McDonald, M. Hoover, D. Butman, R. Striegl, E. Mayorga, C. Humborg, P. Kortelainen, H. Durr, M. Meybeck, P. Ciais & P. Guth (2013) Global carbon dioxide emissions from inland waters. *Nature,* 503**,** 355-359.

Remucal, C. K. (2014) The role of indirect photochemical degradation in the environmental fate of pesticides: a review. *Environmental Science: Processes & Impacts,* 16**,** 628-653.

Rethmeier, J., A. Rabenstein, M. Langer & U. Fischer (1997) Detection of traces of oxidized and reduced sulfur compounds in small samples by combination of different high-performance liquid chromatography methods. *Journal of Chromatography A,* 760**,** 295-302.

Rickard, D. 2012. *Sulfidic Sediments and Sedimentary Rocks*. Amsterdam: Elsevier.

Rickard, D. & G. W. Luther III (2007) Chemistry of Iron Sulfides. *Chemical Reviews,* 107**,** 514-562.

Ritchie, J. D. & E. M. Perdue (2003) Proton-binding study of standard and reference fulvic acids, humic acids, and natural organic matter. *Geochimica et Cosmochimica Acta,* 67**,** 85-96.

Rosen, E. & R. Tegman (1971) A preparative and X-ray powder diffraction study of the polysulfides Na2S2, Na2S4, and Na2S5. *Acta Chemica Scandinavica,* 25**,** 3329–3336.

Rozan, T. F., S. M. Theberge & G. Luther III (2000) Quantifying elemental sulfur (S0), bisulfide (HS-) and polysulfides (Sx2-) using a voltammetric method. *Analytica Chimica Acta,* 415**,** 175-184.

Saeed , A. I., V. Sharov, J. White, J. Li, W. Liang, N. Bhagabati, J. Braisted, M. Klapa, T. Currier, M. Thiagarajan, A. Sturn, M. Snuffin, A. Rezantsev, D. Popov, A.

Ryltsov, E. Kostukovich, I. Borisovsky, Z. Liu, A. Vinsavich, V. Trush & J. Quackenbush (2003) TM4: a free, open-source system for microarray data management and analysis. *Biotechniques,* 34**,** 374-378.

Safinowski, M., C. Griebler & R. U. Meckenstock (2006) Anaerobic Cometabolic Transformation of Polycyclic and Heterocyclic Aromatic Hydrocarbons: Evidence from Laboratory and Field Studies. *Environmental Science & Technology,* 40**,** 4165–4173.

Schiff, J. A. & H. Fankhauser. 1981. Assimilatory Sulfate Reduction. In *Biology of Inorganic Nitrogen and Sulfur,* eds. H. Bothe & A. Trebst, 153-168. Berlin, Heidelberg: Springer Berlin Heidelberg.

Schippers, A., T. Rohwerder & W. Sand (1999) Intermediary sulfur compounds in pyrite oxidation: implications for bioleaching and biodepyritization of coal. *Applied Microbiology and Biotechnology,* 52**,** 104-110.

Schmidt, F., M. Elvert, B. P. Koch, M. Witt & K.-U. Hinrichs (2009) Molecular characterization of dissolved organic matter in pore water of continental shelf sediments. *Geochimica et Cosmochimica Acta,* 73**,** 3337-3358.

Schmidt, F., B. P. Koch, M. Elvert, G. Schmidt, M. Witt & K. U. Hinrichs (2011) Diagenetic transformation of dissolved organic nitrogen compounds under contrasting sedimentary redox conditions in the Black Sea. *Environmental Science & Technology,* 45**,** 5223-5229.

Schmidt, F., B. P. Koch, M. Witt & K.-U. Hinrichs (2014) Extending the analytical window for water-soluble organic matter in sediments by aqueous Soxhlet extraction. *Geochimica et Cosmochimica Acta,* 141**,** 83-96.

Schmidt, M. & H. Heinrich (1958) Beitrag zur Lösung des Problems der Wackenroderschen Flüssigkeit. Über Säuren des Schwefels, XII. *Angewandte Chemie,* 70**,** 572-573.

Schmitt-Kopplin, P., A. Gelencsér, E. Dabek-Zlotorzynska, G. Kiss, N. Hertkorn, M. Harir, Y. Hong & I. Gebefügi (2010) Analysis of the Unresolved Organic Fraction in Atmospheric Aerosols with Ultrahigh-Resolution Mass Spectrometry and Nuclear Magnetic Resonance Spectroscopy: Organosulfates As Photochemical Smog Constituents. *Analytical Chemistry,* 82**,** 8017-8026.

Schmitt-Kopplin, P. & A. Kettrup (2003) Capillary electrophoresis-electrospray ionization-mass spectrometry for the characterization of natural organic matter: an evaluation with free flow electrophoresis-off-line flow injection electrospray ionization-mass spectrometry. *Electrophoresis,* 24**,** 3057-3066.

Schmitt-Kopplin, P., G. Liger-Belair, B. P. Koch, R. Flerus, G. Kattner, M. Harir, B. Kanawati, M. Lucio, D. Tziotis, N. Hertkorn & I. Gebefügi (2012) Dissolved organic matter in sea spray: a transfer study from marine surface water to aerosols. *Biogeosciences,* 9**,** 1571-1582.

Schouten, S., W. de Graaf, J. S. Sinninghe Damsté, G. B. van Driel & J. W. de Leeuw (1994) Laboratory simulation of natural sulphurization: II. Reaction of multi-functionalized lipids with inorganic polysulphides at low temperatures. *Organic Geochemistry,* 22**,** 825-834.

Schouten, S., G. B. van Driel, J. S. Sinninghe Damsté & J. W. de Leeuw (1993) Natural sulphurization of ketones and aldehydes: A key reaction in the formation of organic sulphur compounds. *Geochimica et Cosmochimica Acta,* 57**,** 5111-5116.

Schug, K. & H. M. McNair (2002) Adduct formation in electrospray ionization. Part 1: Common acidic pharmaceuticals. *Journal of Separation Science,* 25**,** 759-766.

Schug, K. & H. M. McNair (2003) Adduct formation in electrospray ionization mass spectrometry II. Benzoic acid derivatives. *Journal of Chromatography A,* 985**,** 531-539.

Seidel, M., M. Beck, T. Riedel, H. Waska, I. G. N. A. Suryaputra, B. Schnetger, J. Niggemann, M. Simon & T. Dittmar (2014) Biogeochemistry of dissolved organic matter in an anoxic intertidal creek bank. *Geochimica et Cosmochimica Acta,* 140**,** 418-434.

Shen, Y., F. H. Chapelle, E. W. Strom & R. Benner (2014) Origins and bioavailability of dissolved organic matter in groundwater. *Biogeochemistry,* 122**,** 61-78.

Sholkovitz, E. R. & D. Copland (1981) The coagulation, solubility and adsorption properties of Fe, Mn, Cu, Ni, Cd, Co and humic acids in a river water. *Geochimica et Cosmochimica Acta,* 45**,** 181-189.

Simpson, A. J., D. J. McNally & M. J. Simpson (2011) NMR spectroscopy in environmental research: From molecular interactions to global processes. *Progress in Nuclear Magnetic Resonance Spectroscopy,* 58**,** 97-175.

Simpson, A. J., M. J. Simpson & R. Soong (2012) Nuclear Magnetic Resonance Spectroscopy and Its Key Role in Environmental Research. *Environmental Science & Technology,* 46**,** 11488-11496.

Simpson, M. J. & A. J. Simpson. 2014. *NMR Spectroscopy: A Versatile Tool for Environmental Research.* New York: John Wiley & Sons Inc.

Sinninghe Damsté, J. S. & J. W. De Leeuw (1990) Analysis, structure and geochemical significance of organically-bound sulphur in the geosphere: State of the art and future research. *Organic Geochemistry,* 16**,** 1077-1101.

Sinninghe Damsté, J. S., W. Irene, C. Rijpstra, J. W. de Leeuw & P. A. Schenck (1988) Origin of organic sulphur compounds and sulphur-containing high molecular weight substances in sediments and immature crude oils. *Organic Geochemistry,* 13**,** 593-606.

Sinninghe Damsté, J. S., W. I. C. Rijpstra, A. C. Kock-van Dalen, J. W. De Leeuw & P. A. Schenck (1989) Quenching of labile functionalised lipids by inorganic sulphur species: Evidence for the formation of sedimentary organic sulphur compounds at the early stages of diagenesis. *Geochimica et Cosmochimica Acta,* 53**,** 1343-1355.

Skakovskii, E. D., S. A. Lamotkin, S. I. Shpak, L. Y. Tychinskaya, O. A. Gaidukevich & A. I. Lamotkin (2006) Application of NMR spectroscopy for analysis of the composition of pine needle essential oil. *Journal of Applied Spectroscopy,* 73**,** 275-279.

Sleighter, R. L., Y.-P. Chin, W. A. Arnold, P. G. Hatcher, A. J. McCabe, B. C. McAdams & G. C. Wallace (2014) Evidence of Incorporation of Abiotic S and N into Prairie Wetland Dissolved Organic Matter. *Environmental Science & Technology Letters,* 1**,** 345-350.

Sleighter, R. L. & P. Hatcher. 2011. Fourier Transform Mass Spectrometry for the Molecular Level Characterization of Natural Organic Matter: Instrument Capabilities, Applications, and Limitations. In *Fourier Transforms - Approach to Scientific Principles,* ed. G. Nikolic, 295-320. Rijeka: InTech.

Sleighter, R. L. & P. G. Hatcher (2007) The application of electrospray ionization coupled to ultrahigh resolution mass spectrometry for the molecular characterization of natural organic matter. *Journal of Mass Spectrometry,* 42**,** 559-574.

Sleighter, R. L., Z. Liu, J. Xue & P. G. Hatcher (2010) Multivariate Statistical Approaches for the Characterization of Dissolved Organic Matter Analyzed by Ultrahigh Resolution Mass Spectrometry. *Environmental Science & Technology,* 44**,** 7576-7582.

Stedmon, C. A., S. Markager & R. Bro (2003) Tracing dissolved organic matter in aquatic environments using a new approach to fluorescence spectroscopy. *Marine Chemistry,* 82**,** 239-254.

Stenson, A. C., A. G. Marshall & W. T. Cooper (2003) Exact Masses and Chemical Formulas of Individual Suwannee River Fulvic Acids from Ultrahigh Resolution Electrospray Ionization Fourier Transform Ion Cyclotron Resonance Mass Spectra. *Analytical Chemistry,* 75**,** 1275-1284.

Steudel, R. 2003. *Elemental Sulfur and Sulfur-Rich Compounds I.* Berlin: Springer.

Steudel, R., G. Holdt, T. Göbel & W. Hazeu (1987) Chromatographic Separation of Higher Polythionates SnO_6^{2-} (n = 3…22) and Their Detection in Cultures of Thiobacillus ferroxidans; Molecular Composition of Bacterial Sulfur Secretions. *Angewandte Chemie International Edition,* 26**,** 151-153.

Stookey, L. L. (1970) Ferrozine - a new spectrophotometric reagent for iron. *Analytical Chemistry,* 42**,** 779–781.

Stubbins, A., J. F. Lapierre, M. Berggren, Y. T. Prairie, T. Dittmar & P. A. Del Giorgio (2014) What's in an EEM? Molecular Signatures Associated with Dissolved Organic Fluorescence in Boreal Canada. *Environmental Science & Technology,* 48**,** 10598-10606.

Sudasinghe, N., J. R. Cort, R. Hallen, M. Olarte, A. Schmidt & T. Schaub (2014) Hydrothermal liquefaction oil and hydrotreated product from pine feedstock characterized by heteronuclear two-dimensional NMR spectroscopy and FT-ICR mass spectrometry. *Fuel,* 137**,** 60-69.

Suzuki, I. (1999) Oxidation of inorganic sulfur compounds: Chemical and enzymatic reactions. *Canadian Journal of Microbiology,* 45**,** 97-105.

Taillefert, M. & T. F. Rozan. 2002. Electrochemical Methods for the Environmental Analysis of Trace Elements Biogeochemistry. In *Environmental Electrochemistry: Analyses of Trace Element Biogeochemistry* eds. M. Taillefert & T. F. Rozan, 2-14. Washington, DC: American Chemical Society.

Takano, B. & K. Watanuki (1988) Quenching and liquid chromatographic determination of polythionates in natural water. *Talanta,* 35**,** 847-854.

Thamdrup, B., K. Finster, J. W. Hansen & F. Bak (1993) Bacterial Disproportionation of Elemental Sulfur Coupled to Chemical Reduction of Iron or Manganese. *Applied and Environmental Microbiology,* 59**,** 101-108.

Thurman, E. M. 1985. *Organic Geochemistry of Natural Waters*. Dordrecht: Nijhoff/Junk.

Thurman, E. M. & R. L. Malcolm (1981) Preparative isolation of aquatic humic substances. *Environmental Science & Technology,* 15**,** 463-466.

Timko, S. A., M. Gonsior & W. J. Cooper (2015a) Influence of pH on fluorescent dissolved organic matter photo-degradation. *Water Research,* 85**,** 266-274.

Timko, S. A., A. Maydanov, S. L. Pittelli, M. H. Conte, W. J. Cooper, B. P. Koch, P. Schmitt-Kopplin & M. Gonsior (2015b) Depth-dependent Photodegradation of Marine Dissolved Organic Matter. *Frontiers in Marine Science,* 2**,** 1-13.

Timko, S. A., C. Romera-Castillo, R. Jaffe & W. J. Cooper (2014) Photo-reactivity of natural dissolved organic matter from fresh to marine waters in the Florida Everglades, USA. *Environmental Science: Processes & Impacts,* 16**,** 866-878.

Traina, S. J., D. C. McAvoy & D. J. Versteeg (1996) Association of Linear Alkylbenzenesulfonates with Dissolved Humic Substances and Its Effect on Bioavailability. *Environmental Science & Technology,* 30**,** 1300-1309.

Tziotis, D., N. Hertkorn & P. Schmitt-Kopplin (2011) Letter: Kendrick-analogous network visualisation of ion cyclotron resonance Fourier transform mass spectra: improved options for the assignment of elemental compositions and the classification of organic molecular complexity. *European Journal of Mass Spectrometry,* 17**,** 415-421.

Vairavamurthy, A., B. Manowitz, G. W. Luther & Y. Jeon (1993) Oxidation state of sulfur in thiosulfate and implications for anaerobic energy metabolism *Geochimica et Cosmochimica Acta,* 57**,** 1619-1623.

Vairavamurthy, A. & K. Mopper (1987) Geochemical formation of organosulphur compounds (thiols) by addition of H2S to sedimentary organic matter. *Nature,* 329**,** 623-625.

Vairavamurthy, A. & K. Mopper. 1989. Mechanistic Studies of Organosulfur (Thiol) Formation in Coastal Marine Sediments. In *Biogenic Sulfur in the Environment*, 231-242. Washington, DC: American Chemical Society.

Vairavamurthy, A., W. Zhou, T. Eglinton & B. Manowitz (1994) Sulfunates: A novel class of organic sulfur compounds in marine sediments *Geochimica et Cosmochimica Acta,* 58**,** 4681-4687.

van Dongen, B. E., S. Schouten, M. Baas, J. A. J. Geenevasen & J. S. Sinninghe Damsté (2003) An experimental study of the low-temperature sulfurization of carbohydrates. *Organic Geochemistry,* 34**,** 1129-1144.

van Krevelen, D. W. (1950) Graphical-statistical method for the study of structure and reaction processes of coal. *Fuel,* 29**,** 269-284.

vanLoon, G. W. & S. J. Duffy. 2011. *Environmental Chemistry - A global perspective*. New York: Oxford University Press Inc.

Vogt, C. & H. H. Richnow (2014) Bioremediation via in situ microbial degradation of organic pollutants. *Advances in Biochemical Engineering/Biotechnology,* 142**,** 123-146.

Wagner, S., R. Jaffe, K. Cawley, T. Dittmar & A. Stubbins (2015a) Associations Between the Molecular and Optical Properties of Dissolved Organic Matter in the Florida Everglades, a Model Coastal Wetland System. *Frontiers in Chemistry,* 3**,** 1-14.

Wagner, S., T. Riedel, J. Niggemann, A. V. Vahatalo, T. Dittmar & R. Jaffe (2015b) Linking the Molecular Signature of Heteroatomic Dissolved Organic Matter to Watershed Characteristics in World Rivers. *Environmental Science & Technology,* 49**,** 13798–13806.

Walker, K. F. (1974) The stability of meromictic lakes in central Washington. *Limnology and Oceanography,* 19**,** 209-222.

Wang, Z., J. Cao & F. Meng (2015) Interactions between protein-like and humic-like components in dissolved organic matter revealed by fluorescence quenching. *Water Research,* 68**,** 404-413.

Wehrli, B. (2013) Biogeochemistry: Conduits of the carbon cycle. *Nature,* 503**,** 346-347.

Weishaar, J. L., G. R. Aiken, B. A. Bergamaschi, M. S. Fram, R. Fujii & K. Mopper (2003) Evaluation of Specific Ultraviolet Absorbance as an Indicator of the Chemical Composition and Reactivity of Dissolved Organic Carbon. *Environmental Science & Technology,* 37**,** 4702-4708.

Wenk, J., M. Aeschbacher, M. Sander, U. v. Gunten & S. Canonica (2015) Photosensitizing and Inhibitory Effects of Ozonated Dissolved Organic Matter on Triplet-Induced Contaminant Transformation. *Environmental Science & Technology,* 49**,** 8541-8549.

Wenk, J., U. von Gunten & S. Canonica (2011) Effect of Dissolved Organic Matter on the Transformation of Contaminants Induced by Excited Triplet States and the Hydroxyl Radical. *Environmental Science & Technology,* 45**,** 1334-1340.

Wetzel, R. G. 2001. *Limnology, Third Edition: Lake and River Ecosystems*. San Diego: Academic Press.

Wiedemeier, T. H., H. S. Rifai, C. J. Newell & J. T. Wilson. 1999. *Natural Attenuation of Fuels and Chlorinated Solvents in the Subsurface*. New York: John Wiley & Sons, Inc.

Winderl, C., B. Anneser, C. Griebler, R. U. Meckenstock & T. Lueders (2008) Depth-Resolved Quantification of Anaerobic Toluene Degraders and Aquifer Microbial Community Patterns in Distinct Redox Zones of a Tar Oil Contaminant Plume. *Applied and Environmental Microbiology,* 74**,** 792-801.

Wisotzky, F. & P. Eckert (1997) Sulfat-dominierter BTEX-Abbau im Grundwasser eines ehemaligen Gaswerksstandortes. *Grundwasser,* 2**,** 11-20.

Xu, Y. & M. A. A. Schoonen (1995) The stability of thiosulfate in the presence of pyrite in low-temperature aqueous solutions. *Geochimica et Cosmochimica Acta,* 59**,** 4605-4622.

Xu, Y., M. A. A. Schoonen, D. K. Nordstrom, K. M. Cunningham & J. W. Ball (2000) Sulfur geochemistry of hydrothermal waters in Yellowstone National Park,

Wyoming, USA. II. Formation and decomposition of thiosulfate and polythionate in Cinder Pool. *Journal of Volcanology and Geothermal Research,* 97**,** 407-423.

Yamashita, Y., R. Jaffé, N. Maie & E. Tanoue (2008) Assessing the dynamics of dissolved organic matter (DOM) in coastal environments by excitation emission matrix fluorescence and parallel factor analysis (EEM-PARAFAC). *Limnology and Oceanography,* 53**,** 1900-1908.

Yang, L., J. Hur & W. Zhuang (2015) Occurrence and behaviors of fluorescence EEM-PARAFAC components in drinking water and wastewater treatment systems and their applications: a review. *Environmental Science and Pollution Research,* 22**,** 6500-6510.

Yassine, M. M., E. Dabek-Zlotorzynska, M. Harir & P. Schmitt-Kopplin (2012) Identification of weak and strong organic acids in atmospheric aerosols by capillary electrophoresis/mass spectrometry and ultra-high-resolution Fourier transform ion cyclotron resonance mass spectrometry. *Analytical Chemistry,* 84**,** 6586-6594.

Yu, Z.-G., S. Orsetti, S. B. Haderlein & K.-H. Knorr (2015a) Electron Transfer Between Sulfide and Humic Acid: Electrochemical Evaluation of the Reactivity of Sigma-Aldrich Humic Acid Toward Sulfide. *Aquatic Geochemistry,* 22**,** 117–130.

Yu, Z. G., S. Peiffer, J. Gottlicher & K. H. Knorr (2015b) Electron transfer budgets and kinetics of abiotic oxidation and incorporation of aqueous sulfide by dissolved organic matter. *Environmental Science & Technology,* 49**,** 5441-5449.

Zeng, T. & W. A. Arnold (2013) Pesticide Photolysis in Prairie Potholes: Probing Photosensitized Processes. *Environmental Science & Technology,* 47**,** 6735-6745.

Zerkle, A. L., A. Kamyshny, L. R. Kump, J. Farquhar, H. Oduro & M. A. Arthur (2010) Sulfur cycling in a stratified euxinic lake with moderately high sulfate: Constraints from quadruple S isotopes. *Geochimica et Cosmochimica Acta,* 74**,** 4953-4970.

Zhang, J.-Z. & F. J. Millero (1993) The products from the oxidation of H2S in seawater. *Geochimica et Cosmochimica Acta,* 57**,** 1705-1718.

Zhang, Y., M. A. van Dijk, M. Liu, G. Zhu & B. Qin (2009) The contribution of phytoplankton degradation to chromophoric dissolved organic matter (CDOM) in eutrophic shallow lakes: Field and experimental evidence. *Water Research,* 43**,** 4685-4697.

Zhou, Z. & L. Guo (2012) Evolution of the optical properties of seawater influenced by the Deepwater Horizon oil spill in the Gulf of Mexico. *Environmental Research Letters,* 7**,** 1-12.

Zhou, Z., L. Guo, A. M. Shiller, S. E. Lohrenz, V. L. Asper & C. L. Osburn (2013) Characterization of oil components from the Deepwater Horizon oil spill in the Gulf of Mexico using fluorescence EEM and PARAFAC techniques. *Marine Chemistry,* 148**,** 10-21.

Zopfi, J., T. G. Ferdelman & H. Fossing (2004) Distribution and fate of sulfur intermediates—sulfite, tetrathionate, thiosulfate, and elemental sulfur—in marine sediments. *Geological Society of America Special Papers,* 379**,** 97-116.

Zsolnay, A. (1999) Differentiating with fluorescence spectroscopy the sources of dissolved organic matter in soils subjected to drying. *Chemosphere,* 38**,** 45-50.

Curriculum vitae

Personal information

Date of Birth: December 24th, 1986
Nationality: German

Gronsdorfer Straße 9 o
85540 Haar (Germany)
Phone: 0177/7408708
Email: sabine.dvorski@gmail.com

Scientific work experience

10/2012 – 03/2016	**PhD candidate, Helmholtz Zentrum München GmbH, Research Unit Analytical Biogeochemistry, Technische Universität München, Chair of Analytical Food Chemistry** Thesis: *Linking the Sulfur and Carbon Cycle by Ultrahigh Resolution Characterization of Dissolved Organic Matter*
12/2014	Lab visit, University of Maryland, Center for Environmental Science, Chesapeake Biological Laboratory, Solomons, USA
11/2014 – 12/2014	Lab visit, Indiana University-Purdue University Indianapolis, USA
06/2013 – 07/2013	Assistance at the isolation of natural organic matter standard reference material, International Humic Substances Society, Minneapolis, USA
01/2012 – 09/2012	Research stay, Helmholtz Zentrum München, Cooperation Group Comprehensive Molecular Analytics
06/2009 – 07/2009	Student assistant, Technische Universität München, Chair of construction chemistry

Education

10/2009 – 11/2011	**Master of Science in chemistry, Technische Universität München,** Thesis: *Studies on the Metabolism and Metabolites of ^{13}C-labeled Panax ginseng by GC-MS*
10/2006 – 10/2009	**Bachelor of Science in chemistry, Technische Universität München,** Thesis: *Uranium in selected environmental samples: Optimization of the quantification with ICP-OES*
09/2004 – 06/2006	**Abitur (University entrance qualification), Michaeli-Gymnasium, Munich,**

List of scientific communications

Publications

Dvorski, S. E.-M., M. Gonsior, N. Hertkorn, J. Uhl, H. Müller, C. Griebler and P. Schmitt-Kopplin (2016) Geochemistry of Dissolved Organic Matter in a Spatially Highly Resolved Groundwater Petroleum Hydrocarbon Plume Cross-Section. *Environmental Science & Technology*, 50, 5536–5546.

Schramek, N., C. Huber, S. Schmidt, S. E.-M.Dvorski, N. Knispel, E. Ostrozhenkova, L.M. Pena-Rodriguez, R.M. Cusido, G. Wischmann and W. Eisenreich (2014) Biosynthesis of Ginsenosides in Field-Grown Panax Ginseng. *JSM Biotechnology & Biomedical Engineering* 2(1): 1033.

Publications in preparation

Dvorski, S. E.-M., A. R. Szalay, J. Uhl, M. Lucio, N. Hertkorn, C. Griebler, T. Lueders and P, Schmitt-Kopplin: Petroleum hydrocarbon degradation by bacterial sulfate reduction and its effect on groundwater dissolved organic matter

Dvorski S. E.-M., J. Uhl, G. K. Druschel and P. Schmitt-Kopplin: Effects of the inorganic sulfur chemistry on the DOM of a meromictic lake

Dvorski S. E.-M., F. C. Kafantaris, J. Uhl, G. K. Druschel, N. Hertkorn and P. Schmitt-Kopplin: Linking the carbon and sulfur cycle: Reactivity study of inorganic sulfur species with dissolved organic matter

Gonsior, M., S. E.-M. Dvorski, N. Hinman, W. J. Cooper, M. Harir, N. Hertkorn and P. Schmitt-Kopplin: Yellowstone Hot Springs are Organic Chemodiversity Hot Spots. (under revision)

Oral Presentations

Kafantaris, F. C., G. Druschel, S. Dvorski, P. Schmitt-Kopplin, Y. and Hu: *Reactivity of elemental sulfur nanoparticles and their role on the biogeochemical cycling of sulfur.* The Geological Society of America (GSA) Annual Meeting 2015. Baltimore, USA.

Dvorski, S., J. Uhl, H. Müller, M. Größbacher, N. Hertkorn, C. Griebler and P. Schmitt-Kopplin: *Linking the sulfur and carbon cycle by ultrahigh resolution characterization of dissolved organic matter.* Goldschmidt 2015, Prag, Czech Republic.

199

Dvorski, S., M. Harir, Y. Li, N. Hertkorn and P. Schmitt-Kopplin: *Linking the sulfur and carbon cycle by ultrahigh resolution characterization of dissolved organic matter.* Helmholtz WasserZentrum München (HWZM) Final Meeting 2015, Neuherberg, Germany.

Dvorski, S., M. Harir, N. Hertkorn and Schmitt-Kopplin P.: *Ultrahigh resolution mass spectrometry of dissolved organic matter from a tar oil contaminated groundwater.* 3rd Helmholtz WasserZentrum München (HWZM) Status Meeting 2014, Neuherberg, Germany.

Dvorski, S., M. Harir, N. Hertkorn and P. Schmitt-Kopplin: *Assessing the importance & formation processes of sulfur organic compounds in freshwaters under various redox conditions.* 2nd Helmholtz WasserZentrum München (HWZM) Status Meeting 2013, Neuherberg, Germany.

Posters

Dvorski, S., J. Uhl, H. Müller, M. Größbacher, N. Hertkorn, C. Griebler and P. Schmitt-Kopplin: *Linking the sulfur and carbon cycle by ultrahigh resolution characterization of dissolved organic matter.* Departements of Environmental Sciences (DES) Day 2015, Neuherberg, Germany.

Druschel, G. K., F. C. Kafantaris, D. A. Fike, P. Schmitt-Kopplin, S. Dvorski and H. Oduro: *Oxidation kinetics of sulfur species with oxygen and peroxide – a field, lab, and computational approach to understanding detailed sulfur speciation.* American Geophysical Union (AGU) Fall Meeting 2014, San Francisco, USA.

Dvorski, S., J. Uhl, C. Kellermann, H. Müller, M. Größbacher, M. Harir, N. Hertkorn, C. Griebler and P. Schmitt-Kopplin: *Ultrahigh resolution mass spectrometry of dissolved organic matter from a tar oil contaminated aquifer along biogeochemical gradients.* Departements of Environmental Sciences (DES) Day 2014, Neuherberg, Germany.

Dvorski, S., J. Westphal, C. Kellermann, H. Müller, M. Größbacher, M. Harir, N. Hertkorn, C. Griebler and P. Schmitt-Kopplin: *Ultrahigh resolution mass spectrometry of dissolved organic matter from a tar oil contaminated aquifer along biogeochemical gradients.* BioGeoMon 2014, Bayreuth, Germany.

Dvorski, S., M. Harir, N. Hertkorn, N. Hinman, M. Gonsior, W. Cooper and P. Schmitt-Kopplin: *Ultrahigh resolution mass spectrometry of natural organic matter from hydrothermal springs.* Goldschmidt 2013, Florence, Italy.

Dvorski, S., Y. Li, M. Harir and P. Schmitt-Kopplin: *Stability of natural organic matter in different solvents analyzed by ultrahigh resolution mass spectrometry.* TUM Graduate School Kick-Off Seminar 2013, Herrsching, Germany.

Eidesstattliche Erklärung

Ich erkläre an Eides statt, dass ich die bei der promotionsführenden Einrichtung Wissenschaftszentrum Weihenstephan für Ernährung, Landnutzung und Umwelt der Technischen Universität München zur Promotionsprüfung vorgelegte Arbeit mit dem Titel:

Linking the sulfur and carbon cycle by ultrahigh resolution characterization of dissolved organic matter

in Chemie am Lehrstuhl für Analytische Lebensmittelchemie unter der Anleitung und Betreuung durch apl.-Prof. Dr. P. Schmitt-Kopplin ohne sonstige Hilfe erstellt und bei der Abfassung nur die gemäß § 6 Abs. 6 und 7 Satz 2 angegebenen Hilfsmittel benutzt habe.

(x) Ich habe keine Organisation eingeschaltet, die gegen Entgelt Betreuerinnen und Betreuer für die Anfertigung von Dissertationen sucht, oder die mir obliegenden Pflichten hinsichtlich der Prüfungsleistungen für mich ganz oder teilweise erledigt.

(x) Ich habe die Dissertation in dieser oder ähnlicher Form in keinem anderen Prüfungsverfahren als Prüfungsleistung vorgelegt.

 (x) Ich habe den angestrebten Doktorgrad noch nicht erworben und bin nicht in einem früheren Promotionsverfahren für den angestrebten Doktorgrad endgültig gescheitert.

Die öffentlich zugängliche Promotionsordnung der TUM ist mir bekannt, insbesondere habe ich die Bedeutung von § 28 (Nichtigkeit der Promotion) und § 29 (Entzug des Doktorgrades) zur Kenntnis genommen. Ich bin mir der Konsequenzen einer falschen Eidesstattlichen Erklärung bewusst.

Mit der Aufnahme meiner personenbezogenen Daten in die Alumni-Datei bei der TUM bin ich

(x) einverstanden

( ) nicht einverstanden

München, den ....